The Role of Calcium Signalling in Autophagy

Thesis

The Open University, Faculty of Science, Technology, Engineering and Mathematics; School of Life, Heath and Chemical Sciences; Walton Hall, Milton Keynes, United Kingdom.

The role of calcium signalling in autophagy

Tala Chehab, BSc

A thesis submission to The Open University for

the degree of Doctor in Philosophy

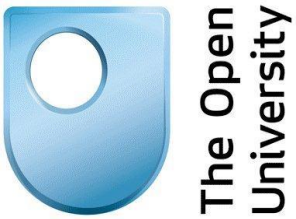

September 2017

DECLARATION

I declare that the work presented in this thesis is a result of my own academic and experimental enquiry. This work does not contain any material submitted for a degree, diploma or any other qualification at the Open University or any other University. Contributions made by other researchers are fully acknowledged in relevant parts of the thesis.

Tala Chehab

September 2017

ABSTRACT

Autophagy is a catabolic process that is important for degradation of cellular components, and for cell survival, and has also been associated with pathological disorders and tumour growth. Autophagy is a complex process; many factors and messengers converge to control steps along the autophagic pathway. Ca^{2+} has been proposed to regulate autophagy. However, Ca^{2+} has been proposed to be both pro- and anti-autophagic. To better understand how Ca^{2+} has these opposing effects, this study investigated in what ways particular sources of Ca^{2+}, and the characteristics of Ca^{2+} signals impacted on autophagy. The fundamental need for Ca^{2+} in the activation of autophagy was demonstrated by loading cells with an exogenous Ca^{2+} buffer, which prevented various stimuli from triggering autophagy.

Autophagy could be activated by inhibiting the transfer of Ca^{2+} from the endoplasmic reticulum to the mitochondrial matrix. This was achieved by expressing an enzyme that prevented Ca^{2+} release from inositol 1,4,5-trisphosphate receptors, inhibition of mitochondrial respiration, and knockdown of the mitochondrial Ca^{2+} uniporter. The triggering of autophagy under these conditions was due to reduced cellular ATP levels. These data suggest that Ca^{2+} signals arising from $InsP_3Rs$ suppress autophagy.

Additional studies used a well-characterised Ca^{2+} transport pathway to generate cellular Ca^{2+} signals, and examined their ability to trigger autophagy. This pathway, known as 'store-operated Ca^{2+} entry' (SOCE), was activated by depleting endoplasmic reticulum Ca^{2+} stores using inhibitors of sarco/endoplasmic reticulum ATPases (SERCA). It was found that sustained cellular Ca^{2+} signals arising via chronic inhibition of SERCA were pro-autophagic. The activation of autophagy absolutely required the presence of extracellular Ca^{2+}, and was not due to cellular stress. Using pharmacological inhibition of various Ca^{2+}-sensitive kinases, it was found that at least part of the autophagy that occurred during SOCE was due to activation of Ca^{2+}/calmodulin-dependent kinase kinase-β (CaMKK-β, also known as CaMKK-2).

ACKNOWLEDGMENTS

First, I would like to thank my supervisors Dr Martin Bootman, Dr Katja Rietdorf and Dr Sarah Allman for their support throughout this life-changing experience. Special thanks to Martin for keeping me inspired and pushing me to my full potential. Thanks to Katja for her attention to detail and helping me develop resilience and critical thinking. I am also grateful to Sarah Allman for her general support throughout the PhD and making me think about things from a different perspective.

I would like to thank our collaborators, Geert Bultynck and Jan Parys for financing part of the PhD and for the opportunity to work in their well-known laboratory in Belgium.

I am forever grateful to Said and Gaurav, my Calcium family, who have shared the ups and downs of the PhD with me. Thanks to Said for bringing tranquillity to the group, and Gaurav for bringing colour in general. I will always remember the random calcium conversations we had (at the most random times-11pm) whilst imaging in the lab. I will not forget to print those beautiful cell images, which are interestingly more beautiful from failed experiments! If they cannot go in the thesis, they are going on the living room wall!

My time during the PhD would not have been the same without my wonderful friends Ketty, Sarah, Sophie, David, Soren, Piotr and last but not least Shereen, the most wonderful office mate. Thanks are also due to Eduardo, for the positive vibes (and maybe singing) and to Julia Barkans, who has always given great advice throughout the years. I would also like to thanks all the lab support staff, academics and administrators who have helped me along the way.

My PhD was also made easier by taking up running, salsa and hula hooping, although these hobbies changed to less sporty ones (gardening) in my writing up phase.

To my sisters Mira and Dana, who have supported me and Youssef and kept me strong through this time. To my aunty Samia for just being the most wonderful and supportive aunt and to all my family in the UK, the Lebanon and Nigeria for supporting me through all stages of my PhD

This thesis is especially dedicated to my mum and dad, my role models. This thesis would definitely not have been possible without the sacrifices they have made for me to reach this stage.

The thesis is also especially dedicated to my son Youssef, who has been so understanding of my PhD commitments from a young age and actually taking an interest in my research along the way. You are my hero.

Finally, I would like to thank my husband for believing in me and getting me through these rollercoaster years.

"There is a paradox in the growth of scientific knowledge. As information accumulates in ever more intimidating quantities, disconnected facts and impenetrable mysteries give way to rational explanations, and simplicity emerges from chaos" ***B. Alberts et al.***

CONFERENCE ITEMS AND PUBLICATIONS

Inhibition of $InsP_3$ receptor signalling induces autophagy (2014)
Chehab, Tala; Rietdorf, Katja; Parys, Jan; Bultynck, Geert and Bootman, Martin
In: 13th International Meeting of the European Calcium Society (13-17 September 2014, Aix-en-Provence, France)

Novel improved Ca^{2+} indicator dyes on the market-a comparative study of novel Ca^{2+} indicators with fluo-4 (2014)
Rietdorf, Katja; Chehab, Tala; Allman, Sarah and Bootman, Martin D.
In: Calcium Signalling: The Next Generation (9-10 October 2014, London, UK)

Inhibition of $InsP_3$ receptor signalling induces autophagy (2014)
Chehab, Tala; Rietdorf, Katja; Parys, Jan B.; Bultynck, Geert and Bootman, Martin D.
In: Calcium Signalling: The Next Generation (9-10 October 2014, London, UK)
Intracellular calcium has a dual role in the regulation of autophagy (2015)

Chehab, Tala; Rietdorf, Katja; Parys, Jan B.; Bultynck, Geert and Bootman, Martin.
In: *6th ECS Workshop: Calcium and Cell Fate* (21-24 June 2015, Seillac, France)

Inhibition of calcium release from InsP3Rs triggers autophagy (2015).
Chehab, Tala; Rietdorf, Katja; Parys, Jan; Bultynck, Geert and Bootman, Martin.
In: Cellular Signalling Abstracts, article no. PC241.

Intracellular calcium: a dual role in autophagy (2016).
Chehab, Tala; Rietdorf, Katja; Parys, Jan B.; Bultynck, Geert and Bootman, Martin In: *Evolution brings Ca2+ and ATP together to control life and death* (16 - 17th March 2016, Chichley Hall, Newport Pagnell).

Intracellular calcium: a dual role in autophagy (2016).
Chehab, Tala; Rietdorf, Katja; Parys, Jan B.; Bultynck, Geert and Bootman, Martin D.
In: *Ubiquitin and Autophagy (Quality control in life processes)* (04-07 July 2016, Frankfurt, Germany).

The sources and characteristics of calcium signals determine whether autophagy is up- or downregulated (2016).
Chehab, Tala; Rietdorf, Katja; Parys, Jan B.; Bultynck, Geert and Bootman, Martin D.
In: *14th International Meeting of the European Calcium Society* (25-29 September 2016, Valladolid, Spain).

The regulation of autophagy by calcium signals: Do we have a consensus? Bootman, Martin D.; Chehab, Tala; Bultynck, Geert; Parys, Jan B. and Rietdorf, Katja (2017). *Cell Calcium*.

Table of Contents

LIST OF FIGURES

LIST OF TABLES

ABBREVIATIONS

AA: Arachidonic acid

AMPK: AMP-activated protein kinases

2-DG: 2-Deoxy-D-glucose

2-APB: 2-Aminoethyl diphenylborinate

Atg: Autophagy related gene

ATP: Adenosine triphosphate

BAPTA-AM: 1,2-bis-(o-aminophenoxy)-ethane-N,N,N′,N′- tetraacetoxymethyl ester

Bax: Bcl-2-associated death promoter

Bcl-2: B-cell lymphoma 2

Bcl-xL: B-cell lymphoma-extra large

Bid: BH3 interacting domain death agonist

Ca^{2+}: Calcium

cADPR: cyclic ADP ribose

CaM: Calmodulin

CaMKK-β: Ca^{2+}/calmodulin-dependent kinase kinase-β

CICR: Ca2+-induced Ca2+ release

CPA: Cyclopiazonic acid

CQ: Chloroquine

CRAC: Ca^{2+} release-activated Ca^{2+}

CytC: Cytochrome C

DAG: Diacylglycerol

DAPK: Death associated protein kinases

DMSO: Dimethyl sulphoxide

DNA: Deoxyribonucleic acid

EGTA: Ethylene glycol-bis(2-aminoethylether)-N,N,N′,N′-tetraacetic acid

ER: Endoplasmic reticulum

ERAD: Endoplasmic reticulum associated degradation

ETC: Electron transport chain

Fura-2: Fura-2-acetoxymethyl ester

GFP: Green fluorescence protein

GPCR: G protein-coupled receptors

HCQ: Hydroxychloroquine

HEK: Human Embryonic Kidney

HeLa: Henrietta Lacks

IMM: Inner mitochondrial membrane

$InsP_3$: Inositol 1,4,5-trisphosphate

$InsP_3R$: Inositol 1,4,5-trisphosphate receptors

LC3: Microtubule-associated protein1 light chain 3

MAM: Mitochondria-associated (ER) membranes

MCU: Mitochondrial Ca^{2+} uniporter

MEF: Mouse embryonic fibroblast

MP: Methyl pyruvate

MPT: Mitochondrial permeability transition

MPTP: Mitochondrial permeability transition pore

mTOR: Mechanistic target of rapamycin

mTORC1: Mechanistic target of rapamycin complex I

NAADP: Nicotinic acid adenine dinucleotide phosphate

NCX: Na^+/ Ca^{2+}exchanger

NEAA: Non-essential amino acids

NMDAR: *N*-methyl-D-aspartate receptor

OMM: Outer mitochondrial membrane

PCD: Programmed cell death

PE: Phosphatidylethanolamine

PERK: (PKR)-like ER kinase

PI3K: Phosphoinositide3-kinase

PKC: Protein kinase C

PLC: Phospholipase C

PMCA: Plasma membrane Ca^{2+}-ATPase

PTP: Permeability transition pore

Rhod-2: Rhodamine based Ca2+ indicator

ROS: Reactive oxygen species

RyR: Ryanodine receptor

SERCA: Sarcoplasmic reticulum/ER Ca^{2+} ATPase

SMOC: Second messenger-operated Ca^{2+}

SOC: Store operated channels

SOCE: Store operated Ca^{2+} entry

STIM1: Stromal interaction protein 1

STIM2: Stromal interaction protein 2

Tg: Thapsigargin

TPC: Two-pore channel

TRPC: Transient receptor potential cation channels

ULK1: Unc-51-like Kinase 1

UPR: Unfolded protein response

UPS: Ubiquitin-proteasome system

VDAC: Voltage-dependent anion channel

VOC: Voltage-gated operated channels

Chapter 1. Introduction

Intracellular ionised calcium (Ca^{2+}) is critical throughout the life and death of a cell [1, 2]. Whether in plants or animals, Ca^{2+} has an important role for growth, development and survival. In plants, Ca^{2+} has a structural role in the cell wall and membranes [3]. In animals, Ca^{2+} has a range of roles as an intracellular messenger controlling diverse processes such as fertilisation, muscle contraction, and cell fate [1, 4]. Additionally to its role as an intracellular messenger, Ca^{2+} can also act as an extracellular 'first messenger' through the Ca^{2+}-sensing receptor (CaSR), a family of G-protein-coupled receptors [5].

This project, entitled 'The Role of Ca^{2+} Signalling in Autophagy', aims to understand the regulation of autophagy (a cell survival process) by cytosolic and mitochondrial Ca^{2+} signals. Specifically, the project sought to develop an understanding of the spatial and temporal characteristics of Ca^{2+} signals that affect autophagy in mammalian cells, and to characterise the relevant sources of Ca^{2+} that lead to the generation of these Ca^{2+} signals.

In 1993, Gordon *et al*. were the first to show a link between autophagy and intracellular Ca^{2+} [6]. Their study demonstrated that both a decrease as well as an increase in cytosolic Ca^{2+} levels was effective in inhibiting autophagy in rat hepatocytes. The study by Gordon *et al*., was the first to hint at a complex role for Ca^{2+} in autophagy regulation. Subsequently, many studies have reported Ca^{2+} to have an inhibitory role in autophagy, while many others have suggested that Ca^{2+} activates autophagy [7]**.** Despite these contrasting views, there is clear evidence that Ca^{2+} plays a role in the regulation of autophagy. It is possible that autophagy regulation occurs by a variety of mechanisms [8]. Understanding the spatial and temporal characteristics of Ca^{2+} signals involved in the induction and inhibition of autophagy is key to resolving some of the apparently contradictory conclusions presented in the published literature. Studying the role of Ca^{2+} channels and sources involved in

autophagy further will hopefully contribute to the understanding of autophagy regulation during disease.

Defects in autophagy are linked to a variety of pathological conditions such as cancer and Alzheimer's disease (AD) [9, 10]. The role of Ca^{2+}, and Ca^{2+}-permeable channels, is quite well understood in cancer, however the regulation of autophagy in this context is a subject of intense current research [8]. Many clinical trials (over twenty) have assessed the efficacy of the autophagy inhibitors chloroquine and hydroxychloroquine (HCQ) in treating different cancers; either as a monotherapy, or in combination with other anticancer agents [11] [12]. The preliminary results of many of these trials show apparent antitumor activity. For example, HCQ (either alone or in combination therapy with tamoxifen), enhances tumour shrinkage [13]. However, these autophagy inhibitors are not specific and can give rise to unexpected side effects in patients. Therefore, more specific and potent autophagy inhibitors are could prove useful in a therapeutic context. Understanding whether, and in which situations, Ca^{2+} signalling stimulates or inhibits autophagy may provide a novel approach to treat cancer, and other diseases [8]. Ultimately, it may be plausible that particular Ca^{2+} channels or Ca^{2+} stores can be new targets for autophagy regulation in disease.

1.1 **Ca^{2+} is a universal and versatile messenger within cells**

The ability of Ca^{2+} to regulate a diverse range of cellular functions is partially due to the fact that cells can modulate Ca^{2+} changes in the context of space, time and amplitude. This is known as spatio-temporal patterning [14]. Fluxes of Ca^{2+} perpetually occur between the cytoplasm and intracellular Ca^{2+} stores such as the endoplasmic reticulum (ER), mitochondria, the nucleus, the Golgi and endosomal organelles such as lysosomes [15]. Communication between organelles can be bidirectional, for example Ca^{2+} can be

transferred from the ER to lysosomes and *vice versa*, or between the ER and mitochondria and *vice versa* [16-18]. This coordinated signalling allows the cell to respond to both internal stimuli (e.g., messengers such as $InsP_3$ and cADPR) and external stimuli (e.g., membrane depolarisation and extracellular agonists) [19].

At rest, cells have an average cytosolic Ca^{2+} concentration of around 100 nM [20]. Following exposure to various physiological stimuli, the cytosolic Ca^{2+} concentration can rise to as high as 1 µM. In the immediate vicinity of open Ca^{2+} channels, the local Ca^{2+} concentration may reach tens or hundreds of micromolar. The process of triggering a cytosolic Ca^{2+} signal, effecting a change in cell behaviour and subsequent recovery to the basal state, can be divided into four stages: 1) exposure to trigger stimuli and signal generation 2) activation of ON mechanisms 3) activation of Ca^{2+}-sensitive processes, and 4) action of OFF mechanisms that remove Ca^{2+} from the cytosol [14].

Trigger stimuli take many forms, including hormonal agonists, neurotransmitters and, growth factors as well as physical stimuli such as mechanical deformation of cell membranes, heat, osmotic changes and variations in pH [1, 21] . Induction of cytosolic Ca^{2+} signals can occur through a variety of mechanisms. Such mechanisms include the production of intracellular messengers and the direct activation of cation channels [14]. The release of Ca^{2+} from intracellular stores and Ca^{2+} entry from the extracellular space are common ways in which cells generate Ca^{2+} signals. The main Ca^{2+} store in non-excitable cells is the ER, and when depleted the ER is replenished by Ca^{2+} entry [22]. The release of Ca^{2+} from intracellular stores occurs as a result of the generation of Ca^{2+}-mobilizing messengers. Although a number of such messengers have been proposed, the four most prominent and clearly established are: inositol 1,4,5-trisphosphate ($InsP_3$), cyclic ADP ribose (cADPR), nicotinic acid adenine dinucleotide phosphate (NAADP), and Ca^{2+} itself [19]. $InsP_3$ can be

hydrolysed to inositol 1,4-bisphosphate ($InsP_2$) by a 5'-phosphatase enzyme, thereby preventing further Ca^{2+} release. Alternatively, $InsP_3$ can be phosphorylated by a 3-kinase enzyme producing inositol 1,3,4,5-tetrakisphosphate ($InsP_4$), which has been suggested to modulate ion channel activity [23] [24]. cADPR releases Ca^{2+} via the activation of ryanodine receptors (RyRs), although some alternative effects of cADPR on Ca^{2+} ATPases have been proposed [25]. Moreover, detectable levels of cADPR seem to exist in cells that do not express RyRs. These data may indicate that cADPR is a relatively constant endogenous regulator of Ca^{2+}-signalling or that it has cellular functions other than Ca^{2+} release [26]. The breakdown product of cADPR is ADP ribose (ADPR), which does not appear to mobilize Ca^{2+} however has been suggested to modulate events that occur during fertilisation [27] [28].

ON mechanisms are those vital for generating Ca^{2+} signals and depend on channels located in the membrane of the internal stores or in the plasma membrane. ON mechanisms result in Ca^{2+} flow into the cytoplasm, increasing its concentration and establishing a Ca^{2+} signal. Although Ca^{2+} signals are derived from messengers mentioned above, a major route of Ca^{2+} entry acting as an ON mechanism is via store-operated calcium entry (SOCE) (discussed in more detail in *Chapter 5*. Ca^{2} itself regulates $InsP_3$ receptor ($InsP_3R$) activity in a biphasic manner; low concentrations of Ca^{2+} (100–300 nM) are stimulatory but higher concentrations (> 300 nM) are inhibitory and switch the channel to an off-state [29]. Additionally, voltage-operated channels (VOCs) and receptor-operated channels (ROCs) are channels that open upon exposure to external stimuli and are discussed in detail in *section 1.2.3 and 1.2.4*. Most of the Ca^{2+} that enters the cytoplasm binds quickly to many cytosolic buffers such as parvalbumin, calbindin-D28K and calretinin, as well as proteins such as calmodulin that are involved in transducing the effects of Ca^{2+} [14].

Following the generation of a Ca^{2+} signal, a range of processes take place to translate this Ca^{2+} signal into a cellular response. Ca^{2+}-binding proteins respond to an increase in Ca^{2+} by undergoing conformational changes which further enable them to activate downstream effectors [30]. Classical sensors include calmodulin (CaM) and troponin C (TnC), which bind Ca^{2+} through EF hands. CaM is involved in the regulation of various processes including smooth muscle contraction, metabolism and gene transcription [31] whereas TnC is responsible for muscle contraction [20].

OFF mechanisms are mechanisms that remove Ca^{2+} from the cytosol to restore the resting state. Once Ca^{2+} has carried out its signalling functions, it is removed from the cytosol by pumps and exchangers. The plasma membrane Ca^{2+} ATPases (PMCA) [32] and Na^{+}/Ca^{2+} exchangers (NCX) [33] remove Ca^{2+} to the extracellular space, whereas sarcoendoplasmic reticulum ATPases (SERCA) transports Ca^{2+} into the ER [34]. The NCX and PMCA have different kinetics; the NCX has a high transport rate but low Ca^{2+} affinity however the PMCA has opposite characteristics. The NCX also functions in a reverse manner, allowing Ca^{2+} entry from the extracellular space. The NCX only functions when there is an electrochemical Na^{+} gradient, and exchanges one for Ca^{2+} every three Na^{+}. Both Ca^{2+} entry and exit is accelerated by phosphorylation of the enzyme [33]. Four PMCA isoforms have been identified. PMCA1 and PMCA4 are expressed in most tissues, whereas PMCA2 and 3 are found in a smaller number of tissues, such as the brain and striated muscle [35]. The distribution of different PMCA isoforms is thought to be inherently linked to the rate of Ca^{2+} clearance, for example fast pumps can be found in cells that generate fast Ca^{2+} transients [36].

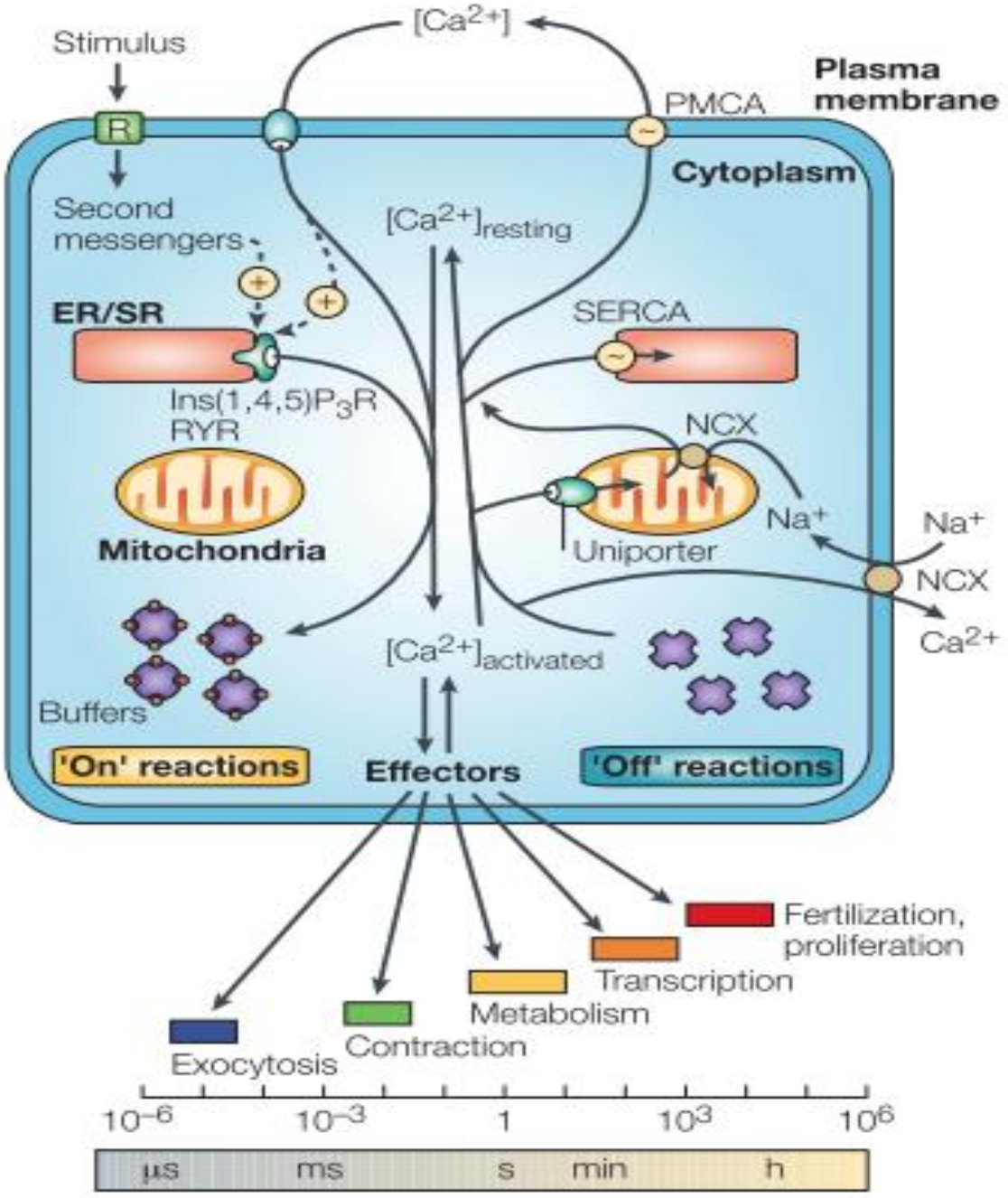

Figure 1.1 Reproduced with permission from Nature Publishing Group: Berridge, MJ,Bootman, MD, Roderick, L. (2003) Calcium signalling: dynamics, homeostasis and remodelling. Ca^{2+}-signalling within the cell. In the 'ON' reactions, stimuli induce the entry of external Ca^{2+} as well as the formation of second messengers. Second messengers release internal Ca^{2+} stored in the ER/SR. Most of this Ca^{2+} (shown as red circles) is bound to buffers and only a small proportion binds to the effectors that trigger a variety of cellular processes. In the 'OFF' reactions, Ca^{2+} leaves the effectors and buffers and is removed from the cell to the outside by various pumps such as the Na^{+}/ Ca^{2+} exchanger (NCX) and the plasma-membrane Ca^{2+}-ATPase (PMCA). The sarco/endoplasmic reticulum Ca^{2+}-ATPase (SERCA), however, pumps Ca^{2+} back into the ER. From: (Berridge *et al.*, 2003).

1.2 Mechanisms and channels of Ca^{2+} entry and exit

Ca^{2+} influx into the cell and its exit occur via channels located on the plasma membrane and organelles such as the ER, mitochondria, lysosomes and the Golgi. The major channels involved in Ca^{2+} signalling are described in this section.

1.2.1 Store-operated Ca^{2+} entry (SOCE)

SOCE is a major Ca^{2+} entry pathway, which is activated in response to depletion of the ER [37]. This mechanism of Ca^{2+} entry, through which intracellular Ca^{2+} stores are replenished, occurs in almost all cell types (with the possible exception of some electrically-excitable cells) [38]. SOCE is vital for short and long term physiological processes such as muscle contraction and cell cycle control [39] and the maintenance of Ca^{2+} signals such as the hormone-induced repetitive Ca^{2+} oscillations detected in non-excitable cells [40, 41].

Following depletion of ER Ca^{2+} stores, stromal interaction protein 1 (STIM1), (a Ca^{2+} sensor on the ER membrane) accumulates at the ER-plasma membrane junctions. STIM1 forms oligomers with, and activates, Orai Ca^{2+} channels on the plasma membrane [42] resulting in influx of Ca^{2+}. Orai channels are well characterised Ca^{2+} release-activated Ca^{2+} (CRAC) channels in non-excitable cells [43-47]. STIM2 is another activator of Orai channels. It is a weaker and slower activator than STIM1, but has been suggested to be mainly responsible for maintaining intracellular Ca^{2+} store levels rather than SOCE activation, given that its EF-hand has a lower affinity for Ca^{2+} [48]. Store-operated currents, I_{crac}, involve the STIM1 activation of Orai channels. Mitochondria also have a vital role in the regulation of I_{CRAC} and control a range of CRAC channel-driven responses including enzyme activation, intercellular communication through paracrine signals and gene expression [49]. Therefore a dynamic interplay exists between the ER, mitochondria and the plasma membrane.

Many studies on SOCE have used Ca^{2+} influx inhibitors such as 2-APB, SKF96365, or gadolinium [50]. Often these inhibitors lack specificity and exert effects on other cellular targets [51] [52]. The canonical transient receptor potential cation channels (TRPC) also have a role in SOCE in many cell types. TRPCs have been shown to cooperate in the development of beating in developing hearts [53]. Upregulation of TRPC expression correlates with increased SOCE and pro-arrythmic spontaneous Ca^{2+} waves [54]. Experiments have shown that cation influx via TRPCs takes place independently of Ca^{2+} store depletion and STIM1 expression [55]. Studies have also shown that TRPCs may be activated by STIM, and that STIM1, Orai and TRPCs act together to promote Ca^{2+} influx [56]. The action of this triad may result from Ca^{2+} entry through a STIM1-Orai interaction subsequently leading to the insertion of TRPC channels into the plasma membrane prolonging SOCE [57]. The interaction of STIM1, Orai and TRPCs results in a current termed $I_{SOC.}$ Both I_{SOC} and I_{CRAC} currents involve STIM1 and Orai isoforms [58].

1.2.2 Messenger-operated Ca^{2+} entry

Messenger-operated Ca^{2+} entry is sometimes referred to as 'second messenger-operated Ca^{2+} entry or SMOC. SMOC can be activated by cellular molecules such as arachidonic acid (AA). Studies by Shuttleworth and colleagues have demonstrated that AA activates a Ca^{2+} entry pathway that involves STIM1 and Orai channels in a different configuration to that required for SOCE. The current derived from AA-dependent activation of Orai channels is denoted I_{ARC}, and has been shown to be necessary for repetitive Ca^{2+} oscillations [59]. $InsP_3Rs$, which are the central route of Ca^{2+} release from intracellular stores, are transmembrane proteins mostly located on the ER membrane [60] and are also found on the plasma membrane [61]. The receptors exhibit greater conductance than CRAC channels, which have a distinctive feature of a small unitary conductance [62].

1.2.3 Receptor-operated Ca^{2+} entry

Receptor operated Ca^{2+} (ROC) entry involves channels which are non-voltage gated [63]. ROC is activated upon binding of an agonist to the extracellular domain of a Ca^{2+} channel, such as the *N*-methyl-D-aspartate receptor (NMDAR) [64]. Receptor activation can lead to Ca^{2+} entry into smooth muscle cells by mechanisms independent of membrane depolarization. ROC channels show varying degrees of Ca^{2+} selectivity [63].

1.2.4 Voltage-Operated Ca^{2+} channels

Electrophysiological studies have indicated the existence of three types of Voltage-Operated Ca^{2+} channels (VOC) - K^+, Na^+ and Ca^{2+} channels [65]. The function of VOC channels is closely connected with the activity of enzymes and phosphorylation of membrane proteins. Many types of VOC have been described in both the nervous system and peripheral tissues. Based on their pharmacological and biophysical properties, VOC have been classified into high voltage activated (HVA) and low voltage activated (LVA) channels. HVA channels require a relatively large depolarization to induce channel opening and typically open at voltages > –30 mV. LVA channels inactivate within ~100 ms in response to a step voltage change. LVA are fast-inactivating, slow deactivating channels that are initially activated at low holding potentials [66].

1.2.5 Plasma membrane Ca^{2+} ATPase

Located on the plasma membrane, plasma membrane Ca^{2+} ATPase (PMCA) pumps extrude Ca^{2+} into the extracellular space against the electrochemical gradient. The PMCA is an important regulator of the Ca^{2+} concentration in the extracellular space [67]. Four genes encode the PMCA, PMCA 1-4 of which exist more than twenty splice variants [68]. PMCA constitute a minor component of the total protein of the plasma membrane (less than 0.1%) [69].

1.2.6 Sarco/endoplasmic reticulum Ca^{2+} ATPase

SERCA, a P-type ATPase, is responsible for re-establishing the low cytosolic Ca^{2+} concentrations, which are required for normal cell function [70]. There are three different SERCA isoforms, all of which located on the endoplasmic/sarcoplasmic membrane. Three genes encode SERCA; SERCA 1-3 all of which have splice variants [71]. SERCA pumps are responsible for removing Ca^{2+} from the cytosol and consequently replenishing Ca^{2+} levels in the ER [34, 72]. The function of the SERCA pump is modulated by endogenous phospholamban (PLB) and sarcolipin (SLN), which are expressed in cardiac and skeletal muscles [73]. Sequestration of Ca^{2+} occurs coupled with adenosine triphosphate (ATP) hydrolysis [74] and similar to PMCA, SERCA pumps have a low transport rate but high Ca^{2+} affinity [75], which enables them to respond to modest Ca^{2+} elevations. SERCA pumps translocate two Ca^{2+} ions and hydrolyse one ATP for each catalytic turnover [75]. [76].

1.2.7 Na^{+}/Ca^{2+} exchanger

The Na^{+}/Ca^{2+} exchanger (NCX) is found predominantly on the plasma membrane and mitochondria. It can also be found on the inner membrane of the nuclear envelope. The NCX extrudes Ca^{2+} to the extracellular space using the electrochemical gradient of Na^{+}. During each cycle, three Na^{+} ions enter the cell and one Ca^{2+} ion is extruded against its concentration gradient [77, 78]. In mitochondria, the NCX pumps Ca^{2+} from the mitochondrial matrix into the cytosol. The NCX has a low affinity for Ca^{2+}, but a high capacity for Ca^{2+} transport [79]. It is particularly abundant in excitable tissues such as the brain and the heart. The NCX is can also be regulated by pH, ATP, protein kinases such as PKA and Protein Kinase C (PKC) [32]. When mitochondria are in close proximity to the ER, Ca^{2+} release from NCX takes place quickly, otherwise the release takes place in a slower fashion [60]. A fast interchange of Ca^{2+} can also take place during apoptosis, when Ca^{2+} release from

the mitochondria is taken up by the ER quickly in order to potentiate apoptotic signals in a positive feedback manner.

1.2.8 Secretory Pathway Ca^{2+}-ATPases

Secretory Pathway Ca^{2+}-ATPases (SPCA) are localised to the Golgi body and transport Ca^{2+} ions from the cytosol to the lumen of the Golgi following a Ca^{2+} signal. This serves to reduce the cytoplasmic Ca^{2+} concentration to resting levels [80] [81]. Additionally, SPCAs also transport Mn^{2+} ions into the Golgi from the cytosol with high affinity, and thus have a role in the prevention of manganese toxicity [80]. Two isoforms exist, SPCA 1 and 2, of which SPCA1 has splice variants. Similar to SERCA and PMCA, SPCAs are members of the P-type family of ion pumps that require ATP for their function [75].

1.3 ER-Mitochondrial and lysosomal Ca^{2+} signalling

The ER, mitochondria and lysosomes are major organelles involved in shaping Ca^{2+} signals that can trigger a range of cellular responses. Each organelle possesses Ca^{2+} channels responsible for uptake and/or release of Ca^{2+} and is recognised as a Ca^{2+} store.

1.3.1 ER-Mitochondrial Ca^{2+} regulation

The key determinants in mitochondrial Ca^{2+} uptake are the distance between the ER and mitochondria, the cytosolic Ca^{2+} concentration and the spatial and temporal properties of cytosolic Ca^{2+} signals [60]. As well as Ca^{2+} uptake from the ER, mitochondria can also take up Ca^{2+} from the extracellular space through the plasma membrane [82, 83].In the context of cell fate, one particularly important aspect of Ca^{2+} signalling is the flux of Ca^{2+} between the ER and mitochondria [60]. Within the cell, mitochondria are found in close proximity to the ER and there are contact sites between the two types of organelles [84, 85], termed mitochondria-associated (ER) membranes (MAMs) [86] [87]. The typical distances between

mitochondria and the smooth ER in a MAM is ~10-15 nm. Up to 20% of mitochondrial surfaces are in close contact with the ER [88]. ER stress causes an increase of the number of contact sites and the total length of MAMs [89, 90]. MAMs are important for a number of physiological processes; e.g. lipid synthesis, Ca^{2+} uptake into mitochondria, mitochondrial movement and fission, apoptosis, and autophagy [91-93]. Alteration of MAMs have been linked with a number of disease conditions, including cancer [94, 95] and neurodegenerative diseases such as Parkinson's and amyotrophic lateral sclerosis [91, 92, 96-99]. These points of contact means that Ca^{2+} signals arising from $InsP_3Rs$ and RyRs on the surface of the ER originate close to the sites of Ca^{2+} uptake into the mitochondria. They involve the 35kDa channel protein voltage-dependent anion channel (VDAC) in the OMM and the mitochondrial uniporter complex (MCU) in the IMM [89, 100].

Mitochondria consist of two membranes, the outer mitochondrial membrane (OMM) and, the inner mitochondrial membrane (IMM) separated by an intermembrane space [89, 101]. The IMM has many folds in the matrix (cristae) which are the sites of ATP production [102].

Mitochondria are capable of translating many extracellular stimuli into different intracellular actions, such as cell death and ATP production. They sequester Ca^{2+} rapidly during development of a Ca^{2+} signal and release it back slowly during the recovery phase [14]. These abilities mean that mitochondria are crucial to Ca^{2+} signalling within the cell; they have high Ca^{2+} buffering and storage capabilities and the ability to both remove and replenish cytosolic Ca^{2+} [103]. Although this function is highly important to Ca^{2+} signalling, the prime role of mitochondria is ATP production, which takes place through the tricarboxylic acid (TCA) cycle. The uptake of Ca^{2+} to the mitochondrial matrix is important for the activation of three dehydrogenases involved in the TCA cycle; pyruvate dehydrogenase, isocitrate dehydrogenase and 2-oxoglutarate dehydrogenase [104]. The

disturbance of mitochondrial Ca^{2+} homeostasis can contribute to a variety of pathological conditions.

Factors such as Bcl-2 and NADH regulate VDAC [105]. The precise mechanisms of VDAC conductance are still under debate but studies have shown that VDAC are fully opened with high-conductance and weak anion-selectivity at low transmembrane potentials (< 20–30 mV). However this switches to cation selectivity and lower conductance at higher potentials [106]. Once across the OMM, Ca^{2+} traffic across the inner mitochondrial membrane (IMM) takes place through an electrogenic transporter, termed the mitochondrial Ca^{2+} uniporter (MCU) that transports Ca^{2+} down the electrical gradient established by the respiratory chain.

Ca^{2+} release from the ER generates global cytosolic Ca^{2+} signals that peak around 0.5 - 1 µM [18], but within the small volume of the MAMs, the local Ca^{2+} signal reaches around 5 – 10 µM [107]. This Ca^{2+} concentration is sufficient to activate the MCU despite its relatively low affinity for Ca^{2+} (K_d 20 - 50 µM) [93]. Ca^{2+} that accumulates within the mitochondrial matrix is consequently released via the mitochondrial NCX and can be taken back up into the ER via SERCA pumps, in order to restore the ER Ca^{2+} levels [108]. Ca^{2+} cycling between the ER and mitochondria may be enhanced by mitochondrial production of reactive oxygen species ROS, which in turn sensitises the ER Ca^{2+} release channels [109].

Mitochondria regulate the generation and characteristics of cytosolic Ca^{2+} signals [110-113]. Chronic cytosolic Ca^{2+} signals (for example those arising as a result of cell stress or damage) can lead to prolonged mitochondrial Ca^{2+} uptake, and consequent activation of the mitochondrial permeability transition pore, swelling and rupture. Consequently, cytochrome C and other pro-apoptotic factors are released [93]. Dysfunctional or

depolarised mitochondria are removed by mitophagy (a selective type of autophagy) to prevent cellular damage [114, 115].

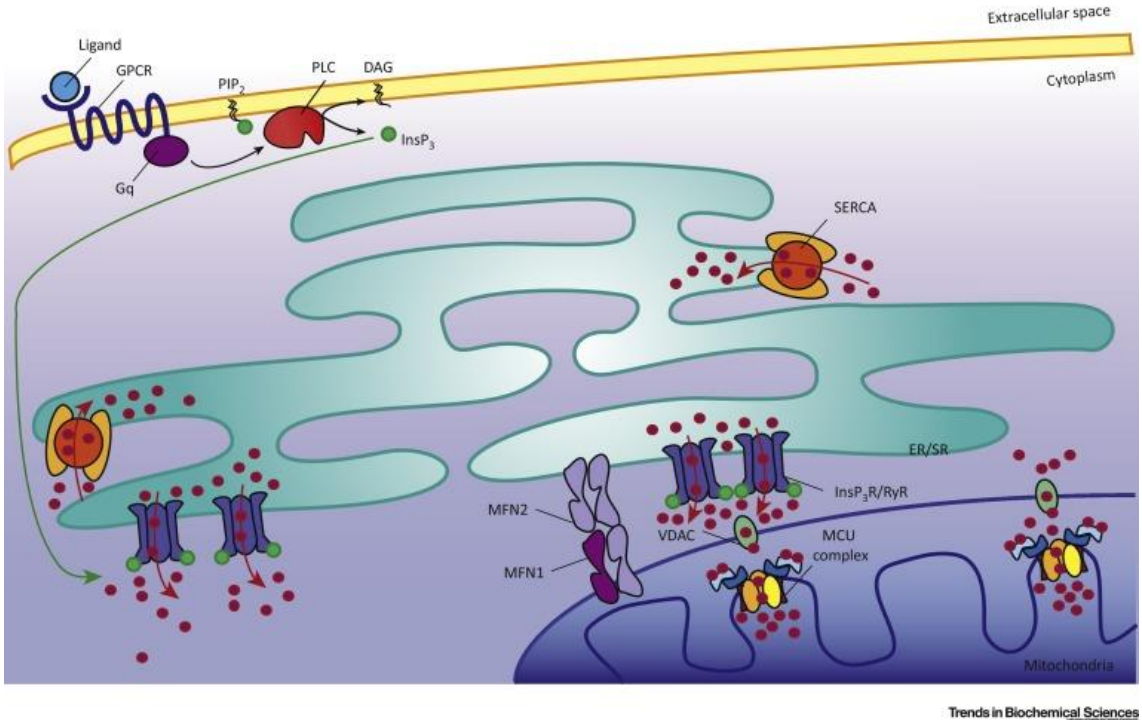

Figure 1.2 reproduced with permission from Elsevier: Raffaello, A, Mammucari, C, Gherardi, G, Rizzuto, R. (2016) Calcium at the Center of Cell Signaling: Interplay between Endoplasmic Reticulum, Mitochondria, and Lysosome. The ER Ca^{2+} Store and mitochondria signalling. Following ligand binding to a G protein-coupled receptor (GPCR), phospholipase C (PLC) is activated and triggers the production of inositol 1,4,5-trisphosphate ($InsP_3$) and diacylglycerol (DAG) from phosphatidylinositol 4,5-bisphosphate (PIP_2). $InsP_3$ binds to $InsP_3$ receptors ($InsP_3Rs$) at the ER surface releasing Ca^{2+} into the cytosol. Since the ER and the mitochondria are close to each other, high [Ca^{2+}] microdomains, allow mitochondria to quickly take up Ca^{2+}. Voltage-dependent anion channels (VDACs) are responsible for the rapid transfer of Ca^{2+} through the outer mitochondrial membrane (OMM) and then accumulation of Ca^{2+} in the mitochondrial matrix occurs via the mitochondrial calcium uniporter (MCU). Many proteins regulate ER–mitochondria contact sites. Red dots are Ca^{2+}.

1.3.2 Lysosomal Ca^{2+} homeostasis

Lysosomes are acidic organelles (pH 4.5-5) that play a central role in degrading and recycling macromolecules delivered by phagocytosis, endocytosis and autophagy. The degradative function of lysosomes relies on lysosomal hydrolases such as cathepsins [116].

Lysosomal distribution has been shown to vary depending on nutrient availability; from a peripheral cellular location in nutrient-rich conditions to perinuclear clustering during nutrient starvation [117]. Aside from their role in degradative pathways, lysosomes are implicated in many cellular processes such as cell death and plasma membrane repair following cell injury.

Lysosomes are also regarded as important intracellular Ca^{2+} stores [118, 119]. Within the endolysosomal system, Ca^{2+} is important for maintaining normal trafficking, recycling, and vesicular fusion events [120]. The Ca^{2+} concentration inside lysosomes can reach up to 600 µM Ca^{2+} [121], a concentration similar to that of the ER and greater than the typical ER luminal Ca^{2+} concentration (~200-500 µM). Since the total volume of lysosomes in the cell is smaller than that of the ER, the amount of Ca^{2+} available for release from this store is lower than that from the ER. Therefore cytosolic Ca^{2+} signals arising from lysosomes are modest in comparison [120].

Ca^{2+} can be released from lysosomes by a potent intracellular Ca^{2+} -releasing second messenger, nicotinic acid adenine dinucleotide phosphate (NAADP). The potential of NAADP to release Ca^{2+} was first demonstrated using sea urchin egg homogenates [122]. NAADP was later established as an intracellular messenger that acts upon stores other than the ER [123]. Ca^{2+} release by NAADP can be amplified by Ca^{2+} -induced Ca^{2+} release (CICR) from neighbouring RYRs and $InsP_3Rs$ [124]. Ca^{2+} released from the ER can also be taken up by the lysosomes, and the Ca^{2+} transfer between lysosomes and the ER is bi-directional [16]. This bi-directional communication is facilitated by the close proximity of the two organelles. Electron microscopy studies have shown that ~80 % of lysosomes in human fibroblasts are located less than 20 nm from the ER [125] , facilitating them functioning as a signalling microdomain.

It has been a matter of long debate which lysosomal Ca^{2+} channel NAADP acts upon. Most evidence shows that NAADP activates Ca^{2+} release via the two-pore channel (TPC) family of proteins [124]. It has been shown that NAADP does not directly bind to TPCs, but to currently unidentified small molecular-weight proteins which then modulates the TPC channel action [126]. However, other lysosomal Ca^{2+} channels have been discussed as target of NAADP. Besides TPCs, the main other lysosomal Ca^{2+} release channels are TRPML1 (transient receptor potential cation channel) and TRPM2 [127-129]. TRPML1, the first Ca^{2+} channel identified on lysosomes, is sensitive to NAADP but studies have not fully confirmed this finding and so its regulation by remains poorly understood [130]. TRPM2s are mostly found in the plasma membrane where they are activated by NAADP [129], but can also be found on the lysosomes where they are activated by cytosolic ADP-ribose [131].

TPCs are localised on endosomes and lysosomes, and do not bind directly to NAADP. Three TPC isoforms exist (TPC1-3) and have been shown to have different functions [132, 133]. TPC1 is important for endosomal trafficking to the Golgi, and TPC2 is important for endosomal trafficking to lysosomes [134]. TPC1 and TPC2 interact with a variety of proteins that are important for cellular Ca^{2+} homeostasis (e.g., Ca^{2+}-binding proteins such as calreticulin and annexins, $InsP_3R$-interacting proteins and STIM), and with trafficking regulators (e.g., Rab GTPases and syntaxins) [135]. Studies have also found that TPCs co-immunoprecipitate with mammalian target of rapamycin (mTOR) [136], with evidence that mTOR binds to TPCs under nutrient-rich conditions consequently inhibiting channel opening. However, when cellular ATP concentrations are low, mTOR is released from TPCs consequently stimulating Ca^{2+} release. mTOR kinase activity is important for this effect but there is dispute about whether mTOR acts upstream of TPCs, as shown in myoblasts [137], or downstream of TPCs, as shown in macrophages [138]. TPCs also interact with leucine-rich repeat kinase 2 (LRRK2), which can stimulate autophagy [136]. TPCs, and NAADP-

induced Ca^{2+} release can increase both autophagy and apoptosis in cells overexpressing LRRK2 [138, 139].

Lysosomes are involved in a secretory pathway known as lysosomal exocytosis, common to all nucleated cell types [140]. Lysosomal exocytosis is important in many processes such as immune responses, cell signalling and plasma membrane repair [141]. Lysosomal exocytosis is a two-step process, where firstly lysosomes relocate from the perinucleus to the close vicinity of the plasma membrane [142]. At the plasma membrane the lysosomes fuse, firstly with each other then with the plasma membrane. This process takes place in response to a rise in intracellular concentration of Ca^{2+} [140]. ATP (found in large amounts in the lysosomes) is released to the extracellular space during lysosomal exocytosis [143] and participates in communication between cells which is mediated by a range of different ATP binding (purinergic) receptors [144].

Transcription factor EB (TFEB), a master gene important for the biogenesis of lysosomes, regulates lysosomal function in order to meet the need of degradation capacity. In nutrient rich conditions, mTOR is associated with the lysosomal membrane and interacts with TFEB to prevent its nuclear translocation. However in nutrient starvation conditions, mTOR-dependent phosphorylation of TFEB is disrupted and TFEB is translocated to the nucleus to drive the transcriptional regulation of genes encoding proteins for autophagosome formation [145].

1.4 Autophagy

Autophagy (derived from the Greek words auto, meaning "self" and phagein, "to eat", “self-eating”), is a catabolic process by which cellular material is degraded. It is important in the maintenance of cellular homeostasis in eukaryotic organisms [146]. It is one of two main routes by which proteins are degraded within the cell, the other being the ubiquitin

proteasome system (UPS). The UPS deals with the rapid removal of short-lived proteins whereas, autophagy deals with long-lived proteins, organelles and non-protein targets (such as lipids, carbohydrate) [147] [148]. The UPS consumes ATP in the degradation process while autophagy generates energy from the degradation of macromolecules [148]. The generation of energy through autophagy is important in the maintenance of cellular homeostasis.

1.4.1 Autophagy in the cell

Autophagy occurs constitutively at basal levels in nutrient-rich, healthy cells, and is stimulated when cells are exposed to stressors. Basal and stimulated autophagy exhibit common characteristics, suggesting the same underlying mechanism [149]. Common cellular stressors include nutrient starvation, mitochondrial depolarization, toxic protein aggregates, infection and mechanical damage [150]. Depending on the nature and duration of the stress and the cell type, cells can display either protective or destructive autophagic responses [151]. The initial response of a cell to a stressful stimulus is often the promotion of pro-survival actions [151]. If these are unsuccessful, destructive pathways such as apoptosis, necrosis and pyroptosis are activated, which eliminate these damaged cells [151]. Autophagy is a key adaptive response to cellular stress, and is largely regarded as a pro-survival process, although it can lead to cellular demise. Autophagy can be divided into three types: macroautophagy, microautophagy and, chaperone-mediated autophagy. Within the literature, ‘autophagy’ usually refers to macroautophagy unless otherwise stated [152]. Macroautophagy, hereafter called autophagy, is the focus of this study.

1.4.2 Mechanism of autophagy

The process of autophagy involves the formation of a double membraned vesicle called an autophagosome, which encapsulates cellular components earmarked for degradation

[153-155] (Figure 1.3). The double membrane vesicle, resembling a ring-like structure, is a hallmark of autophagy and consists of two distinct lipid bilayers (one inner and one outer bilayer), where the source is still debatable [153-155]. This process is modulated by a family of proteins termed 'autophagy-related' proteins (Atgs). To date, over thirty Atg genes have been identified in yeast, the orthologues of which are well conserved throughout eukaryotes [156, 157].

Autophagy induction takes place when signalling pathways trigger the formation of a membrane invagination described as an omegasome, mainly observed on the surface of the ER. However other membranes such as the plasma membrane have been shown to act as sites of initiation [158]. This structure enlarges into a phagophore (either independently of, or associated to, the ER) and targets cellular material in close proximity for digestion. The phagophore elongates and eventually forms the autophagosome [159]. The mature autophagosome then becomes acidified following fusion with a lysosome in a Ca^{2+}-dependent manner, to produce autolysosomes [160]. Unlike autophagosomes, autolysosomes are single-membrane vesicles [161]. The fusion unites the degradative acid hydrolases with the captured cell material. Following breakdown of the cellular material, nutrients such as amino acids and fatty acids are exported back into the cytoplasm by lysosomal permeases [162]. Autophagosomes, (which are neutral in pH) travel towards the smaller lysosomes (0.1 - 1.0 µm, compared to autophagosomes which are 0.5- 1.5 µm) [163]. Since lysosomes are smaller than autophagosomes, autolysosomes produced as a result of fusion undergo functional adjustments in order to maintain the acidic pH for their hydrolytic function to degrade contents [163]. However the exact mechanism of this functional adjustment is unknown. As with other intracellular trafficking events, autophagosomes move through cytoskeleton-dependent action. This movement involves microtubule-associated proteins such as LC3 and actin microfilaments. Interestingly, actin

filaments have been involved in selective types of autophagy in the yeast *S. cerevisiae*, but are not regarded as necessary for non-selective (bulk) autophagy in the same organism [164].

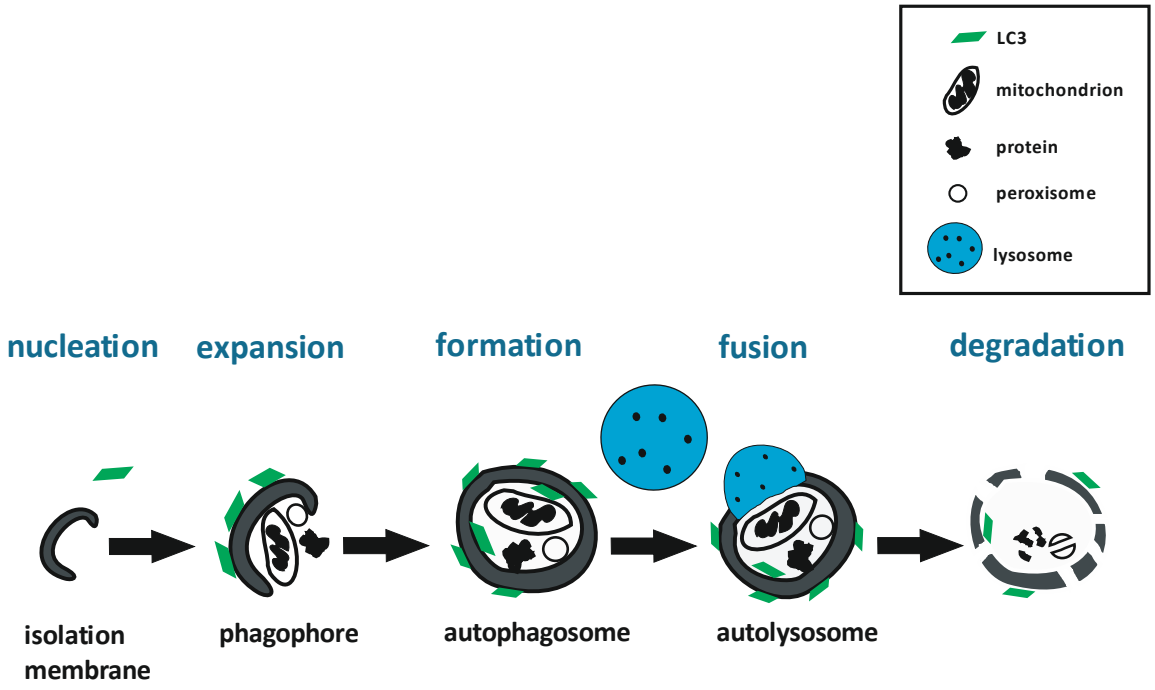

Figure 1.3 The process of autophagy from nucleation to degradation. The process starts with the formation of an isolation membrane, followed by the formation of a double membrane names the autophagosome which targets cellular constituents to be degraded. Following fusion with a lysosome, cell components in the autolysosome are degraded and recycled as nutrients and metabolites back into the cytosol.

1.4.3 Core autophagy machinery

Autophagy is involved in differentiation, development and tissue remodelling in various organisms [165]. It is upregulated in cells undergoing remodelling in the course of differentiation, and was first observed in newborn mice [166]. The morphology of autophagy was first characterized in mammalian cells, however, the molecular components involved in the regulation of autophagy were initially described in yeast [167-169]. The Atg proteins involved in autophagy are frequently classified in six distinct

functional groups, which cooperate to perform important roles in the overall process (Figure 1.4). The functions of these proteins are summarised below [156, 170].

First, UNC-51-like kinase 1 (ULK1, a yeast Atg1 homolog) stimulates autophagy by phosphorylating Beclin-1 and activating VPS34 lipid kinase. ULK1 is a stable cytosolic kinase complex comprised of ULK1, FIP200 (focal adhesion kinase family-interacting protein of 200 kDa), Atg13L and Atg101.

Second, a pathway upstream of mTORC1 involves Vps34 (see section 1.4.4), or PI3-kinase (phosphoinositide 3-kinase, class III), which is a lipid kinase that is conserved throughout eukaryotes. The Vps34 kinase complex is comprised of Vps34, Vps15, Beclin-1 (see sections 1.6.3 and 1.7), and Atg14 or UVRAG. These proteins bind Beclin-1 exclusively. Since Beclin-1 has a vital role in the induction of autophagy, it is often used as a marker of autophagy whereby its expression levels increase upon induction of autophagy [171, 172].

Third, Phosphatidylinositol 3-phosphate (PtdIns3P or PI3P) binding proteins are important in membrane dynamics and the regulation of trafficking. The majority of PI3P are connected with endosomal membranes and with the autophagosome preassembly machinery, most probably at the endoplasmic reticulum [173].

Fourth is the Atg5-Atg12 ubiquitin-like conjugation system, including the E3-ligase-like complex comprised of Atg5-Atg12- Atg16L. The Atg5-Atg12 complex is involved with the expansion of autophagosomal membranes.

Fifth is the microtubule-associated protein 1-light chain 3 (LC3) phosphatidylethanolamine (PE) conjugation system, where PE is conjugated to LC3 by the Atg5-Atg12- Atg16L complex. LC3 has been used as an autophagosome marker in autophagy studies, where cytosolic LC3-I is transformed to a membrane-bound form, LC3-II [174] (see section 1.5).

Sixth, Atg9a is a multi-spanning transmembrane protein and the only transmembrane protein among the Atg proteins that is essential for autophagosome formation [175].

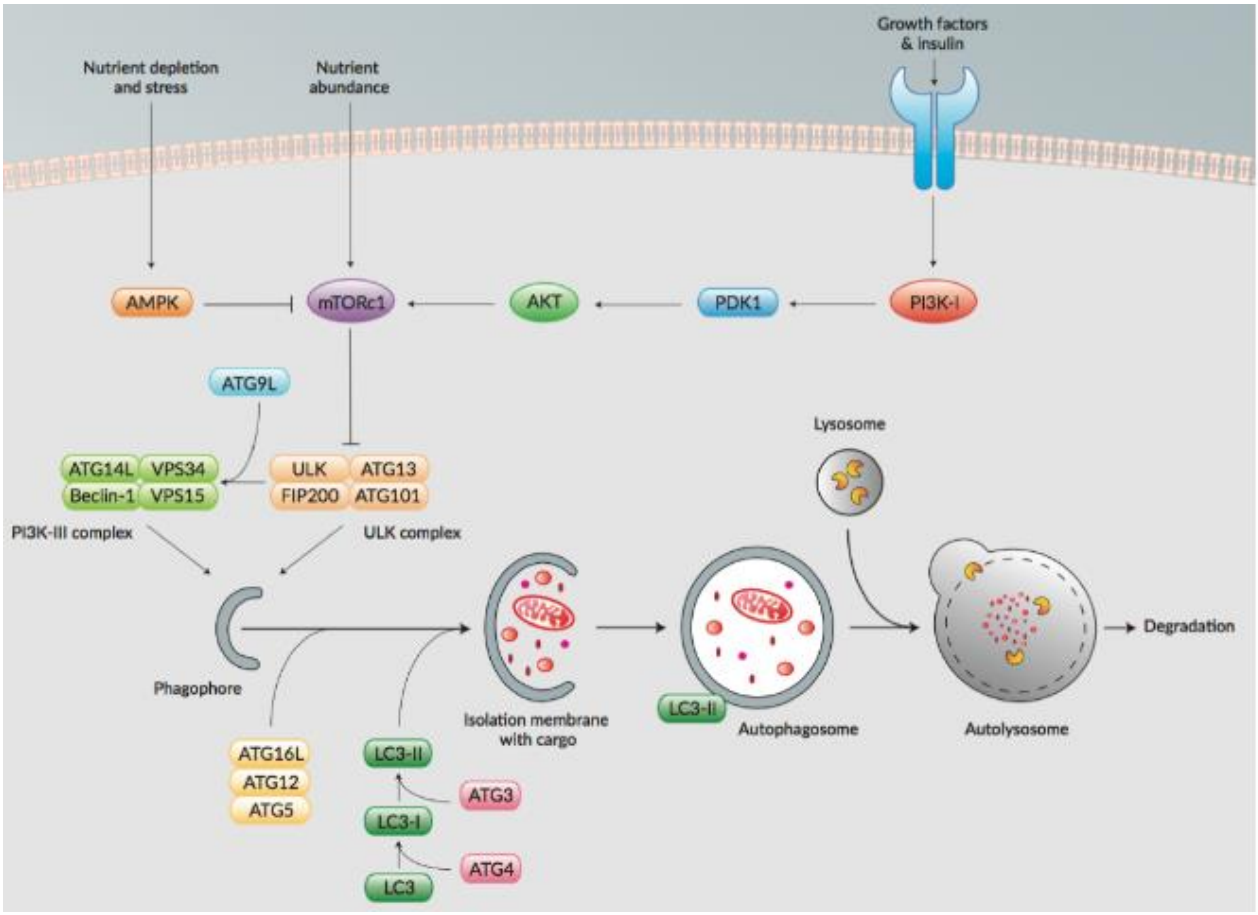

Figure 1.4 reproduced with permission from InvivoGen (www.invivogen.com): Core autophagy proteins involved in the different stages of the autophagy process. The ULK1, Atg13 & FIP200 complex forms to initiate phagophore formation. The Atg5-Atg12 complex is important in the elongation of the phagophore membrane.

1.4.4 Control of autophagy by mTOR

A major regulator for starvation-induced autophagy (in mammalian systems) is the mTOR pathway. mTOR is a highly conserved serine/threonine kinase with a large molecular size (c. 300 kDa). It belongs to the phosphatidylinositol kinase-related kinase (PIKK) family [176] and is capable of responding to signals from many stimuli (including amino acids, oxygen, growth factors and stress) to coordinate cell growth and maintain metabolic homeostasis [177]. As mTOR has been linked to many cellular events it has been linked to a variety of pathological states, including cancer and neurodegenerative diseases [178, 179].

mTOR binds many proteins forming two distinctive protein signalling complexes, mTORC1 (mTOR complex 1) and mTORC2 (mTOR complex 2). mTORC1 contains raptor (KOG1 ortholog), GβL/mLst8, PRAS40 and DEPTOR, and mTORC2 (mTOR complex 2) contains rictor (Avo3 ortholog), GβL/mLst8, Sin1 (Avo1 ortholog), PRR5/protor and DEPTOR [150]. The activation of mTOR occurs downstream of Akt/PKB (a pathway commonly dysregulated in human cancers including breast cancer) [180]. Biochemical approaches in mammals led to the discovery of mTOR as the physical target of rapamycin, which forms a gain-of-function complex with the intracellular FK506-binding protein (FKBP12). The complex directly interacts with, and inhibits mTORC1, but not mTORC2 [181].

mTORC2 is involved in the regulation of phosphorylation and activation of Akt/PKB, PKC, serum- and glucocorticoid induced protein kinase 1. The inhibition of mTORC2 triggered autophagy and atrophy in skeletal muscle cells under fasting conditions [176].However, the autophagy induction by mTORC2 inhibition is mediated mainly by FoxO3, a transcription factor downstream of Akt that is involved in autophagy gene expression.

The mTORC1 complex is sensitive to both growth factors and nutrients, and the presence of amino acids has been shown to be crucial for activation of the mTORC1 kinase [150]. Cellular stress leads to negative regulation of mTORC1 activity, which in turn leads to the stimulation of autophagy. In growth promoting conditions, mTORC1 phosphorylates and inhibits ULK1 downstream, inhibiting autophagosome formation.

Aside from nutrient starvation, other common methods of inducing autophagy via the mTOR pathway involve treatment with pharmacological agents such as rapamycin, Torin and PP242. The classical mTOR inhibitor rapamycin suppresses mTORC1 activity when applied acutely [182]. Since the activation of mTOR is involved in stimulating cell growth and protein synthesis, mTOR inhibitors such as PP242 and rapamycin have potential uses

as drugs for molecular-targeted therapy against many malignancies such as leukaemia [183]. These inhibitors have been shown to have different potencies in different cell lines [184]. For example, PP242 was shown to suppress cell growth more potently than rapamycin in several leukaemia cell lines such as T-Lymphoblastic and Jurkat cells.

The yeast orthologue of mTOR (TOR) is regulated by the availability of nutrients such as nitrogen and carbon. TORC1 and mTORC1 containing raptor, are important regulators of translation and ribosome biogenesis in both yeast and mammalian cells, and are also responsible for autophagy stimulation [169][171] in response to starvation .

Vps34 has been shown to regulate autophagy in response to nutrients by producing and accumulating PI(3)P, at specific locations during early steps of autophagy induction [150]. Deficiency of the mammalian Vps34 suppressed leucine responsive activation of mTORC1, proposing that Vps34 may act upstream of mTORC1 signalling [176]. In agreement with this finding, it has been shown that Ca^{2+} and CaMdependent signalling regulate mTORC1 via Vps34 in HeLa cells in response to leucine [185]. However, the relationship between mTORC1 and Vps34 appears to be complex since Vps34 is not essential for TORC1 signalling in *Drosophila* [186]. The complexity of this relationship could be due to the difference between the mammalian and *Drosophila* systems [187]. It is possible that some of the Vps34 complexes function upstream and others downstream of mTORC1. Further investigation is necessary to clarify the relation between mTORC1 and Vps34 complexes and their crosstalk throughout the whole autophagy processes.

1.4.5 Induction of autophagy

A common method for induction of autophagy *in vitro* is to remove growth factors and amino acids from the extracellular medium of cells. These starvation conditions lead to the inhibition of mTOR kinase and the subsequent induction of autophagy through well-

characterised mechanisms [188] [189]. Not all autophagy signals are dependent upon mTOR transduction; some amino acid (leucine) signalling can suppress autophagy in an mTOR-independent manner [190, 191]. Autophagy can also be induced independently of mTOR by small-molecule enhancers of the cytostatic effects of rapamycin (SMERs) [192].

The absence of essential amino acids (specifically leucine) is believed to be a particularly important in the induction of autophagy [193]. Depletion of amino acids induces autophagy in variety of cultured cell lines, however the sensing mechanism is not fully understood. Individual amino acids have been shown to exert differing effects on autophagy; for example leucine, tyrosine, phenylalanine, glutamine, proline, histidine, tryptophan, methionine, and alanine have been shown to suppress autophagy in *ex vivo* perfused liver [194]. These profiles are likely related to differences in amino acid metabolism between tissues**.** Additionally to insulin and amino acid signalling, many other factors are involved in autophagy regulation [195]. These include Bcl-2, reactive oxygen species (ROS) [196-198], Ca^{2+} [199] and AMP-activated protein kinase (AMPK) [200].

1.4.6 Selective autophagy

Autophagy was initially considered to be an essential but non-selective process. Bulk autophagy, which takes place during nutrient starvation, is thought to be non-selective toward its substrates. Recently evidence has shown that autophagy can also be selective. This allows for the specific targeting and elimination of of abnormal protein aggregates, lipid droplets, dysfunctional organelles and invading pathogens [201]. The mechanisms of cargo recognition in such cases are not yet fully understood [202], but what is known is that this process involves ubiquitination. Many autophagy-specific receptors such as P62/SQSTM (hereafter referred to as p62) control the selective autophagy by tethering cargo to the site of autophagosomal engulfment [203]. P62 is a scaffold protein for atypical

PKC, extracellular signal-regulated kinase (ERK)1, nuclear factor-κB and caspase-8. The p62 receptor possesses multiple domains, including an LC3-interacting region (LIR). Most p62 protein in the cell is found in the cytoplasm and the nucleus, as well as the autophagosomes and lysosomes. It is also localised to autophagy substrates such as protein aggregates and damaged organelles [204]. Before autophagic clearance, p62 'tethers' the ubiquitinated cargo to the nascent autophagosome, which carries ubiquitin-like modifiers (UBL) proteins such as LC3 on its surface [205]. Defects in autophagy results in accumulation of p62. Many types of selective autophagy have been identified and include xenophagy (microbes and viruses), ribophagy (ribosomes), mitophagy (mitochondria) and reticulophagy (ER).

1.4.6.1 Mitophagy

Since mitochondria are essential for regulating cellular energy homeostasis, mitophagy has been the subject of extensive research and has been recently proposed to play critical roles in diseases [206]. As the name suggests, mitophagy is the selective degradation of mitochondria by autophagy. In addition to quality control, mitophagy is important for the maintenance of mitochondrial number [207] and the elimination of mitochondria during the development of specialized cells such as reticulocytes [208].

Lemasters *et al*., initially found that mitochondria are selectively targeted for autophagy following a loss in their membrane potential. This suggests that the process of mitophagy is key to the removal of damaged mitochondria [209]. A number of factors interact specifically with damaged mitochondria; notably PTEN-induced kinase 1 (PINK1). PARKIN, a protein implicated in autosomal recessive monogenic Parkinson's disease (PD), has also been found to bind selectively to damaged mitochondria [210], and it has been suggested that PARKIN may therefore have a role in this selective autophagy process.

PARKIN and Pink-1 act together through a complex interplay of phosphorylation and ubiquitination [211]. A number of groups have reported that the recruitment of PARKIN to

impaired mitochondria requires PINK1 expression and its kinase activity [208, 212, 213]. Following translocation to the mitochondrial surface, PARKIN ubiquitylates many OMM proteins, such as VDAC and some components of the translocase of the OMM (TOM) complex (TOM70, TOM40 and TOM20)[208]. These consequently recruit other proteins to mitochondria to initiate mitophagy [214]. Overexpression of PARKIN is typically used to induce mitophagy and can be employed as a tool to identify mitochondrial E3 ligase substrates as endogenous PARKIN expression is low in many cell lines. Mitophagy can be confirmed by flow cytometry using mitochondrial dyes [215]. It is vital to confirm that changes in mitochondrial mass are truly as a consequence of autophagy and not because of reduced mitochondrial biogenesis.

1.4.6.2 Ribophagy

Ribosomes constitute half of the cell's protein mass [216] and so represent an important source of amino acids. Studies of nutrient starvation conditions in *S.cerevisiae* have revealed that ribosomes are degraded faster than other cytoplasmic components. This is suggestive of a selective degradation process [217]. The transport of ribosomes to the degradative organelles in yeast relies on core autophagy proteins such as Atg1 and Atg7. Catalytically inactive mutants of ubiquitin protease (Ubp3) exhibit defects in the degradation of ribosomes resulting in cell death. This study reveals that ubiquitination plays a key role in this process and, also that ribosomal turnover is important for cell survival under conditions of nutrient starvation [218]. Additionally, ribophagy is a significant process as has been shown to contributes to the downregulation of protein translation, a process that relies on large amounts of energy and the availability of amino acids [218].

1.5 Methods for measuring autophagy

Tools employed for studying autophagy include immunoblotting and fluorescence microscopy. Biochemical detection of the membrane-associated form of LC3-II can be carried out by immunoblotting. LC3-I is conjugated to PE following autophagy activation to form LC3-II and consequently recruited to the autophagosomal membrane. The ratio of LC3-I and LC3-II can be detected using immunoblotting. A band with a different molecular weight is observed after modification of LC3-II (LC3-I: 18 kDa, LC3-II: 16 KdA). LC3 is expressed as three isoforms in mammalian cells, LC3A, LC3B and LC3C, but only LC3B-II is linked with increased levels of autophagic vesicles. The use of anti-LC3B specific antibodies are employed for such analysis [215].

Endogenous LC3B-II protein can be quantified by immunofluorescence [215]. In addition, it can be visualised via the use of fluorescent markers into the cell system, such as green fluorescent protein (GFP) and red fluorescent protein (RFP). GFP-tagged LC3, in which GFP is expressed as a fusion protein at the amino terminus of LC3, is a common marker used to monitor autophagy in such systems. Since GFP-LC3 will be localised to, autophagosomes and autolysosomes, these structures can be visualised as punctate or ring structures (autophagosomes and autolysosomes that are 0.5-1.5 μm in diameter). The lipidated form of LC3 (LC3-II) is observed as bright green punctae associating with phagophore and autophagosomal membranes. As vesicles mature, LC3-II present on the outer autophagosome membrane is delipidated and released for recycling back to LC3-I [219]. When autophagosomes fuse with lysosomes the acidic content of the lysosomes quench the GFP fluorescence and therefore punctae are no longer apparent. Determination of the number of autophagosome by fluorescence is one method by which cellular autophagy can be quantified. An increased number of autophagosomes usually reflects an increase in

autophagic activity. However, it is important to note that autophagosomes are intermediate structures in a dynamic pathway. An accumulation of autophagosomes may result from either autophagy induction, or suppression of degradation steps. A block of any step downstream of autophagosome formation will result in an increase of the number of autophagosomes.

Systems such as those described above are widely used to gain insight into the process of autophagy. Counting GFP-positive punctate is, however, a laborious and potentially subjective task. This can be somewhat ameliorated by the use of computer software. In addition, over-expressed GFP–LC3 has the potential to be incorporated into protein aggregates or endosomal vesicles independent of autophagy.

LC3 tagged to both GFP and a red fluorescent protein (mRFP or mCherry), called 'tandem reporter', provides an alternative method to visualise autophagy processes [220]. The red fluorescence is not quenched at low pH. This tandem tool allows the visualisation of phagophores and autophagosomes with both green and red fluorescence that can be overlaid. Since the green fluorescence is quenched in mature autophagosomes, these appear as red fluorescent punctae.

Other proteins such as WD repeat domain, phosphoinositide interacting 1 (WIPI-1, a mammalian ortholog of Atg17) can be fluorescently tagged and used to detect autophagy. WIPI-1 is more rapidly recycled and enables more proximal events such as the development of nascent phagophore membranes to be observed [221]. WIPI-1 also co-localizes with LC3-positive membranes therefore WIPI-1-positive punctae can be used together with LC3-II staining as a measure of autophagy.

Recent research has shown that autophagy does not depend solely on LC3 but also relies on GABARAPs, a subfamily of Atg8 proteins [222], and in these instances, alternative

methods must be employed. To analyse autophagic flux in such conditions, cytosolic proteins such as lactate dehydrogenase (LDH) can be analysed. A sequestration assay can be employed to measure the transfer of the autophagic cargo marker enzyme LDH from the cytosol to autophagic vesicles, which is later degraded by the lysosome [223].

Measuring flux through the autophagic pathway in its entirety – from autophagosome production through to lysosomal degradation – may therefore be regarded as a more reliable representation of autophagic activity [224] [225]. Measuring long-term protein degradation (for example of p62) by e.g. Western Blotting has been used as a means of measuring autophagy. However, factors other than autophagy could be influencing the degradation of proteins, for instance the UPS is also active during inhibition of mTOR by rapamycin [226] [224]. Autophagic flux can be measured by selectively inhibiting the specific stages of autophagy using pharmacological agents. Lysosomal activity can be blocked using lysosomal protease inhibitors, such as bafilomycin A1 (BafA1) and chloroquine (CQ) [215, 227]. These compounds inhibit autophagosome degradation, resulting in an accumulation of autophagosomes.

In addition to the use of BafA1 to inhibit the autophagic flux, inhibitors of autophagy induction such as Chloroquine (CQ), 3-Methyladenine (3-MA) and Wortmannin can be employed to exert influence upon specific points of the pathway (Figure 1.5). CQ is a lysosomotropic agent commonly used to neutralise lysosomal pH and inhibit lysosomal degradation [163]. 3-MA inhibits the Vps34 complex and consequently the production ofPI3P, which is needed for nucleation of phagophores. One limitation of this approach is that chronic incubation with 3-MA can induce autophagy through via the inhibition of class I PI3-kinases [228]. Wortmannin is another inhibitor of PI3-Kinase [228] that is commonly used to inhibit the nucleation step of autophagy.

Other methods for detecting selective types of autophagy (such as mitophagy) also exist. These are described in section 1.4.6.

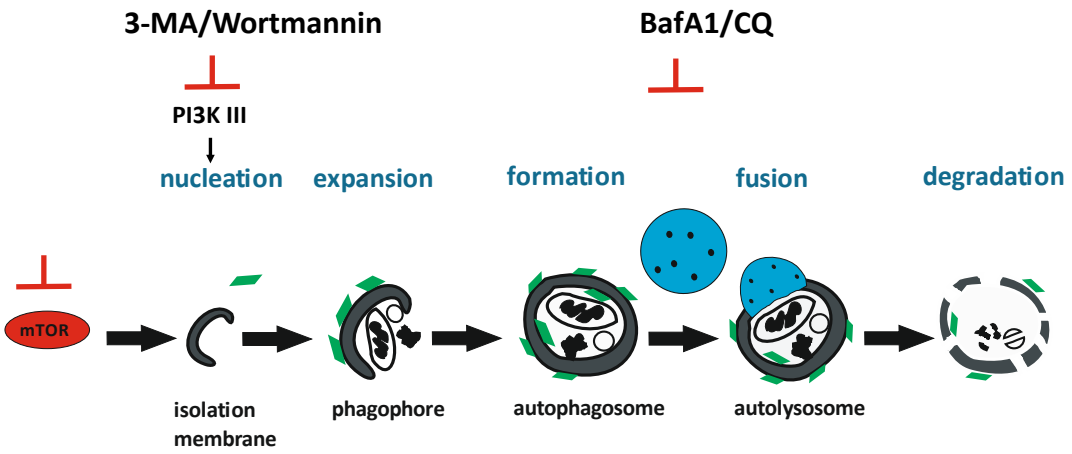

Figure 1.5. Schematic representation of the autophagy process and common inhibitors used to modulate different stages of autophagy. 3-MA: 3-methyladenine, BafA1: Bafilomycin A1, CQ: Chloroquine

1.6 Autophagy in health and disease

Autophagy is implicated in many human diseases ranging from neurodegenerative disorders, cardiovascular diseases and various forms of cancer [229, 230].

1.6.1 Neurodegenerative diseases

Alzheimer's disease (AD) is characterized by the presence of the hallmark extracellular amyloid-beta (Aβ) plaques and accumulations of abnormally processed tau (the neurofibrillary tangles) in the brain. Compared to non-neuronal cells, neurons are dependent on high basal autophagy for survival. It is the major degradative pathway in neuronal cells [231]. There is evidence to suggest that defects in the autophagy-lysosomal pathway occurs before any signs of pathological hallmarks [229]. Therapeutic targeting of the autophagy network in this context has focused upon promoting autophagy [232].

Factors such as ageing and metabolic/oxidative stress contribute to the accumulation of materials including multivesicular bodies, dense bodies, and autophagosomes. The latter have shown to contain greater levels of *amyloid precursor protein (*APP), and processing enzymes required for Aβ generation. Neurons grown in cell culture and transgenic mice deficient of Beclin-1 show accumulation of APP and Aβ. However, Beclin-1 over-expression reduces Aβ accumulation. Beclin-1 deficiency has been shown to impair late stages in the autophagosomal-lysosomal pathway, and promote neurodegeneration in mice. Beclin-1 levels are also reduced in affected grey matter of patients with early stages of AD [233].

Lysosomal proteases such as cathepsin are important in autophagy and are involved directly in substrate clearance. Inhibiting these proteases has been shown to increase amyloid pathologies and memory deficits in an AD mouse model [234]. Other therapeutic studies have shown that rapamycin reduces Aβ and Tau pathology resulting in an improvement in cognition [235], if treatment precedes the onset of plaque and tangle accumulation. Moreover rapamycin treatment of *Drosophila* over-expressing wild-type and mutant tau showed an increased tau clearance. Arctigenin, can inhibit both Aβ production and stimulate its clearance through mTOR inhibition (thereby autophagy stimulation) in APP transgenic AD model mice. This study also showed that memory impairment was reduced in these mice [10]. Enhancing lysosomal production or function (or both) could be another therapeutic approach. Yang *et al.* [236] showed that increasing lysosomal activity in the brain of a transgenic AD mouse model of reduced Aβ levels and deposits. While some evidence points to defective autophagic clearance, irregular autophagy induction can also lead to accumulation of autophagosomes containing Aβ and APP [10].

Autophagy is also implicated in Huntington's disease (HD) and Parkinson's disease (PD). In PD autophagy is vital for the clearance of α-synuclein (α-syn), a major component of Lewy

bodies that characterize PD [237]. Over-expression of Beclin-1 reduces the accumulation of α-syn and enhanced neuropathological features in the mouse model [238]. HD is linked to the expansion of the polyglutamine (polyQ) tract in huntingtin (Htt). Autophagy enhances the turnover of Htt [239], and studies of Atg knockout (autophagy deficient) *Caenorhabditis elegans* worms have shown increases in the formation of Htt aggregates and toxicity [240].

1.6.2 Cardiovascular diseases

Autophagy occurs at low levels under normal conditions in the myocardium, and defects in autophagy can lead to cardiac dysfunction and heart failure. A build-up of autophagosomes was observed in myocardial biopsy samples from patients with cardiovascular diseases (such as hypertension and congestive heart failure) [241]. Induction of autophagy in cardiac myocytes reduced the accumulation of misfolded proteins known to contribute to cardiac diseases [242]. mTOR inhibitors have been shown to promote the stabilization of atherosclerotic plaques [243]. Deficiency of LAMP2 in mice has been shown to result in autophagosome accumulation and defective degradation of long-lived proteins, which may contribute to the incidence of cardiomyopathy [244].

Verapamil, an L-type calcium channel blocker used in the treatment of hypertension and cardiac arrhythmia, induces autophagy and is antiproliferative in cultured vascular smooth muscle cells (VSMC). Moreover, commonly used cardiovascular drugs such as β-receptor agonists and β-receptor blockers have also been shown to alter autophagy levels in the cardiovascular system but a better understanding of their autophagic mechanism of action is required [243].

1.6.3 Cancers

Autophagy has been shown to have a dual role in cancer with evidence showing that autophagy may act as a tumour suppressor, particularly in the early stages of tumour initiation, while it can also enhance cancer cell survival in harsh conditions such as nutrient deficiency and hypoxia (common to many established and solid tumors) [245]. In addition, autophagy has been linked to the therapeutic resistance of breast cancer [246]. Elevated autophagy is often seen in cancer cells exposed to radiation and chemotheraptic agents [227]. Attempts to inhibit autophagy in order to ameliorate such effects have therefore attracted great interest. A number of studies have also suggested that autophagy inhibition by genetic or chemical means has the potential to induce apoptotic cell death and inhibit tumour cells growth [247, 248].

Cancer cells have a re-modelled phenomenon termed the 'Warburg effect', a metabolism where ATP is produced through increased glycolysis and reduction of lactic acid, rather than ATP production via oxidation of pyruvate within the mitochondria [249]. A variety of cancer cell lines have been shown to be addicted to the ER-mitochondrial Ca^{2+} fluxes to keep up with their uncontrolled proliferation, whereas non-tumorigenic cells slow down their cell cycle in when mitochondrial metabolism is limited so that failed cytokinesis and necrosis do not occur [250, 251]. Metastatic cancer cells are also sensitive to $InsP_3R$ inhibition. For example, when breast cancer cells were treated with the $InsP_3R$ inhibitor 2-APB, or following $InsP_3R$ knockdown, cell death was increased and was linked to amplified activation of autophagy involving Atg5 upregulation. Knockdown of Atg5, or the inhibition of autophagy repressed the breast cancer cell death [252].

1.6.3.1 Autophagy as a tumour promotor

Mechanisms by which autophagy promotes tumorigenesis include the inhibition of p53 tumour suppressor protein and supporting the metabolic function of mitochondria. Cancer cells have been shown to be more dependent on autophagy than normal cells and tissue, mostly due to unique characteristics of the tumour microenvironment and the increased metabolic demands as a consequence of deregulated proliferation [253].

Autophagy is elevated in RAS-transformed cancer cells and enhances their growth, survival [254] and metastasis [255]. Moreover findings have shown that that RAS-driven cancers may be "autophagy addicted", relying upon elevated levels of autophagy for survival [254]. The essential autophagy gene *Atg7* was deleted alongside with $KRAS^{G12D}$ activation in mouse models to study role of autophagy in spontaneously arising lung cancer. Tumour-specific *Atg7* deficiency caused the accumulation of dysfunctional mitochondria with an induction of p53, proliferative arrest, and cell death reducing tumour size. In spite of the reduction in tumour size and the generation of benign instead of malignant neoplasms, animals with *Atg7*-deficient tumours didn't extend their life span because the mice died of pneumonia instead of cancer. Autophagy defects in tumours, have been shown to trigger inflammation, which may trigger pneumonia. These studies propose that inactivating autophagy can divert progression of lung carcinomas to a benign disease, which could be an advantage if it can be achieved in the clinic with an autophagy inhibitor [253]. RAS-driven cancers not only rely on autophagy for survival, RAS activation also promotes cell signalling events involved in autophagy induction by upregulating Beclin-1 expression and BNIP3 expression through the RAS/RAF/ERK pathway [256].

The tumour microenvironment contributes to cancer cell survival and metastasis and is a complex system composed of a variety of cells including adipocytes, immune cells, fibroblasts, vascular endothelial cells, mesenchymal stems cells (MSCs), and many

cytokines [257]. The characteristics of the tumour microenvironment can induce autophagy by activating various pathways. For example autophagy is upregulated by activating the AMPK pathway to protect cancer cells against nutrient starvation by providing their nutrients. In response to hypoxia, hypoxia inducible factor HIF-1α is translocated to the nucleus and causes a rapid induction of the BH3-only proteins which displace Beclin1 from Bcl-2, leading to the induction of autophagy [188].

1.6.3.2 Autophagy as a tumour suppressor

Studies have shown that that the essential autophagy gene Beclin-1 is mono-allelically lost in up to 75 % of human prostate, breast, and ovarian cancers [253]. The death-associated protein kinase (DAPK), a Ca^{2+}-activated protein kinase that phosphorylates Beclin-1 and therefore disrupts Beclin-1/BcL-2 complex and induces autophagy, is commonly silenced in many human cancer types [256]. Beclin-1 protein levels have also been shown to be reduced in many brain cancers.

A crucial connection between autophagy and tumour suppression is through the regulation of reactive oxygen species (ROS) [258]. Increased ROS production stimulates carcinogenesis. Since mitochondria are the main source of intracellular ROS, mitophagy helps to minimise damage. Inhibition of autophagy in different animal models leads to accumulation of defective mitochondria. Defects in the autophagic process are linked with the accumulation of protein aggregates and the autophagy substrate p62/SQSTM1 (commonly elevated in human tumours). Such factors are associated with increased production of ROS and ER stress. In fact studies have shown that genetic inactivation of p62 in various models have reversed tumorigenic development observed in autophagy-deficient cells. An anti-inflammatory role of autophagy has also been suggested [256]. Degenhardt *et al*., have shown that autophagy inhibition in apoptosis-deficient tumour

cells promote necrotic cell death, local inflammation, and tumour growth [245]. These results suggest that autophagy restricts tumour necrosis and local inflammation.

Autophagy is mainly regarded as a pro-survival process but, under certain conditions, an increase in autophagic flux may cause cell death in part due to the tumour suppressor effects of autophagy [256]. Studies in an ovarian cancer cells showed that ectopic expression of Ras stimulates autophagic cell death through the upregulation of Beclin-1 and Noxa, a BH3-only protein [259]. Autophagy also has a role in cell senescence, which can be a major barrier to malignant transformation. This role might explain its tumour suppressor effects. Studies in fibroblasts showed that autophagy is activated during RAS-induced senescence and inhibition of autophagy delayed the oncogene-facilitated senescence [260].

1.6.4 Therapies, clinical trials and challenges

Many methods exist for measuring autophagy *in vitro*, however few methods exist for the assessment of this dynamic process in a living organism (especially in humans). This raises questions such as how can one be sure that autophagy was indeed inhibited or stimulated in patient treatments. Therefore there is a need to develop reliable biomarkers for autophagy assessment in clinical trials. Anticancer drugs such as hormonal agents, DNA damaging agents, microtubule-targeted drugs, death receptor agonists, antimetabolites, antiangiogenic agents, histone deacetylase inhibitors, and kinase inhibitors have all demonstrated an effect on autophagy [261].

HCQ, a derivative of the anti-malarial chloroquine (CQ), and an inhibitor of lysosomal acidification, is the only autophagy inhibitor that is clinically-approved [13]. Preclinical trials show that HCQ (which is less toxic than CQ) leads to tumour shrinkage alone or in

combination therapy. For example, in breast cancer cells, HCQ and tamoxifen were more effective at inhibiting autophagy than the monotherapy in oestrogen receptor-positive breast cancer cell lines [262]. HCQ nanocarriers have also been used to improve the pharmacokinetic properties. However studies of HCQ have shown that high doses of the drug (up to 1200 mg/day) only show modest inhibition *in vivo* and are not always consistent. HCQ has also been shown to contribute to defective lysosomal function, which can consequently cause lysosomal storage disease [263]. Therefore there is a demand for more active autophagy inhibitors and an understanding of mechanism of action [13].

1.7 Autophagic cell death

Apoptosis, a form of programmed cell death (PCD), is well characterised. However, there is substantial evidence suggesting that there may be other forms of PCD for example autophagic PCD, a type II programmed cell death process. Unlike apoptosis, autophagic PCD does not require DNA fragmentation or caspase activation [264].Autophagic cell death, termed autosis, is morphologically different from apoptosis and results from sustained excessive levels of cellular autophagy [265]. Autosis is accompanied with increased autolysosomes in dying cells that lack features of apoptosis and necrosis. Autosis has been shown to be regulated by Na^+,K^+-ATPase [266]. The process has been mainly observed from morphologic studies (i.e. cell death associated with autophagosomes/autolysosomes). This observation stems from evidence suggesting cells with autophagic features in regions where PCD is occurring. A lack of appropriate experimental systems to study autophagic PCD is one of the reasons why the mechanism remains poorly defined [267].

Evidence has shown that apoptotic death is faster than autophagic death and that autophagic cell death acts as an alternative to apoptosis. For example, growth factor–deprived wild-type cells go through a rapid apoptotic death whereas growth factor–

deprived *bax*$^{-/-}$, *bak*$^{-/-}$ cells, which are unable to undergo apoptosis, undergo slow death characterized by progressive self-cannibalization[264]. Deficiency in apoptosis due to the absence of Bax and Bak allows autophagy to progress to such an excessive extent that cells eventually die.

These observations raise the question whether autophagic activity in such cells is the cause of death or, an attempt to prevent it [268]. In situations where cell death occurs following sustained periods of autophagy, genetic or pharmacological inhibition of the autophagy process should prevent cell death. Indeed, *in vitro* inhibition of autophagy has been shown to prevent cell death. For example, the pharmacologic inhibitor of autophagy 3–MA, partially inhibits death in populations of starved hepatocytes derived from carcinogen-treated rats, in serum-deprived PC12 cells, and in TNF-treated human T lymphoblastic leukaemia cells. However, in a number of these studies, autophagy was observed in cells thought to die by apoptosis, and it was presumed that autophagy triggered apoptosis instead of having a direct role in cell death [264].

Additionally, studies have shown Atg5, Atg6 and Atg7 are involved in both autophagic cell death and in pro-survival autophagy. However their expression levels vary between the two events. In pro-survival autophagy their levels remain low whereas in autophagic death the proteins are upregulated [267].

The molecular connections between autophagy and apoptosis are complex. The therapeutic potential of autophagy for treating cancers and other diseases relies on the complicated interactions between the apoptotic and autophagic mechanisms [268]. Most cancer therapeutics induce cytotoxic stress on cancer cells that eventually trigger programmed cell death [269] and research has shown that autophagy can protect cells

against treatment with anti-cancer drugs [11]. Understanding these connections is therefore critical to know when and how to modulate autophagy for therapeutic gain.

During nutrient starvation, autophagy is usually the dominant process stimulated in the cell to provide energy in form of ATP, thereby achieving a metabolic state which is anti-apoptotic [270]. Other stimuli may promote an apoptotic response, and many molecules can stimulate both process.

At the root of autophagy-apoptosis interactions are two autophagy proteins, p62 (important for RAS-induced tumorigenesis) and the tumour suppressor Beclin-1 [268]. p62 is important in the selective autophagy of many proteins and interacts directly with many apoptotic and survival pathway proteins including ERK, TRAF6 (this regulates NF-kB survival pathways) and caspase-8 [271]. Beclin-1 interacts directly with anti-apoptotic Bcl-2. When Bcl-2 and Beclin-1 are bound, Beclin-1 is unable to trigger autophagy. The process is only triggered when Beclin-1 is released from Bcl-2 by pro-apoptotic BH3 proteins, when Beclin-1 is phosphorylated by DAPK or when Bcl-2 is phosphorylated by JNK [272]. Studies have shown that overexpression of DAPK in tumour cell lines (such as HeLa, MCF-7, or HEK 293T cells) leads to cell death displaying characteristic autophagic features [273]. Overexpression of Bcl-2 or Bcl-XL can hinder autophagy. Apoptosis can also inhibit autophagy through caspase-3-dependent cleavage of Beclin-1, resulting in a truncated protein that is unable to stimulate autophagy. These results show that apoptotic components regulating Beclin-1 can either stimulate or inhibit autophagy depending on BH3 proteins and caspase activities [272].

The pro-apoptotic BH3-only proteins, Bim and Bid directly trigger oligomerisation of Bax and Bak on the outer membrane of the mitochondria, leading to release of cytochrome c. Other members of the pro-apoptotic BH3-only proteins are Bad and Bik. In this case, the

BH3 domain of these proteins binds and antagonises anti-apoptotic Bcl-2 proteins and sensitises cells to apoptosis. BH3-only proteins can also regulate autophagy, for example the over-expression of Bnip3 (a hypoxiainducible, BH3 domain containing protein) increased autophagy levels and non-apoptotic cell death [274].

DAPK also acts as a mediator of ER stress-induced caspase activation and autophagic cell death in primary fibroblasts. Loss of DAPK reduces the accumulation of the active form of caspase-3, and the accumulation of LC3-II, thereby partially inhibiting cell death. Loss of DAPK has not been shown to affect ER stress or the unfolded protein response (UPR) signalling pathway. This suggests that DAPK acts downstream of the ER stress response to facilitate apoptosis and autophagy [275].

Calpains, a family of Ca^{2+}-dependent cysteine proteases localised in the cytosol, have also been shown to be involved in both apoptosis and autophagy processes. Increased levels of cytosolic Ca^{2+} allow calpains to translocate to the intracellular membrane, where they are activated by autocatalytic hydrolysis. Calpain-mediated cleavage of anti-apoptotic proteins such as Bcl-2 promotes apoptosis [273]. Calpains can also trigger necrosis by cleaving the Na^{+}/Ca^{2+} exchanger in the plasma membrane. This results in sustained secondary intracellular Ca^{2+} overload [276]. In relation to autophagy, loss of the calpain small 1 regulatory subunit (CAPNS1) resulted in the inhibition of autophagy under conditions of nutrient starvation, rapamycin treatment, and etoposide treatment. This inhibition of autophagy sensitises cells to apoptotic cell death events, suggesting that calpain-mediated autophagy plays a protective role against apoptosis [273]. Caspase inhibition have also been reported to induce autophagic cell death; chemical inhibition of cysteine proteases with z-VAD-fmk (a broad spectrum caspase inhibitor) can cause autophagic cell death in L929 mouse fibrosarcoma and the human Jurkat T cell lymphoma

cell types. This effect is likely to involve the combined inhibition of one or more caspases, including caspase-8, as well as other proteases such as a calpain [270].

Although autophagy is able to specifically degrade components of the apoptotic machinery (such as mitochondria and caspase-8), the significance of these events in relation to modifying the extent of cell death in a physiological or disease setting is unclear. For example, only mitochondria recognised as damaged or defective are thought to be targeted specifically by mitophagy. Therefore a question that remains unanswered is: even with autophagy being upregulated in a cell, why would an apoptotic stimulus still not cause cytochrome c release from the mitochondria untargeted by autophagy to induce apoptosis? One suggestion is that in a population of cells where some die and some survive, the molecular mechanisms (such as Beclin-1 or p62 cleavage), only take place in those cells that do eventually die and, these cells have lower levels of autophagy. Therefore, a clear mechanistic understanding of how autophagy can inhibit apoptosis for any defined apoptotic pathway is still lacking. Gaining knowledge on how proteins involved in autophagy and apoptosis can control the balance between cell death and survival can potentially help determine the approach in targeting autophagy in disease [268]. It is likely that cells have different sensitivity thresholds and can influence whether autophagy or apoptosis will occur. In some situations, a mixed phenotype of both apoptosis and autophagy is observed at the single-cell level [270].

1.8 Autophagy and ER stress

The ER is a site of synthesis, folding and post-processing of proteins in the cell.

Genetic and environmental factors that disrupt the function of the ER cause misfolded and unfolded proteins to accumulate in the ER lumen. This accumulation results in ER stress.

Factors disrupting ER function include Ca^{2+} depletion from the ER, viral infections, high protein demand, increased concentration of ROS and inflammatory cytokines. ER stress-mediated cell dysfunction and death has been implicated in many disorders, including diabetes and neurodegeneration. Ogata *et al*., have also shown that tumour cells stimulate autophagy for survival to avoid ER stress-induced toxicity [277].

Eukaryotic cells respond to ER stress by triggering the unfolded protein response (UPR); a signalling network which acts to alleviate this stress and restore ER homeostasis, promoting cell survival. Depending on the severity and duration of the ER stress, the UPR branches into two streams, survival or programmed cell death. The Bcl-2 family of proteins is essential to the cell death arm of the UPR pathway. It is usually under irrecoverable ER stress conditions that the UPR promotes apoptosis through intrinsic and extrinsic pathways [278]. Three ER transmembrane proteins initiating the UPR are Inositol Requiring 1 (IRE1), PKR-like ER kinase (PERK), and Activating Transcription Factor 6 (ATF6). In normal cell conditions, the ER chaperone immunoglobin binding protein (BiP) (which ensures correct folding of newly synthesised proteins) binds to the luminal domains of these master regulators rendering them inactive. However upon ER stress, BiP dissociates from these sensors [279].

Once activated, the UPR regulates downstream effectors resulting in adaptive response, feedback control, and cell fate regulation. The adaptive response includes upregulation of molecular chaperones and protein processing enzymes thereby increasing folding and handling efficiency. Translation is also attenuated for a few hours to minimise ER workload and reduce additional accumulation of unfolded proteins. An increase in ER-associated protein degradation (ERAD) and autophagy occur to clear unwanted proteins. ERAD involves translocation of misfolded or aggregated ER proteins to the cytoplasm where they are degraded by the ubiquitin proteasome system [280].

In the canonical ERAD system, terminally misfolded proteins are ubiquitylated and targeted for degradation by the ubiquitin–proteasome system (UPS). However, activation of autophagy by UPR transducers functions as a non-canonical ERAD pathway. Autophagic degradation was originally considered as a secondary response to ER stress, and activated only when the canonical UPS was overwhelmed by an excess of ubiquitylated proteins [281]. However, recent evidence shows that autophagy removes misfolded proteins that either form aggregates or are not efficiently processed by the canonical ERAD system [281]. In general it is now known that autophagy-dependent ERAD deals with both soluble and insoluble forms of misfolded proteins, whereas UPS-dependent ERAD targets only soluble misfolded proteins [282]. ER stress activates autophagy, however prolonged or excessive autophagy is often associated with cell death [283]. ER stress mediated autophagy induction can take place through varying mechanisms depending on cell types and stimuli in question. A link between autophagosome formation and ER expansion induced by ER stress has been shown by electron microscopy studies in yeast, revealing that ER volume increases 5-fold under ER stress and with a concomitant increase in autophagosome formation [278]. Evidence has shown that the UPR and autophagy are dynamically interconnected, and that ER stress can either stimulate or inhibit autophagy. However the molecular signals that control the changeover between induction and inhibition of autophagy remained undefined. Additionally, mitochondrial function is also associated with the UPR and autophagy in ER stress conditions with emerging roles by E3 ubiquitin ligases in regulating these processes by fine-tuning their magnitude and duration [281].

RIPK1, an emerging determinant of cell fate in response to cellular stress, was also shown to have a role in autophagy in response to ER stress. RIPK1 was found to be upregulated in melanoma cells treated with ER stressors tunicamycin (TM) and thapsigargin (Tg) along

with upregulated autophagy. RIPK1 has been shown to be important for protecting melanoma cells from TM- or Tg-induced apoptosis by increasing autophagy. Knockdown of RIPK1 inhibited autophagy and rendered the cells sensitive to cell death by TM or Tg [284]. Targeting the RIPK1 autophagy mechanism may therefore be valuable in order to enhance sensitivity of melanoma cells to therapeutic agents that induce ER stress.

1.9 The complex role of Ca^{2+} in autophagy

Differing spatiotemporal patterns of Ca^{2+} have been shown to both promote autophagy as well as suppress autophagy process. On the one hand, evidence indicates that intracellular Ca^{2+} signals, arising mainly from $InsP_3Rs$, suppress autophagy. Conversely, elevated cytosolic Ca^{2+} concentrations have also been shown to promote autophagic process [285]. Figure 1.6 represents some of the ways Intracellular Ca^{2+} regulates autophagy.

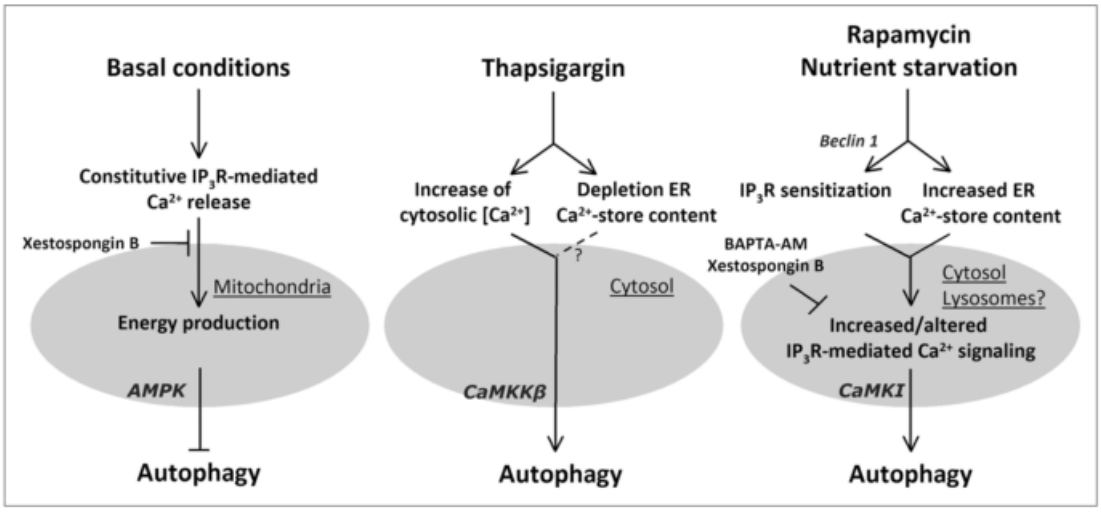

Figure 1.6 Intracellular Ca^{2+} signalling regulates autophagy. In basal conditions, IP_3R-mediated Ca^{2+} release towards mitochondria enhances mitochondrial ATP production and consequently inhibits autophagy through inactivation of AMPK. Centre: once Ca^{2+} mobilising agents, like thapsigargin, are added, the ER Ca^{2+} store is emptied causing a gradual increase in cytosolic Ca^{2+}, leading to autophagy activation through the calcium/calmodulin kinase (CaMKK-β) and AMPK pathway. Upon rapamycin addition (an inhibitor of mTOR) or nutrient starvation, the $InsP_3R$ becomes sensitised through Beclin 1 and increased ER Ca^{2+} store content, enhancing $InsP_3R$ mediated Ca^{2+} signalling and essentially triggering autophagy (Decuypere, *et al.*, 2013).

1.9.1 Ca^{2+} inhibits autophagy

Many studies reporting Ca^{2+} as an inhibitor of autophagy focus on $InsP_3Rs$ [286-288]. Elevations in cytosolic $InsP_3$ concentrations produced in cells occur after stimulation by (for example) hormones, growth factors or antibodies. This causes $InsP_3R$ mediated Ca^{2+} release from the ER into the cytosol [4]. $InsP_3$-mediated inhibition of autophagy has been studied in $InsP_3R$ triple knock out (TKO) chicken DT40 B lymphocytes, which showed higher autophagy levels than their wild-type counterparts [288]. Expressing type 1 or 3 $InsP_3R$ reduced autophagy levels in TKO cells. In contrast, ryanodine receptor expression, another ER Ca^{2+} release channel, does not reduce the elevated autophagy levels found in the TKO cells. However, although it is clear that $InsP_3Rs$ are important, the mechanisms involved are still debated. Other groups have shown decreased mTOR activity in TKO cells while AMPK activity did not change, and have demonstrated that cytosolic Ca^{2+} elevation acts to maintain elevated mTORC1 activity and thereby inhibiting autophagy [289].

Antagonists of voltage-operated Ca^{2+} channels (VOCC) and of $InsP_3$ signalling enhance autophagy by inhibiting calpain (Ca^{2+}-sensitive proteases) activity [290]. Inhibition of calpains activated an mTOR-independent autophagic clearance of aggregated proteins in neuronal cells [291]. It was suggested that Ca^{2+} influx was necessary for constitutive calpain-mediated cleavage of Atg5, thereby preventing induction of autophagy.

Resveratrol, a natural polyphenol, causes cell cycle arrest and cancer cell death by apoptosis and was found to inhibit SOCE in prostate cancer cells, causing ER stress and autophagy [292]. Tg, widely used to induce long lasting cytosolic Ca^{2+} signals and depleting ER Ca^{2+}, was shown to stimulate autophagy [293]. Other studies have shown that Tg blocked autophagic flux by preventing the maturation of autophagosomes into autolysosomes. In another study, Tg did not block autophagosome formation, but it

inhibited the fusion of autophagosomes with lysosomes. Tg has also been shown to inhibit nutrient starvation-induced autophagy [294]. These results show that Tg has a dual role in autophagy with more evidence for it activating autophagy. It could be that these dual roles are a consequence of a balance between cellular responses to elevated cytosolic Ca^{2+} concentration versus loss of ER Ca^{2+} stores.

SOCE, a major route of Ca^{2+} influx in many excitable and non-excitable cells, also has a role in autophagy. Inhibition of SOCE led to colorectal cancer cell death through apoptosis [295]. However, inhibition of SOCE also evoked a concomitant triggering of autophagy that delayed the onset of apoptosis by preventing cytochrome c release from mitochondria. Blocking autophagy increased colorectal cancer cell death. In this context, Ca^{2+} influx via SOCE prevented the triggering of autophagy via a Ca^{2+}/CaMKII/AKT pathway [295].

1.9.2 Ca^{2+} activates autophagy

Studies reporting Ca^{2+} as an activator of autophagy mostly make use of the SERCA inhibitors such as Tg or Ca^{2+} mobilising agents like ionomycin, ATP or resveratrol that all lead to elevated cytosolic Ca^{2+} levels and consequently elevated levels of autophagy [296]. However, exactly how these elevations lead to autophagy activation has not been fully elucidated, with data implicating many Ca^{2+} sources.

The importance of cytosolic Ca^{2+} in autophagosome formation was shown in one of the first studies where adding BAPTA-AM, a potent intracellular cytosolic Ca^{2+} chelator (more potent for Ca^{2+} than magnesium), prevented the induction of autophagy in MCF-7 cells. Høyer-Hansen *et al.* further demonstrated that autophagy occurred by the Ca^{2+}-dependent activation of AMP activated protein kinase, which required upstream activation of the CaMKK-β [199].

Sakaki *et al.* showed that Tg, used to deplete intracellular Ca^{2+} stores, induced autophagy in hepatocytes due to ER stress and the misfolding of proteins [293]. Autophagy in this study was shown to act as a pro-survival process, since the application of 3-MA reduced cell survival following Tg treatment. While these treatments have either directly or indirectly lead to an increase in Ca^{2+} in the cytosol, data showed that nutrient starvation induced autophagy was also inhibited by BAPTA-AM, suggesting that nutrient starvation might also lead to autophagy through enhanced Ca^{2+} signalling. Additionally, BAPTA-AM loading reduces the number of autophagosomes at basal levels (in cells kept in a medium replete with nutrients) and also prevents the formation of new ones in response to stimulation. This implies that a Ca^{2+} signal is important for maintaining the basal level of autophagic flux and for autophagy induction when mTOR is inhibited. The origin of such signals and the effectors involved are not fully known. BAPTA-AM was shown to prevent endosome/lysosome fusion, revealing that BAPTA-AM not only prevents the triggering of autophagy but also inhibits the processing of autophagosomes.

Studies on autophagy induced by amino acid starvation (through the inhibition of mTORC1) have shown that withdrawing essential amino acids lead to an increase in cytosolic Ca^{2+} deriving from both intracellular stores and the extracellular medium. An induction of AMPK via CaMKK-β (important for mTORC1 inactivation) was presented and the inactivation of AMPK has shown that induction of autophagy was attenuated [297]. AMPK was also shown to evade mTORC11 inhibition and can induce autophagy by phosphorylating ULK1 [298]. Furthermore, the Ca^{2+}/CaMKK-β/ AMPK signalling pathways has been commonly proposed in the involvement of increased autophagy in a variety of cell lines. Experimental conditions such as stimulation with ionomycin, vitamin D and $InsP_3$ generating agonists in cancer cells [199] and in neuronal cells treated with resveratrol, promoted autophagic clearance of amyloid-beta peptide via CaMKK/AMPK [296]. Other studies involving the CaMKK/AMPK

pathway include the induction of autophagy in endothelial progenitor cells by oxidized low-density lipoproteins through SOCE [299].

Further evidence of Ca^{2+} acting as an inducer of autophagy was the finding from Gao *et al.* [300] that Ca^{2+} phosphate precipitates could induce autophagy in a concentration dependent manner when transfected into HEK293 and MEF cells. This autophagy induction is also inhibited by BAPTA-AM. They also show that autophagy mediated by Ca^{2+} phosphate was Beclin-1 dependent and not dependent on CaMKK-B as the use of STO-609 (inhibitor of CaMKK-B) did not block autophagy.

TRPML3 Ca^{2+}channels located at the plasma membrane and intracellular vesicles, were also shown to have role in induction of autophagy. Knockdown of TRPML3 by siRNA reduced autophagy in response to many stimuli such as tunicamycin, nutrient starvation and SERCA inhibition in HeLa cells [301].

Many of the reports of Ca^{2+} stimulating autophagy stem from imposition of Ca^{2+} signals by treatments such as ionophores and SERCA inhibitors. Only a few reports have examined the role of natural agonist stimulation such as ATP, given that ATP is an agonist of purinergic receptors on many cell types. ATP is released from cells through connexin hemichannels for paracrine signalling [302]. It can also be released from dying cells to act as a pro-inflammatory molecule. Studies have shown that ATP can induce autophagy through G-protein coupled P2Y receptors [303] and ionotropic P2X receptors [304]. Autophagy induction through P2X receptors enhanced inflammatory signalling in hepatocytes but in macrophages, autophagy induction in response to ATP was very fast due to a Ca^{2+} influx, which helped in the clearance of mycobacteria from cells [305]. Evidence also showed that the concentration of extracellular ATP has a role in the fate of hepatoma cells, either autophagic or apoptotic [306].The role of $InsP_3Rs$ has been studied fairly well in relation to

autophagy, however Less is known about the role of RyRs in autophagy in comparison with $InsP_3Rs$. Autophagy induced by knockout of $InsP_3Rs$ was reversed by re-expression of functional $InsP_3Rs$, but not by functional RyRs [115]. Insulin withdrawal leads to cell death via autophagy in neural stem cells alongside cytosolic Ca^{2+} signals arising from type 3 RyRs [307]. Stimulation of RyR activity amplified cell loss also. In neonatal cardiac myocytes, $InsP_3R$-mediated Ca^{2+} release but not RyR $InsP_3R$-mediated Ca^{2+} release inhibits autophagy [308]. However, in adult cardiac myocytes, where type 2 RYRs expression is reduced, increased autophagy was linked to decreased mitochondrial metabolism [286]. This is similar to the effect of reduced $InsP_3R$ expression in other cell types. Expression of type 3 RyRs in HEK293 cells inhibited autophagic flux, however pharmacological inhibition of ectopically expressed RyRs in HEK293 cells, increased autophagic flux [309]. It was proposed that RyR-mediated Ca^{2+}-release inhibited autophagic flux by preventing autophagosome-lysosomal turnover.

1.9.3 Mitochondrial Ca^{2+} uptake and autophagy

Ca^{2+} uptake into mitochondria has been shown to prevent AMPK-activated autophagy [310]. Ca^{2+} stimulates the citric acid cycle within the mitochondrial matrix by activating pyruvate dehydrogenase, α-ketoglutarate dehydrogenase and isocitrate dehydrogenase and increasing electron flow through the electron transport chain for ATP production. Therefore it is unsurprising that the inhibition of mitochondrial Ca^{2+} uptake renders cells susceptible to bio-energetic crisis [311]. Studies where $InsP_3Rs$ have been inhibited (pharmacologically or genetically) show that autophagy can be induced independent of mTORC1 [286]. Moreover, in support of these findings, reduced expression of MCU upregulated autophagy in HeLa cells [312]. However, mitochondrial depolarisation, thought to inhibit Ca^{2+} uptake did not show elevated autophagy using autophagic markers [286].

The Bax inhibitor-1 (BI-1/TMBIM6), a member of the transmembrane Bax-Inhibitor Motif-containing protein family (TMBIM) is an ER membrane protein with important cell death functions [313] and was found to promote autophagy by reducing $InsP_3R$-mediated Ca^{2+} transport to the mitochondria [314]. BI-1/TMBIM6's ability to lower the ER Ca^{2+} store occurs by forming a Ca^{2+}-permeable channel [315] and/or directly sensitizing $InsP_3Rs$ (outside the MAMs) [316]. SERCA overexpression, to restore normal ER Ca^{2+} loading suppressed BI-1/TMBIM6-induced autophagy and mitochondrial energetics. The $InsP_3R$ antagonist xestospongin B (XeB) was found to stimulate autophagy in various cell lines, but not in DT40 cells that had a triple knockout of all $InsP_3R$ isoforms (DT40 TKO) [287]. In breast cancer cells, the induction of autophagy by inhibiting $InsP_3Rs$ led to cell death and reduction of tumour growth [252].

Evidence has also shown that $InsP_3Rs$ are necessary for the induction of autophagy. For example, incubating cells with XeB can not only induce autophagy, but when applied to cells under nutrient starvation conditions, it inhibits autophagy [317]. $InsP_3Rs$ associate with Beclin 1, an important protein for phagophore formation, and inhibit autophagic flux by limiting Beclin 1 availability for Vps34-complex formation. In response to rapamycin and starvation, $InsP_3Rs$ scaffolding with Beclin 1 cause a direct sensitization of $InsP_3R$ that is required to induce autophagy [317]. Moreover, expression of the $InsP_3$-binding domain of $InsP_3Rs$ (prevents $InsP_3R$ activation/opening) abolished autophagy induced by XeB or nutrient starvation [287]. Additionally, the knockout of all three $InsP_3R$ isoforms in HEK cells, which inhibits all agonist-induced Ca^{2+} release prevented resveratrol-induced autophagy [318].

Tumour cells which rely on autophagy for proliferation can involve $InsP_3R$-mediated Ca^{2+} signalling. In renal cancer cells, upregulation of type 1 $InsP_3R$ increased autophagy and

consequently tumour survival [319]. However, inhibiting $InsP_3R$-mediated Ca^{2+} release was demonstrated to kill tumour cells in higher numbers than non-tumorigenic cells although both cell types are able to induce autophagy similarly [320]. Autophagy was not responsible for tumour cell death in that study; inhibiting autophagy in fact instead caused an increased cell death. $InsP_3R$ inhibition in cancer cells causes a bio-energetic crisis resulting in failure to complete mitosis, leading to necrotic death when tumour cells undergo division. The effect of $InsP_3R$ inhibition could be overcome by incubating cells with a membrane permeant form of pyruvate to stimulate the citric acid cycle, consistent with a metabolic defect downstream of IP_3R inhibition due to a decreased rate of mitochondrial respiration.

1.10 Aims

Given the contradicting literature on the role of Ca^{2+} Signalling in Autophagy, one aim in the thesis was to study the regulation of autophagy by cytosolic and mitochondrial Ca^{2+} signals. Specifically, the aim was to understand the spatial and temporal characteristics of Ca^{2+} signals that regulate autophagy in two mammalian cell lines. The relevant sources of Ca^{2+} that lead to the generation of these Ca^{2+} signals will also be investigated. The first chapter presented establishes robust cellular systems as tools to study the regulation of autophagy by Ca^{2+}, whilst ensuring viability, without extruding Ca^{2+} indicators, or triggering unwanted autophagy or other cellular processes. Tools include fluorescence and electron microscopy and using Ca^{2+} indicators to record Ca^{2+} signalling in parallel with autophagy measurements.

The second chapter investigates the regulation of autophagy by Ca^{2+} release from $InsP_3Rs$. The aim is to inhibit Ca^{2+} signalling from the ER across to mitochondria with the expression of $InsP_3$ 5'-phosphatase. By doing so, we aim to explore putative links between preventing $InsP_3R$ function and mitochondrial Ca^{2+} uptake, cellular ATP concentration, and ER stress,

which have all been suggested to regulate autophagy. Moreover, the role of $InsP_3R$ activity for cell cycle progression and sensitivity towards apoptotic stimuli will be examined.

The last chapter investigates the role of Ca^{2+} influx via store-operated Ca^{2+} entry (SOCE) on autophagy with the use of Cyclopiazonic acid (CPA), an inhibitor of SERCA. Using CPA, intracellular Ca^{2+} stores become depleted and SOCE takes place. This tool will enable the distinction between Ca^{2+} signals arising from intracellular stores and SOCE and will hopefully reconcile some of the contradictory data on SOCE in literature. Where there is a link between Ca^{2+} and autophagy upregulation/downregulation, cellular pathways such as CaMKK2 will be investigated.

Chapter 2: Materials & methods

2.1 Chemicals and solutions

Chemical or solution	Supplier	Catalogue number
2-Aminoethoxydiphenyl borate (2-APB)	Sigma	D9754-5G
2-Deoxy-D-glucose (2-DG)	Calbiochem	25972
3-Methyladenine (3-MA)	Sigma	M9281-100 MG
Ampicillin	Thermo Fisher	11593027
Antimycin A	Sigma	A8674-25MG
ATP determination kit	Molecular Probes	A22066
Bafilomycin A1 (BafA1)	LC Labs	B-1080
BAPTA-AM	AAT Bioquest	21001
Cyclopiazonic acid (CPA)	Sigma	C1530-5 MG
Cyto-ID autophagy kit	Enzo Life Sciences	ENZ-51031-0050
DharmaFECT	Dharmacon	T-2001-01
Dimethylsulfoxide (DMSO)	Sigma	276855-100ML
Dithiothreitol (DTT)	Sigma	D-9163
Dulbecco's Modified Eagle Medium (DMEM)	HyClone	SH30022.02
EGTA	Sigma	E-0396
Ethanol, absolute	Fisher Scientific	E/0650DF/17
Foetal bovine serum (FBS)	Gibco	10500
Fura-2-AM	Thermo Fisher	F1221
Geneticin, powder (G-418 sulfate)	Thermo Fisher	11811-023
Gö 6983 (PKC inhibitor)	Sigma	G1918-500UG
Hydrogen peroxide- 30 % (w/w) in H_2O	Sigma	H1009-5ML
Ionomycin, free acid	Sigma	I9657
jetPEI DNA transfection reagent	Source Bioscience	101-01N
Kanamycin	Thermo Fisher	11815024
KN-92	Calbiochem	422709

Chemical or solution	Supplier	Catalogue number
KN-93 (CaMKII inhibitor)	Calbiochem	422708
Laminin	Sigma	L2020-1MG
L-glutamine	Thermo Fisher	25030081
Luciferase from *Photinus pyralis* (firefly) (for use with the ATP kit)	Sigma	L9506-2MG
MCU antibody	Sigma	HPA016480
Menadione	Selleckchem	S1949
Methyl pyruvate	Sigma	371173-25G
Minimal Essential Medium (MEM) amino acids (50X)	Thermo Fisher	11130051
MTT (thiazolyl blue tetrazolium bromide)	Sigma	M2128
Nocodazole	Sigma	M1404
Non-essential amino acids (100 X)	Thermo Fisher	11140050
NuPAGE LDS sample buffer (4X)	Thermo Fisher	NP0007
Oligomycin A	Sigma	75351-5MG
Paraformaldehyde (PFA)	Sigma	P6148
Penicillin-Streptomycin	Thermo Fisher	15140122
Phosphate-buffered saline (PBS)	Sigma	P3813
Pierce™ BCA protein kit	Thermo Scientific	23225
Pierce™ ECL	Thermo Scientific	32109
Pluronic F-127	Thermo Fisher	P-3000MP
Power SYBR®Green PCR Master Mix	Thermo Fisher	4367659
Propidium iodide	Sigma	P4170-10MG
Protease Inhibitor Cocktail Set III, EDTA-Free	Calbiochem	539134
QIAprep Spin Miniprep Kit	Qiagen	27104
Rapamycin	Enzo Life Sciences	BML-A275- 0025
Rhod-2-AM, ultrapure	AAT Bioquest	21062

Chemical or solution	Supplier	Catalogue number
RNA extraction kit High-Capacity RNA-to-cDNA™ Kit	Thermo Fisher	4387406
RNase A	Alfa Aesar	J62232
RNeasy kit	Qiagen	74104
RU360	Santa-Cruz	sc-222265
SB 216763	Selleckchem	S1075
siRNA MCU (ON-TARGETplus Human MCU siRNA SMARTpool)	Dharmacon	L-015519-02
siRNA control (ON-TARGETplus Non-targeting siRNA)	Dharmacon	D-001810-10
Sodium pyruvate	Thermo Fisher	11360070
STO-609	Stratech	C17-900-SGC
Tali® cellular analysis slides	Tali®	T10794
Thapsigargin	Thermo Fisher	T7458
ThioflavinT	Sigma	T3516
Tissue culture inserts (0.4 µm)	Greiner	665641
Trypsin-EDTA solution	Gibco	25200-056
U-73122 hydrate	Sigma	U6756
Wheat Germ Agglutinin (WGA)	Thermo Fisher	W11262

Table 2.1 *List of chemicals or solutions used, with their relevant supplier and catalogue number. The name of the chemical and its acronym or abbreviation used in the text are shown.*

2.2 Cell culture

2.2.1 Cell lines used

HeLa cells

HeLa cells are an immortalised human epithelial cervical cell line that proliferate as attached cells. With regard to ER Ca^{2+} release channels, HeLa cells mainly express $InsP_3R1$ and $InsP_3R3$. Some RYR2 expression has been shown [321]. Early studies have shown that these cells can be transiently activated by histamine through H1 receptors [322].

HEK-293 cells

HEK-293 cells (hereafter denoted 'HEK cells') are immortalised human embryonic kidney cells that were developed by Frank Graham [323], and have since been an important cell line for use in biology, virology and molecular biology research. HEK cells are epithelial cells that mainly express $InsP_3R2$ and $InsP_3R3$ [324].

GFP-LC3 HEK cells and GFP-LC3 HeLa cells

HeLa and HEK cell lines stably expressing GFP-LC3 were a gift from The Katholieke Universiteit (KU), Leuven and The Babraham Institute respectively. The GFP-LC3 HeLa cells were initially observed to be heterogenous in GFP-LC3 expression, which made it difficult to find appropriate settings for imaging. The GFP-LC3 HeLa cells were therefore sub-cloned to obtain a population of cells with a more homogenous GFP-LC3 expression. Cells were seeded onto glass coverslips at 4 x 10^4 cells /mL in 12 well plates for 48 hours before use. GFP-LC3 HEK cells were grown on laminin-coated glass coverslips 48 hours before imaging. The laminin coating was applied by adding a 25 µg/mL laminin solution (made up in PBS) to ethanol- and PBS-washed coverslips for one hour at 37°C. After removal of the laminin the coverslips were left to air dry before seeding with cells.

RFP-GFP-LC3 HeLa cells

This cell line was created by stably transfecting RFP-GFP-tagged LC3 in HeLa cells during this project. RFP-GFP-tagged LC3 is a tandem sensor that was used for monitoring the various stages of autophagy. Compared to GFP-LC3 expressing cells, where it is only possible to monitor autophagosome activity, the RFP-GFP-LC3 cell line can be used to assess the full autophagic flux and distinguish between autophagosomes and

autolysosomes. Cells were seeded on glass coverslips at 4 x 10^4 cells /mL in 12 well plates for 48 hours before use.

Two-pore channel null (TPC) 1/2 (WT and $^{-/-}$) MEF cells

TPC 1/2 $^{-/-}$ MEF cells and their corresponding wild type MEF cells were obtained from Professor Antony Galione (University of Oxford). Ruas *et al*. (2015) first showed that TPC 1/2$^{-/-}$ knockout in MEF cells abrogates NAADP-induced Ca^{2+} signals. Although there is still some debate about the role of NAADP, it has been shown to play a role in many physiological contexts such as smooth muscle contraction, autophagy and cardiovascular physiology [325]. We used TPC1/2$^{-/-}$ cells, and their corresponding control TCP-expressing MEF cells, were used to study the role of these channels have in the regulation of autophagy. The TPC1/2$^{-/-}$ cells and their corresponding controls were seeded onto glass coverslips at 3 x 10^4 cells /mL in 12 well plates, then transiently transfected with GFP-LC3 24 hours later, and used in experiments 24 hours following transfection.

2.2.2 Growth of cells

All the cell types described above were maintained in DMEM supplemented with 10% FBS, 50 U/mL penicillin and 50 µg/Ml streptomycin in a standard cell culture incubator (i.e. humidified environment with 5% CO_2 at 37°C). For those cell lines that needed continual selection (i.e. HeLa or HEK cells stably expressing GFP-LC3 or RFP-GFP-LC3), 400 µg/mL or 800 µg/mL geneticin was added to the cell culture medium. Cells were passaged every 2 or 3 days depending on confluency, with the aim of keeping them sub-confluent at all times. For passaging, the DMEM surrounding the cells was aspirated, and the cells were superfused with PBS and then incubated with a 0.05% trypsin/0.2% EDTA solution at 37°C for a maximum of 2 minutes. Following dissociation of the cells from their cell culture substrates, the action of trypsin was terminated by addition of fresh DMEM with the

supplements described above. The cells in suspension were counted using a haemocytometer. To obtain the number of cells per mL, the number of cells in a 1 mm^2 square of the haemocytometer grid was multiplied by 10,000. Subsequently, cells were re-suspended in DMEM at the desired density and plated onto 16 mm coverslips (for imaging) or into 25 cm^2 flasks (for perpetuation).

2.2.3 Cell storage and recovery

For long-term storage, cells were re-suspended in freezing media (10% DMSO, 90% FBS v/v), placed in cryo-vials in 1 mL aliquots and frozen at a rate of 1°C per hour to –80°C in a pre-cooled freezing tub, and then kept within in a –80°C freezer or in a liquid nitrogen cryopreservation container. Cells were resuscitated from frozen by thawing at 37 °C and then re-suspended in 4 mL warm complete medium before being transferred to a 25 cm^2 flask. Once the cells were adherent, their surrounding medium was aspirated and replaced with fresh DMEM plus supplements in order to remove the DMSO present in the freezing medium.

2.2.4 Sub-cloning

In order to obtain a population of HeLa cells that expressed a homogenous level of GFP-LC3, cell cloning by serial dilution was carried out in a 96 well plate. The protocol was adapted from the article "Cell cloning by Serial Dilution in 96 Well Plates" (Corning). First, HeLa cells expressing heterogeneous levels of GFP-LC3 were plated at 4,000 cells/200 µL in the first well of a plate (well A1). 100 µL of cell culture medium was added to all wells except for well A1. Using a single channel pipette, 100 µL of the cell solution in well A1 was transferred to well B1, mixing gently and avoiding bubbles. These 1:2 dilutions were sequentially carried out across the columns of wells (i.e. wells A1 – H1) discarding 100 µL from well H1 so that it ended up with the same volume as all the wells above it. 100 µL of

cell culture medium was added to all wells in column 1, giving a final volume of 200 µL for each. Quickly after, 100 µL from the wells in column 1 were transferred to column 2 and all the way across the plate to the last column. As before, 100 µL medium was added to all wells to give a final volume of 200 µL. The plate was placed in a cell culture incubator under standard conditions. Colonies were detectable by microscopy 5 days after plating. Wells that contained a single colony were selected and the cells were sub-cultured into one well of a 12 well plate. Following a few days of growth, 3 wells from the plate were checked for populations where >95% of the cells expressed the fusion protein of interest (GFP-LC3) at approximately the same level. The colonies checked were passaged in T25 flasks individually. Clones displayed stability with time and were expanded and frozen for later use. Autophagy studies, such as inducing cells with rapamycin and nutrient starvation, were also carried out and results showed the same effects with all 3 clones. Transient transfection with $InsP_3$ 5'-phosphatase showed the 3 clones transfected at the same efficiency. Altogether results demonstrated that any of the 3 clones were suitable for use.

2.3 Molecular biology

2.3.1 Transformation of E.coli

100 µL of competent cells (DH5α) (thawed on ice) were added to a cold, sterile tube with 1 - 5 µL DNA. The mixture was heat shocked at 42^{o}C for 2 minutes and returned on ice. 600 µL of LB media (without antibiotics) was added to each tube and incubated at 37^{o}C in an orbital shaker for 1 hour. 100 or 200 µL of the transformation mix was spread onto antibiotic-containing LB agar plates (ampicillin or kanamycin) and incubated at 37^{o}C for 16-24 hours.

2.3.2 Plasmid DNA preparation

Single colonies were picked from the agar plates and used to inoculate 10 mL aliquots of LB media containing the required antibiotic. The colonies were grown at 37^{o}C with gentle agitation in an orbital shaker at 220 rpm overnight until the mixture was cloudy. Bacteria were collected in 5 mL aliquots and plasmid DNA was isolated using a miniprep kit (Qiagen) following the manufacturer's protocol. The resultant plasmid DNA was re-suspended in TE buffer and stored at -20 ^{o}C.

2.4 Transfection

2.4.1 Expression vectors

The following expression vectors are gifts from:

RFP-GFP-LC3: Laboratory of Molecular and Cellular Signaling, KU Leuven Belgium.

GFP-LC3: Laboratory of Molecular and Cellular Signaling, KU Leuven Belgium.

mCherry InsP$_3$ 5'phosphatase: The Babraham Institute, Cambridge.

GFP InsP$_3$ 5'phosphatase: The Babraham Institute, Cambridge.

The mCherry and GFP InsP$_3$ 5'-phosphatase constructs were a gift from Professor Llew Roderick (KU Leuven, Belgium). Sequence information was not given, although the cloning and sequence were verified. The InsP$_3$ 5'-phosphatase was originally cloned by Professor Christophe Erneux [326] and incorporated in a mammalian expression vector. The inactive InsP$_3$ 5'-phosphatase has a D232A mutation, which is known to make the enzyme catalytically inactive [327].

The constructs used encode kanamycin resistance for selection in bacteria and neomycin resistance which allows cells expressing the construct to be selected for using geneticin in mammalian cells.

2.4.2 Transient transfection

Cells were seeded either onto 16 mm glass coverslips in 12-well plates (for imaging experiments), or into 6-well dishes for PCR and transfected at 70 - 80% confluency 24 hours post seeding, and 12 – 24 hours prior to imaging experiments. JetPEI® transfection reagent was used for DNA transfection in all studies in accordance with the manufacturer's instruction. In brief, DNA encoding the gene of interest and NaCl, and similarly JetPEI and NaCl, were mixed together and vortexed. The JetPEI/NaCl mix was added to the DNA/NaCL mix, vortexed and incubated for 15-30 minutes at room temperature (the amount of DNA and solution volumes are shown in Table 2.2). Following incubation, ~100 µL of the resulting solution was added dropwise to the DMEM surrounding the cells.

	DNA mix		**Transfection reagent mix**	
HeLa and HEK cells	DNA	NaCl (150 mM)	Jetpei	NaCl (150 mM)
	1 µg	50 µL	2 µL	50 µL
MEF cells	1 µg	50 µL	8 µL	50 µL

Table 2.2 *Ratio of Jetpei to DNA (per well of a 12-well plate).*

2.4.3 Stable transfection

The RFP-GFP-LC3-expressing HeLa cells were generated by initially following the transient transfection protocol, but then selecting test clones using the colony isolation procedure described in section 2.2.4. To maintain the RFP-GFP-LC3 expression, a 'kill curve' of

geneticin-dependent cell death was established to determine the minimal antibiotic concentration at which non-transfected cells would die. For this, HeLa cells were seeded in a 24-well plate and incubated for 72 hours with geneticin concentrations ranging from 50 µg/mL to 1,000 µg/mL. Clones were selected and amplified, and then tested with rapamycin and bafilomycin to ensure that the RFP-GFP-LC3 reporter construct was sensitive to inducers of autophagy.

2.4.4 siRNA transfection

HeLa and HEK cells were seeded in 6-well plates in antibiotic-free complete medium (DMEM+FBS) and were transfected with siRNA solutions 48 hours post seeding. DharmaFECT (Dharmacon) was used to facilitate siRNA transfections, using the manufacturer's protocol. In brief, in separate tubes, the siRNA (Tube 1) and the appropriate DharmaFECT transfection reagent (Tube 2) were diluted with serum-free medium and incubated for 5 minutes at room temperature. Contents of tube 1 were added to tube 2, mixing carefully. The mix was incubated for 20 minutes at room temperature. Antibiotic-free complete medium was added to the mix for a final MCU siRNA concentration of 25 nM. Culture medium from wells of the 6-well plate were replaced with the appropriate transfection medium to each well. Cells were incubated for 72 hours before lysates were collected for western blotting analysis using antibodies directed against the MCU and to confirm inhibition of gene expression. Control transfections were performed in parallel using a negative control siRNA (non-silencing). siRNA sequences are shown in Table 2.3.

siRNA	Sequence
non-targeting	UGGUUUACAUGUCGACUAA UGGUUUACAUGUUGUGUGA UGGUUUACAUGUUUUCUGA UGGUUUACAUGUUUUCCUA
Human MCU siRNA	GAUCAGGCAUUGUGGAAUA GUUUUGACCUAGAGAAAUA ACUGAGAGACCCAUUACAA GUAAUGACACGCCAGGAAU

Table 2.3 *siRNA sequences used in transfection experiments.*

2.5 Quantification of ATP in cells

2.5.1 Solutions used

2-deoxyglucose solution: this solution is similar to complete imaging medium (section 2.10), but with replacement of D-glucose by 5.5 mM 2-deoxyglucose.

To determine ATP concentration in cells, a luciferase-based luminescence assay was used. HeLa and HEK cells were seeded at a density of 40,000 cells per well in 12-well plates. Where necessary, cells were transfected (e.g. with $InsP_3$ 5'-phosphatase) 12 hours post seeding. Various treatments (e.g. oligomycin, antimycin and 2-deoxyglucose solution) were added to cells within a well, and the cells further incubated for 1 hour. At the appropriate sampling time, the media surrounding the cells was carefully aspirated and cells were washed twice with PBS, before the addition of 0.5 mL boiling distilled water. This boiling water method (adapted from Hu *et al*.) was used to lyse cells and extract ATP instead of other methods that involve chemicals such as perchloric acid or Tris-borate, which were found to interfere with the luciferin-luciferase system. Additionally, the boiling water method of ATP extraction was found to be effective in inhibiting ATPases, and thereby prevent post-lysis degradation of ATP. Following lysis, cells were suspended by repeated pipetting and then centrifuged at 12,000g for 5 minutes at 4°C. 10 µL of the supernatant

was used for luminescence measurement using the ATP Determination Kit (Molecular Probes). The ATP measurement protocol was carried out as per the manufacturer's instructions in a 96 well plate. This involved the addition of 90 µL of a reaction solution that consists of Luciferin, DTT, Luciferase and a reaction buffer provided in the kit. The reaction buffer consists of 500 mM Tricine buffer, pH 7.8, 100 mM $MgSO_4$, 2 mM EDTA and 2 mM sodium azide. 10 µL ATP standard solution and sample supernatants were added to the reaction buffer for a final volume of 100 µL. The plate was then placed in an OPTIMA FluoStar plate reader for luminescence detection at 560 nm.

Luciferase solution (purchased as a powder separately from Sigma) was prepared by diluting the powder in 1 M Tris-buffer (composition: 6.05g TrisBase in 30 mL dH_20, pH adjusted to 7.3 using HCl then made up to 50 mL with dH_20). A standard curve of ATP concentrations (spanning 50 to 2,000 nM) was generated by serial dilutions from a stock solution containing 10 µM ATP. This standard curve was used to relate luciferase output from the cell samples to ATP concentration.

2.6 Determining cell viability using an MTT assay

To determine potential changes in cell viability or metabolism, the colorimetric MTT metabolic activity assay was carried out on cells cultured in 96 well plates. HEK and HeLa cells were cultured at 1×10^4 cells/well overnight in a cell culture incubator under standard conditions. Where indicated, cells were transfected (e.g. with $InsP_3$ 5'-phosphatase) for 12 hours. To induce cell death, 100 µM menadione (a pro-apoptotic agent) was added to some cells, but not the cells in the control wells, and they were returned to the incubator for a further 12 hours. Subsequently, the cell culture medium surrounding the cells was aspirated, and was replaced with 60 µL/well of MTT solution (5 mg/mL constituted in dH_20,) and incubated for 2 to 4 hours in a cell culture incubator under standard conditions. After

incubation, the MTT solution was aspirated and 100% DMSO (100 µL/well) was added to dissolve the purple formazan precipitate formed in the assay. The plate was then placed in an OPTIMA FluoStar plate reader, and the absorbance of each well was measured at 540 nm.

2.7 Measuring endoplasmic reticulum stress

WT HeLa cells were seeded onto 16 mm glass coverslips in 12-well plates for 48 hours before use. Some cells were transfected with $InsP_3$ 5'-phosphatase 12 hours post seeding and on the day of experimentation, some coverslips were treated with hydrogen peroxide for 1.5 or 3 hours, or with DTT for 1, 2 or 4 hours for use as positive controls. Cells were incubated with 0.5 µM thioflavin T in the last 10 minutes of treatment and visualised in the GFP mode on the Leica wide-field microscope for measuring overall fluorescence intensity. DTT, which causes ER stress by interfering with disulfide bond formation, was made up fresh on each day of experimentation.

Quantitative reverse transcription PCR (qRT-PCR) (section 2.8) was carried out as another tool for measuring ER stress in HEK cells.

2.8 Quantitative real-time PCR

HEK and HeLa cells were seeded at a density of 8 x 10^4/mL in 6-well plates and were either transfected with $InsP_3$ 5'-phosphatase the next day for 24 hours or incubated with other treatments such as H_20_2 for 3 hours two days post-seeding. Following the experimental treatments, total RNA was extracted from both cell types using an RNeasy kit (Qiagen). RNA was quantified using a Nanodrop (NanoDrop™ One, Thermo Scientific) and 0.5 µg RNA was transcribed into cDNA using a High-Capacity RNA-to-cDNA™ Kit (Thermo Fisher). cDNA was used at a 1/20 dilution, and qRT-PCR was performed using Power SYBR®Green PCR Master Mix (Thermo Fisher) in a reaction volume of 25 µl on an BioRad DNA Engine Opticon 2 Real-

Time Cycler. Primer sequences (synthesised by Eurofins Genomics) are shown in Table 2.4. Thermal cycling conditions were 95°C for 5 minutes following PCR Master Mix addition, followed by 40 cycles comprising: 95°C for 30 seconds, 58°C for 30 seconds and 72°C for 30 seconds. At the end of the PCR cycling, melting curves were investigated to determine the amplification of a single product and the absence of primer dimers. A melting curve shows the change in fluorescence detected when double-stranded DNA (dsDNA) with an incorporated dye dissociates, or "melts" into single-stranded DNA (ssDNA) as the reaction's temperature is raised. For example, when double-stranded DNA bound with SYBR Green I dye is heated, a sudden decrease in fluorescence is detected when the melting point (the temperature at which 50% of DNA is denatured) is reached. This is due to dissociation of the DNA strands and a consequent release of the dye. SYBR®Green dye is able to detect any double-stranded DNA including primer-dimers, contaminating DNA and PCR products from mis-annealed primers therefore by viewing the melting curve, one can ensure that the desired amplicon is detected.

2.8.1 Analysis of real-time PCR

Ct (threshold cycle) values, which show the number of cycles taken to detect a real signal from the samples, are obtained at the end of the PCR assay and are used for quantification. Results were calculated and normalised against GAPDH as endogenous control using the **2^-ΔΔCt** method [328]. . The fold change in mRNA was calculated using the following equations:

$$2^{-\Delta\Delta Ct}, \text{ where } \Delta\Delta Ct = \Delta CTE - \Delta CTC$$

(Δ represents change, CTE are Ct experimental values, and CTC are Ct control values).

$$\Delta CTE = TE - HE$$

(TE: gene tested experimental, HE: housekeeping gene experimental)

ΔCTC = TC-HC (TC: gene tested control (untreated), HC: housekeeping gene control).

One-way ANOVA or one-sample t-tests were applied to determine the differences in mRNA expression between samples using a hypothetical value of 1 (control). A P value < 0.05 was considered as the threshold for statistical significance.

Gene	**Primer sequence (5' to3')**
GAPDH Forward	AGGGCTGCTTTTAACTCTGGT
GAPDH Reverse	CCCCACTTGATTTTGGAGGGA
GRP78/BiP Forward	ACGTGGAATGACCCGTCTGT
GRP78/BiP Reverse	AACCACCTTGAACGGCAAGA

Table 2.4 *Oligonucleotides primers used for PCR with their relevant sequence.*

2.9 Western blotting

2.9.1 Western blotting solutions

Running buffer: contains 190 mM Glycine, 0.1% SDS and 25 mM Tris-HCL (pH 8.3).

Stripping buffer: contains 2% SDS, 62.5 mM Tris (pH 6.7) and 100 mM β-mercaptoethanol.

TRIS-buffered saline (TBS) (pH 7.6): contains 10 mM TRIS-HCL and 150 mM NaCL

TRIS-buffered saline + Tween (TBST): contains 0.05% Tween-20 and TBS.

Laemmli sample buffer: contains 3% SDS, 4 mM EDTA (pH 8.0), 500 nM sucrose, 0.005% Bromophenol blue and 80 mM Tris/HCL (pH 7.0).

Transfer buffer: contains 192 mM Glycine, 25 mM Tris-HCL and 20 % Methanol.

Ponceau-S: contains 0.1% w/v Ponceau-S and 1% v/v Glacial acetic acid.

Blocking buffer: contains 8% w/v non-fat dry milk in TBST.

*Lysis buffer: t*his solution was used for preparing cell lysates for western blotting. Lysis buffer contained 40 mM Na_3VO_4, 20 mM Tris-HCL (pH 7.6), 140 mM NaCl, 1% Triton X-100 and a cocktail of protease inhibitors (freshly added at 1/100 to the lysis buffer before use).

2.9.2 Preparation of cell lysates

Cells were grown in 25 cm^2 flasks to obtain sufficient amounts for immunoblotting (or 6-well plates for MCU siRNA (section 2.4.4)). Cell lysates were prepared on ice, with reagents at ice-cold temperatures and centrifuges pre-cooled to 4°C. The medium surrounding the cells was aspirated, and the cells were washed. Cells were displaced from culture flasks using a cell scraper and then centrifuged 10,000 RPM for 5 minutes. The pellet was washed with PBS and re-suspended in 500 µL lysis buffer, placed on a shaker for 30 minutes, and centrifuged again for 5 minutes at 10,000 rpm. The supernatant was kept and analysed for protein content.

2.9.3 Protein determination

To quantify the amount of protein in cell lysates, a protein assay kit involving bicinchoninic acid (BCA) was used in a 96-well plate format with 10 µL Bovine serum albumin (BSA) standard and 2 µL samples in duplicates. The BCA reagent was prepared by adding 4% copper (II) sulphate to BCA at a ratio of 1:50. BCA reagent was added to each well of the plate and incubated at 37°C for 30 minutes, during which time a change of colour took place. Absorbance values were obtained by reading the plate at 562 nm on either the OPTIMA or FLEXSTATION plate readers. Protein concentration in the lysates was calculated

by reference to a standard curve obtained by adding the BCA mix to wells in the 96-well plate that contained a range of BSA Concentrations (0, 0.025, 0.125, 0.5, 0.75, 1, 1.5 and 2 mg/mL).

2.9.4 Gel Electrophoresis

Pre-cast gels were used to resolve proteins within the cell lysates. The gels used were 4-12% Bis-Tris (NuPAGE) or 4-20% Tris-glycine (NOVEX). To prepare for Western blotting, cell lysates (1µg/µL in 15µL) were diluted in 4x NuPAGE LDS (for Bis-Tris gels) or Laemmli sample buffer (for Tris-glycine gels) and heated to 75°C for 5 minutes. The comb associated with the pre-cast gels was removed, and the wells were washed to remove any bubbles or residue. The electrophoresis chamber was filled with running buffer (or MES 20x for Bis-Tris gels; NOVEX) and the heated samples were loaded onto wells alongside molecular weight protein standards (Novex Sharp Pre-stained protein standard, Thermofisher). Once assembled in the electrophoresis system (Invitrogen), gels were subjected to 125 - 180 V until the sample buffer had reached the bottom of the gel.

2.9.5 Transferring proteins from the gel to membranes for staining

Gels were carefully removed from their associated glass plates. The proteins within the gels were subsequently transferred to either Immobilon-P polyvinylidine difluoride (PVDF) or nitrocellulose membranes transfer. The gel and appropriate membrane were sandwiched between sponges and filter papers soaked in transfer buffer. PVDF membranes were soaked in methanol for 15 seconds, followed by dH_20water for 2 minutes, and then pre-soaked along with the sponges in transfer buffer. Nitrocellulose membranes were only briefly soaked in transfer buffer before sandwiching. The sandwich was then placed in a Novex Mini-cell system (Invitrogen). The inner chamber was filled with transfer buffer and the outer chamber with water. Proteins were transferred from gel to membrane by

application of 100 V for 1 hour at 4°C (PVDF) or 30 V for 2.5 hours at room temperature (nitrocellulose).

2.9.6 Immunodetection

Following the transfer step described above, the membranes were stained with Ponceau-S to visualise protein transfer and to ensure equal transfer of samples. The membranes were consequently washed in distilled water, and incubated for 1 hour in blocking buffer at room temperature on a rocking plate. The membranes were then incubated overnight at 4°C in blocking buffer with primary antibody. The primary antibodies used in this study are listed in Table 2.5. The following day, the antibody solution was replaced with TBS-T, and the membrane was placed on a rocking plate for 1 hour at room temperature, with the TBS-T exchanged every 10 minutes. The membranes were then incubated in the appropriate horse radish peroxidase (HRP)-conjugated secondary antibody in TBS-T-milk for 1 hour at room temperature on a rocking plate. This was followed by washes in TBS-T for 1 hour with the TBS-T exchanged every 10 minutes. The secondary antibodies used in this study are listed in Table 2.6. An additional wash was carried out in TBS without tween just before the protein detection step. Finally, the membranes were incubated in enhanced chemiluminescence (ECL) reagent for 2 minutes. Excess reagent was drained before detecting protein bands using a G:BOX gel doc system (Syngene) running Genesys software or ChemiDoc imaging system (BIO-RAD). Analysis was carried out using either ImageJ software or BIO-RAD Image Lab.

Antibody	Supplier	Catalogue number	Source	immunogenic protein/peptide	Dilution
Beclin-1	Santa Cruz	sc-48341	mouse	amino acids 1-300 of BECN1 of human origin	1/500
Calreticulin (CRT)	Abcam	ab92516	rabbit	amino acid sequence is in the first 100.	1/1000
GAPDH	Sigma	G8795	mouse	full length from rabbit GAPDH	1/50,000
LC3	Nanotools	0231-100/ LC3-5F10	mouse	peptide conjugated to hemocyanin. epitope: N-terminus of LC3-B.	1/200
MCU	Sigma	HPA016480	rabbit	Coiled-coil domain-containing protein 109A recombinant protein epitope signature tag (PrEST)	1/200
P62	CST	5114	rabbit	the epitope surrounding Gly410 is ~10-20 amino acids long	1/10,000
SERCA2	CST	9580	rabbit	residues near the amino terminus of human ATP2A2/SERCA2	1/500

Table 2.5. *Primary antibodies used in Western blotting.*

Antibody	Supplier	Catalogue number	Source	Dilution
peroxidase-conjugated anti-mouse IgG	Thermo Fisher	R-21455	Rabbit	1/2500
peroxidase-conjugated anti-rabbit IgG	abcam	ab6721	Goat	1/5000

Table 2.6. *Secondary antibodies used in Western blotting.*

2.10 Calcium recording

2.10.1 Solutions used

Complete imaging medium and starvation medium

During the experiments described in this study, cells were either maintained in culture medium in a cell culture incubator (i.e. humidified environment with 5% CO_2 at 37°C), or when they were removed from the incubator, cells were superfused with an extracellular solution based on a formulation that has been used in my lab for a number of years [329].

'Complete imaging medium' was designed to support the long-term survival of cells outside the cell culture incubator, whilst ensuring that autophagy was not activated. Complete imaging medium contained 121 mM NaCl, 5.4 mM KCl, 0.8 mM $MgCl_2$, 1.8 mM $CaCl_2$, 6 mM $NaHC0_3$, 5.5 mM D-Glucose, 25 mM Hepes (adjusted to pH 7.35 using 5 M NaOH), plus nutrients (10 % FBS, 2 mM L-glutamine, 1 x amino acids, 1 mM sodium pyruvate). As shown in the *Results*, the omission of these nutrients caused the activation of autophagy. In which case, this solution was denoted 'starvation medium'. It is important to note that each cell line required different types of amino acids in the complete imaging medium. For example, non-essential amino acids were used for HeLa cells, however HEK cells required both non-essential and essential amino acids (MEM).

Ca^{2+}-free solutions

Where it was necessary, solutions were configured to be Ca^{2+} free by omitting $CaCl_2$ during their preparation, and addition of 1 mM EGTA to chelate contaminating Ca^{2+} from the double distilled water. Care was taken to ensure that the solution was still at pH 7.35 after the addition of EGTA.

2.10.2 Fluorescent calcium dyes

Cytosolic and mitochondrial Ca^{2+} changes were tracked using fluorescent indicator dyes. Fluorescent Ca^{2+} indicators are negatively charged, hydrophilic compounds that cannot easily cross the plasma membrane. To overcome this problem, acetoxymethyl (AM) ester groups are added to mask the negative charges on the carboxyl groups, therefore allowing the molecule to cross the plasma membrane. The AM form of indicators such as Fura-2 is not Ca^{2+} sensitive. Once inside the cell, endogenous esterases cleave the AM ester groups leaving a charged Ca^{2+}-sensitive molecule remaining in the cell. The indicators used in these studies were Fura-2 and Rhod-2. Fura-2 AM was synthesised in 1985 in Professor Roger Tsien's laboratory [330] and has the substantial benefit of being a 'ratiometric indicator'. In essence, the ratiometric capability of Fura-2 was ideal for the long-term imaging experiments presented in this study. Ratiometric measurements account for differences in indicator loading between cells in a field of view, as well as the progressive loss of indicator due to indicator leakage or photobleaching [331]. Rhod-2 AM was also synthesised in Professor Tsien's laboratory [330] and is a single-wavelength indicator that can be used in conjunction with Fura-2 as it has different excitation and emission spectra. Rhod-2 is a cationic molecule and therefore preferentially accumulates with the matrix of actively respiring mitochondria due to the potential difference across the inner mitochondrial membrane. Rhod-2 has been widely used for measurement of mitochondrial Ca^{2+} uptake. Both indicators can be co-loaded into cells, allowing simultaneous recording of the cytosolic and mitochondrial Ca^{2+} concentration.

BAPTA-AM (10 µM), used to chelate intracellular Ca^{2+} (Figure 3.24), was loaded into cells for 1 hour prior to imaging at room temperature.

To prepare cells for imaging experiments, following tryspinisation cells were re-suspended in DMEM and plated onto 16 mm diameter glass coverslips for 48 hours prior to use at 70-80% confluency. Prior to imaging, the 16 mm glass coverslips with adherent cells were mounted in a circular imaging chamber that was designed to fit on the stage of the Leica DMI6000 microscope that was used in these studies. Cells were loaded with either 1 µM Fura-2 AM and/or 5 µM Rhod-2 in complete imaging medium for 30 minutes at room temperature. Subsequently, the Ca^{2+} indicator was aspirated, and the cells were superfused with fresh complete imaging medium and left for another 30 minutes to allow the ester groups on the fluorescent indicator to hydrolyse. Fura-2 stock solutions were made at 1 or 2 mM in DMSO containing 20% F-127 pluronic, aliquoted into single-use aliquots and kept at -20 ˚C. An aliquot was diluted in complete imaging immediately prior to use.

To record Ca^{2+} signals, a field of cells on the coverslip was selected based on an even indicator loading and healthy appearance. A vacuum aspirator was set up in the imaging chamber to facilitate superfusion of the cells with experimental solutions. Imaging parameters such as excitation/emission light wavelength, exposure time, rate of image capture and pixel binning, were set using the Leica proprietary software. At the beginning of every recording, the basal fluorescence of Fura-2- or Rhod-2-loaded cells was recorded for 1 minute (unless otherwise stated in the figure legends) followed by addition experimental treatments (e.g. CPA, ionomycin, etc). A wash off period was sometimes incorporated (where stated in the figure legends) before any agonist additions. Fura-2 was alternately excited at 340 nm and 380 nm wavelengths (ultraviolet filter set), and emitted light >500 nm was recorded. Rhod-2 was excited at 540-552 nm (red filter set), and emitted light was recorded at 580-620 nm. For most experiments a 63x objective oil immersion was used (NA = 1.25). Fluorescence images (464 by 364 pixels) were captured using a 12-bit

DFC360 FX Digital Camera on the Leica DMI6000 light microscope which uses a halogen lamp as a light source.

2.10.3 Analysis of Fura-2 and Rhod-2 recordings

Video recordings were analysed using ImageJ software. Cells were outlined individually, and their raw fluorescence pixel intensity values at both 340 nm and 380 nm excitation were sampled and exported into a Microsoft Excel spreadsheet. A non-cellular area was used to sample the background signals at both the 340 nm and 380 nm excitation wavelengths. The 340 nm/380 nm ratio for each cell was calculated in Excel using the formula:

Ratio = (fluorescence recorded from cell X with 340 nm excitation – background fluorescence at 340 nm excitation)/ (fluorescence recorded from cell X with 380 nm excitation – background fluorescence at 380 nm excitation)

The background-subtracted 340 nm/380 nm ratio was then used in GraphPad Prism to plot graphs, and to calculate outcomes such as the percentage of responding cells, peak response amplitudes and percentage of oscillating cells.

2.11 Measuring autophagy and autophagy vesicles

2.11.1 Solutions used

Complete imaging medium and starvation medium

During the experiments described in this study, cells were either maintained in culture medium in a cell culture incubator (i.e. humidified environment with 5% CO_2 at 37°C), or treated with a complete imaging medium (see section 2.10) at room temperature to ensure that autophagy was not activated. As shown in the *Results*, the omission of nutrients (10 % FBS, 2 mM L-glutamine, 1 x amino acids, 1 mM sodium pyruvate) caused the activation of autophagy. In which case, this solution was denoted ‘starvation medium’. It is important

to note that each cell line required different types of amino acids in the complete imaging medium. For example, non-essential amino acids were used for HeLa cells, however HEK cells required both non-essential and essential amino acids (MEM).

2.11.2 GFP-LC3 punctae quantitation

Prior to use, GFP-LC3 HeLa or HEK cells were seeded on 16 mm coverslips and allowed to adhere and grow for 48 hours in a standard cell culture incubator before use. To visualise GFP-LC3 punctae, the glass coverslips with adherent cells were mounted in the imaging chambers described earlier and placed on the stage of the Leica DMI6000 light microscope. GFP was excited using 450-490 nm light, and emission of 500-550 nm. Autophagosome numbers in all autophagy studies were counted manually or using Image J (using the cell counter plugin or the manual thresholding function) and were from time to time verified in blind fashion by an independent observer. Punctae are dot like structures that are brighter in fluorescence than the overall background of the cell. Punctae were shown to be of similar size across the cells. Punctae were displayed as single dots and aggregations were very rarely seen. Using this criteria, the number of punctae per cell were counted and used a measure for analysing data. Expressing data in this manner is generally the preferred in autophagy research compared to for example “percentage of cells with GFP-LC3 punctae”.

2.11.3 Cyto-ID reagent detection kit

Cyto-ID dye (Enzo Life Sciences), is a cationic amphiphilic tracer fluorophore that was used in this study to assess numbers of autophagic vesicles in situations where GFP-LC3 expression was not appropriate (e.g. with MEF cells). The protocol was followed as per the manufacturer’s instructions. In summary, cells were exposed to various treatments then washed twice with the assay buffer provided with the Cyto-ID kit. 5% FBS was added to the assay buffer to preserve cells and prevent the induction of autophagy, since autophagic

cells can be easily dislodged during washing. Subsequently, a solution containing Hoechst 33342 Nuclear Stain and the autophagosome-specific Cyto-ID indicator was added to cells for 30 minutes at 37 °C. The cells were then washed with fresh assay buffer before being mounted in an imaging chamber and placed on the stage of the Leica DMI6000 microscope. The Cyto-ID-labelled punctae were visualised using a 63x objective and the same experimental settings as described earlier for imaging GFP-LC3-labelled punctae.

2.11.4 RFP-GFP-LC3 HeLa cells

The RFP-GFP-LC3 tandem reporter was used to assess autophagic flux where autophagosomes are evident as punctae with both green and red emission (from GFP and RFP, respectively), and autolysosomes are evident as punctae solely with red emission (from RFP only). The RFP-GFP-LC3-expressing cells were imaged using the Leica DMI6000 light microscope using the 63x objective using similar conditions to those employed for monitoring GFP-LC3, but with the addition that RFP was simultaneously monitored. RFP was excited using 590-650nm light, and the emitted light >660 nm was recorded.

2.11.5 Electron microscopy

2.11.5.1 Solutions used:

0.2 M Sörenson's phosphate buffer: 18 mM NaH_2PO_4, and 82 mM Na_2HPO_4 (pH7.4).

Transmission electron microscopy was used to study the structure and size of autophagic vesicles in HEK cells. First, HEK cells were seeded into the top of transwell inserts (1 cm^2, Corning Costar) in a 12-well plate. The transwell system consists of a top chamber containing porous membrane (pores of 0.4 μm) on which cells grow, and is filled with 0.5 mL of cell culture medium, and a bottom chamber that contains 1.5 mL of PBS. The cells were seeded at a density of 100,000 cells per insert and incubated for 2 days in a standard

cell culture incubator (37°C with 5% CO_2). Transwell inserts were coated with laminin before seeding HEK cells.

Following cell incubation, the liquids from both parts of the transwell were removed and the cells were washed three times using Hanks' balanced salt solution (Sigma). The cells were then fixed by application of a 2.5% glutaraldehyde solution for 1 hour at room temperature. The fixative was removed by washing the filter three times with 0.1 M Sörenson's phosphate buffer (PB) and stored in this buffer at 4°C. Samples were then processed by Drs Igor Kraev and Radka Gromnikova in The Open University's electron microscopy facility. The processing included post-fixation, dehydration and embedding in resin. Cultures were post-fixed in a solution containing 1% osmium tetroxide and 1.5% ferricyanide (to enhance membrane labelling) in 0.1 M PB for 1 hour. They were then washed three times in 0.1 M PB. The membrane of the transwell insert that contained cells was removed and dehydrated in series of ethanol solutions as follows: 30% ethanol for 5 minutes, 50% for 5 minutes, 70% for 10 minutes, 100% for 10 minutes twice, and 100% ethanol with a molecular sieve (type 3A, Sigma) for 10 minutes. The molecular sieve dehydrates ethanol since atmospheric water absorbed when the ethanol bottle is open can decrease the percentage of ethanol. The membranes were then incubated in a mixture of 100% ethanol and epon resin in 1: 1 ratio overnight. After that, the membranes were embedded in epon resin and formed blocks were polymerized at 60°C for 48 hours. The blocks were then microsectioned at 80 nm thickness with a diamond knife (Diatome). The sections were mounted onto pioloform-coated copper grids and counter stained in 3.5% uranyl acetate and lead citrate. The grids were imaged using a transmission electron microscope JEM 1010 (Jeol, Japan) Using an 80 kV electron beam gun for excitation and a spot size of 2 µm. A XR40 camera (Advance microscopy techniques; AMT, Woburn, MA,

USA) was used for capturing images and the software used for capturing images was AMT Image Capture Engine (AMT, Woburn, MA, USA).

2.12 Analysis of cell cycle progression

HEK cells were seeded in 12-well plates, and transiently transfected with DNA constructs as described in the *Results*. The positive control for cell cycle arrest (G2-M arrest) was nocodazole (100 nM for 12 hours). 24 hours post transfection, the medium surrounding the cells was aspirated, and the cells were fixed using a 4% paraformaldehyde (PFA) solution for 30 mins at room temperature. The cells were then scraped, centrifuged and washed with PBS. A mix of RNAse A (10 µg/mL), 0.1 % Triton X-100 and propidium Iodide (1 µg/mL) was added to the cells and incubated for 30 minutes in the dark. Subsequently, 25 µL of the cell solution was aliquoted into the slots on slides compatible with a Tali cytometer (Invitrogen). Data analysis was performed on the cytometer itself, firstly by gating debris and aggregates out of the analysis by setting the correct size of HEK cells (5 - 20 µm). Threshold gates were set for each phase of the cell cycle using the untreated sample (normal cell cycle histogram) and these settings were held constant across treated samples and the Relative fluorescence units (RFU) were displayed with their corresponding numbers and percentages of cells for each phase of the cell cycle. The data were analysed with a Two-way ANOVA using Tukey's post-hoc multiple comparisons test. A P value < 0.05 was considered as the threshold for statistical significance.

Chapter 3: Validating autophagic flux measurements using HeLa and HEK cell lines, and examining the necessity of cellular Ca^{2+} signalling for autophagy.

3.1 Introduction

Over the past decades there has been extensive research focusing on understanding the causes and mechanisms underlying autophagy, such as the discovery of evolutionarily-conserved genes that regulate autophagy. Numerous techniques have been established to monitor dynamic autophagic flux, and to modulate it at various stages in order to understand its function and regulation [225]. The first methods in autophagy research (dating back to the 1950s) largely involved the use of electron microscopy [152]. Autophagosomes could be identified using this technique due to their obvious double membrane. However, this is not the case with autolysosomes, which are delimited by a single membrane (as described in detail in *Chapter 1: Introduction)*. The use of fluorescence microscopy, enzyme assays and Western blotting and, molecular tools such as expression of fluorescently-tagged proteins and organelle markers, as well as techniques for preventing expression of particular proteins have increasingly been used to complement electron microscopy studies. Many of these techniques have the added advantage that they enable the investigation of the process in live cells [152, 332].

A common approach for studying the induction of autophagy is to monitor the formation of autophagosomes by following the coalescence of GFP-tagged LC3 (GFP-LC3). GFP-tagged LC3 shows a largely diffuse distribution in resting cells, with a few brightly fluorescent spots (‘punctae’), which range from ~0.5 to ~1.5 µm in diameter. These punctae reflect LC3 molecules coupling with the nascent phagophore and autophagosomal vesicles [333]. The few GFP-LC3 punctae in resting cells reflect a constitutive basal level of autophagy, whereas the number of GFP-LC3 punctae increases upon induction of autophagy [152]. Counting the

number of punctae can provide a quantitative assay for autophagic induction providing that certain control experiments are performed to ensure that autophagic flux, and not a blockage of vesicle processing, is being measured [334].

The studies described here used HeLa and HEK cell lines that stably express GFP-LC3, in addition to other cell lines when required. Both HeLa and HEK cells were employed in this study in order to establish whether the responses seen were somewhat generic, or whether there was a cell type-dependence to the relationship between Ca^{2+} signalling and autophagy. Since the published literature describing the regulation of autophagy by Ca^{2+} is contradictory in places, it was considered that using two independent cell lines might help establish some consistent mechanisms. HeLa cells are ideal for this project because they are well understood from the perspective of Ca^{2+} signalling [335], they have highly reproducible responses to various agonists, and they can be readily transfected using standard cationic lipid reagents [336]. HEK cells are widely studied in the autophagy field, they have been widely used for studying various aspects of Ca^{2+} signalling, and they can also be readily transfected [337].

The work presented in this Chapter describes the characterisation of HEK and HeLa cells as tools to study the regulation of autophagy by Ca^{2+}. It is essential to characterise the robustness of the cellular systems that were going be used in order to establish conditions in which the cells could be maintained on a fluorescence imaging microscope whilst ensuring viability, without extruding Ca^{2+} indicators, or triggering unwanted autophagy. The primary goal here was to determine experimental conditions where autophagic flux and cellular Ca^{2+} signals could be measured in real time, whilst analysing both processes simultaneously in the same cells. Moreover, cells can react to prolonged Ca^{2+} signals by remodelling their signalling toolkits [19] triggering stress responses and/or dying [338]. It

was therefore considered that an ideal experimental approach would be one where cells were investigated for a minimal duration whilst still yielding statistically significant outcomes for both autophagy and cellular Ca^{2+} signals. To be able to quantify autophagic flux in response to changes in cellular Ca^{2+} signalling and homeostasis, it was important to establish the response of HEK and HeLa cells to known activators and inhibitors of autophagy. Finally, the data in this chapter examines the necessity of cellular Ca^{2+} signals for triggering of autophagy in different conditions.

3.2 Results

Imaging medium contains Ca^{2+} (complete imaging medium)	**Imaging medium does not contain Ca^{2+} (Ca^{2+}-free medium)**
All figures (Figure 3.1 to 3.24)	none

Table 3.1 *Experiments of Chapter 3 which were carried out in either complete imaging medium or Ca^{2+}-free medium.*

3.2.1 GFP-LC3-expressing HeLa and HEK cells remain viable, and autophagy is not activated in an extracellular medium that mimics their cell culture environment.

Initial experiments sought to establish a medium whereby HeLa and HEK cells could be imaged on the stage of the fluorescence microscope for a prolonged period, but did not undergo cell death, and maintained basal levels of autophagy. Standard culture medium was not suitable for this purpose as it contains phenol red, which would have interfered with fluorescence recordings, and the pH buffering would not have been stable outside the environment of a gassed incubator. Therefore a supporting medium was established, based on standard HEPES-buffered imaging medium (*Chapter 2: Materials and Methods)* compatible with fluorescence imaging [294, 339, 340].

To begin imaging experiments, glass coverslips bearing growing cells were removed from the gassed incubator and the cell culture medium surrounding the cells was replaced with the medium used for imaging experiments. The glass coverslips were then transferred to imaging chambers, and the cells were superfused with fresh HEPES-buffered imaging medium. The solution change was performed as rapidly as possible so that there was no period in which the cellular integrity could be affected (e.g., due to drying out or a pH change), but without causing mechanical damage to the cells. The data presented in Figure 3.1 show that HeLa cells suspended in HEPES-buffered medium supplemented with non-essential amino acids (NEAA), 10% FBS, 2 mM L-glutamine and 1 mM sodium pyruvate (hereafter referred to as 'complete imaging medium') maintained basal levels of GFP-LC3 punctae for up to 4 hours. The GFP-LC3 punctae could be readily quantified by manual counting (*Chapter 2: Materials and Methods)*, and elaborated below. Superfusion of cells with imaging medium that did not contain the supplemented nutrients provoked a significant increase in the number of GFP-LC3 punctae following 1- or 4-hour incubations, consistent with an increase in autophagy.

All four supplements were required to suppress the increase in GFP-LC3 punctae (Figure 3.2). Sodium pyruvate was added to the medium due to its common addition to cell culture medium as an additional source of energy. FBS was also added to the medium, as studies have shown that serum starvation induces autophagy in many cell lines including astrocytes. Reports have shown that L-glutamine deprivation induces autophagy [341, 342] and was therefore added to the complete imaging medium. L-glutamine is a NEAA, which is not present in the NEAA solution used in this study. It was therefore necessary to add L-glutamine to the complete imaging medium. Given that DMEM contains a mixture of non-essential and essential amino acids, we added amino acids to the complete imaging medium to ensure that autophagy was not activated. HeLa cells required addition of NEAA,

whereas HEK cells also required the addition of essential amino acids.Since the purpose of this study was to examine the role of Ca^{2+} signalling in autophagy, no further investigations were made into medium constitution or different supplement combinations. Media in which all four supplements were omitted (hereafter termed 'starvation medium') was used in this study to trigger starvation-induced autophagy.

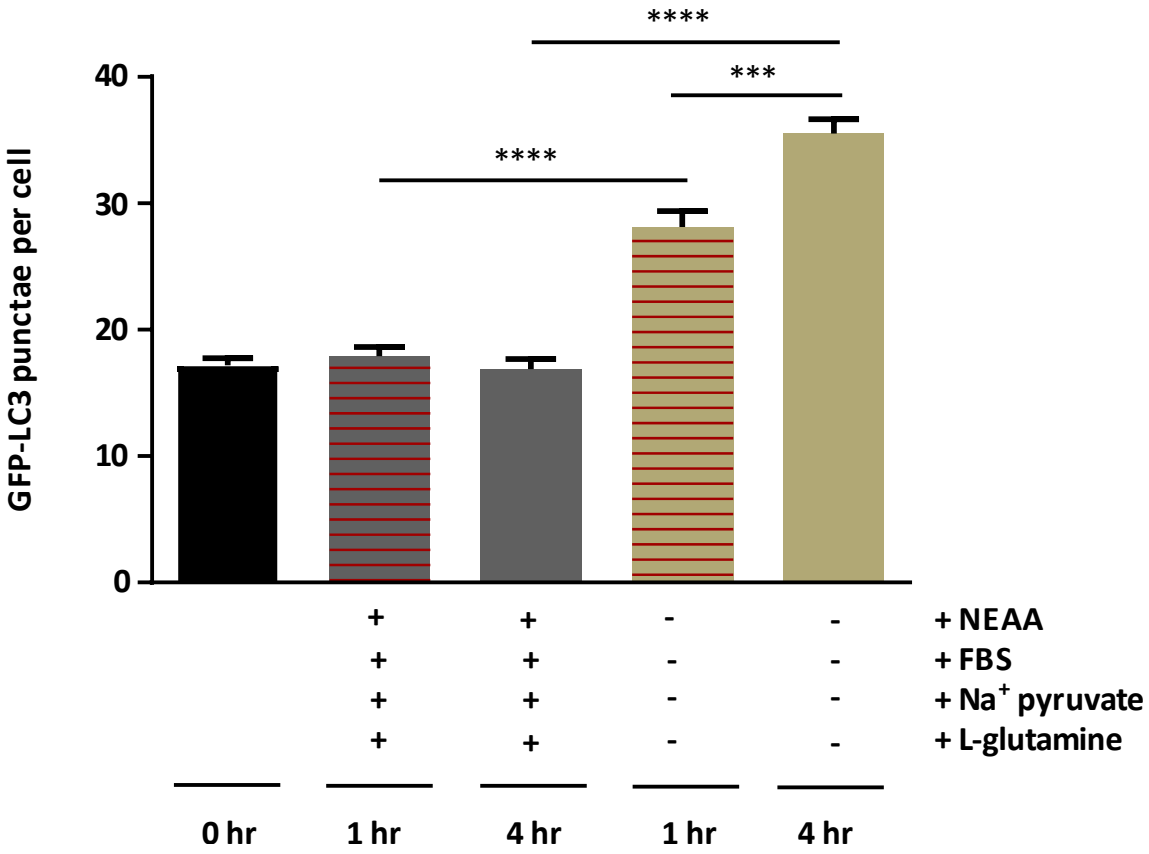

Figure 3.1. The phenol red–free 'complete imaging medium' used for live cell imaging prevented the accumulation of GFP-LC3 punctae. The column graph is a quantitative representation of the effect of the nutrient-replete extracellular medium, which was used in this study, on GFP-LC3 punctae accumulation in HeLa cells. The complete imaging medium is similar to the medium in which the cells were cultured (i.e., containing NEAA, sodium pyruvate, L-glutamine and 10% FBS), but with HEPES and without phenol red. It was critical to this project that the complete imaging medium supported long-term survival of the cells and did not lead to the induction of autophagy. Removing the four nutrients led to elevated numbers of GFP-LC3 punctae in a time–dependent manner. The data are mean ± S.E.M of 3 - 5 experiments (35 - 60 cells per condition). The data were analysed with a one-way ANOVA test. *** indicates $p < 0.001$ and **** indicates $p < 0.0001$.

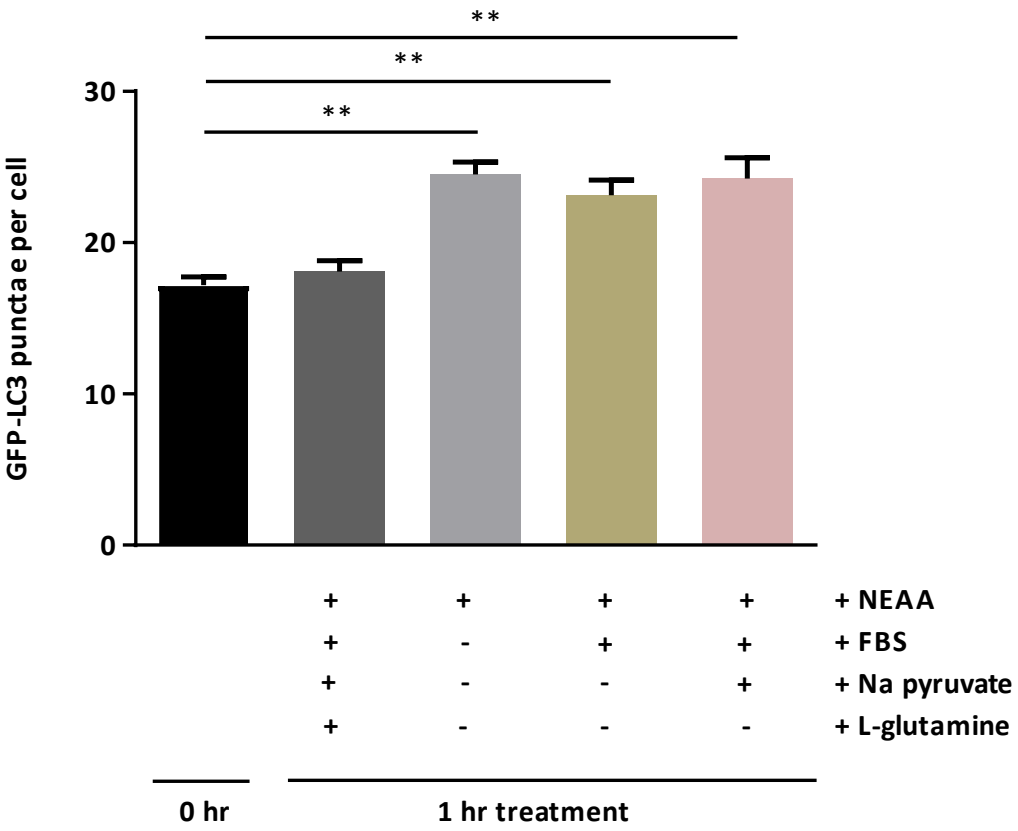

Figure 3.2. Optimisation of the composition of a phenol red–free medium for live cell imaging and to prevent induction of autophagy. The column graph is a quantitative representation of the effect of removing specific nutrients from HeLa cells suspended in a HEPES-buffered phenol red–free medium on GFP-LC3 punctae accumulation in HeLa cells. A nutrient-replete extracellular medium (complete imaging medium; black and dark grey bars), similar to the medium in which the cells were cultured, maintained the basal level of GFP-LC3 punctae. Removing any of the nutrients led to elevated numbers of GFP-LC3 punctae. The data are mean ± S.E.M of 3 experiments (40 - 60 cells per condition). The data were analysed with a one-way ANOVA test. ** indicates $p < 0.01$.

To ensure that the complete imaging medium could suppress the accumulation of GFP-LC3 punctae and maintain cell viability over a longer period of time, and to establish that the 1- and 4-hour time points analysed for the data presented in Figures 3.1 and 3.2 were not nearing the end of cell viability, both HeLa and HEK cells were incubated in the complete imaging medium for 12 hours. As shown by the cell images in Figures 3.3A and 3.4A, there was no obvious deterioration of the cells: they remained firmly attached with no evident morphological changes such as membrane blebbing, which could indicate a loss of viability. In addition, there was no increase in GFP-LC3 punctae accumulation in either cell type following the 12-hour incubation in complete imaging medium (Figures 3.3 and 3.4). These data indicate that the complete imaging medium was able to adequately support the cells' long term nutritional needs, whilst also being compatible with fluorescence imaging.

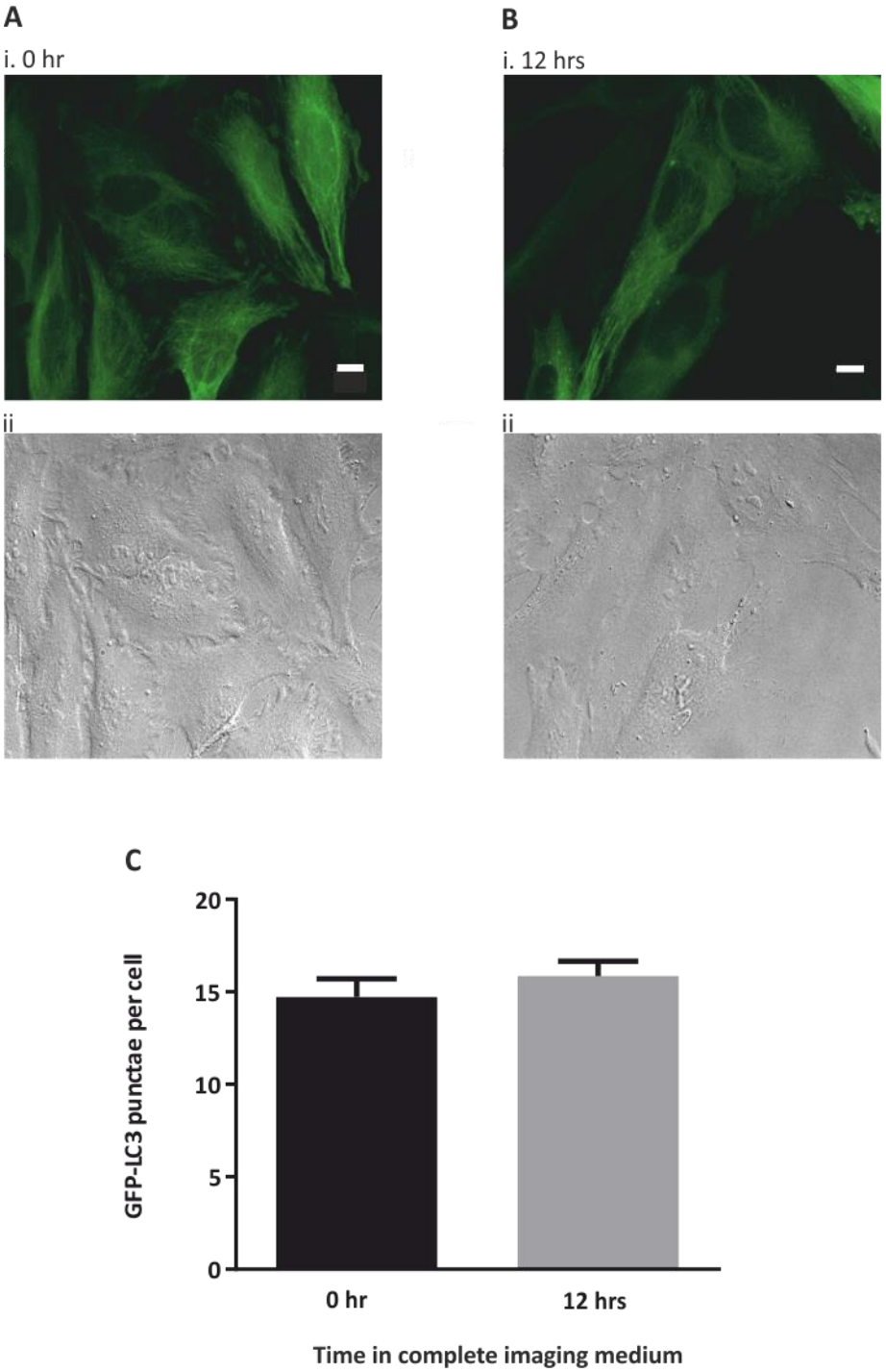

Figure 3.3. Complete imaging medium maintained HeLa cell viability and basal levels of GFP-LC3 punctae for up to 12 hours. Panels A and B show representative images of HeLa cells incubated in complete imaging medium, which contained the same supplements as the usual cell culture environment (i.e., amino acids, sodium pyruvate, L-glutamine and 10% FBS). Panels A and B show GFP-LC3 fluorescence (Ai and Bi) and bright field images (Aii and Bii) of cells at the start of incubation with complete imaging medium, and following a 12-hour incubation, respectively. Similar numbers of GFP-LC3 punctae were observed at both time points. The images in panels Aii and Bii illustrate that the cells appeared comparable in terms of shape, size and attachment. Panel C is a quantitative representation of GFP-LC3 punctae in the cells following incubation with complete imaging medium. The data are mean ± S.E.M of 3 experiments (40 - 45 cells per condition). The data were analysed with an unpaired t-test. The scale bars in Panels A and B represent 10 µm.

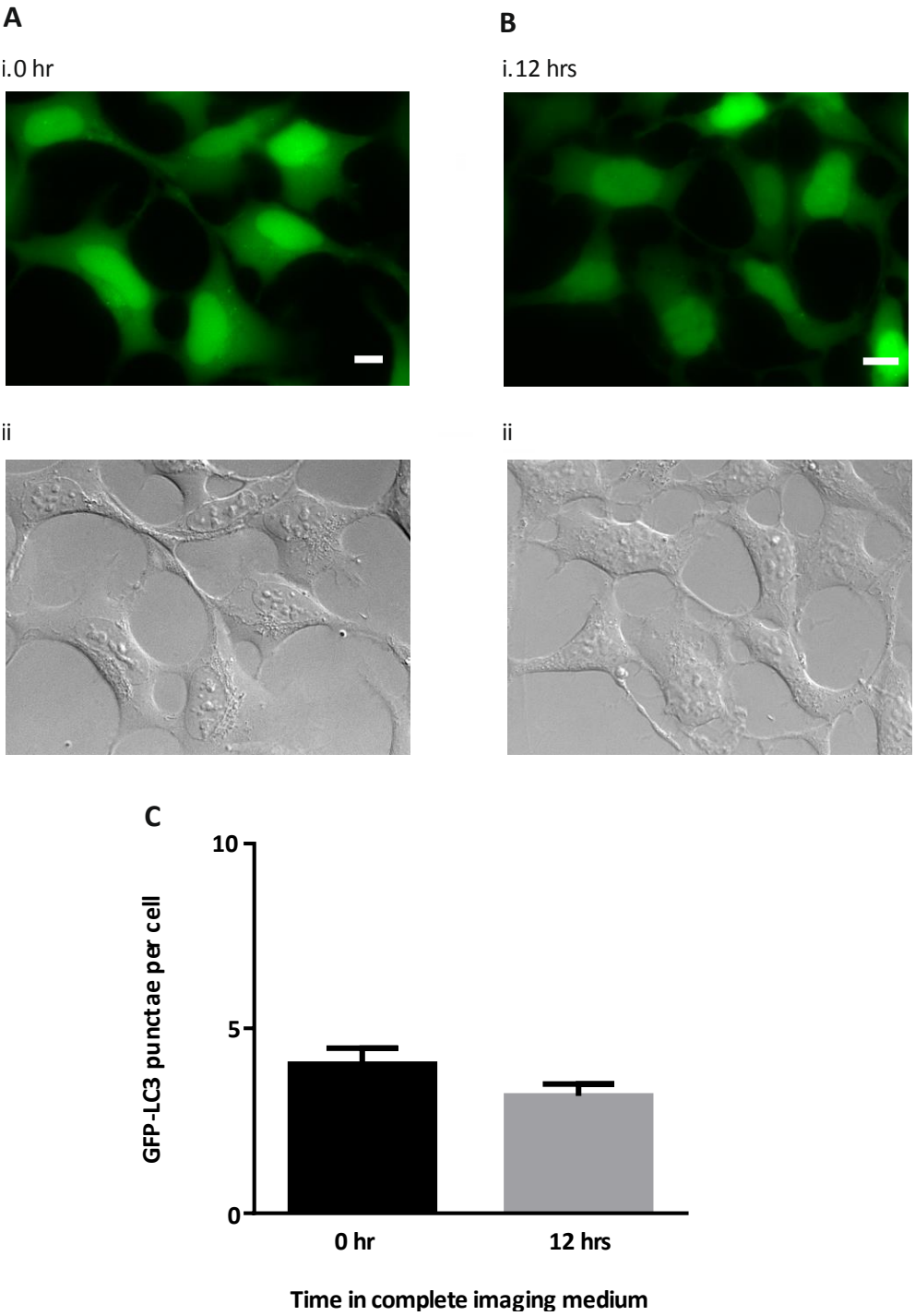

Figure 3.4. Complete imaging medium maintained HEK cell viability and basal levels of GFP-LC3 punctae for up to 12 hours. Panels A and B show representative images of HEK cells incubated in complete imaging medium, which contained the same supplements as the usual cell culture environment (i.e., amino acids, sodium pyruvate, L-glutamine and 10% FBS). Panels A and B show GFP-LC3 fluorescence (Ai and Bi) and bright field images (Aii and Bii) of cells at the start of incubation with complete imaging medium, and following a 12-hour incubation, respectively. Similar numbers of GFP-LC3 punctae were observed at both time points. The images in panels Aii and Bii illustrate that the cells appeared comparable in terms of shape, size and attachment. Panel C is a quantitative representation of GFP-LC3 punctae in the cells following incubation with complete imaging medium. The data are mean ± S.E.M of 3 experiments (50 - 70 cells per condition). The data were analysed with a paired t-test. The scale bars in Panels A and B represent 10 µm.

3.2.2 The induction of autophagy by nutrient starvation

Nutrient starvation is a key physiological stimulus for induction of autophagy [150]. Images of HeLa cells showing an increase of GFP-LC3 punctae following incubation in starvation medium are depicted in Figure 3.5. HEK cells also showed an increase in the number of GFP-LC3 punctae following incubation in a starvation medium (Figure 3.6). However, HEK cells had a lower basal number of GFP-LC3 punctae, a lesser accumulation of punctae following starvation, and reached a maximal punctae accumulation within 1 hour of incubation in starvation medium.

The visualisation of GFP-LC3 punctae is a convenient way to monitor autophagy and is compatible with Ca^{2+} imaging, which also requires recording of fluorescence. Autophagosomes are normally short-lived vesicles that form and undergo degradation within tens of minutes [162]. However, several reports have demonstrated that accumulation of autophagosomes can arise not only from the induction of autophagy, but also from the artificial blockade of autophagic degradation [152, 334]. If autophagic degradation is blocked, GFP-LC3 punctae may progressively accumulate within cells solely due to on-going basal autophagy and the lack of processing of GFP-LC3-labelled autophagosomes, rather than increased levels of autophagy. It is therefore essential to establish that an increased accumulation of GFP-LC3 punctae is due to the induction of new autophagosome formation (i.e., increased 'autophagic flux'), and is not caused by the blockade of autophagic vesicle processing. Application of bafilomycin A1 (BafA1), an inhibitor of vacuolar-type H^+-ATPases that prevents the fusion of autophagosomes with lysosomes, is commonly used for this purpose [343, 344]. In this study, where formation of GFP-LC3 punctae was used to monitor autophagy, it would be expected that BafA1 would cause an increased number of GFP-LC3 punctae under conditions in which there was an

increased autophagic flux. In contrast, if an observed accumulation of GFP-LC3 punctae reflected the blockade of autophagic flux, BafA1 would not be expected to cause any further increase in the number of GFP-LC3 punctae. Importantly, incubation of either HeLa or HEK cells in starvation medium that included BafA1 (0.1 μM) had a greater number of GFP-LC3 punctae compared to cells in starvation medium only (Figures 3.7 and 3.8). These observations support the notion that counting GFP-LC3 punctae can reflect a genuine induction of autophagic flux in both cell types.

Another control experiment that allows genuine autophagy induction to be distinguished from aberrant accumulation of LC3-II is the use of 3-methyladenine (3-MA) [152, 345, 346]. 3-MA inhibits Vps34 (a class III PI3-kinase) and thereby prevents the production of PI3P necessary for forming nascent autophagic vesicles. However, care has to be taken in the use of 3-MA, since long term treatment can trigger autophagy due to its additional inhibition of class I PI3-kinases [228]. In this study, 3-MA was used to confirm that the various treatments caused the accumulation of GFP-LC3 punctae due to the activation of the canonical autophagy pathway. An example of the effect of 3-MA on GFP-LC3 puncta accumulation in HEK cells incubated in starvation medium is shown in Figure 3.9. The inclusion of 3-MA during incubation of the cells in starvation medium suppressed the accumulation of GFP-LC3 punctae (Figure 3.9).

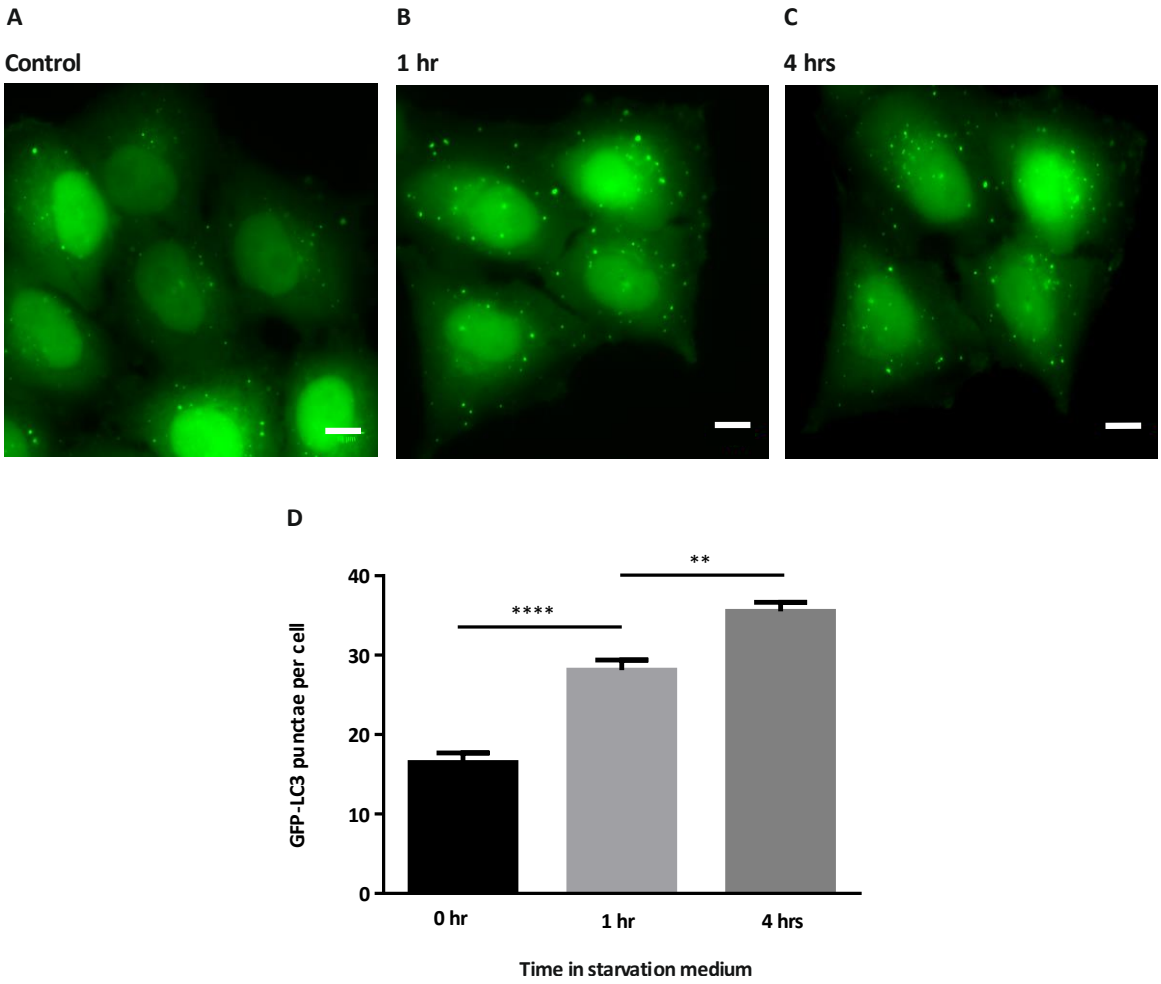

Figure 3.5. Induction of GFP-LC3 accumulation in HeLa cells following incubation in starvation medium. Panel A is a representative image of cells in complete imaging medium. Panels B and C are representative images of cells in starvation medium following a 1- or 4-hour incubation, respectively. The green (GFP-LC3) punctae represent autophagosomes within the cells. Relatively few GFP-LC3 punctae, due to a basal level of autophagy, are visible in A. Whereas, more GFP-LC3 punctae are visible in Panels B and C. Panel D is a quantitative representation of the effect of starvation on autophagy; the number of GFP-LC3 punctae per cell increased progressively with time. The data are mean ± S.E.M of 3 experiments (55 - 90 cells per condition). The data were analysed with a one-way ANOVA test. ** indicates $p < 0.01$ and **** indicates $p < 0.0001$. The scale bars in Panels A-C represent 10 µm.

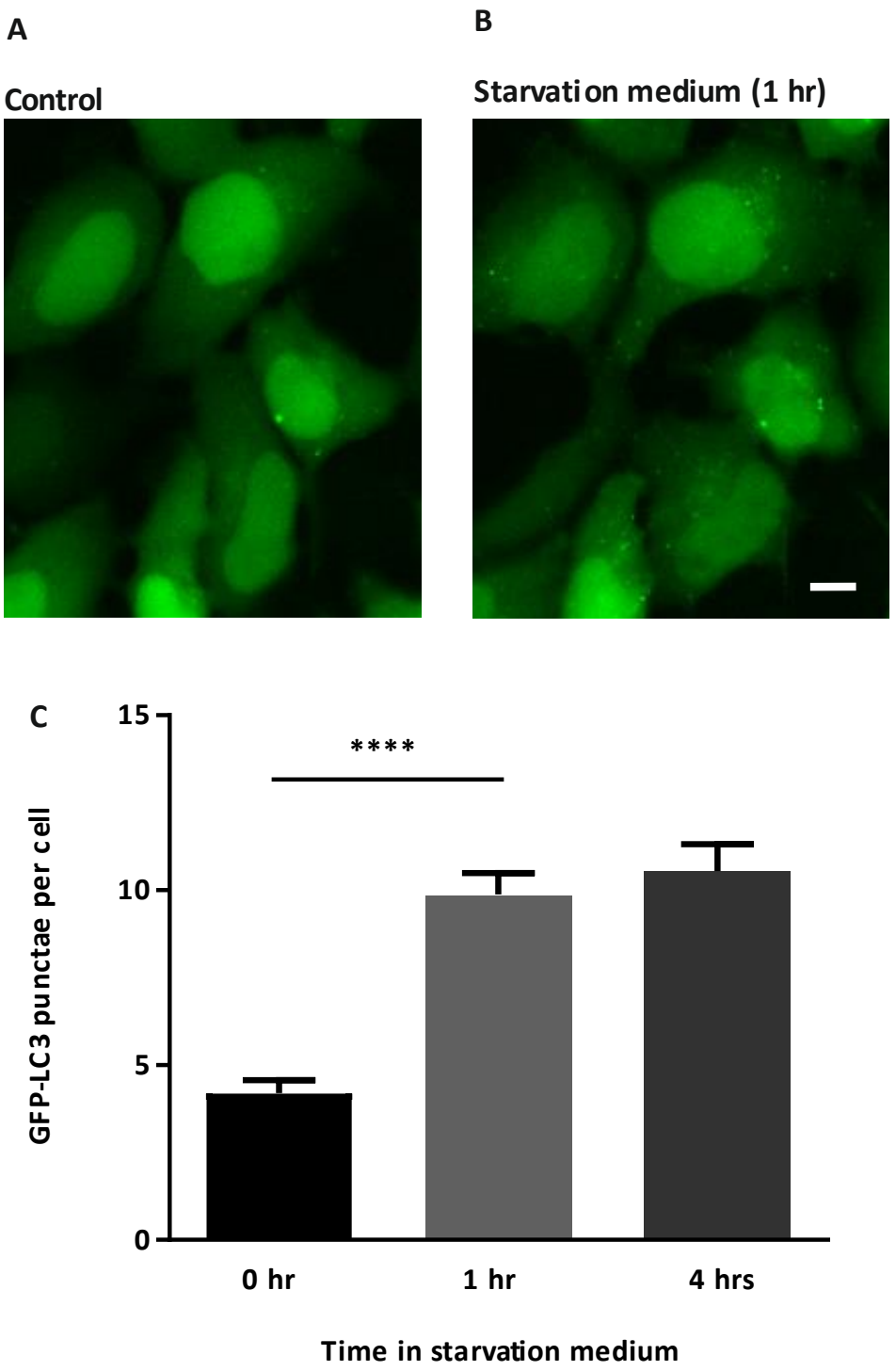

Figure 3.6. Induction of GFP-LC3 punctae accumulation in HEK cells by incubation in starvation medium. Panel A is a representative image of HEK cells maintained in complete imaging medium. Panel B is a representative image of the same cells as in Panel A, but following a 1-hour incubation in starvation medium. Relatively few GFP-LC3 punctae (due to basal autophagy) are visible in Panel A. Greater numbers of punctae are visible in Panel B (following starvation). Panel C is a quantitative representation of the effect of starvation on autophagy. The number of GFP-LC3 punctae per cell significantly increased after 1 hour and remained elevated for a further 3 hours. The data are mean ± S.E.M of 3 - 9 experiments (25 - 60 cells per condition). The data were analysed with a one-way ANOVA test. **** indicates $p < 0.0001$. The scale bar in Panel B indicates 10 µm.

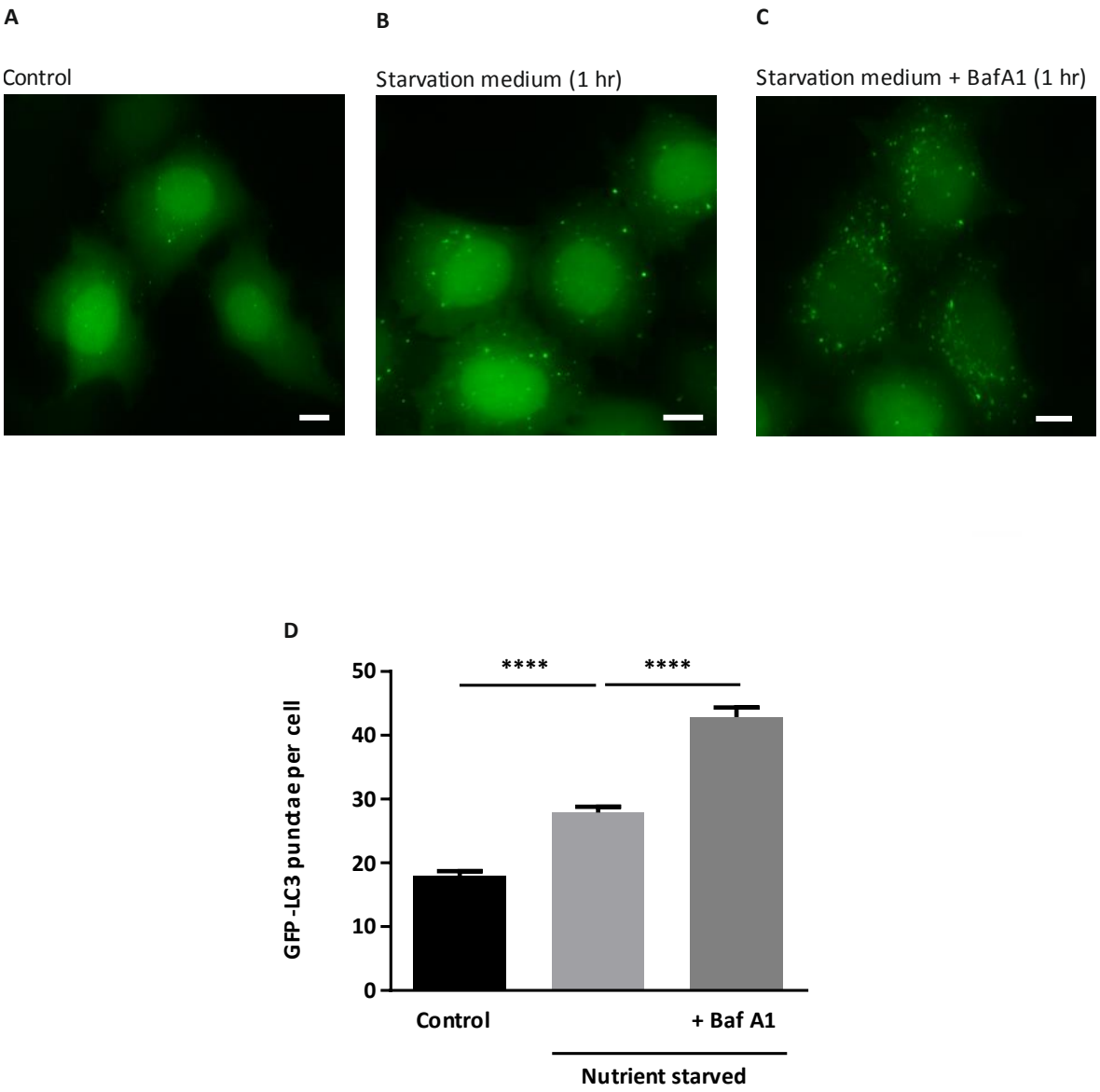

Figure 3.7. Nutrient starvation increased GFP-LC3 punctae accumulation in HeLa cells. Panel A is a representative image of cells in complete imaging medium. Panels B and C are representative images of cells following a 1-hour incubation in starvation medium, in the absence or presence of BafA1 (0.1 µM) respectively. Panel D is a quantitative representation of the effect of nutrient starvation on accumulation of autophagosomes; more GFP-LC3 punctae were observed following starvation, with greater punctae accumulation in the presence of BafA1 indicating that starvation increased autophagic flux. The data are mean ± S.E.M of 3 experiments (55 - 70 cells per condition). The data were analysed with a one-way ANOVA. **** indicates $p < 0.0001$. The scale bars in Panels A - C indicate 10 µm.

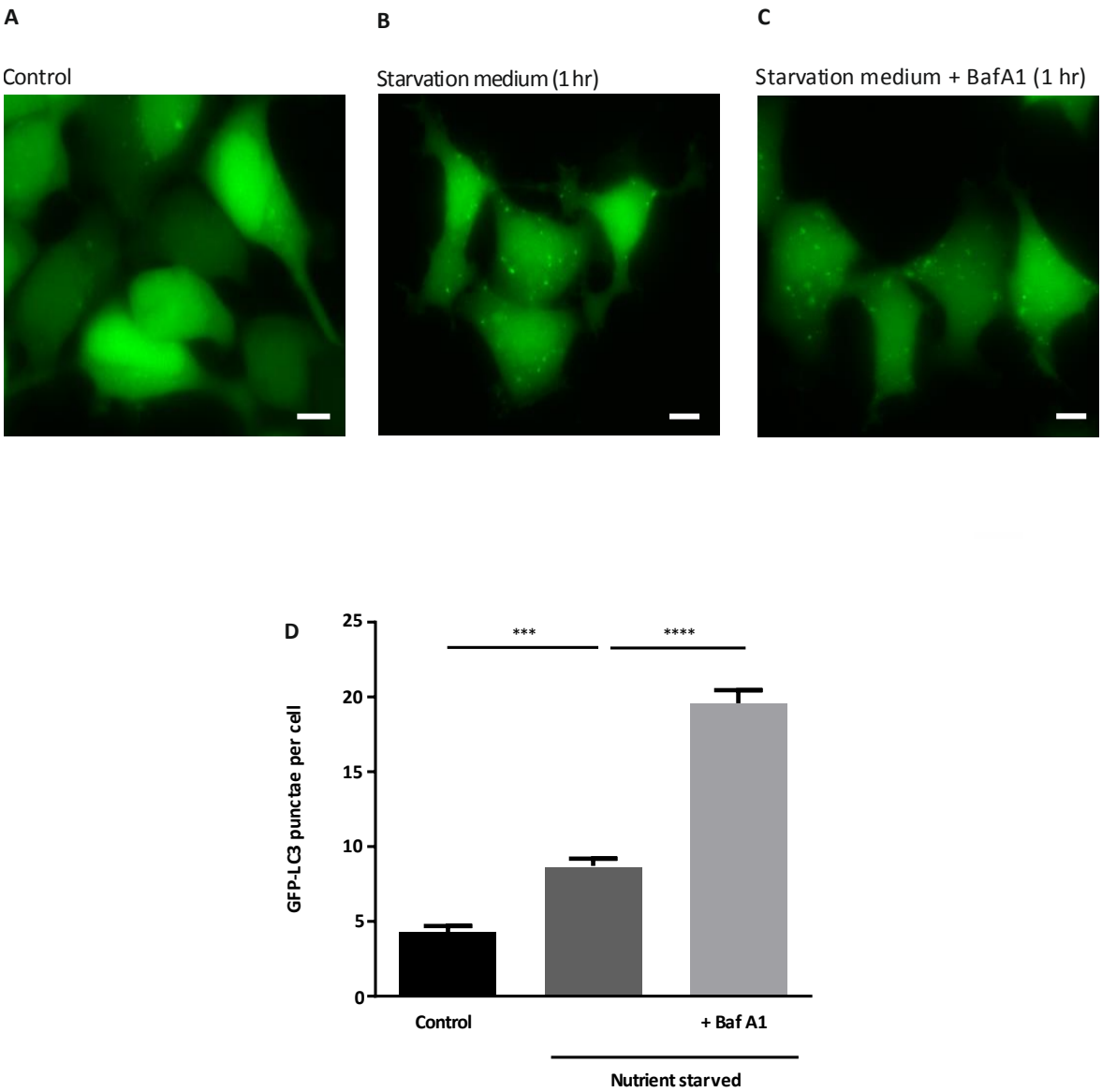

Figure 3.8. Nutrient starvation increased GFP-LC3 punctae accumulation in HEK cells. Panel A is a representative image of cells in complete imaging medium. Panels (B) and C are representative images of cells following a 1-hour incubation in starvation medium, in the absence or presence of BafA1 (0.1 µM) respectively. Panel D is a quantitative representation of the effect of nutrient starvation on accumulation of autophagosomes; more GFP-LC3 punctae were observed following starvation, with greater punctae accumulation in the presence of BafA1 indicating that starvation had increased autophagic flux. The data are mean ± S.E.M of 3 experiments (50-70 cells per condition). The data were analysed with a one-way ANOVA. *** indicates $p < 0.001$ and **** indicates $p < 0.0001$. The scale bars in panels A - C indicate 10 µm.

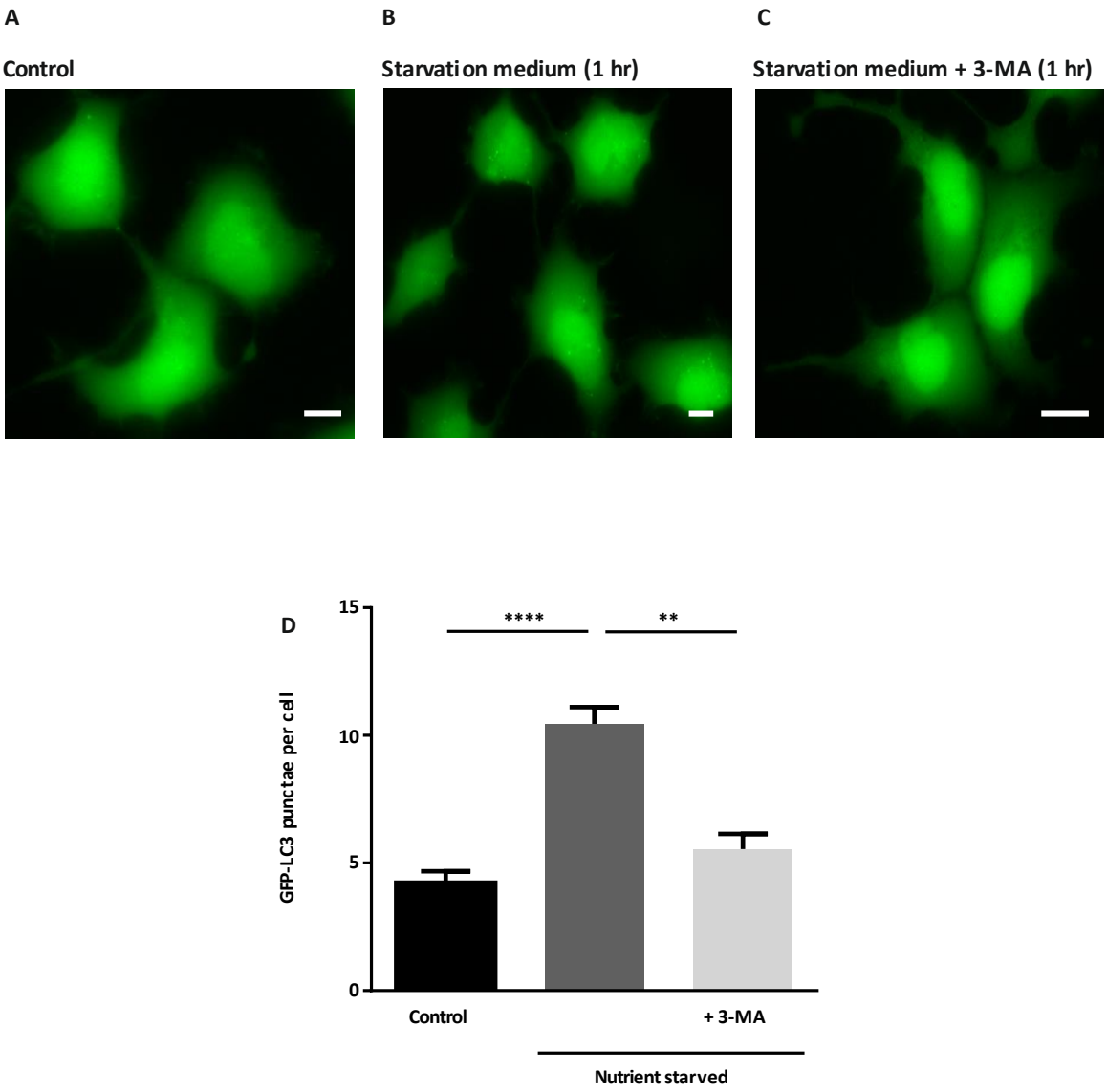

Figure 3.9. 3-MA, an inhibitor of class III PI3-kinase, inhibited induction of GFP-LC3 punctae accumulation by nutrient starvation in HEK cells. Panels A, B and C are representative images that show cells as follows: A in complete imaging medium, B following a 1-hour incubation in starvation medium, and C following 1-hour incubation in starvation medium supplemented with 3-MA (5 mM). Panel D is a quantitative representation of the effect of nutrient starvation, and nutrient starvation + 3-MA, on autophagy; the number of GFP-LC3 punctae per cell was increased by nutrient starvation, but was suppressed to near basal levels by 3-MA. The data are mean ± S.E.M of 2 - 3 experiments (40 – 50 cells per condition). The data were analysed with a one-way ANOVA. ** indicates $p < 0.01$ and **** indicates $p < 0.0001$. The scale bars in Panels A - C represent 10 µm.

3.2.3 The triggering of autophagy by rapamycin occurred over the same time course as the induction of autophagy by nutrient starvation

In addition to nutrient starvation, a commonly used method of inducing autophagy is application of rapamycin [152, 347, 348]. Rapamycin is an antifungal agent that inhibits the mechanistic target of rapamycin (mTOR) [349, 350]. Since rapamycin is a well-known activator of autophagy, it was used in this study to verify that the accumulation of GFP-LC3 punctae within the HeLa and HEK cells represented an autophagic response. In addition, rapamycin was used as a positive control to establish that cells were viable and displayed increased autophagy before carrying out various experimental conditions on the same day. Initial experiments determined the optimal rapamycin concentration and incubation time to use for inducing autophagy in HeLa and HEK cells.

Addition of rapamycin to cells maintained in complete imaging medium triggered the accumulation of GFP-LC3 punctae (Figure 3.10). Similar to the effect of nutrient starvation, rapamycin induced an increase in GFP-LC3 punctae over 1 to 4 hours. As shown in Figure 3.10, an increase in GFP-LC3 punctae was observed following incubation of cells with 0.1 and 1 μM rapamycin, with more GFP-LC3 punctae being evident at the higher rapamycin concentration. These data indicate that rapamycin induced GFP-LC3 punctae accumulation in a time- and concentration-dependent manner.

As described in *Chapter1: Introduction*, LC3 (or LC3-I) is a cytosolic protein that is converted to LC3-II prior to membrane association, and is upregulated on induction of autophagy. Although sometimes difficult to interpret [225], Western blotting of LC-I and LC3-II has been used in many studies to assess activation of autophagy. Autophagic responses can typically be validate by calculating either the ratio of LC3-I to LC3-II, or the ratio of LC3-II to an endogenous protein such as GAPDH [215]. Western blotting experiments were

therefore carried out to determine LC3 protein modification following treatment of cells with rapamycin (1 μM, 1 hour) (Figure 3.10B). Rapamycin treatment caused an increase of LC3-II compared to the control levels.

Similarly to nutrient starvation, the addition of rapamycin in the presence of BafA1 (0.1 μM) caused a greater number of GFP-LC3 punctae per cell compared to treatment with rapamycin only (Figure 3.11). The effect of BafA1 supports the idea that rapamycin induced an increase in autophagic flux. Moreover, addition of 3-MA during the incubation of cells with rapamycin significantly reduced the increase in GFP-LC3 punctae accumulation in both HeLa and HEK cells (Figures 3.12 and 3.13).

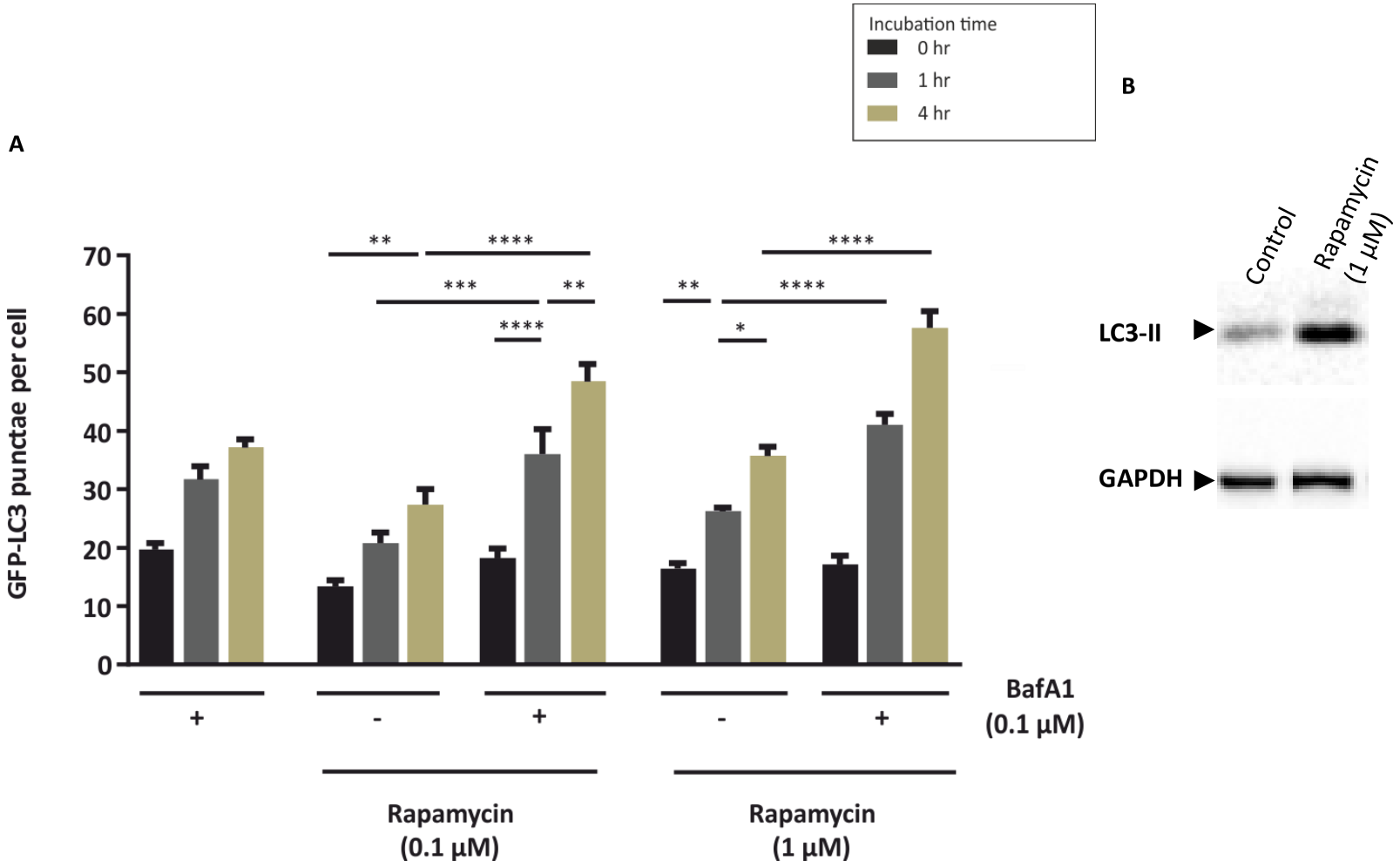
A
Incubation time
0 hr
1 hr
4 hr
GFP-LC3 punctae per cell
70
60
50
40
30
20
10
0
**
****
***
**
****
**
****
*
****
+
-
+
-
+
BafA1
(0.1 µM)
Rapamycin
(0.1 µM)
Rapamycin
(1 µM)
B
Control
Rapamycin
(1 µM)
LC3-II
GAPDH

Figure 3.10. Rapamycin (an inhibitor of mTOR) stimulated GFP-LC3 punctae accumulation in a time- and concentration-dependent manner in HeLa cells maintained in complete imaging medium. Panel A shows a quantitative representation of the effect of rapamycin concentration, and incubation time, on GFP-LC3 punctae accumulation; rapamycin causes a progressive increase in GFP-LC3 punctae accumulation in a time- and concentration-dependent manner. Greater GFP-LC3 punctae accumulation was obtained in the presence of BafA1, indicating an increased autophagic flux. The data are mean ± S.E.M of 3 - 5 experiments (30 - 70 cells per condition). The data were analysed with a one-way ANOVA test. * indicates $p < 0.05$, ** indicates $p < 0.01$, *** indicates $p < 0.001$ and **** indicates $p < 0.0001$. Panel B shows a Western blot for LC3-II protein in lysates from rapamycin-treated (1 hour incubation with 1 µM rapamycin), or untreated cells. GAPDH was used as a loading control (n = 1).

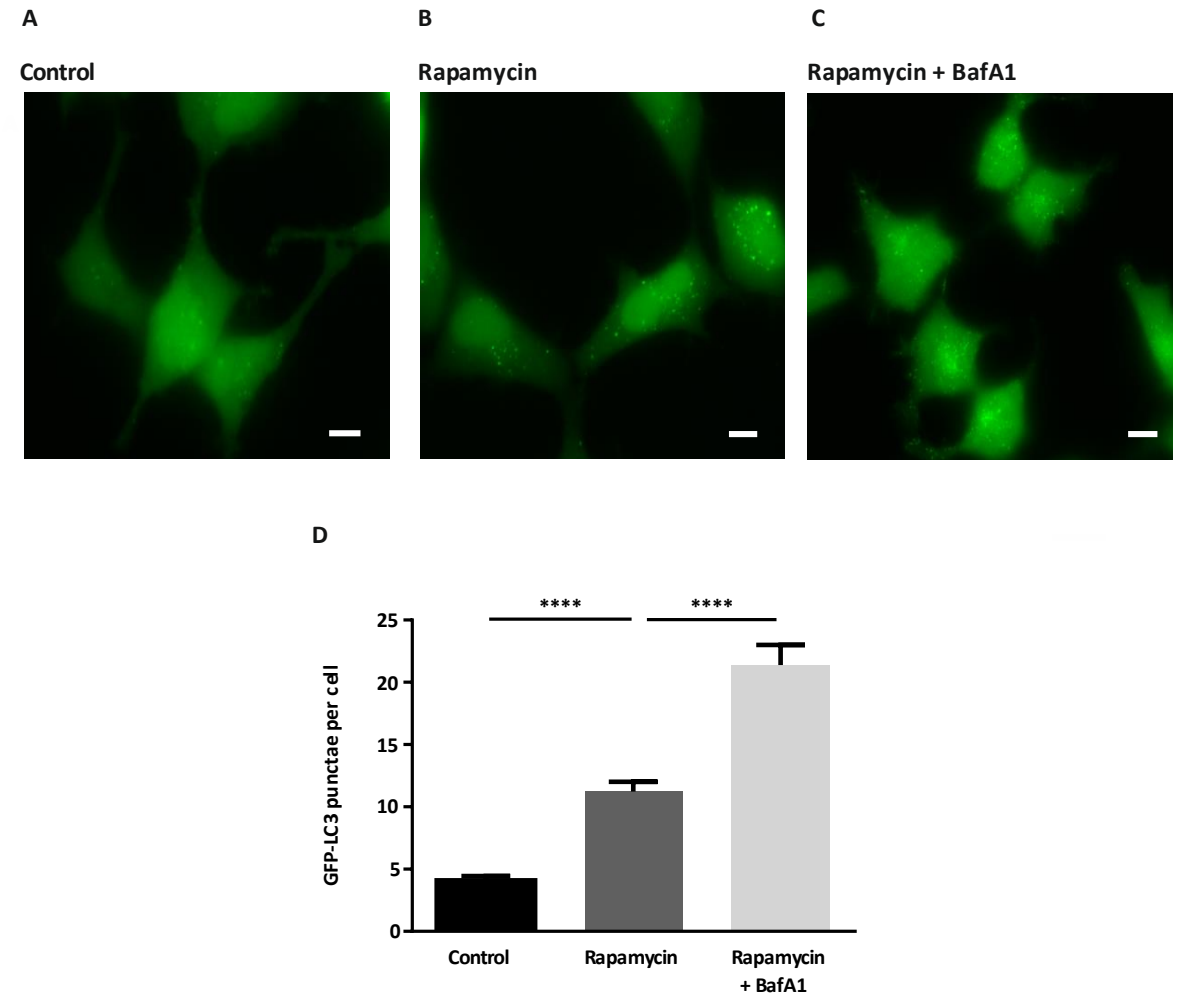

Figure 3.11. Rapamycin stimulated GFP-LC3 punctae accumulation in HEK cells. Panel A is a representative image of cells in complete imaging medium. Panels B and C are representative images of cells in complete imaging medium following a 1-hour incubation with rapamycin (2 µM) in the absence, or presence, of BafA1; 0.1 µM), respectively. Panel D is a quantitative representation of the effect of rapamycin on GFP-LC3 punctae accumulation; an increase in GFP-LC3 punctae was caused by rapamycin, with greater punctae accumulation in the presence of BafA1. The data are mean ± S.E.M of 3 experiments (45 - 70 cells per condition). The data were analysed with a one-way ANOVA. **** indicates $p < 0.0001$. The scale bars in Panels A - C indicate 10 µm.

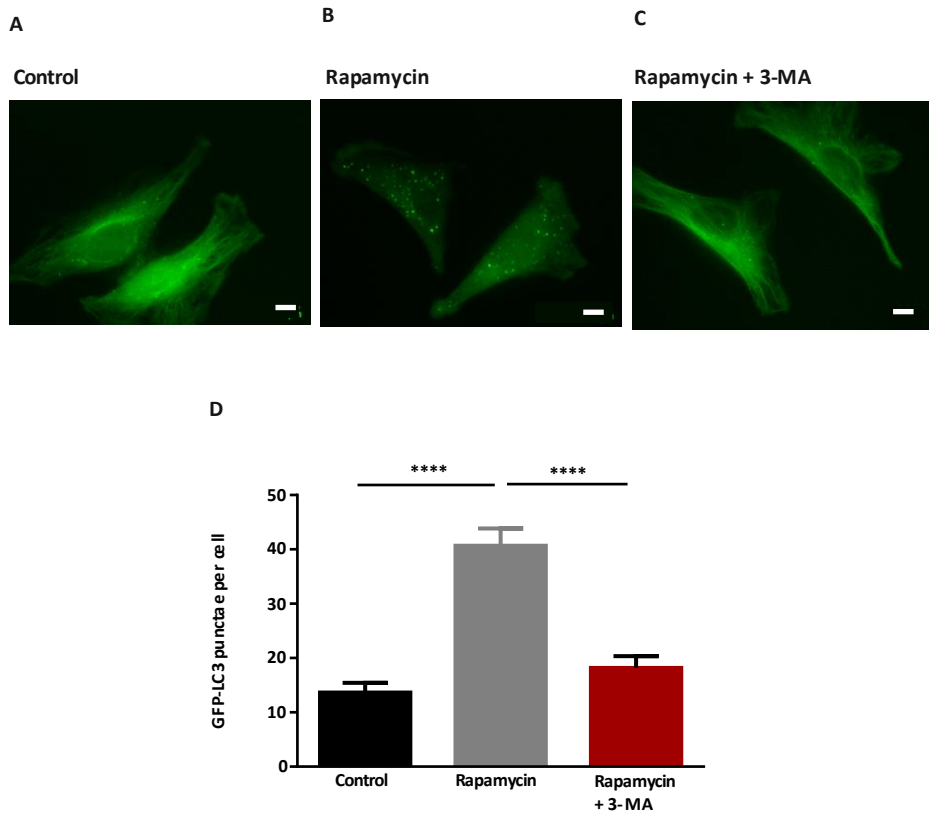

Figure 3.12. 3-MA, an inhibitor of class III PI 3-Kinases, inhibited GFP-LC3 punctae accumulation in HeLa cells. Panels A, B and C are representative images that show: A, the basal level of GFP-LC3 punctae in cells maintained in complete imaging medium, B, elevated levels of GFP-LC3 punctae following a 1-hour incubation with rapamycin (1 µM), and C, low levels of GFP-LC3 punctae following 1-hour treatment with rapamycin (1 µM) and 3-MA (5 mM). Panel D is a quantitative representation of the effect of rapamycin, and rapamycin + 3-MA, on autophagy; the number of GFP-LC3 punctae per cell increased due to addition of rapamycin, but was suppressed to near basal levels by 3-MA. The data are mean ± S.E.M of 3 experiments (25 - 35 cells per condition). The data were analysed with a one-way ANOVA. **** indicates $p < 0.0001$. The scale bars in Panels A - C indicate 10 µm.

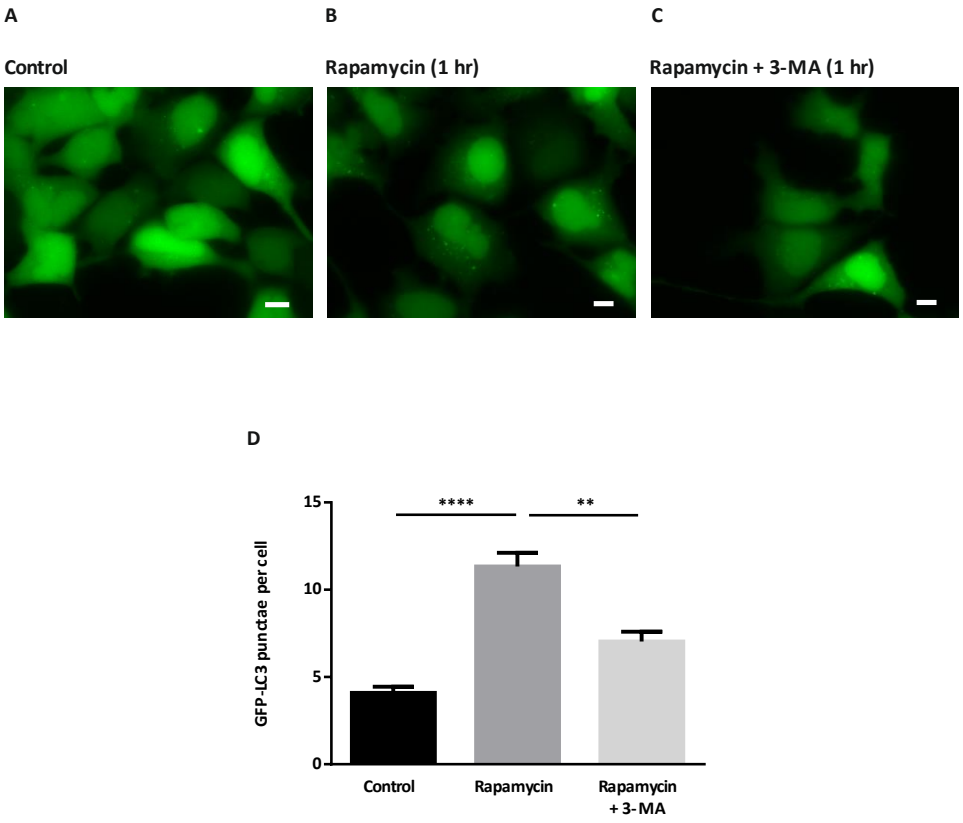

Figure 3.13. 3-MA, an inhibitor of class III PI 3-kinases, inhibited GFP-LC3 punctae accumulation induced by rapamycin in HEK cells. Panels A, B and C are representative images that show cells as follows: A, in complete imaging medium, B, following a 1-hour incubation with rapamycin (2 µM), and C, following 1-hour treatment with rapamycin (2 µM) and 3-MA (5 mM). Panel D is a quantitative representation of the effect of rapamycin, and rapamycin + 3-MA, on GFP-LC3 punctae accumulation; the number of GFP-LC3 punctae per cell was significantly increased by rapamycin alone, but suppressed to near basal levels by 3-MA. The data are mean ± S.E.M of 3 experiments (30-50 cells per condition). The data were analysed with a one-way ANOVA. ** indicates $p < 0.01$ and **** indicates $p < 0.0001$. The scale bars in Panels A - C represent 10 µm.

3.2.4 PP242 (Torkinib), an inhibitor of mTOR, induces autophagy in HeLa cells.

A newer mTOR inhibitor, PP242, was also used as an inducer of autophagy. Consistent with the effect of rapamycin shown above, incubation of HeLa cells in complete imaging medium with PP242 (1 µM, 1 hour) resulted in an increase in GFP-LC3 punctae formation (Figure 3.14).

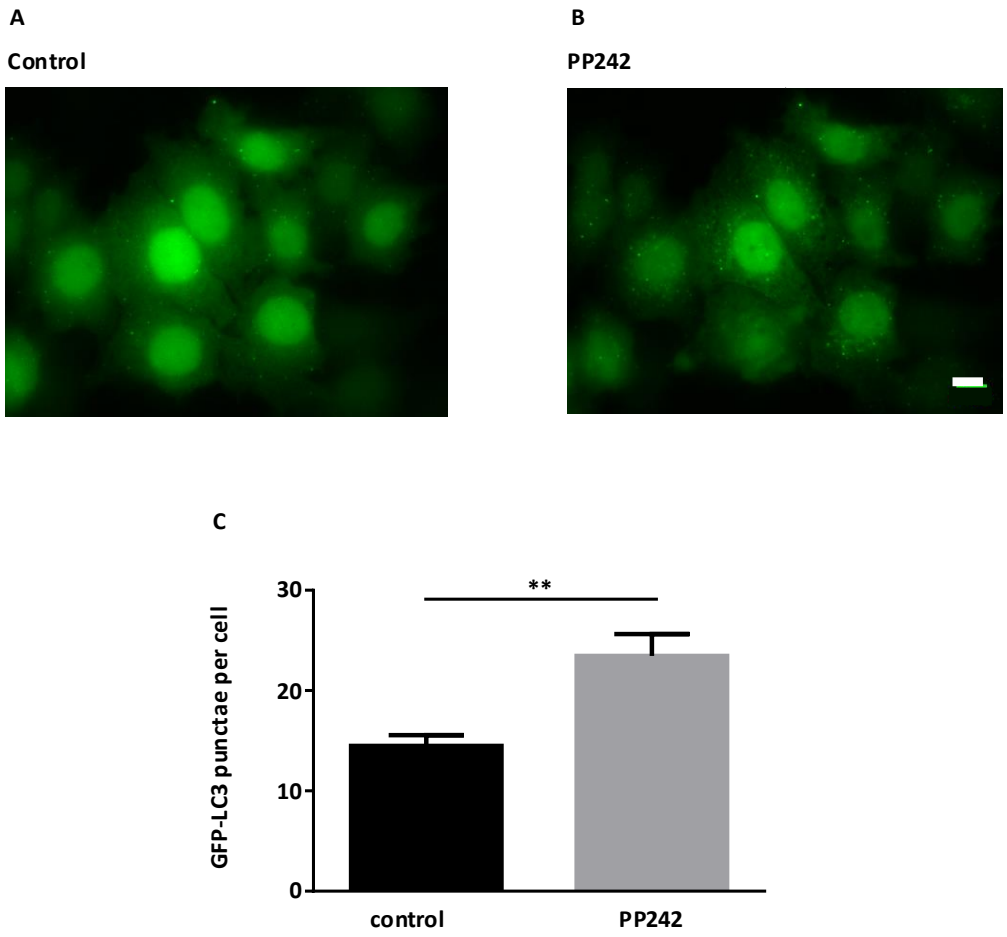

Figure 3.14. Induction of GFP-LC3 punctae accumulation in HeLa cells by the mTOR inhibitor PP242. Panel A is a representative image of cells in complete imaging medium. Panel B is a representative image of cells incubated with PP242 (1 µM) for 1 hour. Panel C is a quantitative representation of the effect of PP242 on GFP-LC3 punctae accumulation. The data are mean ± S.E.M of 3 experiments (30 - 40 cells per condition). The data were analysed with an unpaired t-test. ** indicates $p < 0.01$.

3.2.5 The induction of autophagy in HEK and Hela cells is quantitatively similar at 37°C or room temperature

The bulk of imaging experiments presented in this thesis were performed at room temperature. It is challenging to maintain cells at 37 °C on the stage of an epifluorescence microscope (such as that used here) when solutions are being changed, and because the objective lens is a significant heat sink. Ca^{2+} signals in both HeLa and HEK cells have been extensively characterised at room temperature, and Ca^{2+} indicator dyes (such as Fura-2) are known to be sequestered into organelles or extruded when cells are warmed above room temperature [329, 351, 352]. It was therefore considered that conducting experiments at room temperature would prevent issues observed with temperature changes/gradients and preserve Fura-2 loading. However, it was important to ensure that basal autophagy and the altered accumulation of GFP-LC3 punctae in response to nutrient starvation, rapamycin, BafA1 and 3-MA were not affected by the lower temperature.

The data presented in Figures 3.15 and 3.16 shows results obtained from cells examined on the same day, and using the same experimental solutions, but at either room temperature (approximately 20 – 22°C) or 37°C. Similar numbers of GFP-LC3 punctae were evident in control cells before any experimental manipulations at either temperature. Incubation of cells in starvation medium or with rapamycin, caused a comparable increase of GFP-LC3 punctae in cells maintained at room temperature or 37°C. Moreover, BafA1 augmented the number of GFP-LC3 punctae observed during incubation of cells with rapamycin, whilst 3-MA prevented an increase in GFP-LC3 punctae number at either temperature. These observations indicate that the induction of autophagy by pharmacological or physiological means, and the actions of BafA1 and 3-MA, are similar at room temperature or 37°C.

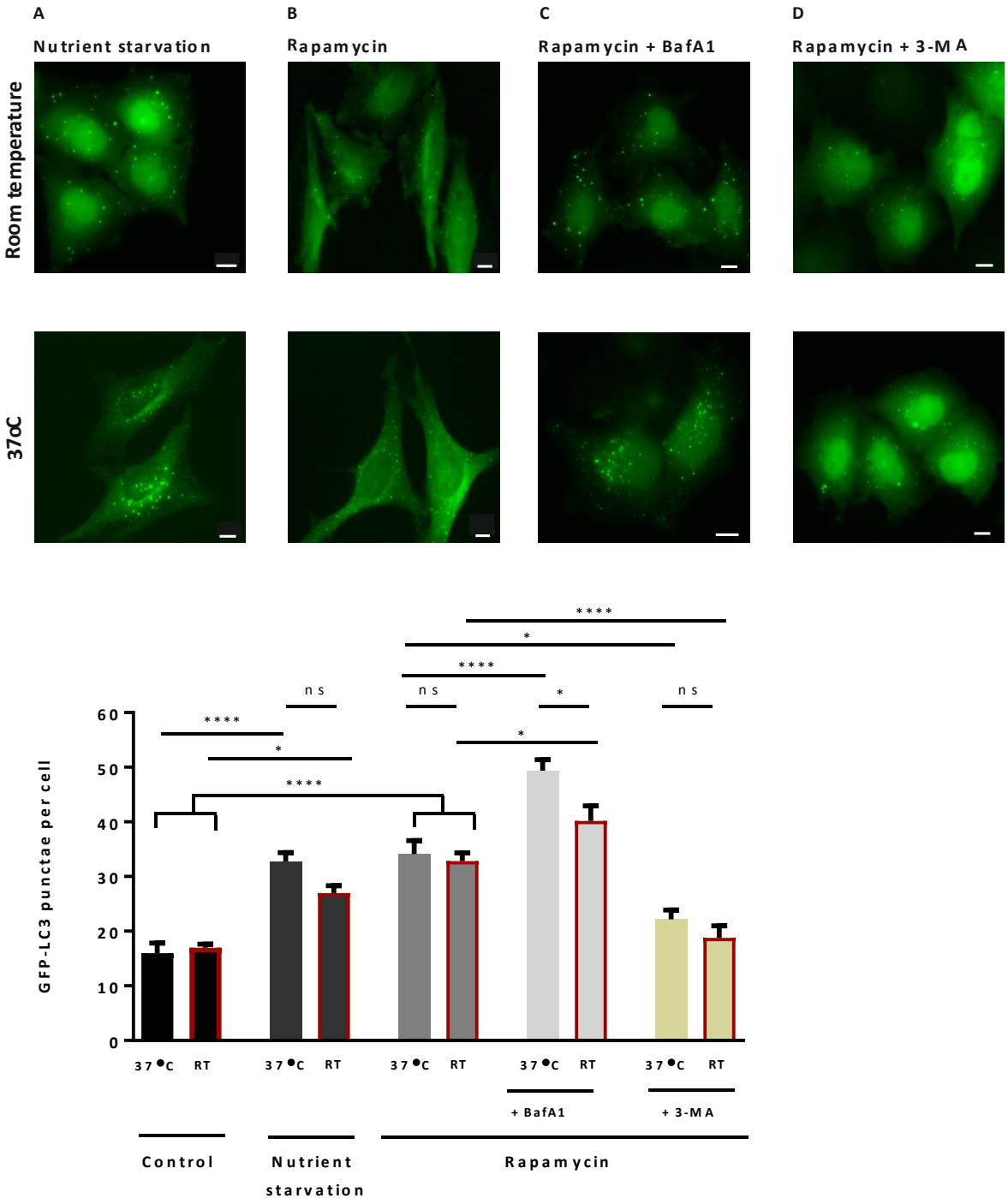

Figure 3.15. The induction of GFP-LC3 punctae accumulation in HeLa cells is quantitatively similar in cells at 37°C or room temperature. Panels A-D represent images of HeLa cells following a 1-hour incubation with either starvation medium, rapamycin (1µM), rapamycin + BafA1 (0.1µM), or rapamycin + 3-MA (5mM), respectively, at room temperature or 37°C. Panel E is a quantitative representation of the effect of temperature on GFP-LC3 punctae accumulation during the various treatments; there were quantitatively similar increases in GFP-LC3 punctae caused by nutrient starvation or rapamycin at both temperatures. The induction of GFP-LC3 accumulation was blocked by 3-MA with both temperatures. The data are mean ± S.E.M of 3 experiments per temperature (25 - 50 cells per condition). The data were analysed with a one-way ANOVA test. * indicates $p < 0.05$, **** indicates $p < 0.0001$. The scale bars in Panels A - D indicate 10 µm.

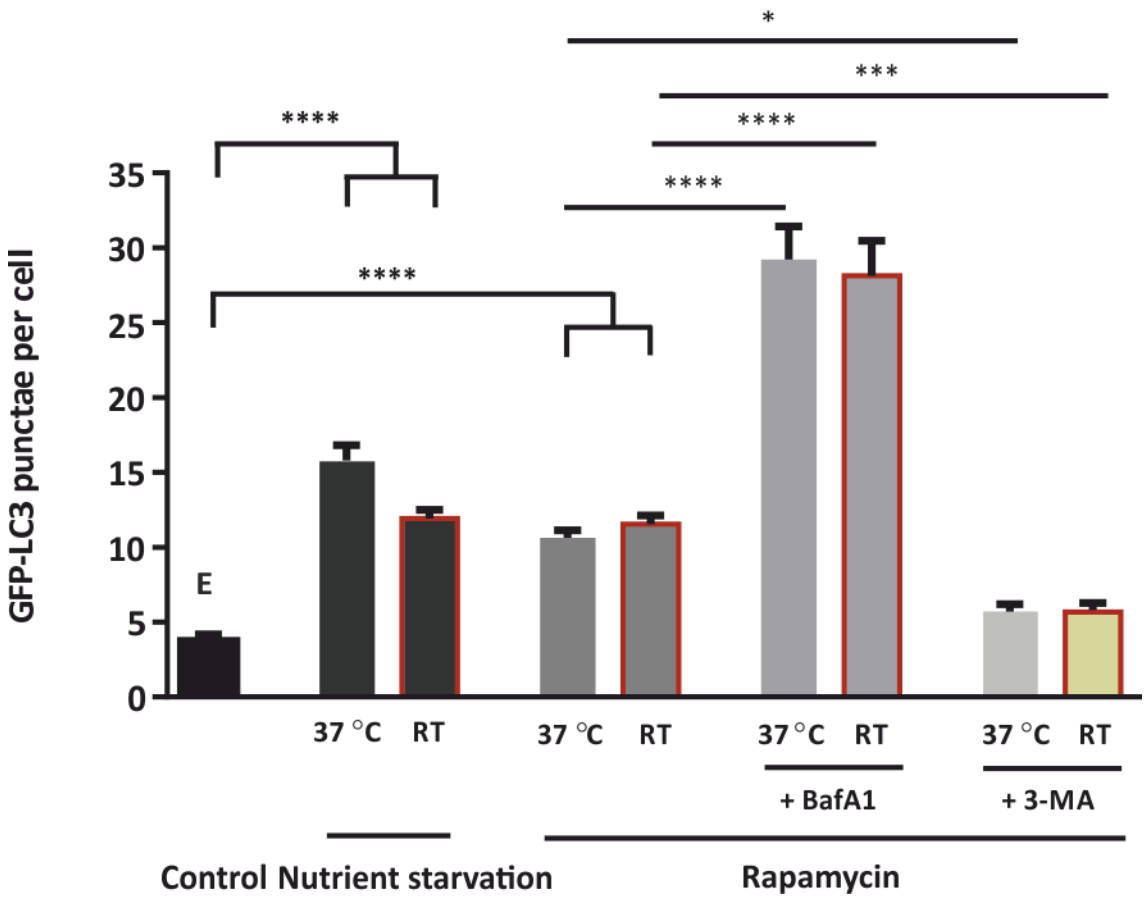

Figure 3.16. Induction of GFP-LC3 punctae accumulation in HEK cells is quantitatively similar at 37°C or room temperature. The column graph is a quantitative representation of the effect of temperature on GFP-LC3 punctae accumulation during the various treatments indicated; there were quantitatively similar increases in GFP-LC3 punctae caused by either nutrient starvation or rapamycin (2µM) at both temperatures. The induction of GFP-LC3 punctae accumulation was blocked by 3-MA (5mM) at both temperatures. The data are mean ± S.E.M of 3 experiments per temperature (40 - 100 cells per condition). The data were analysed with a one-way ANOVA test. * indicates $p < 0.05$, ** indicates $p < 0.01$, *** indicates $p < 0.001$ and **** indicates $p < 0.0001$. The scale bars in Panels A - D indicate 10 µm.

3.2.6 Additional methods to measure the induction of autophagy: Cyto-ID® green autophagy stain

Cyto-ID® green, a cationic amphiphilic tracer dye, was recently developed to enable acute labelling of autophagic vesicles with minimal staining of lysosomes [353]. The advantages of a fluorescent autophagic indicator such as the Cyto-ID autophagy stain are that it is compatible for use with flow cytometry, fluorescence microscopy and high throughput screening. Moreover, it can stain autophagic vesicles within minutes, so cells do not have to be transfected or undergo clonal selection, for example to express a fluorescent protein. In this study, Cyto-ID green was used as another method of verifying the induction of autophagy by various treatments, and to assess its potential to be used in situations where GFP-LC3 expression was not appropriate.

The Cyto-ID green autophagy stain was found to label discrete punctae within HeLa cells, similar in size and distribution to those observed in cells expressing GFP-LC3 (Figure 3.17A). Incubation of HeLa cells with starvation medium, or addition of rapamycin, increased the number of Cyto-ID green-labelled punctae. Moreover, concurrent application of BafA1 during the incubation with rapamycin increased the number of Cyto-ID green-labelled punctae. Whereas, the addition of 3-MA during the incubation with rapamycin decreased the number of Cyto-ID green-labelled punctae. Control experiments, using GFP-LC3-expressing HeLa cells, were conducted in parallel using the same reagents and solutions, and qualitatively similar responses were observed (Figure 3.17B). These observations suggest that Cyto-ID green can be used as an alternative to GFP-LC3 for detection of autophagic vesicles. However, one notable difference between the Cyto-ID green-labelled cells and cells expressing GFP-LC3 was that Cyto-ID consistently indicated a higher number of punctae.

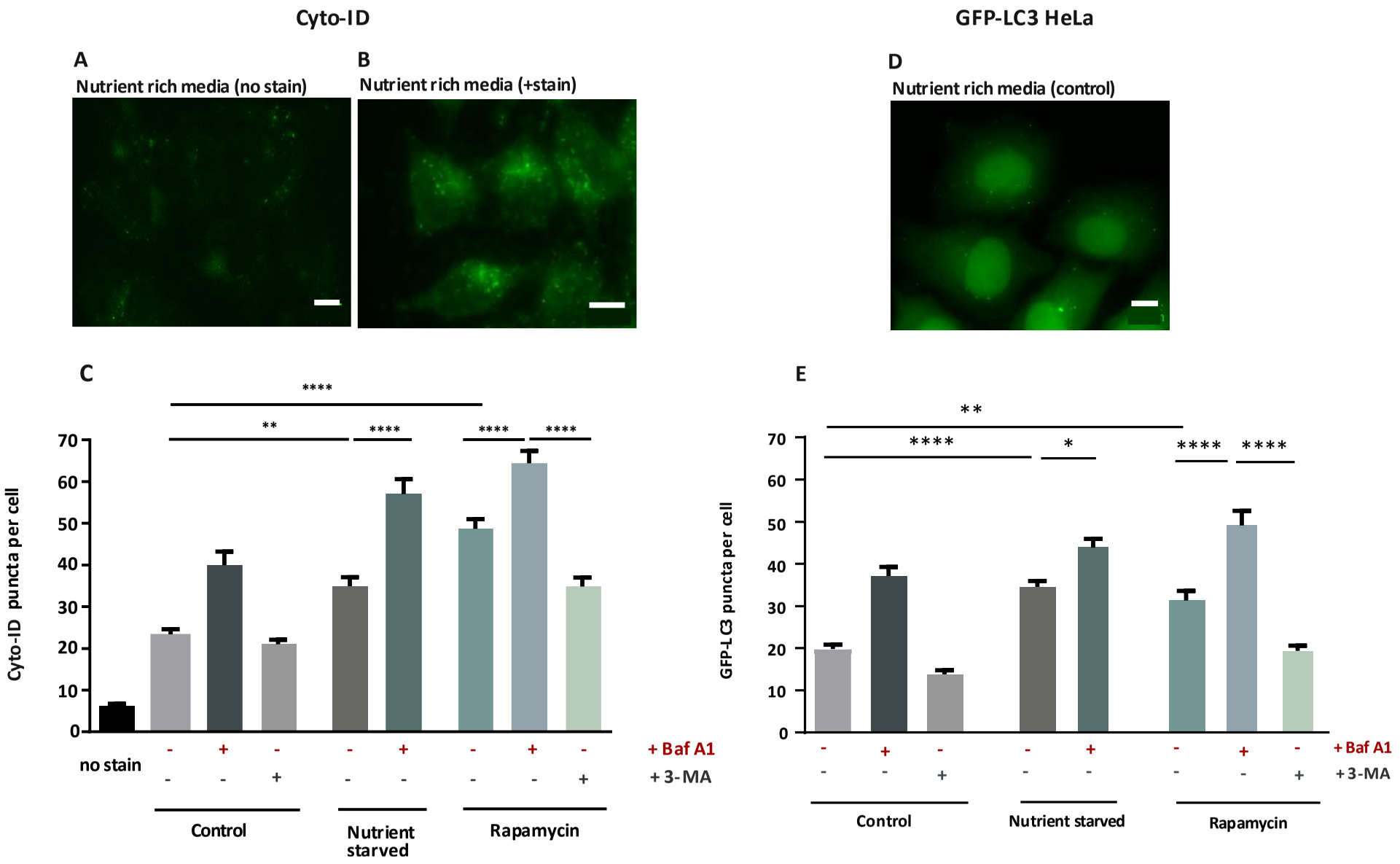
Cyto-ID
A
Nutrient rich media (no stain)
B
Nutrient rich media (+stain)
GFP-LC3 HeLa
D
Nutrient rich media (control)
C
Cyto-ID puncta per cell
no stain
+ Baf A1
+ 3-MA
Control
Nutrient starved
Rapamycin
E
GFP-LC3 puncta per cell
Control
Nutrient starved
Rapamycin

Figure 3.17. Detection of autophagy in HeLa cells with CYTO-ID®, a selective stain for autophagic vesicles. HeLa cells (either wild type, or GFP-LC3-expressing) were incubated in complete imaging medium, starvation medium or complete imaging medium supplemented with rapamycin, and the other treatments indicated, for 1 hour. The wild type HeLa cells were further incubated with CYTO-ID® green autophagy detection reagent for 10 min at 37°C. Panels A and B are representative images of wild type HeLa cells in complete imaging medium in the absence or presence of CYTO-ID®. Panel D is a representative image of GFP-LC3 HeLa cells in complete imaging medium. Panels C and E are quantitative representations of the effects of the various treatments on autophagic vesicle numbers measured using the CYTO-ID® kit or GFP-LC3, respectively. The data are mean ± S.E.M of 3 experiments (30 - 50 cells per condition). The data were analysed with one-way ANOVA. * indicates $p < 0.05$, ** indicates $p < 0.01$, and **** indicates $p < 0.0001$. The scale bars in Panels A, B and D indicate 10 µm.

3.2.7 Electron microscopy

As discussed at the beginning of this Chapter, electron microscopy has been used in many previous studies to establish the presence and form of autophagic vesicles [152, 354]. Experiments were therefore undertaken to explore whether electron microscopy could be used as a quantitative approach to measuring autophagic flux. As depicted in Figures 3.18 and 3.19, autophagic vesicles could be clearly identified within cells under nutrient-replete conditions, and also following stimulation of autophagy by rapamycin and nutrient starvation. The autophagic vesicles were similar in shape and form, but were heterogeneous in terms of their contents. With some autophagic vesicles, it was possible to identify the contents of the engulfed structures within the lumen of the vesicle (Figure 3.19). Whilst it was relatively simple to observe autophagic vesicles using electron microscopy, it was found to be a labour-intensive method that could only provide quantitative data with a significant investment of time. Moreover, distinguishing autophagosomal structures from other vesicles was sometimes difficult. The preparation for electron microscopy required the transfer of cells from imaging buffer to a fixation solution for an hour, thereby making it difficult to match Ca^{2+} imaging with quantitation of autophagy.

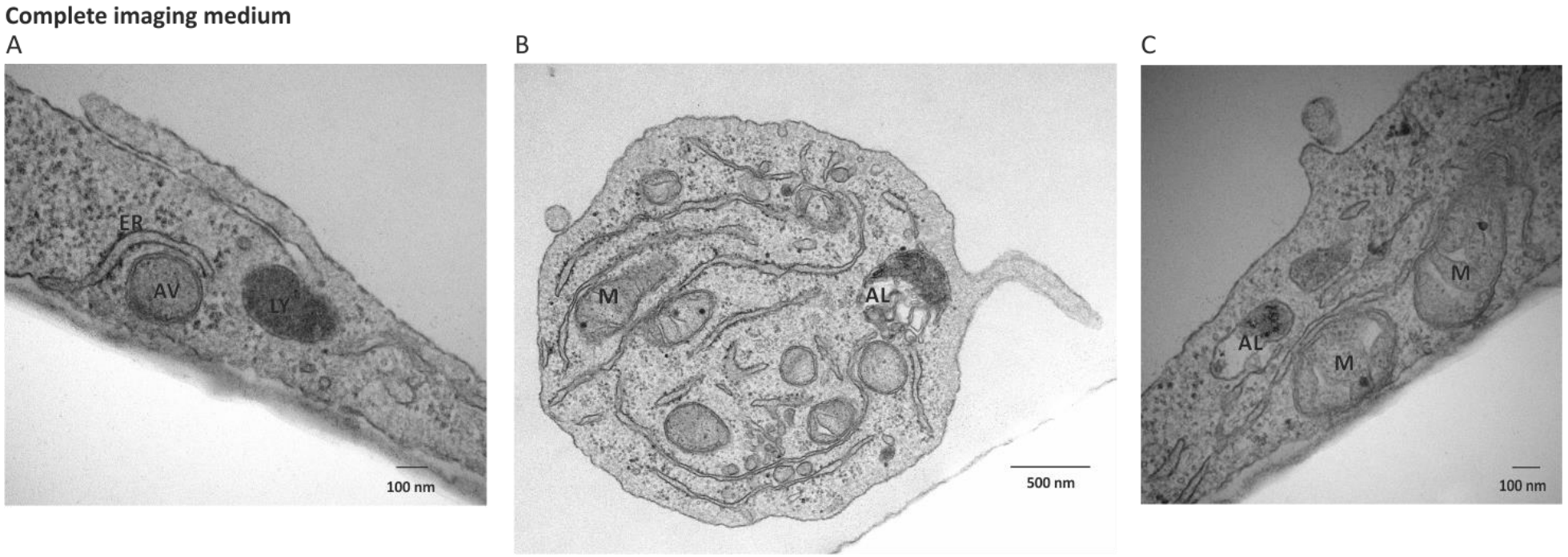

Figure 3.18. Detection of autophagic vesicles in HEK cells using electron microscopy. Panels A – C are electron micrographs showing sections of different cells that were incubated in complete imaging medium. Labels indicate autophagosomes and autolysosomes in various locations within the cells, along with mitochondria, ER and lysosomes. Heterogeneity in the contents of autophagosomes is evident. AL: autolysosome, AV: autophagosome, ER: endoplasmic reticulum, M: mitochondria, LY: lysosome.

A (Starvation medium)

i

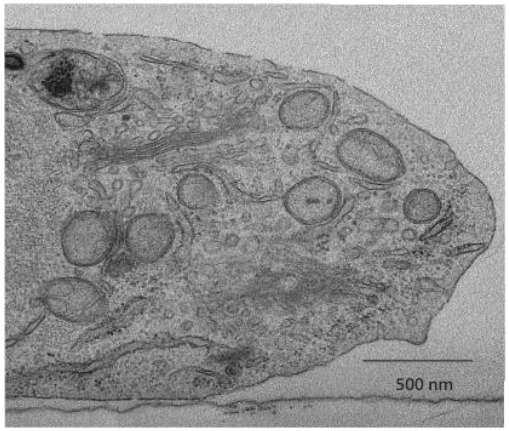

ii

iii

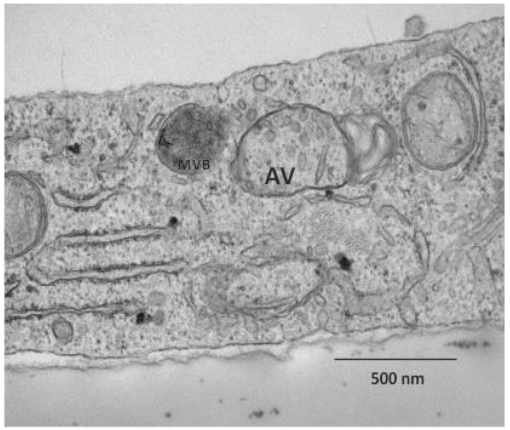

B (Rapamycin)

i

ii

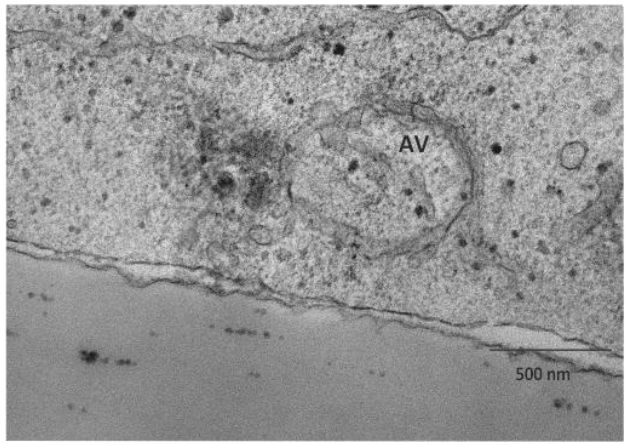

iii

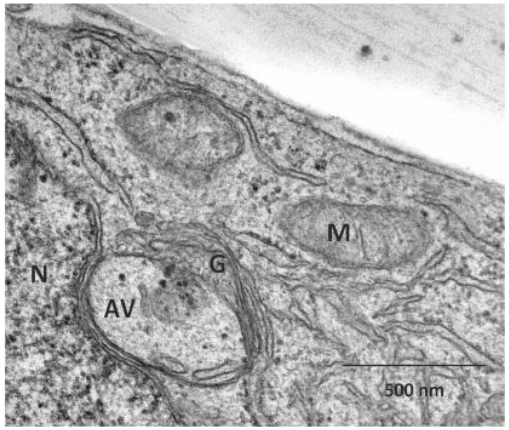

Figure 3.19. Detection of autophagic vesicles in HEK cells using electron microscopy following induction of autophagy with nutrient starvation and rapamycin. Panels A and B are electron micrographs showing sections of different cells that were incubated in starvation medium for 1 hour, or complete imaging medium supplemented with rapamycin (2 µM, 1 hour). The labels indicate autophagosomes and autolysosomes in various locations within the cells, along with mitochondria, ER and lysosomes. Heterogeneity in the contents of autophagic vesicles is evident. Panel (Aii) shows an autophagosome containing a fragment of rough ER. Panel B shows images with an autophagosome containing traces of mitochondrial cristae (i) and pieces of smooth ER (ii). No gross differences in the structure or size of the autophagosomes were obvious between the two treatments. AV: autophagosome, ER: endoplasmic reticulum, G: golgi, LY: lysosome, M: mitochondria, MVB: multivesicular body, N: nucleus.

3.2.8 Using mCherry-GFP-LC3-expressing HeLa cells to assess autophagic flux

Due to its relatively simple use in microscopy and high-throughput screening, GFP-LC3 has been employed in many studies of autophagy. A refinement of this approach was the development of a mCherry-GFP-LC3 dual-colour reporter construct with both green and red fluorescent proteins appended to the LC3 protein [220] . This mCherry-GFP-LC3 tandem fluorescent reporter labels nascent autophagosomal membranes and autophagosomes with both green and red fluorescence emission. However, when autophagosomes fuse with lysosomes the acidic conditions within the lumen of the autolysosome quenches the fluorescence from the GFP moiety. In contrast, the red fluorescence from mCherry is not quenched by the acidity of the autolysosomes, but eventually disintegrates due to autophagic protein degradation. The mCherry-GFP-LC3 tandem fluorescent reporter therefore allows visualisation of autophagosomes as punctae with overlapping green and red fluorescence, and mature autolysosomes as punctae with red fluorescence only (Figure 3.20A) [225].

A stable HeLa cell line expressing mCherry-GFP-LC3 was created in this study (*Chapter 2: Materials and Methods*). As shown in Figure 3.20, the mCherry-GFP-LC3-expressing HeLa Cells displayed both green and red punctae when incubated in complete imaging medium. Incubation of cells with rapamycin increased the total number of green + red punctae indicative of an increase in autophagy (Figure 3.20). Addition of BafA1 increased the number of autophagosomes (green + red fluorescence), and decreased the number of autolysosomes (red fluorescence only), when applied by itself, or concurrently with rapamycin. The increase in the number of autophagosomes caused by BafA1 tallies with the results described earlier, which were obtained using the GFP-LC3 construct. The decrease in the number of autolysosomes by BafA1 was an expected result, as the compound has been shown to block the fusion of autophagosomes with lysosomes, in

which case the progression from red + green punctae to red only punctae cannot occur. These observations are consistent with the use of fluorescently-tagged LC3 reporter constructs to quantitatively monitor the induction of autophagy, and the utility of BafA1 as a blocker of autophagic flux.

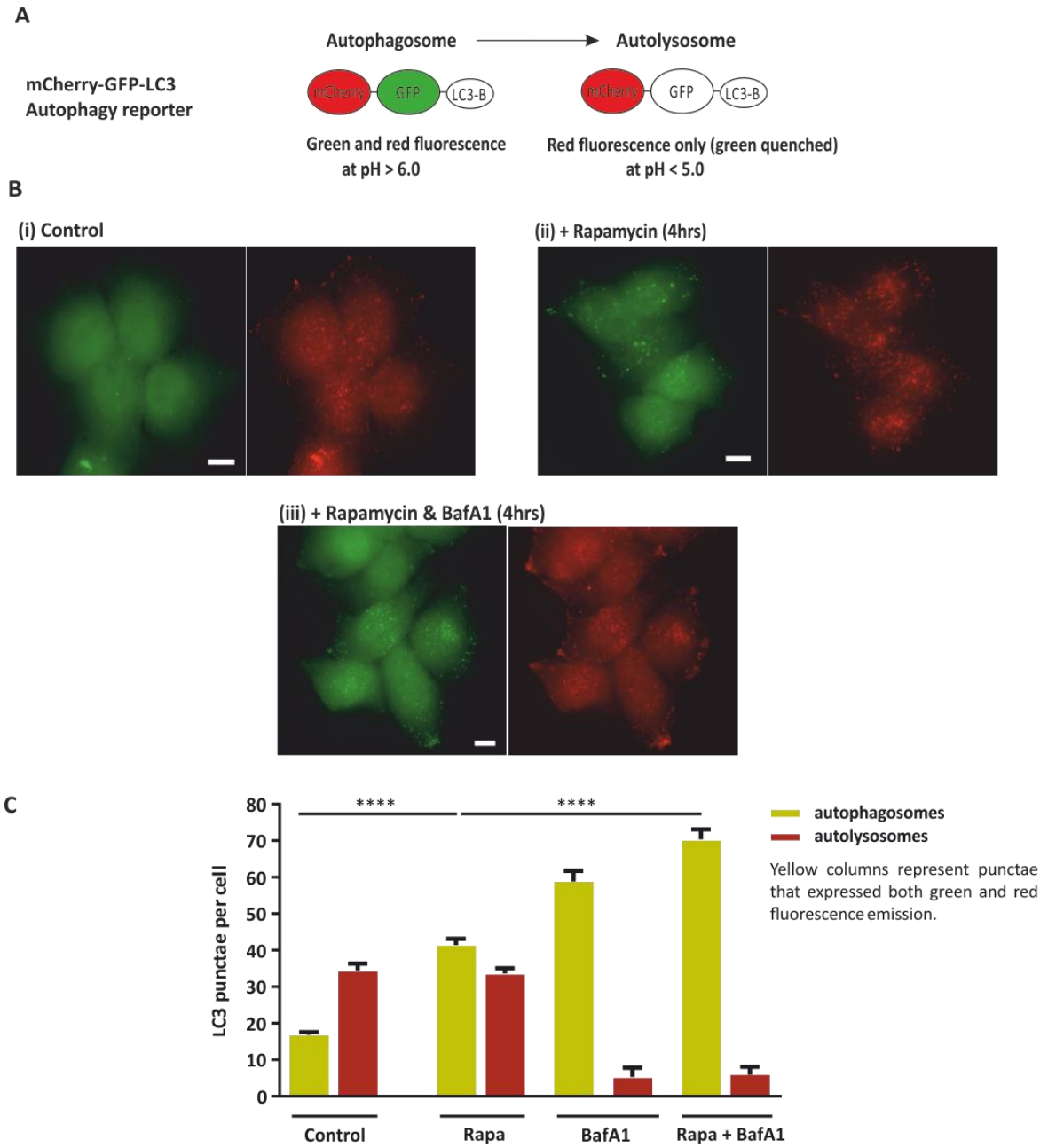

Figure 3.20. Quantitation of autophagy using an mCherry-GFP-LC3 reporter in HeLa cells. Cells were stably transfected with a plasmid encoding mCherry-GFP-LC3. Panel A illustrates how this reporter can be used to assess autophagic flux. GFP is quenched in the acidic autolysosomal compartment, whereas mCherry remains fluorescent. Therefore, autophagosomes are evident as punctae with both green and red emission (from GFP and mCherry, respectively) and autolysosomes are evident as punctae that have red emission (from mCherry only). Panel B shows representative images of (i) cells in complete imaging medium, (ii) cells in complete imaging medium supplemented with rapamycin (1 µM) for 4 hours, and (iii) cells in complete imaging medium supplemented with rapamycin (1 µM) and BafA1 (0.1 µM) for 4 hours. Panel C is a quantitative representation of the effects of rapamycin and rapamycin + BafA1 on numbers of green and red punctae. Rapamycin and BafA1 increased the total number of punctae (whether green or red). BafA1 also reduced the proportion of red-only punctae, consistent with a reduced autophagic flux. The data are mean ± S.E.M of 3 - 4 experiments (40 - 80 cells per condition). The data were analysed with a one-way ANOVA. **** indicates $p < 0.0001$. The scale bars in Panel B indicate 10 µm.

3.2.9 Quantification of fluorescent autophagic vesicles

The GFP-LC3 punctae quantitation presented so far have been expressed as 'punctae per cell'. However, whilst counting the number of punctae per cell is a common method presented in the published literature, it is important to note that there is some variability in the size of cells. It was therefore considered whether cell size could influence the quantitation of autophagy. As an alternative to calculating the number of GFP-LC3 punctae per cell, the number of GFP-LC3 punctae per cell area was also determined, using the same cells in each case to allow a direct comparison. As illustrated in Figure 3.21, both methods of calculating GFP-LC3 punctae numbers gave qualitatively similar outcomes. Using either method, there was a clear, statistically significant, increase in GFP-LC3 punctae caused by treatment of the cells with 1 or 2 μM rapamycin (1 or 2 hours), and an even greater number of GFP-LC3 punctae in cells incubated with rapamycin and 0.1 μM BafA1 (1 or 4 hours). Since determination of the number of punctae per cell is simpler and less time consuming, it was adopted as the method of punctae quantitation in this study.

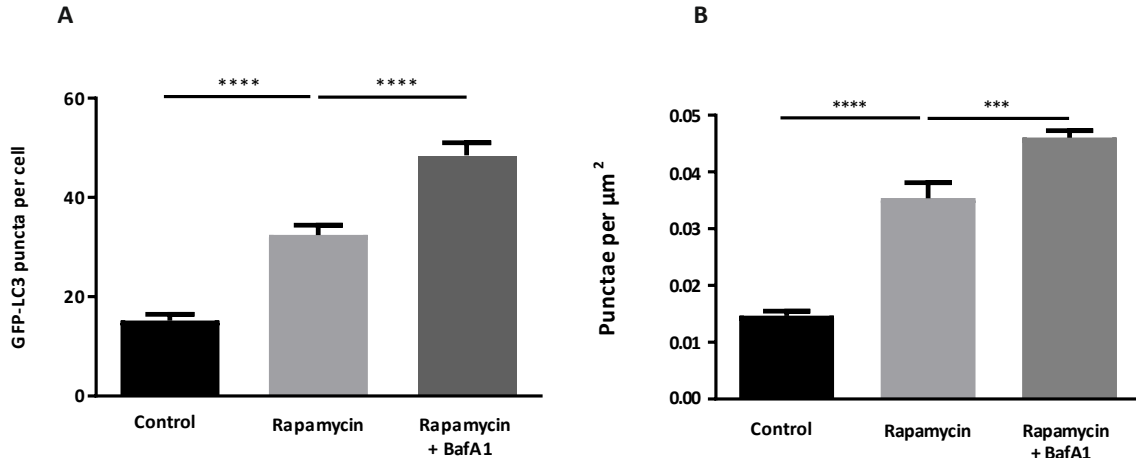

Figure 3.21. Analysis of GFP-LC3 punctae as number of punctae per cell or number of punctae per cell area. Panels A and B depict data from the same experiments analysed in two different ways. Panel A represents data expressed as the number of punctae per cell and panel B represents data expressed as number of punctae per cell area. Both analyses show that rapamycin (1 µM) induced a significant increase in the number GFP-LC3 punctae in HeLa cells, with a further increase in GFP-LC3-labelled punctae accumulation in cells concurrently incubated with rapamycin (1 µM) and BafA1 (0.1 µM). The data are mean ± S.E.M of 3 experiments (30 - 40 cells per condition). The data were analysed with a one-way ANOVA test. **** indicates $p < 0.0001$.

An important consideration when capturing images of cells to calculate the number of GFP-LC3 punctae is that there are different possible focal planes at which images may be captured. Since autophagic vesicles are ~500 - 1500 nm in diameter, it is likely that they may not be evident in all possible focal planes. Failing to capture all GFP-LC3 punctae within a cell through choosing an inappropriate focal plane for image capture could lead to an underestimation of the induction of autophagy. Therefore, it was important to determine whether quantitation of GFP-LC3 punctae was affected by altering the focal plane for image capture. The scatter plots shown in Figure 3.22 depict the identification of GFP-LC3 punctae from cell images within the same cells, but captured at three different focal planes. It is evident that whilst there was some variability in the numbers of GFP-LC3 punctae measured in each cell at the three focal planes, overall it made little difference to the calculated average number of punctae.

In this study, the quantitation of GFP-LC3 punctae was performed manually by counting individual discrete fluorescent spots within each cell in a field of view. This was a preferred method since it allowed quality control for images and cells that were non-optimal (e.g., out of focus images or evidently imperfect cells). However, to establish that the manual method of counting was not under- or over-estimating punctae, a comparison with an automated analysis was performed. For this purpose, the ImageJ Cell Counter plug-in was used to measure the GFP-LC3 punctae within cells, and the data from this automated analysis was compared to the quantitation of the same cells using the manual approach. The settings used for the Cell Counter Plug-in are described in *Chapter 2: Materials and Methods*. As depicted in Figure 3.23, both the manual and automated methods gave similar number of punctae in cells incubated in complete imaging medium, or following incubation of cells in complete imaging medium supplemented with rapamycin to simulate autophagy.

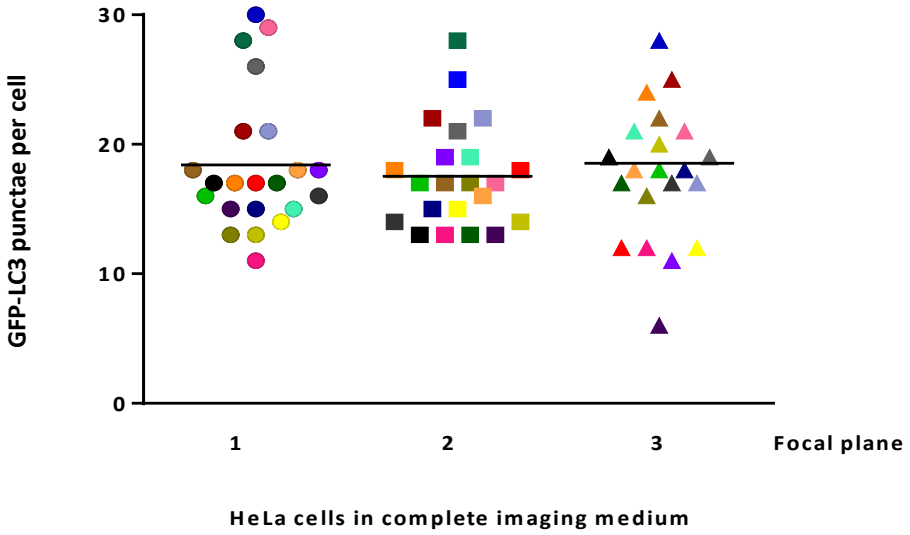

Figure 3.22. Quantitation of GFP-LC3 punctae at 3 different focal planes within the same cells. The scatter plots show the number of GFP-LC3 punctae observed within the same field of HeLa cells imaged at three distinct focal planes. Each cell is represented by a dot, square or triangle of the same colour. There were no significant differences in the average number of GFP-LC3 punctae per cell obtained using any of the focal planes.

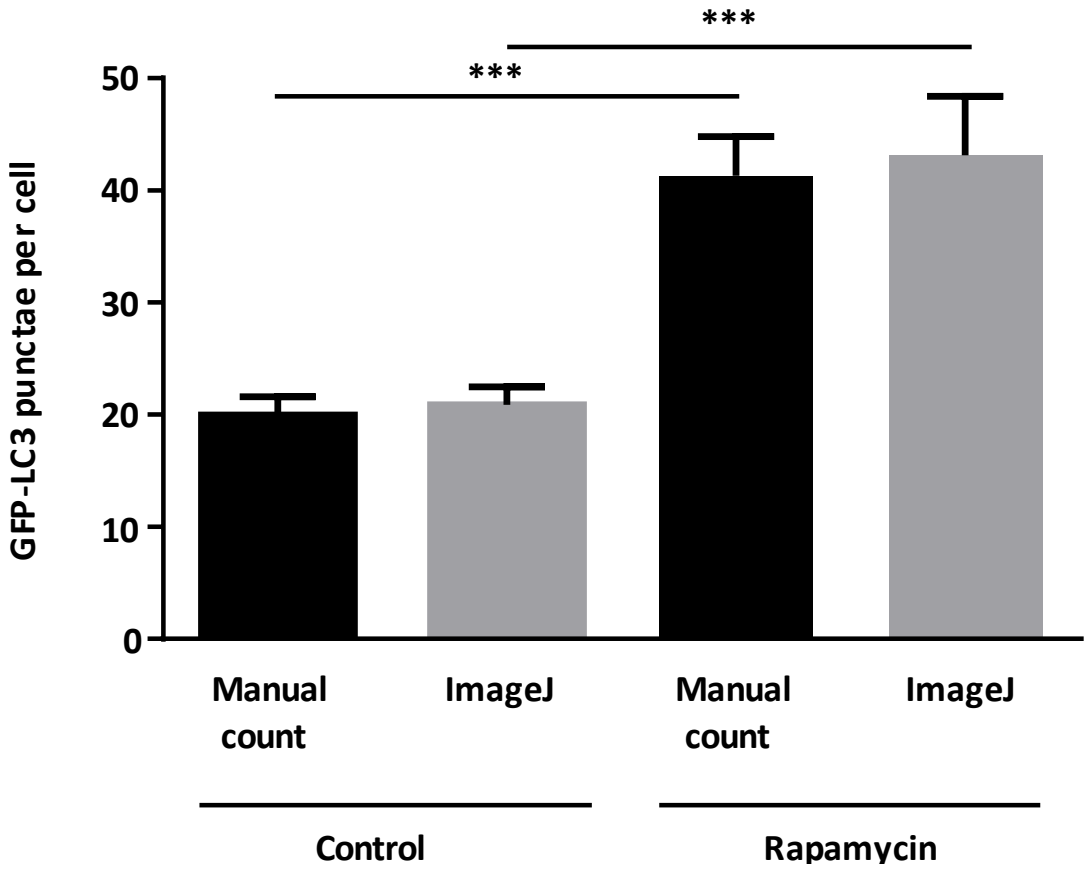

Figure 3.23. Quantitation of GFP-LC3 punctae in HeLa cells using ImageJ or manual counting. Punctae were counted manually by two independent researchers, the cell counter ImageJ plugin, or the threshold function in ImageJ. The number of punctae within cells incubated in complete imaging medium, or within cells incubated in complete imaging medium supplemented with 1 µM rapamycin were similar whether counted manually or using an automated approach with ImageJ. The data are mean ± S.E.M of 3 experiments. The data were analysed with a one-way ANOVA test. *** indicates $p < 0.001$.

3.2.10 Cytosolic Ca^{2+} is required for the induction of autophagy by rapamycin in HeLa cells

The key aim of this study was to investigate the regulation of autophagy by cellular Ca^{2+} signals. Previous reports have shown that loading cells with BAPTA-AM, a high-affinity intracellular Ca^{2+} buffer, prevented the induction of autophagy [297, 355]. BAPTA-AM has been commonly used in autophagy studies, and has consistently indicated that cytosolic Ca^{2+} is required for the induction of autophagy, although it is unclear how Ca^{2+} regulates autophagy [2][356]. In agreement with these findings, it was observed that loading cells with BAPTA-AM significantly reduced the level of GFP-LC3 punctae observed within cells incubated in complete imaging medium, and also prevented the increase in GFP-LC3 punctae that was usually observed following incubation of cells with rapamycin (Figure 3.24). These results support the hypothesis that Ca^{2+} signalling is a vital element of canonical mTOR-dependent autophagy. Despite the widespread use of BAPTA-AM to explore the role of Ca^{2+} in autophagy, there are few studies where experiments are performed to ensure that the BAPTA-AM loading conditions were actually sufficient to suppress cellular Ca^{2+} signals over the timecourse in which autophagy was measured. As depicted in Figure 3.24, the BAPTA-AM loading conditions used in this study were sufficient to prevent an increase in cytosolic Ca^{2+} concentration following the addition of histamine, a normally potent agonist for causing Ca^{2+} signals in HeLa cells [3].

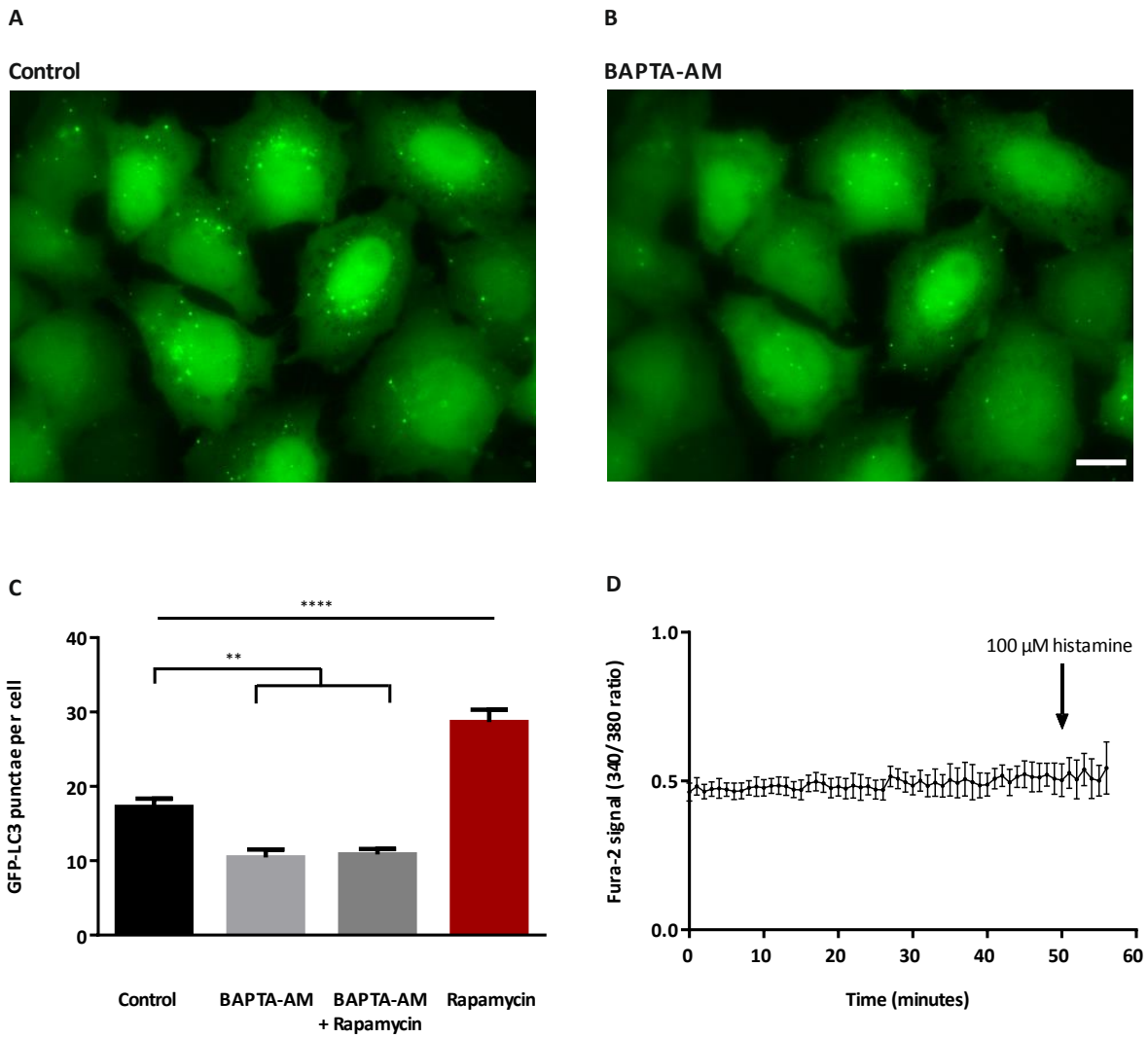

Figure 3.24. Chelating intracellular Ca^{2+} with BAPTA-AM prevented the induction of autophagy in HeLa cells. Panel A is a representative image of cells in complete imaging medium. Panel B is a representative image of cells incubated in complete imaging medium and that were loaded with 10 µM BAPTA-AM for 1 hour prior to imaging. Panel C is a quantitative representation of the effect of BAPTA-AM loading on autophagy in untreated cells, and cells incubated with 1 µM rapamycin; the number of GFP-LC3 punctae per cell due to basal autophagy was decreased following BAPTA-AM loading. In addition, BAPTA-AM prevented the accumulation of GFP-LC3 punctae by rapamycin. Panel D is the profile of cytosolic Ca^{2+} in cells pre-loaded with BAPTA-AM before imaging (10 µM for 1 hour). To assess the ability of BAPTA-AM to buffer Ca^{2+}, 100 µM histamine was added to the cells for the final 5 minutes of the recording. The data are mean ± S.E.M of 3 experiments (15 - 50 cells per condition). The data were analysed with a one-way ANOVA test. ** indicates $p < 0.01$ and **** indicates $p < 0.0001$. The scale bar in Panel B indicates 10 µm.

3.3 Summary

The work described in this chapter characterised the utility of two cell lines (HeLa and HEK) for studying the regulation of autophagy by Ca^{2+}. Emphasis was placed on using the accumulation of GFP-LC3 punctae as a real-time, direct assay for induction of autophagy in these cell lines. A key advantage of visualising GFP-LC3-labelled punctae formation as an assay of autophagy is that that it can be performed simultaneously with Ca^{2+} imaging. In theory, it would be possible to follow autophagy and Ca^{2+} signals within individual cells in a field of view, although that was not performed in this study. Particular attention was given to control experiments that are necessary when using GFP-LC3 punctae accumulation to distinguish an increased autophagic flux from effects on autophagosome processing. Several experimental systems were examined, including recording of GFP-LC3 fluorescence, tandem mCherry-GFP-LC3 fluorescence, electron microscopy, and labelling of autophagosomes with CYTO-ID® green. In addition, preliminary experiments using Western blotting for endogenous LC3 protein were performed.

The key findings in this Chapter are:

- The accumulation of GFP-LC3 punctae was increased by known activators of autophagy (starvation, rapamycin, PP242) (Figures 3.7 and 3.8, 3.10 and 3.11, 3.14 respectively), and was enhanced by BafA1, which is consistent with an increase in autophagic flux. Moreover, the accumulation of GFP-LC3 punctae was inhibited by the PI3-kinase inhibitor 3-MA. Similar increases in punctae formation were observed with a tandem mCherry-GFP-LC3 fluorescent reporter (Figure 3.20) and application of the acute autophagosome stain CYTO-ID® green (Figure 3.17).

- An extracellular medium that mimicked the cells' culture environment maintained cell viability, and did not induce an increase in GFP-LC3 punctae accumulation for up to 12 hours (Figures 3.3 and 3.4). This medium, termed complete imaging medium, required NEAA, 10% FBS, 2 mM L-glutamine and 1 mM sodium pyruvate to prevent induction of GFP-LC3 punctae accumulation (Figure 3.1).

- Nutrient starvation and rapamycin increased GFP-LC3 punctae accumulation in HeLa and HEK cells to similar extents at 37°C and room temperature (Figures 3.15 and 3.16).

- Simultaneous, real-time recordings of cytosolic Ca^{2+} and GFP-LC3 punctae accumulation are possible (Figure 3.24).

- GFP-LC3 punctae can be reliably measured using a wide-field microscope despite the focal plane chosen perhaps not capturing all GFP-LC3 punctae (Figure.322).

- Images from electron microscopy reveal autophagic vesicles in HEK cells with evidently different cargoes (Figures 3.18 and 3.19). However, this technique is not the most efficient for use as a quantitative assay.

- Loading of cells with BAPTA-AM reduced both the basal and rapamycin-stimulated GFP-LC3 punctae accumulation, suggesting that cytosolic Ca^{2+} is critical for autophagy (Figure 3.24).

3.4 Discussion

The work described in this chapter aimed to characterise assays for studying the induction of autophagy, and determining their reliability for use with live cell imaging experiments. A key aim was to find experimental conditions that allowed the recording of Ca^{2+} signals and autophagy together within the same cells. Real-time visualization of both activities is an

ideal situation, and could potentially simplify some of the complex results reported in literature. In addition, the minimal experimental times that allowed both Ca^{2+} signals and autophagy to be measured with statistically significant data sets were a sought. It is important to bear in mind that physiological Ca^{2+} signalling events are usually brief events in the cell [19]. Deviation from a physiological pattern may activate autophagy, potentially due to cellular stress and adaptive responses [293] and not necessarily because of naturally occurring Ca^{2+} signals. Moreover, since stimuli such as hormones, thapsigargin and ionomycin trigger Ca^{2+} signals within tens of seconds, and the formation and processing of autophagic vesicles occurs over minutes, it could be argued that there is no need for the extended (e.g., many hours) incubations that that have been reported in the literature.

To verify that the assays used in this study could reliably detect autophagy, different stimuli were employed to induce autophagy in the HeLa and HEK cell lines. In particular, rapamycin and nutrient starvation were used to inhibit mTORC1 and thereby activate the canonical autophagic pathway (Figures 3.5-3.13). Numerous studies have demonstrated that rapamycin [357, 358] and nutrient starvation [359, 360] induce autophagy in various cell types. However, the incubation times and concentrations of rapamycin used are not always the same. For example, in HeLa cells, rapamycin was shown to cause an increase in autophagy following a 2-hour incubation [347], whereas a 24-hour incubation was shown to induce autophagy in pancreatic islet cells [361]

To induce starvation conditions, studies have used serum or amino acid withdrawal to induce autophagy [297, 362, 363]. However, as with rapamycin, the incubation times have been variable. Moreover, a variety of media are widely used in autophagy research. These include Hank's balanced salt solution (HBSS) [364], Earle's Balanced Salt Solution (EBSS) [365], PBS [366] and DMEM [341]. Similar to the approach used in the present work, some

studies have induced autophagy with Krebs buffer as a starvation medium, however, incubation times are longer. For example a 4-hour incubation in Krebs buffer induced autophagy in HEK293 cells [367] and a 6-hour incubation was used to induce autophagy in HeLa cells [368].

Despite the variability in time of incubation and/or concentration of rapamycin, and the different types of starvation medium used, there is general consensus that they activate a *bona fide* autophagic response. Moreover, measurement of punctae/autophagic vesicle accumulation has been used in significant number of publications to indicate a stimulation of autophagy [152, 347, 369, 370]. The results presented in this chapter concur with the established evidence for the utility of measuring GFP-LC3 punctae as a microscopy-based method for real-time monitoring of autophagic flux. It was considered that using the tandem mCherry-GFP-LC3-expressing cells to assess autophagic flux could be advantageous because both autolysosomes and autophagosomes could be estimated simultaneously. However, it was found to be highly labour intensive to look for overlapping red/green punctae within the cell images. Moreover, the essential advantage of using the tandem mCherry-GFP-LC3 is evidence of continual autophagic flux, which can readily be assessed by the inclusion of BafA1.

Cytosolic Ca^{2+} has been shown to have a dual role in the regulation of autophagy [7, 371]. However, one of the few consistent findings that emerges from the literature is that loading cells with BAPTA-AM blocks autophagy [317, 355]. Indeed, BAPTA-AM appears to be an effective inhibitor of autophagy in almost all conditions [290]. Exactly how BAPTA-AM blocks autophagy is currently unclear. It has been proposed that BAPTA-AM simply buffers Ca^{2+} signals that trigger autophagy [310]. However, there are observations suggesting that a number of different steps within the autophagic pathway may be blocked by BAPTA-AM

loading. For example, BAPTA-AM loading of cells (using conditions that inhibited autophagy) did not affect the production of PI3P by Vps34, but changed the accumulation of the PI3P-binding protein WIPI-1 to nascent phagophore membranes [372]. Also, BAPTA-AM was found to prevent endosome/lysosome fusion [373]. These results reveal that BAPTA-AM does not just inhibit the stimulation of autophagy by experimentally-evoked Ca^{2+} signals, but also inhibits steps in the formation and processing of autophagosomes. The source and nature of the Ca^{2+} signals necessary for these putative Ca^{2+}-sensitive steps is unclear [290].

The results presented in this chapter indicate that chelating cytosolic Ca^{2+} with BAPTA-AM prevented the induction of autophagy, whether under basal conditions, or when autophagy was stimulated via application of rapamycin (Figure 3.22). Although many published studies have invoked a role for Ca^{2+} in the regulation of autophagy through the use of BAPTA-AM loading, control experiments are seldom performed to show the effectiveness of BATPA-AM at buffering cytosolic Ca^{2+} signals. It is well known that cells can extrude Ca^{2+} indicators, especially at 37°C, most likely through ABC transporters, and they may also be able to remove BAPTA-AM from the cytosol too. It was therefore important to show that BAPTA-AM was buffering cytosolic Ca^{2+} in this study, over the same experimental time and conditions that were used for recording GFP-LC3 punctae formation. A simple test that can be performed at the end of an experiment to examine the buffering of cytosolic Ca^{2+} by BAPTA-AM is the stimulation of cells with an $InsP_3$-generating agonist. An example of this simple control experiment is depicted in Figure 3.24, which demonstrates that BAPTA-AM loading abrogated Ca^{2+} signals evoked by the $InsP_3$-generating agonist histamine, indicating that the Ca^{2+} chelator was retained inside the cells and was effective.

Electron microscopy images showed that autophagic vesicles in cells under nutrient rich conditions, and those formed during nutrient starvation or treatment with rapamycin, appeared similar in size and shape (Figures 3.18 and 3.19). Clustering of autophagic vesicles has been highlighted before, particularly under conditions where autophagic flux was blocked [372]. Although the contents of the autophagic vesicles were heterogeneous, there were no obvious signs of abnormalities in the size or shape of the vesicles compared to other published images. Since, only one, or a few, autophagic vesicles could be detected at most in one image, electron microscopy was not deemed suitable for quantitative measurements in the present study.

Cyto-ID® autophagy stain, a recently developed amphiphilic tracer dye, was used to label autophagosomes in HeLa cells (Figure 3.17). A notable difference between the Cyto-ID green-labelled cells and cells expressing GFP-LC3 was that Cyto-ID consistently indicated a higher number of punctae. Plausibly this difference could be accounted for by the labelling of autophagic vesicles as well as other acidic organelles, such as lysosomes or endosomes etc., which are not detected with GFP-LC3. Although, specific staining for those compartments would be required to validate this notion. Despite the increased numbers of punctae labelled, the Cyto-ID® green stain indicated a statistically significant increase in autophagic flux following either nutrient starvation or treatment with rapamycin (Figure 3.17). The punctae observed with cyto-ID were similar in size and distribution to those observed in cells expressing GFP-LC3.

An important limitation with use of GFP-LC3 to monitor autophagy is that LC3 can associate with ubiquitinated protein aggregates, particularly if LC3 is overexpressed by transient transfection [215]. This limitation can lead to misinterpretation of results. These aggregates have been described in many systems and are also referred to as aggresome-

like induced structures (ALIS), SQSTM1/p62 bodies/sequestosomes and inclusions [374]. In addition to the LC3 proteins, GABARAP (γ-aminobutyric acid receptor-associated protein) are a subfamily of Atg8 proteins that are involved in vesicle processing, and are subject to lipidation under autophagy-inducing conditions [375]. GABARAPs have been shown to associate with phagophores during closure, and moreover, it was shown that cytoplasmic cargo sequestration by autophagy depends on GABARAPs [222]. Therefore, analysing autophagic flux by using GFP-LC3 alone may not account for the development and processing of all autophagic vesicles. Additional techniques to assess macroautophagic cargo sequestration could be helpful, such as using the transfer of the cytosolic protein lactate dehydrogenase to autophagic vesicles [223].

In conclusion, the results presented in this chapter establish that monitoring GFP-LC3 punctae accumulation is a convenient, reliable method for assaying autophagic flux using conditions that are also suitable for measuring cytosolic Ca^{2+} signals. Other techniques may provide some additional advantages, but are ether more labour intensive or cannot be performed simultaneously with Ca^{2+} measurements. Two media were established for these experiments. Complete imaging medium supported cell viability and prevented the induction of autophagy for at least 12 hours whereas starvation medium induced autophagy within an hour. These media were used for the experiments reported in the rest of this thesis. The results indicate that factors such as the experimental temperature, focal imaging plane or manual/automated method of punctae counting did not alter the ability to gather reliable data. Moreover, the results confirmed that BAPTA-AM loading blocks the induction of autophagy under conditions in which cytosolic Ca^{2+} is clearly buffered. The source and characteristics of Ca^{2+} signals that regulate autophagy are unknown, and are examined in the following chapters.

Chapter 4: Ca^{2+} flux from $InsP_3$ receptors to mitochondria suppresses autophagy by maintaining cellular ATP

4.1 Introduction

As discussed in *Chapter 1: Introduction*, various studies have suggested that intracellular Ca^{2+} signals can positively and negatively regulate autophagic flux. Exactly how Ca^{2+} signals switch cells between pro-autophagic and anti-autophagic states is not very clear. It is likely that the source and characteristics of Ca^{2+} signals are critical in determining cellular responses. Inositol 1,4,5-trisphosphate receptors ($InsP_3Rs$) are one source of Ca^{2+} signals proposed to control autophagic flux. Studies have shown that a reduction in $InsP_3$ signalling can be pro-autophagic. For example, treatment of cells with lithium triggers autophagy in a mTOR-independent manner [286, 291]. Lithium gradually depletes the cells' capacity to produce $InsP_3$ through inhibiting the recycling of inositol from inositol monophosphates [376]. Evidence has also shown that $InsP_3Rs$ are necessary for autophagy. For example, Cd^{2+} -induced autophagy was abolished by $InsP_3R$ inhibition with 2-APB [377], and starvation-induced autophagy was reduced with the addition of xestospongin B, an $InsP_3R$ antagonist [318].

Mitochondrial Ca^{2+} signalling is an important aspect of Ca^{2+} signalling (Figure 1.2). The close distance of mitochondria to ER Ca^{2+} stores [100] means that Ca^{2+} signals arising from RyRs and $InsP_3Rs$ on the surface of the ER occur near the sites of Ca^{2+} uptake into the mitochondria. ER-mitochondria contact sites termed mitochondria-associated membranes (MAMs) [96] are important for a number of physiological processes, including lipid synthesis, mitochondrial movement and fission, apoptosis, and autophagy [91, 92]. Mitochondrial Ca^{2+} uptake involves the mitochondrial uniporter complex (MCU), located in the inner mitochondrial membrane and the voltage-dependent anion channel (VDAC), located in the outer mitochondrial membrane. The local Ca^{2+} signal within the MAMs (~10

μM) [107] is sufficient for activating the MCU despite its low affinity for Ca^{2+} (K_d 20 - 50 μM) [93]. Ca^{2+} is consequently released from mitochondria through the mitochondrial Na^+/Ca^{2+} exchanger (NCLX) [108], and taken back up into the ER via SERCA, restoring the Ca^{2+} level in the ER.

Ca^{2+} uptake by mitochondria has been shown to prevent AMPK-activated autophagy [288, 312, 378]. Mitochondrial Ca^{2+} uptake has been shown to stimulate the citric acid cycle [379]. Furthermore, Ca^{2+} within the mitochondrial matrix increases the rate of ATP production by the ATP synthase [380, 381]. In addition to its role in maintaining of ATP production, the Ca^{2+} transfer from $InsP_3Rs$ to mitochondria has been shown to be necessary to support the cell cycle of cancer cells. It was demonstrated that inhibition of $InsP_3Rs$ preferentially killed tumour cells, but not non-tumourigenic cells, due to a metabolic catastrophe that resulted in necrotic death [378]. These observations that $InsP_3R$-mediated Ca^{2+} release prevents the induction of autophagy, and plays a role in the survival of cancer cells, could be highly significant in terms of developing new therapies to prevent tumours, and provided the impetus for the work presented in this chapter.

4.2 Aims of the chapter

One aim of this chapter was to investigate the role of Ca^{2+} signalling between $InsP_3R$ and mitochondria in regulating autophagy. The principle experimental approached used in this study was to prevent $InsP_3R$ function in a specific manner, whilst still allowing the cellular expression of $InsP_3Rs$ since they are a binding site for proteins that are involved in autophagy, such as Beclin1 [382] and mTOR [383]. It was therefore considered that inhibiting $InsP_3R$ expression, for example via the use of siRNA, may alter the expression or distribution of $InsP_3R$-associated proteins and thereby affect autophagic responses indirectly. Moreover, preventing $InsP_3R$ expression has not always proven to be helpful in

deciphering the role of these channels in autophagy. For example, DT40 cells that are null for $InsP_3R$ expression have provided conflicting evidence about the role of these channels in both basal and triggered autophagic flux [287, 288].

To prevent the activation of $InsP_3Rs$ cells were transfected with an $InsP_3$ 5'-phosphatase; an enzyme that dephosphorylates $InsP_3$ into $InsP_2$ and inorganic phosphate [384, 385]. Whilst $InsP_3$ is an intracellular messenger that stimulates the release of Ca^{2+} from $InsP_3$ receptors on the ER, $InsP_2$ does not activate $InsP_3$ receptors, and consequently, Ca^{2+} release from the $InsP_3Rs$ is prevented. The experimental approach of using $InsP_3$ 5'-phosphatase to elucidate the specific contribution of $InsP_3Rs$ to particular cellular processes has been used before by my laboratory, for example to reveal the role of $InsP_3Rs$ in the response of cardiac myocytes to hypertrophic stimuli [386]. In addition to the specificity afforded by using an enzymatic approach to prevent $InsP_3R$ function, it was possible to use a mutated form of the enzyme, which has no catalytic activity, as a control for transfection and expression of an exogenous protein.

Additional results presented in this chapter explored putative links between preventing $InsP_3R$ function and mitochondrial Ca^{2+} uptake, cellular ATP concentration, and ER stress, which have all been suggested to regulate autophagy. Moreover, the necessity of $InsP_3R$ activity for cell cycle progression and sensitivity towards apoptotic stimuli was also examined. The overall rationale for these studies was to obtain a significant insight into the role played by $InsP_3Rs$ in autophagy and other cell death-linked phenomena.

4.3 Results

Imaging medium contains Ca^{2+} (complete imaging medium)	Imaging medium does not contain Ca^{2+} (Ca^{2+}-free medium)
All figures (Figure 4.1 to 4.32)	none

Table 4.1 *Experiments of Chapter 4 which were carried out in either complete imaging medium or Ca^{2+}-free medium.*

4.3.1 Transfection of HeLa and HEK cells with $InsP_3$ 5-'phosphatase

For the experiments described in this chapter that involved expression of $InsP_3$ 5'-phosphatase, cells were transfected with a plasmid in which $InsP_3$ 5'-phosphatase was fused in-frame with GFP or a red fluorescent protein called 'monomeric cherry' (hereafter called GFP-$InsP_3$ 5'-phosphatase or mCherry-$InsP_3$ 5'-phosphatase, respectively). The green or red fluorescent tags were essential to find those cells that had been successfully transfected. The plasmids encoding GFP-$InsP_3$ 5'-phosphatase or mCherry-$InsP_3$ 5'-phosphatase were transfected into cells using jetPEI, a commercial cell transfection reagent, as per the manufacturer's instructions. The GFP-$InsP_3$ 5'-phosphatase or mCherry-$InsP_3$ 5'-phosphatase were used for experiments involving Ca^{2+} imaging, as described below. Both constructs were found to be similarly efficacious. When GFP-LC3-expressing HEK or HeLa cells were used for experiments, the mCherry-$InsP_3$ 5'-phosphatase was transfected. In brief, the GFP-LC3 HeLa cells were incubated for 12 - 24 hours with jetPEI reagent mixed with 1 μg of mCherry-$InsP_3$ 5'-phosphatase plasmid DNA. A plasmid construct that encoded an inactive mCherry-tagged $InsP_3$ 5'-phosphatase was used to control for transfection. This was important to determine whether transfection itself caused any cellular stresses, plausibly upregulating autophagy as a consequence. As shown in Figures 4.1 and 4.2, $InsP_3$ 5'-phosphatase-transfected HeLa and HEK cells displayed increased autophagy. However, expression of the inactive form of the $InsP_3$ 5'-phosphatase did not evoke any change in GFP-LC3 punctae formation. To confirm the pro-autophagic

effect of the $InsP_3$ 5'-phosphatase, Western Blotting was used as an alternative technique. As shown in 4.1D, intensity of the LC3-II band in $InsP_3$ 5'-phosphatase-transfected cells was increased compared to that of control conditions.

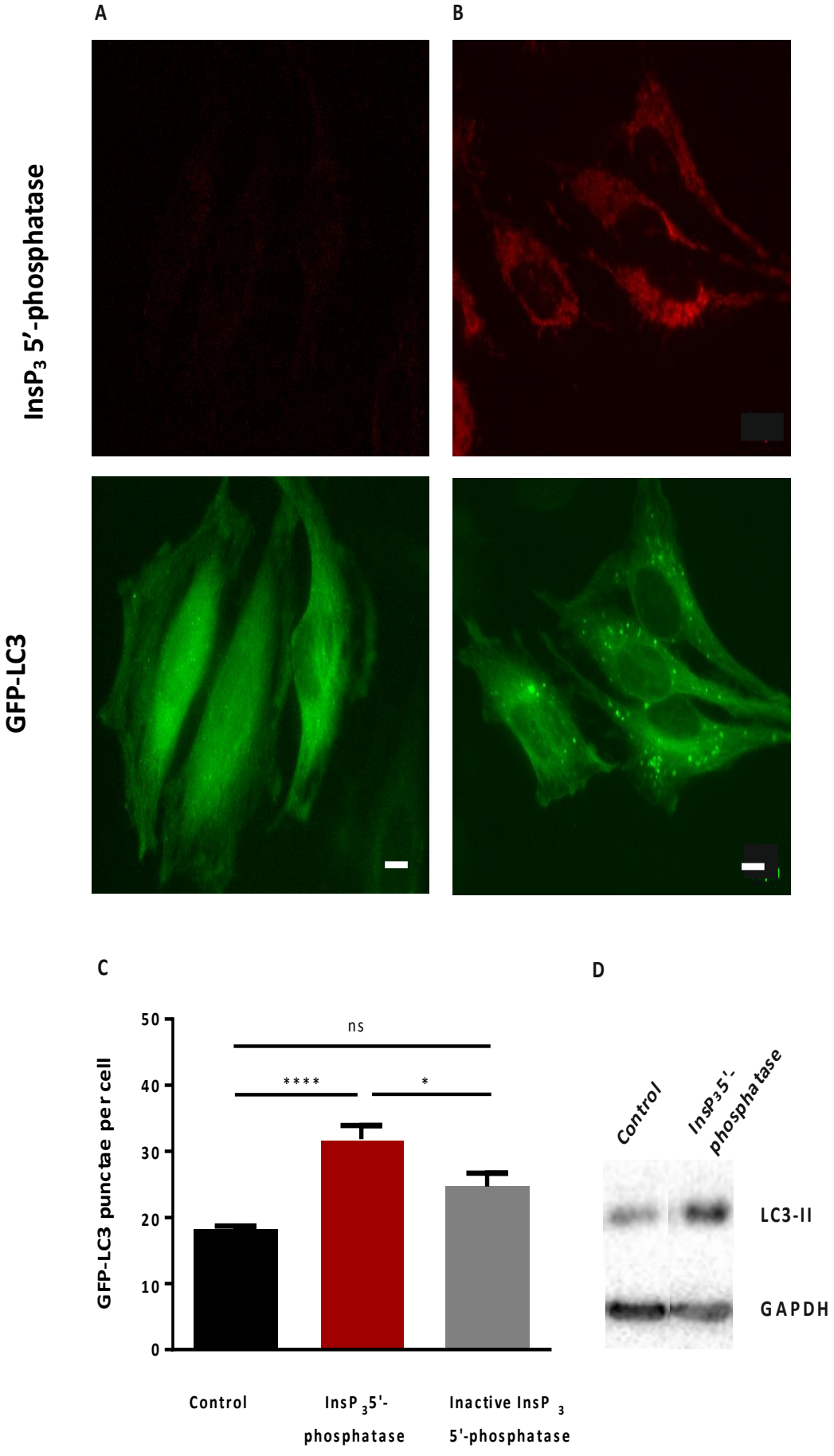
A
B
InsP3 5'-phosphatase
GFP-LC3
C
D
GFP-LC3 punctae per cell
50
40
30
20
10
0
ns
****
*
Control
InsP 3 5'-
phosphatase
Inactive InsP 3
5'-phosphatase
Control
InsP3 5'-
phosphatase
LC3-II
GAPDH

Figure 4.1. HeLa cells transfected with $InsP_3$ 5'-phosphatase displayed increased autophagy. Panel A represents untransfected HeLa cells, with a basal level of autophagy. Panel B depicts cells transfected with mCherry-tagged $InsP_3$ 5'-phosphatase (12-hour transfection), showing an increased number of GFP-LC3 punctae. Note that the autophagy depicted in this figure was solely due to the expression of the $InsP_3$ 5'-phosphatase; the cells were maintained in cell culture medium whilst in the incubator, and then in complete imaging medium for visualisation on the microscope. Panel C is a quantitative representation of the effects of transfecting the $InsP_3$ 5'-phosphatase, and the inactive form of the enzyme, on autophagy. Whereas the $InsP_3$ 5'-phosphatase triggered significant autophagy, cells expressing the inactive enzyme showed similar numbers of GFP-LC3 puncate to control cells. The data are mean ± S.E.M of 3 - 7 experiments (30 - 70 cells per condition). The data were analysed with a one-way ANOVA. * indicates $p < 0.05$ and **** indicates $p < 0.0001$. The scale bars in Panels A and B indicate 10 μm. Panel D is a Western blot showing the expression of LC3-II protein with GAPDH as a loading control; the intensity of the LC3-II band was increased in $InsP_3$ 5'-phosphatase-expressing cells (n = 1).

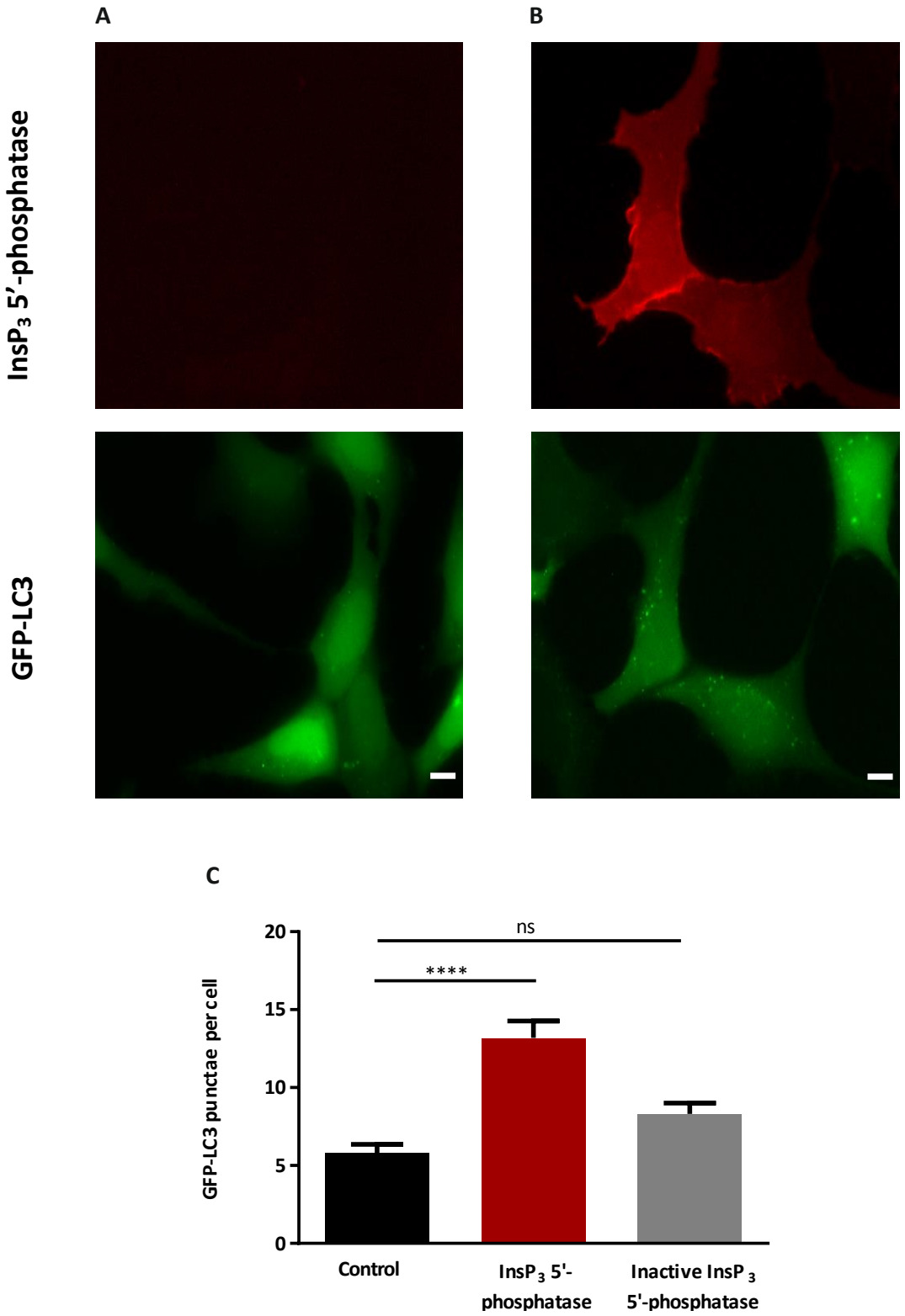

Figure 4.2. HEK cells transfected with $InsP_3$ 5'-phosphatase displayed increased autophagy. Panel A represents untransfected HEK cells, with a basal level of autophagy. Panel B shows cells transfected with mCherry $InsP_3$ 5'-phosphatase (12-hour transfection), with an increased number of GFP-LC3 punctae. Panel C is a quantitative representation of the effects of $InsP_3$ 5'-phosphatase, and the inactive form of the enzyme, on autophagy, with the latter showing similar level autophagy to control cells. The data are mean ± S.E.M of 3 - 5 experiments (40 - 55 cells per condition). The data were analysed with a one-way ANOVA. **** indicates $p < 0.0001$. The scale bars in Panels A and B indicate 10 µm.

4.3.2 Agonist responses in $InsP_3$ 5'-phosphatase-transfected cells and non-transfected cells

To examine how expression of the $InsP_3$ 5'-phosphatase affected cellular Ca^{2+} signalling, cells were loaded with Fura-2 and Rhod-2 to monitor cytosolic and mitochondrial Ca^{2+} responses, respectively. To provoke Ca^{2+} signals the cells were superfused with complete imaging medium supplemented with histamine (for HeLa cells), or ATP (for HEK cells). Both of these agonists trigger the production of $InsP_3$ and mobilisation of Ca^{2+} from stores, with sub-maximal and maximal agonist concentrations of ~2.5 µM and 100 µM. The averaged population results presented in Figure 4.3, and the example single cell traces shown in Figure 4.4, indicate that HeLa and HEK cells transfected with the $InsP_3$ 5'-phosphatase (GFP form) showed substantially reduced cytosolic and mitochondrial Ca^{2+} responses, compared to non-transfected cells. From these data, the percentage of cells that responded to agonist stimulation, and showed Ca^{2+} oscillations, were calculated. These analyses also confirmed that HeLa and HEK cells expressing the $InsP_3$ 5'-phosphatase had lesser responses to either 2.5 µM or 100 µM agonist concentrations compared to non-transfected cells (Figures 4.5 and 4.6). Expression of a catalytically inactive $InsP_3$ 5'-phosphatase did not significantly affect the response of HEK cells to ATP (Figure 4.6).

It is important to note that Rhod-2 can become compartmentalised in both mitochondria and the cytosol [387]. Therefore, additional control experiments were carried out to determine whether Rhod-2 signals reflected mitochondrial or cytosolic Ca^{2+} responses, or a mixture of both. To this end, cells were incubated with oligomycin (5µM) and antimycin A (5 µM) to depolarise mitochondria, and prevent Ca^{2+} uptake via the mitochondrial uniporter. The results presented in Figure 4.7 show that indeed there was some Rhod-2 in the cytosol, since oligomycin and antimycin A did not entirely abolish Rhod-2 responses. However, there was a significant decrease in Rhod-2 responses following oligomycin and

antimycin A application suggesting that a proportion of the Rhod-2 signal emanated from mitochondria. Moreover, although the Fura-2 and Rhod-2 signals were temporally similar, they did not exactly mirror each other (Figure 4.4), consistent with the notion that they arose from separate cellular compartments. Taken together, these data indicated that expression of the $InsP_3$ 5'-phosphatase abrogated $InsP_3R$-evoked Ca^{2+} signals in both the cytosol and mitochondria.

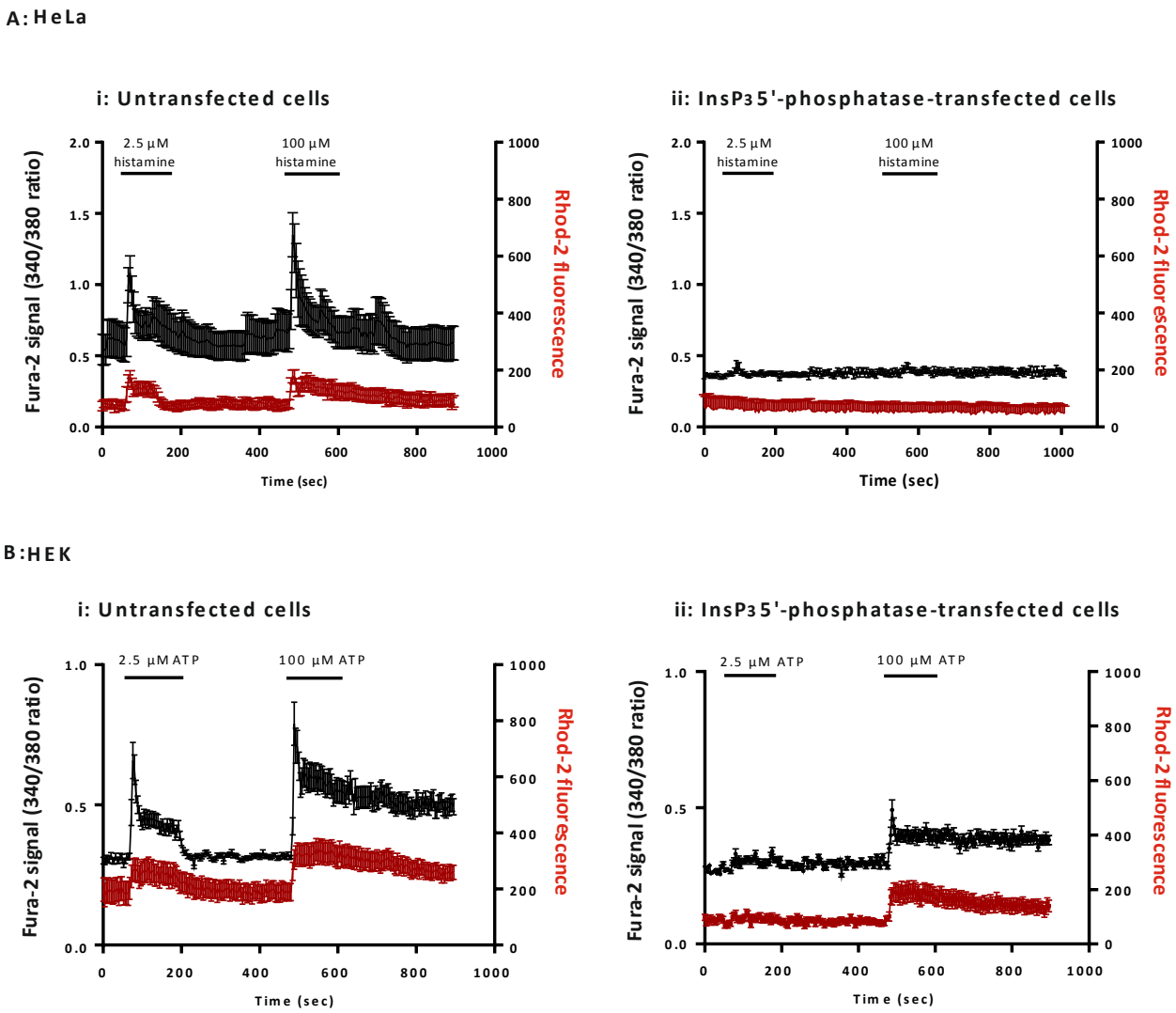

Figure 4.3. Cytosolic and mitochondrial Ca^{2+} signals were concomitantly reduced in $InsP_3$ 5'-phosphatase–expressing HeLa and HEK cells. The traces in Panels A and B represent recordings from Fura-2- and Rhod-2-loaded HeLa (A) and HEK (B) cells. Cytosolic and mitochondrial Ca^{2+} signals were monitored in untransfected cells (Panels Ai and Bi), or in cells transfected with $InsP_3$ 5'-phosphatase (GFP form) (Panels Aii and Bii). Ca^{2+} signals were evoked by addition of a submaximal and a maximal agonist concentration (histamine or ATP; 2.5 and 100 µM); larger Ca^{2+} signals were observed in untransfected cells, whereas less prominent Ca^{2+} transients were shown in $InsP_3$ 5'-phosphatase-transfected cells. The data are representative of 3 experiments for each cell type. The data expressed as mean ± S.E.M (total cells: 75 untransfected and 35 transfected HeLa cells; 100 untransfected and 65 transfected HEK cells).

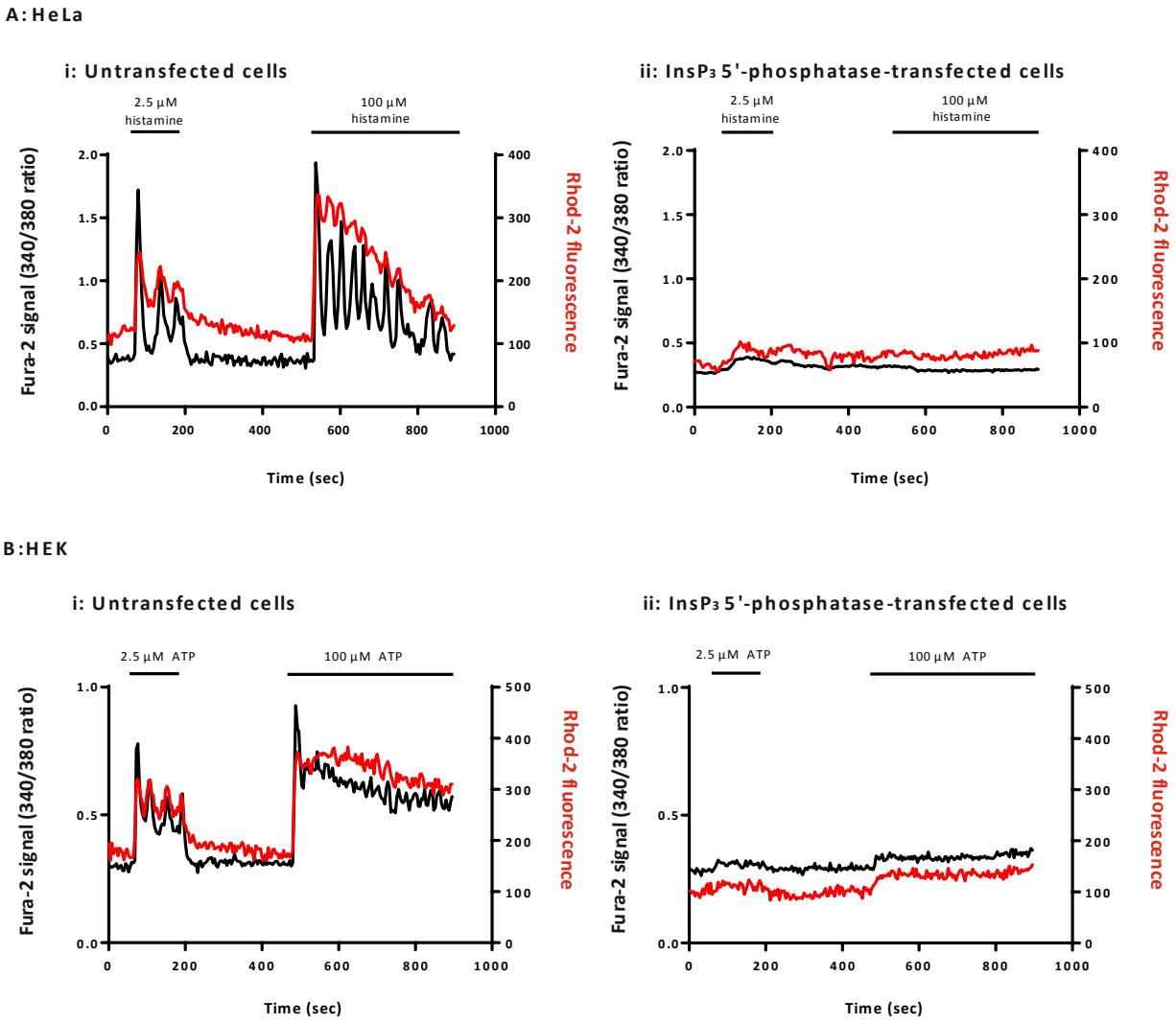

Figure 4.4. Cytosolic and mitochondrial Ca^{2+} signals were concomitantly reduced in $InsP_3$ 5'-phosphatase–expressing HeLa and HEK cells. The traces in Panels A and B represent Fura-2 and Rhod-2 recordings from individual HeLa and HEK cells. Cytosolic (black traces) and mitochondrial (red traces) Ca^{2+} signals were monitored in untransfected cells (Panels Ai and Bi), or in cells transfected with $InsP_3$ 5'-phosphatase (GFP form) (Panels Aii and Bii). Ca^{2+} signals were evoked by addition of a submaximal and a maximal agonist concentration (histamine or ATP; 2.5 and 100 µM); larger Ca^{2+} signals were observed in untransfected cells, whereas less prominent responses were shown in $InsP_3$ 5'-phosphatase-transfected cells.

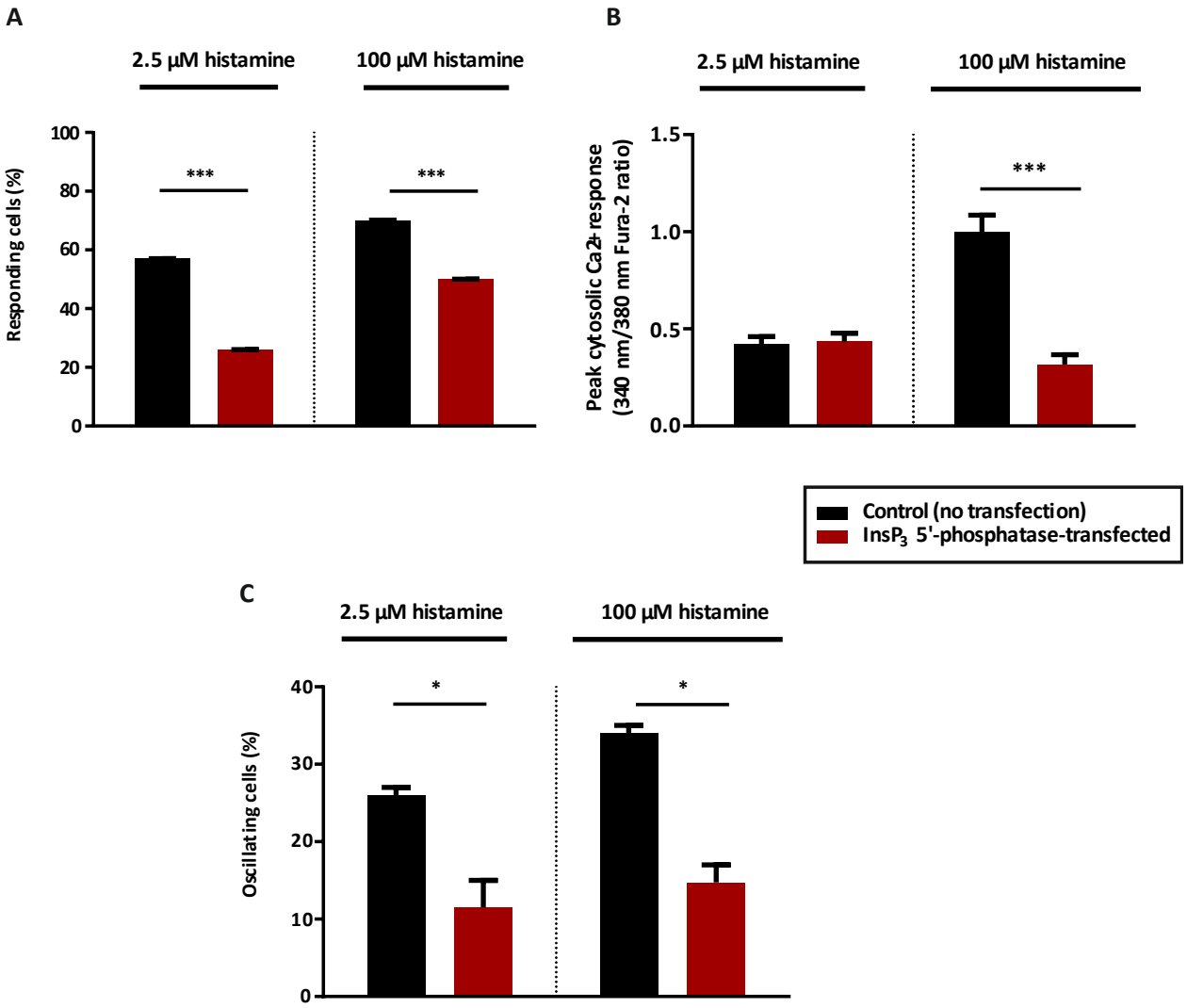

Figure 4.5. Expression of $InsP_3$ 5'-phosphatase reduced histamine-evoked Ca^{2+} signals in GFP-LC3-expressing HeLa cells. Panels A - C show that HeLa cells transfected with an $InsP_3$ 5'-phosphatase (mCherry form) had a lesser response to both 2.5 µM and 100 µM histamine compared to non-transfected cells. Panels B and C represent data of responding cells only. The data are mean ± S.E.M of 3 experiments. The data were analysed with a one-way ANOVA. * indicates $p < 0.05$ and *** indicates $p < 0.001$.

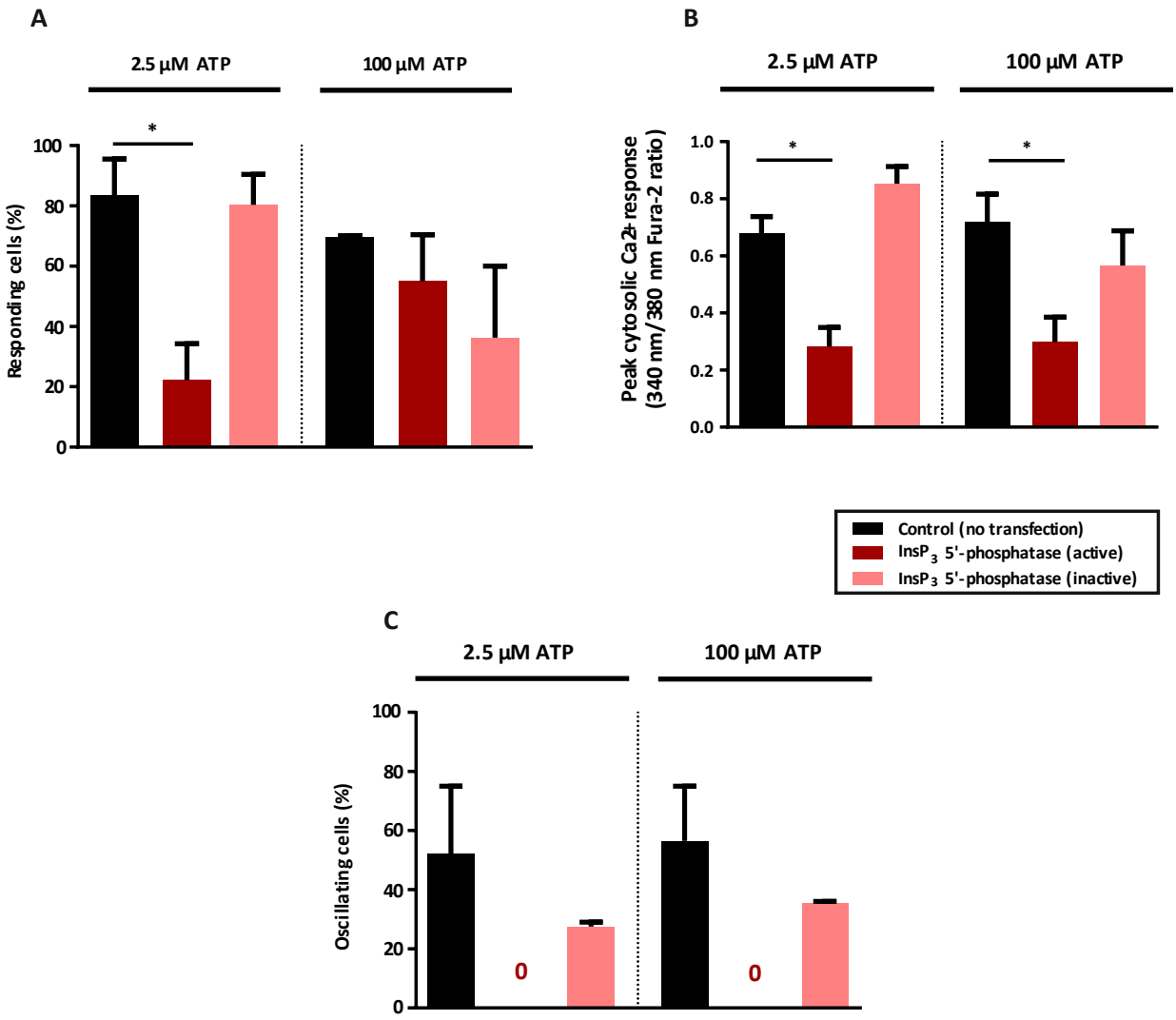

Figure 4.6. Expression of $InsP_3$ 5'-phosphatase reduced ATP-evoked Ca^{2+} signals in GFP-LC3-expressing HEK cells. Panels A - C show that HEK cells transfected with an $InsP_3$ 5'-phosphatase (mCherry form) had a lesser response to both 2.5 µM and 100 µM ATP compared to non-transfected cells, or cells transfected with a catalytically inactive $InsP_3$ 5'-phosphatase. The data are mean ± S.E.M of 3 experiments. The data were analysed with a one-way ANOVA. * indicates $p < 0.05$.

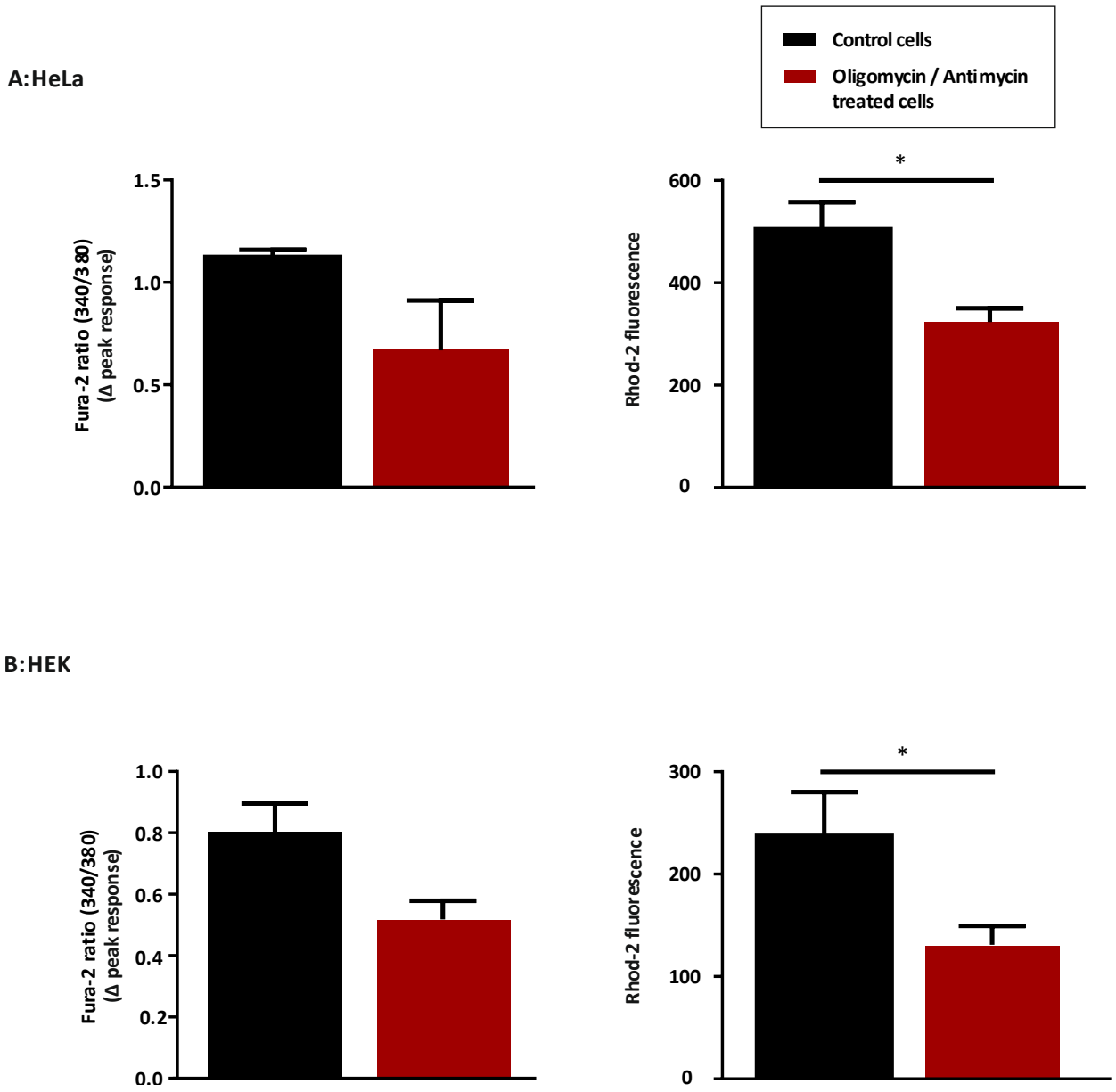

Figure 4.7. Mitochondrial depolarisation decreased mitochondrial Ca^{2+} uptake, but did not affect cytosolic Ca^{2+} signals, in HeLa and HEK cells. Cytosolic and mitochondrial Ca^{2+} signals were simultaneously monitored by loading cells with both Fura-2 and Rhod-2. Following indicator loading, cells were either left untreated, or were treated with 5 µM oligomycin and antimycin A for 5 minutes prior to imaging. Ca^{2+} signals were evoked by the addition of 100 µM histamine to HeLa cells, or 100 µM ATP to HEK cells (Panels A and B, respectively). The column graphs represent the difference between Fura-2 and Rhod-2 fluorescence signals before histamine/ATP addition and the peak responses observed following stimulation of the cells with the agonist. Cells treated with oligomycin and antimycin A showed a reduction in Rhod-2 peak fluoresence compared to control cells. There was a residual response of Rhod-2 in oligomycin- and antimycin A-treated cells, which is likely have been due to Rhod-2 in the cytosol since whole cells, and not just mitochondrial regions, were measured in the analysis. The data are representative of 2-3 experiments for each cell type (100 – 150 cells per condition). The data were analysed with a one-way ANOVA. * indicates $p < 0.05$.

4.3.3 $InsP_3$ 5'-phosphatase expression did not correlate with GFP-LC3 punctae number

In order to evaluate any correlation between different levels of protein expression and induction of autophagy, HeLa cells showing different intensities of mCherry fluorescence (following transfection with 1 μg of the mCherry-tagged $InsP_3$ 5'-phosphatase plasmid DNA) were evaluated for autophagy levels. It was postulated that greater $InsP_3$ 5'-phosphatase protein expression (assessed by the intensity of mCherry fluorescence) could result in a more substantial number of GFP-LC3 punctae due to increased inhibition of $InsP_3R$-mediated Ca^{2+} release. However, no correlation was found between mCherry fluorescence and the number of GFP-LC3 punctae (Figure 4.8), suggesting that even low levels of the $InsP_3$ 5'-phosphatase efficiently inhibited Ca^{2+} release from $InsP_3$ receptors and triggered autophagy.

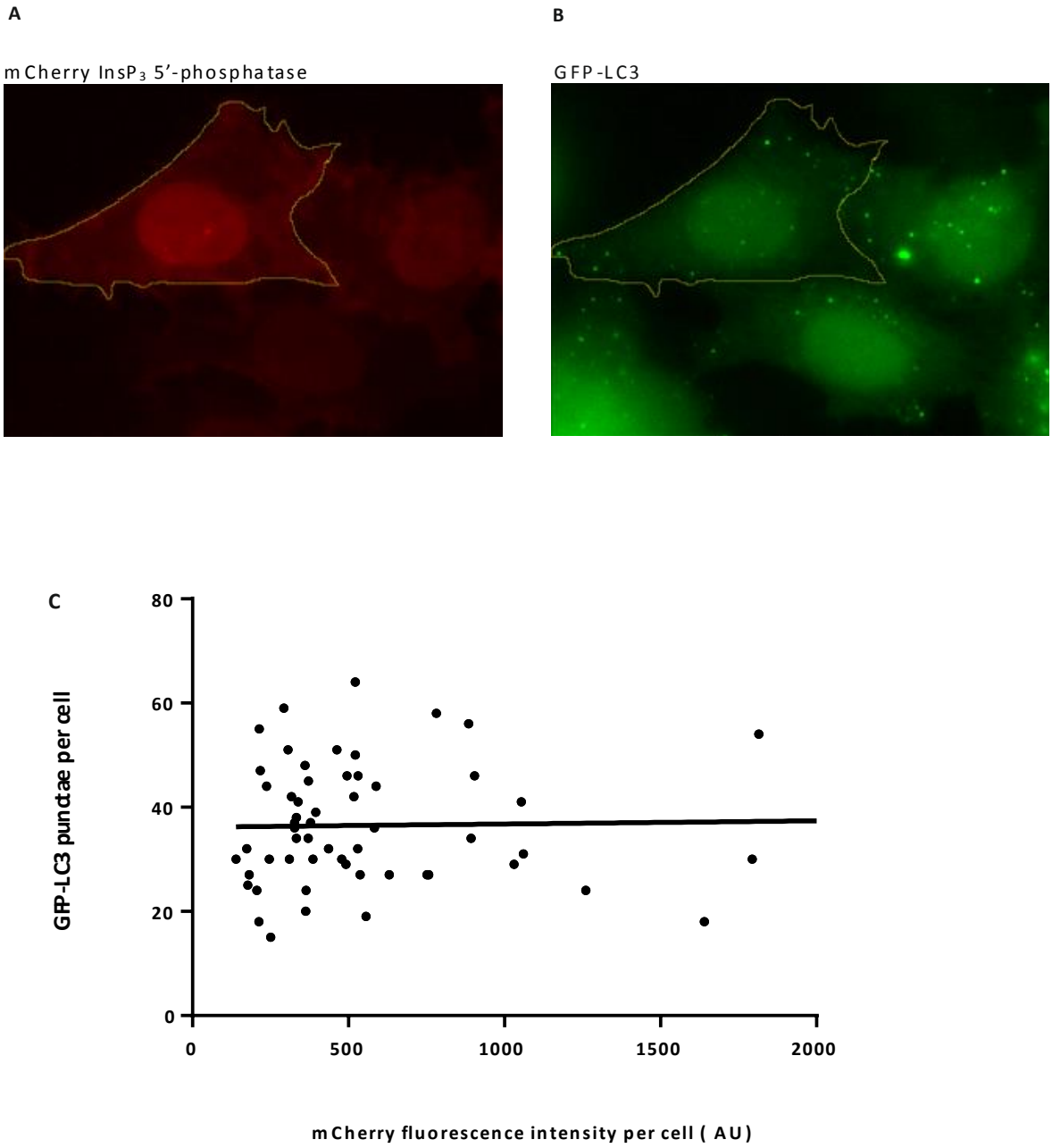

Figure 4.8. Correlation of $InsP_3$ 5'-phosphatase transfection and GFP-LC3 punctae in HeLa cells. Panel A is a representative image of cells transfected with 1 μg mCherry $InsP_3$ 5'-phosphatase (12-hour transfection). Panel B shows the consequent induction of autophagy. The level of $InsP_3$ 5'-phosphatase expression is reflected by the mCherry fluorescence intensities in individual cells. Panel C is a plot of mCherry-$InsP_3$ 5'-phosphatase intensity versus induction of autophagy for individual cells (55 cells from 5 independent experiments). Line of best fit was plotted using analysis of linear regression ($R^2 = 0.0006$).

4.3.4 Inhibition of $InsP_3Rs$ with 2-APB induced autophagy

The data presented above show that transfection of cells with an $InsP_3$ 5'-phosphatase triggered autophagy. From this result, it would be expected that other blockers of $InsP_3R$ function would have a similar effect. Therefore, the action of 2-aminoethoxydiphenyl borate (2-APB), a well-known inhibitor of $InsP_3Rs$ [388], was examined. Consistent with the effect of expressing the $InsP_3$ 5'-phosphatase, acute application of 2-APB (100 μM for 1 hour) increased the accumulation of GFP-LC3 punctae and also reduced histamine-evoked cytosolic Ca^{2+} signals (Figure 4.9).

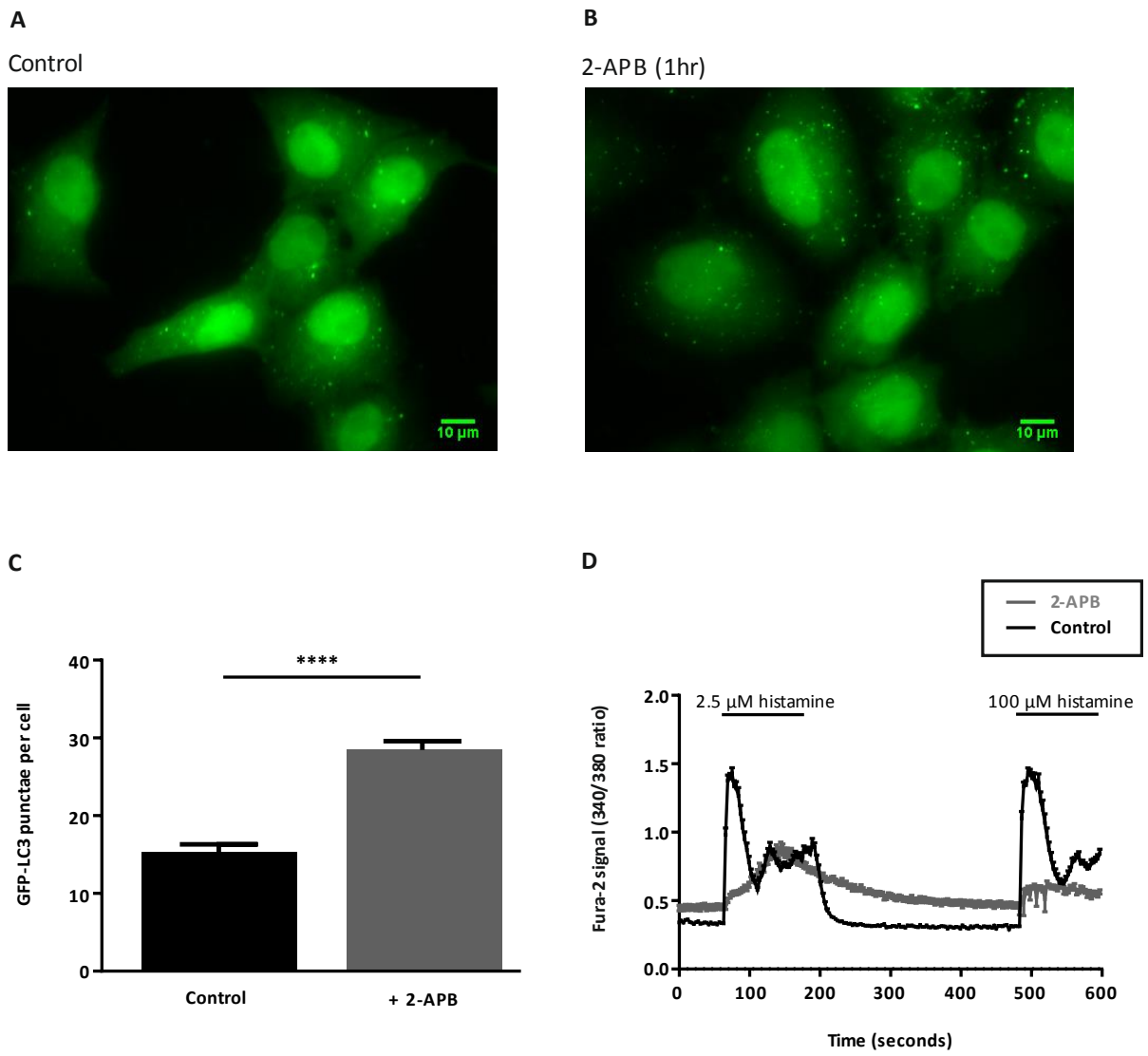

Figure 4.9. Inhibition of $InsP_3Rs$ with 2-APB induced autophagy in HeLa cells. Panel A is a representative image of cells in complete imaging medium. Panel B is a representative image of the same cells following a 1-hour incubation with 2-APB (100 µM). Panel C is a quantitative representation of the effect of 2-APB on autophagy. Panel D shows averaged Ca^{2+} signals upon addition of 2.5 µM and 100 µM histamine to cells following 2-APB treatment, or to cells that were not treated with 2-APB. Larger Ca^{2+} signals were observed in the untreated cells, whereas less prominent peaks are shown in 2-APB treated cells. The data are mean ± S.E.M of 3 experiments (70 - 90 cells per condition). The data were analysed with a one-way ANOVA test. **** indicates $p < 0.0001$.

4.3.5 The phospholipase C inhibitor U-73122 induced autophagy

Another tool that is widely used for inhibiting Ca^{2+} release from $InsP_3Rs$ is U-73122, an inhibitor of phospholipase C. Essentially, this compound prevents the production of $InsP_3$, and as a consequence Ca^{2+} release from $InsP_3$ receptors is abrogated. Incubation of cells with U73122 increased the accumulation of GFP-LC3 punctae (Figure 4.10), although the effect of the phospholipase C inhibitor was slower, and not as big as that with 2-APB (Figure 4.9). The accumulation of GFP-LC3 punctae during incubation with U73122 is consistent with the results obtained using both the $InsP_3$ 5'-phosphatase and 2-APB. The slower action of U73122 might point to it giving a weaker inhibition of $InsP_3R$-mediated Ca^{2+} signals compared to the other treatments.

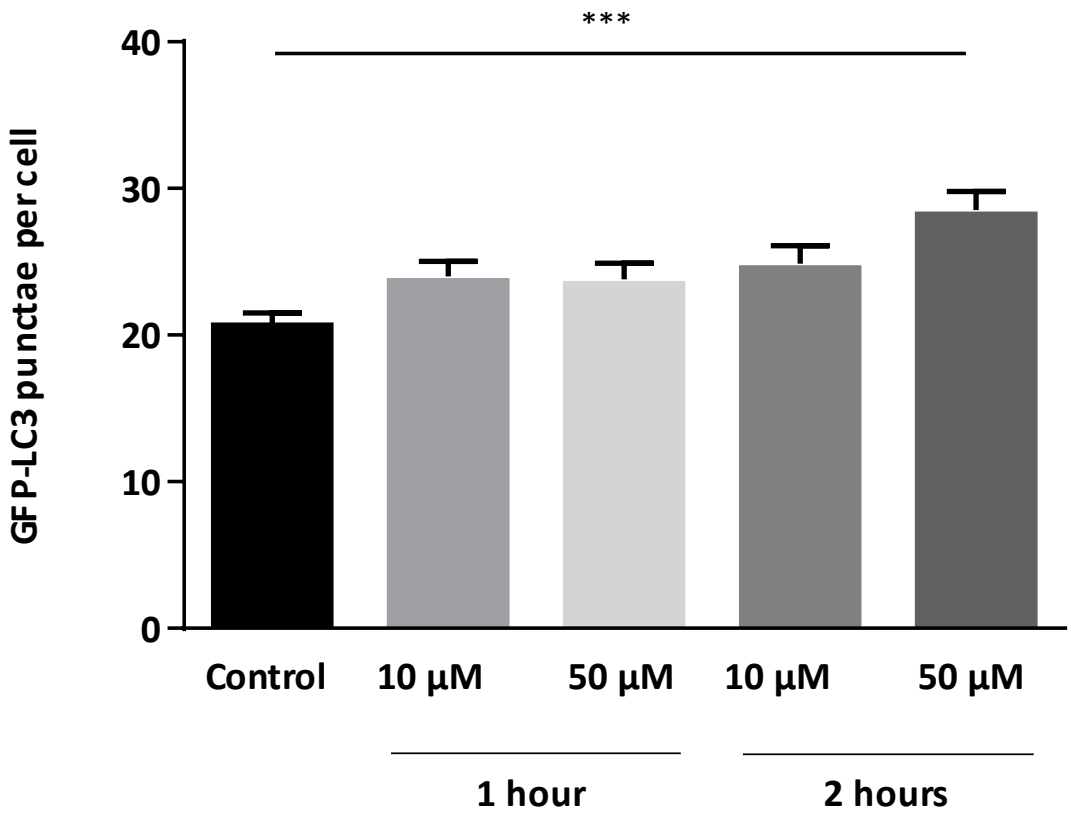

Figure 4.10. The phospholipase C inhibitor U73122 induced autophagy in HeLa cells. The graph shows a quantitative representation of the effect of 10 µM and 50 µM U73122 on autophagy, following a 1- or 2-hour incubation. The number of GFP-LC3 punctae per cell increased following a 2-hour incubation with 50 µM U73122. Cells were incubated with U73122 in complete imaging medium. The data are mean ± S.E.M of 3 experiments (30 - 60 cells per condition). The data were analysed with a one-way ANOVA test. *** indicates $p < 0.01$.

4.3.6 Rapamycin and $InsP_3$ 5'-phosphatase did not show a synergistic or additive effect on the induction of autophagy

The data presented in this Chapter so far has demonstrated that Inhibition of $InsP_3R$-mediated Ca^{2+} signalling induced autophagy. To explore if there was an interaction between autophagy caused by reduced $InsP_3R$ opening and that arising via mTOR inhibition, cells were transfected with the $InsP_3$ 5'-phosphatase and simultaneously treated with rapamycin. For these experiments, two different amounts of mCherry-$InsP_3$ 5'-phosphatase (0.2 μg or 1 μg) were used to transfect the cells, with the intention of evoking different levels of autophagic response that might reveal additivity/synergy with rapamycin. However, with HeLa cells, both amounts of mCherry-$InsP_3$ 5'-phosphatase plasmid DNA gave a similar number of GFP-LC3 punctae (Figure 4.11), consistent with the data shown in Figure 4.8 that the expression of $InsP_3$ 5'-phosphatase has an all-or-none effect, rather than being concentration dependent. With HEK cells, 1 μg of the mCherry-$InsP_3$ 5'-phosphatase plasmid DNA gave a robust transfection and induction of autophagy (Figure 4.12). Whereas, 0.2 μg of mCherry-$InsP_3$ 5'-phosphatase plasmid DNA was not sufficient for triggering autophagy. Despite the concentration of mCherry-$InsP_3$ 5'-phosphatase plasmid DNA used to transfect the cells, concurrent application of rapamycin did not give any additional increase in GFP-LC3 punctae numbers (Figures 4.11 and 4.12). It is plausible that rapamycin and $InsP_3$ 5'-phosphatase induced autophagy through the same canonical pathway. This would explain why the addition of rapamycin to $InsP_3$ 5'-phosphatase-transfected cells did not increase autophagy to a higher level than the $InsP_3$ 5'-phosphatase alone.

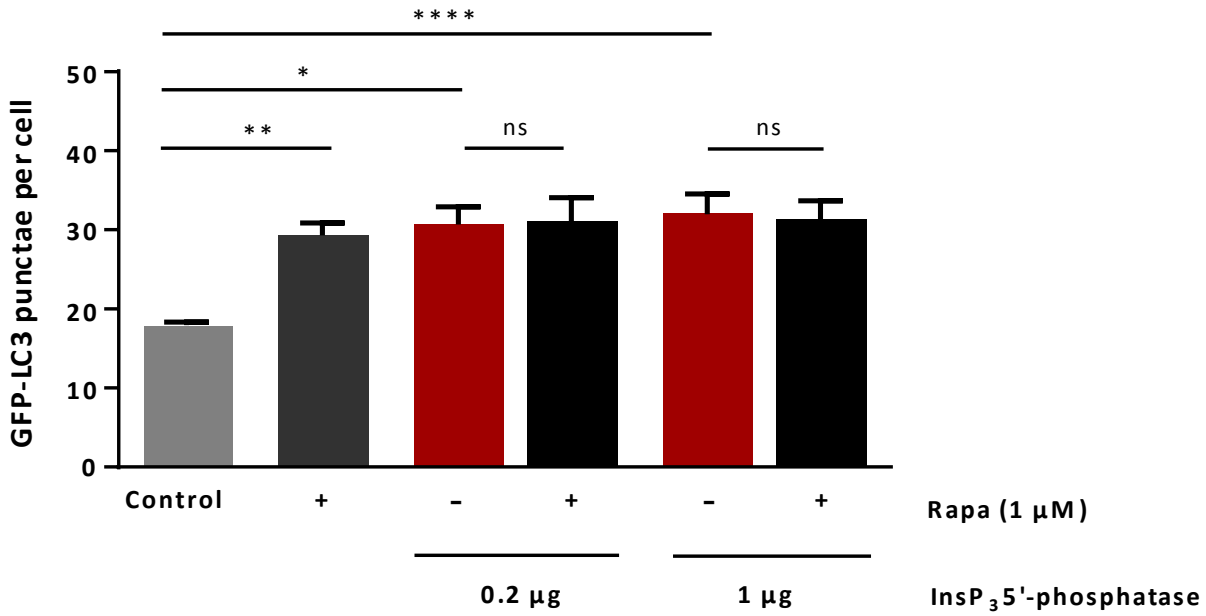

Figure 4.11. Rapamycin and $InsP_3$ 5'-phosphatase did not have an additive effect on autophagy in HeLa cells. The bar graph shows a quantitative representation of the effect of rapamycin on autophagy levels in cells that were either untransfected, or transfected with an mCherry-$InsP_3$ 5'-phosphatase construct. The data are mean ± S.E.M of 3 experiments (30 - 50 cells per condition) and were analysed with a one-way ANOVA. * indicates $p < 0.05$, ** indicates $p < 0.01$ and **** indicates $p < 0.001$.

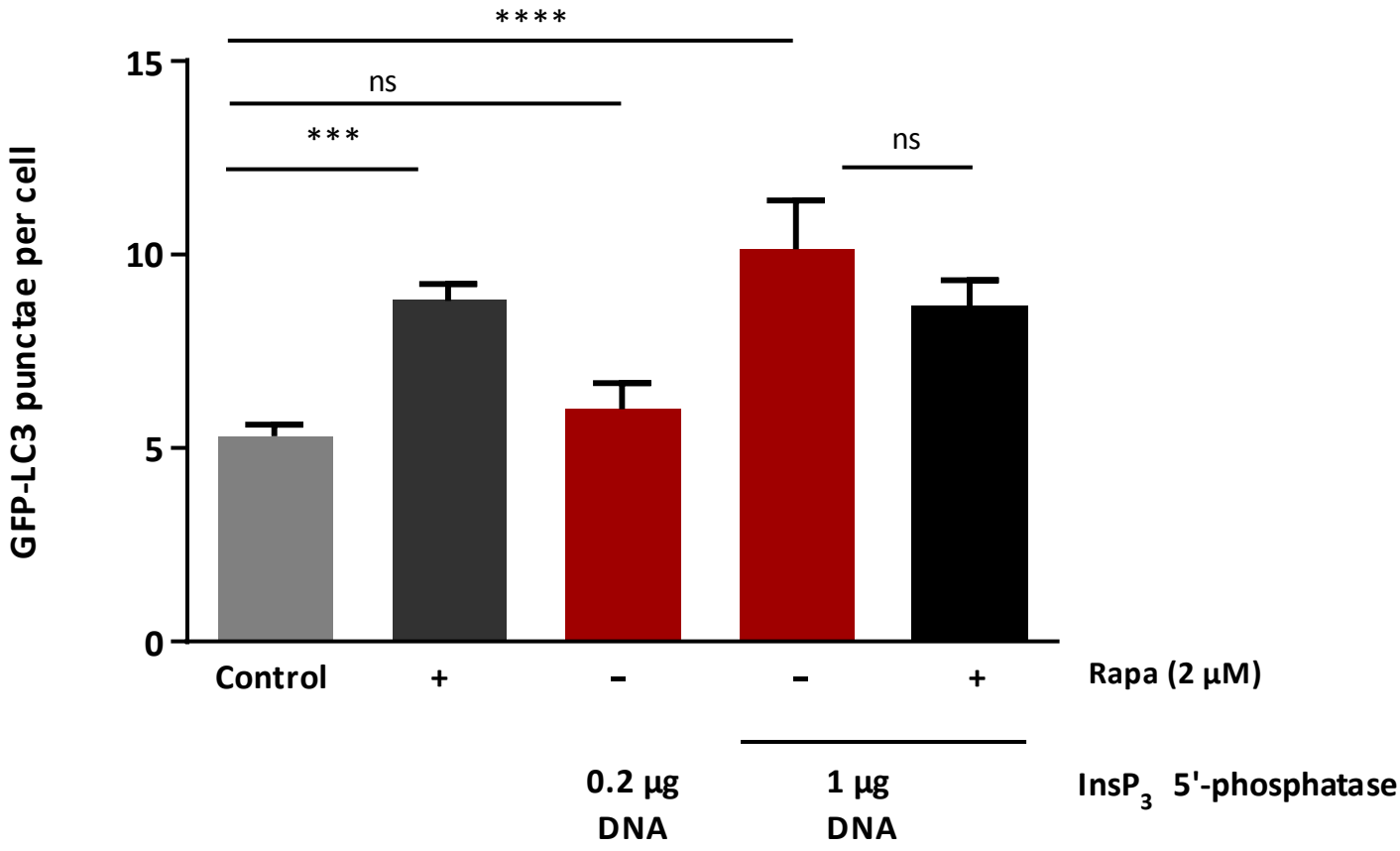

Figure 4.12. Rapamycin and $InsP_3$ 5'-phosphatase did not have an additive effect on autophagy in HEK cells. The column graph shows a quantitative representation of the effect of rapamycin on autophagy in cells that were either untransfected, or transfected with an mCherry-$InsP_3$ 5'-phosphatase construct. The data are mean ± S.E.M of 3 experiments (30 - 75 cells per condition) and were analysed with a one-way ANOVA. *** indicates $p < 0.001$ and **** indicates $p < 0.0001$.

4.3.7 BAPTA-AM inhibited autophagy induced by $InsP_3$ 5'-phosphatase

The accumulation of GFP-LC3 punctae following expression of the $InsP_3$ 5'-phosphatase, suggests that $InsP_3R$-mediated Ca^{2+} release provides a signal that suppresses autophagy. In this situation, Ca^{2+} signals would be anti-autophagic. However, one of the most consistent methods for preventing the induction of autophagy is the buffering of Ca^{2+} using BAPTA-AM (Chapter 3, Figure 3.24), and in this context Ca^{2+} signals would be pro-autophagic. To examine the interplay between these Ca^{2+} signals, the effect of BAPTA-AM loading on $InsP_3$ 5'-phosphatase was examined. For these experiments, cells were pre-incubated with BAPTA-AM (10 μM for 1 hour at room temperature), concurrently with Fura-2 loading in the final hour of the 12–hour transfection with $InsP_3$ 5'-phosphatase. As shown earlier (Figures 4.1 and 4.2), transfection of HeLa and HEK cells with the mCherry-$InsP_3$ 5'-phosphatase induced the accumulation of GFP-LC3 punctae (Figures 4.13 and 4.14). With both HeLa and HEK cells that were loaded with BAPTA-AM in the number of GFP-LC3 punctae was reduced to basal, or even sub-basal, levels. These data are consistent with a scheme in which $InsP_3Rs$ provide a Ca^{2+} signal that suppresses autophagy, and so prevention of $InsP_3R$-mediated Ca^{2+} release switches on autophagy. At the same time, another Ca^{2+} signal, which can be buffered by BAPTA-AM loading, is required for autophagy to occur. The nature and source of the Ca^{2+} signal that is buffered by BAPTA-AM is unclear. However, it obviously cannot be from $InsP_3Rs$.

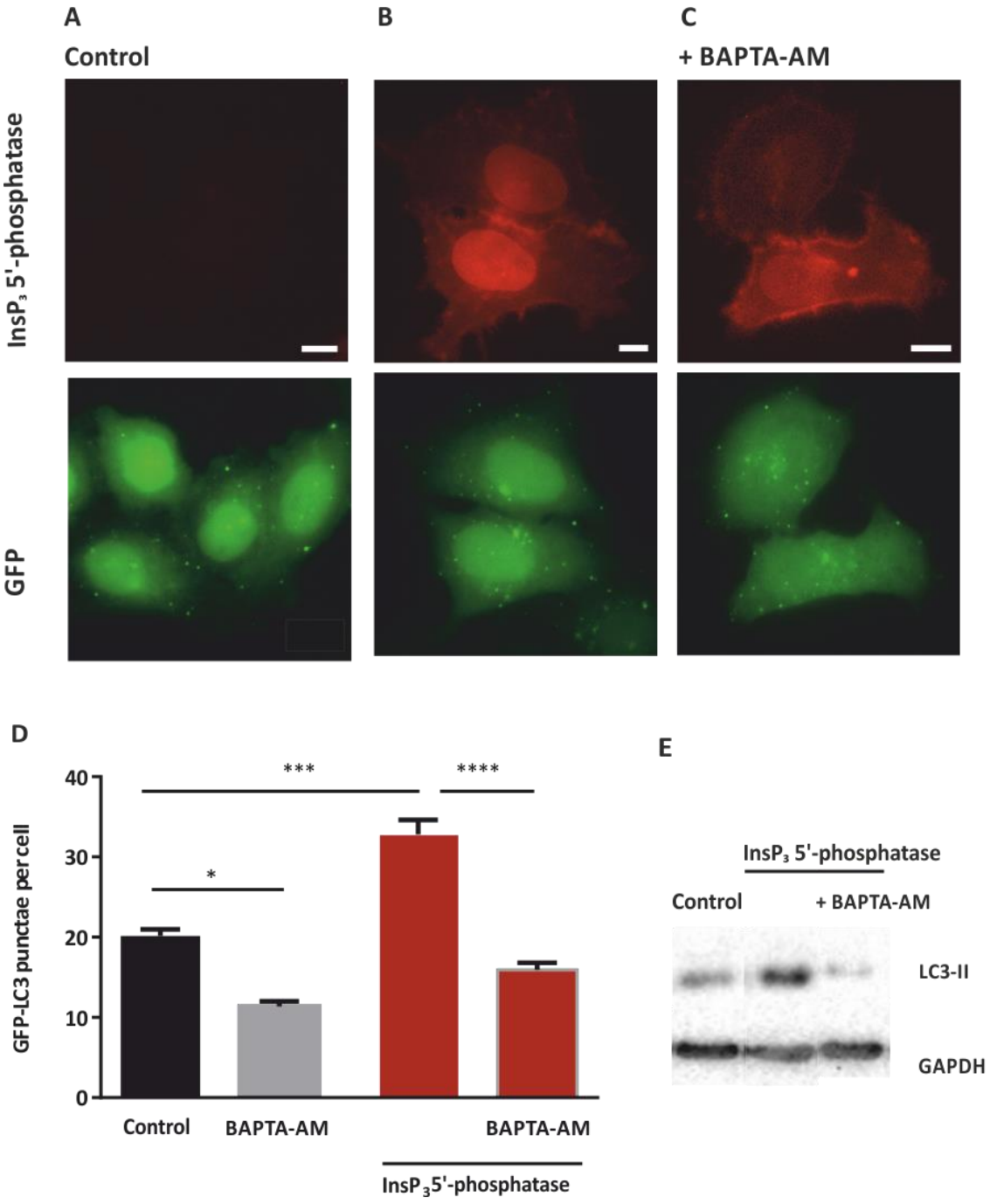
A
Control
B
C
+ BAPTA-AM
InsP3 5'-phosphatase
GFP
D
GFP-LC3 punctae per cell
40
30
20
10
0
***
****
*
Control
BAPTA-AM
BAPTA-AM
InsP3 5'-phosphatase
E
InsP3 5'-phosphatase
Control
+ BAPTA-AM
LC3-II
GAPDH

Figure 4.13. Preincubation of HeLa cells with BAPTA-AM inhibited the induction of autophagy by $InsP_3$ 5'-phosphatase. Panel A represents GFP-LC3 cells that are untreated (control). Panel B represents cells transfected with mCherry-tagged $InsP_3$ 5'-phosphatase (12-hour transfection), showing an increased number of GFP-LC3 punctae. Panel C represents cells treated with 10 µM BAPTA-AM for one hour at the 11^{th} hour of $InsP_3$ 5'-phosphatase transfection; the number of GFP-LC3 punctae was similar to those at basal level (control). Panel D is a quantitative representation of the effects of $InsP_3$ 5'-phosphatase and BAPTA-AM on autophagy. The data are mean ± S.E.M of 3 - 4 experiments (40 - 60 cells per condition). The data were analysed with a one-way ANOVA. * indicates $p < 0.05$, *** indicates $p < 0.001$ and **** indicates $p < 0.0001$. The scale bars in Panels A-C indicate 10 µm. Panel E is a Western blot showing the expression of LC3-II protein with GAPDH as a loading control (note that two of the blot columns were shown in Figure 4.1). The intensity of the LC3-II band was increased in $InsP_3$ 5'-phosphatase-expressing cells, but reduced by BAPTA-AM loading (*n* = 1).

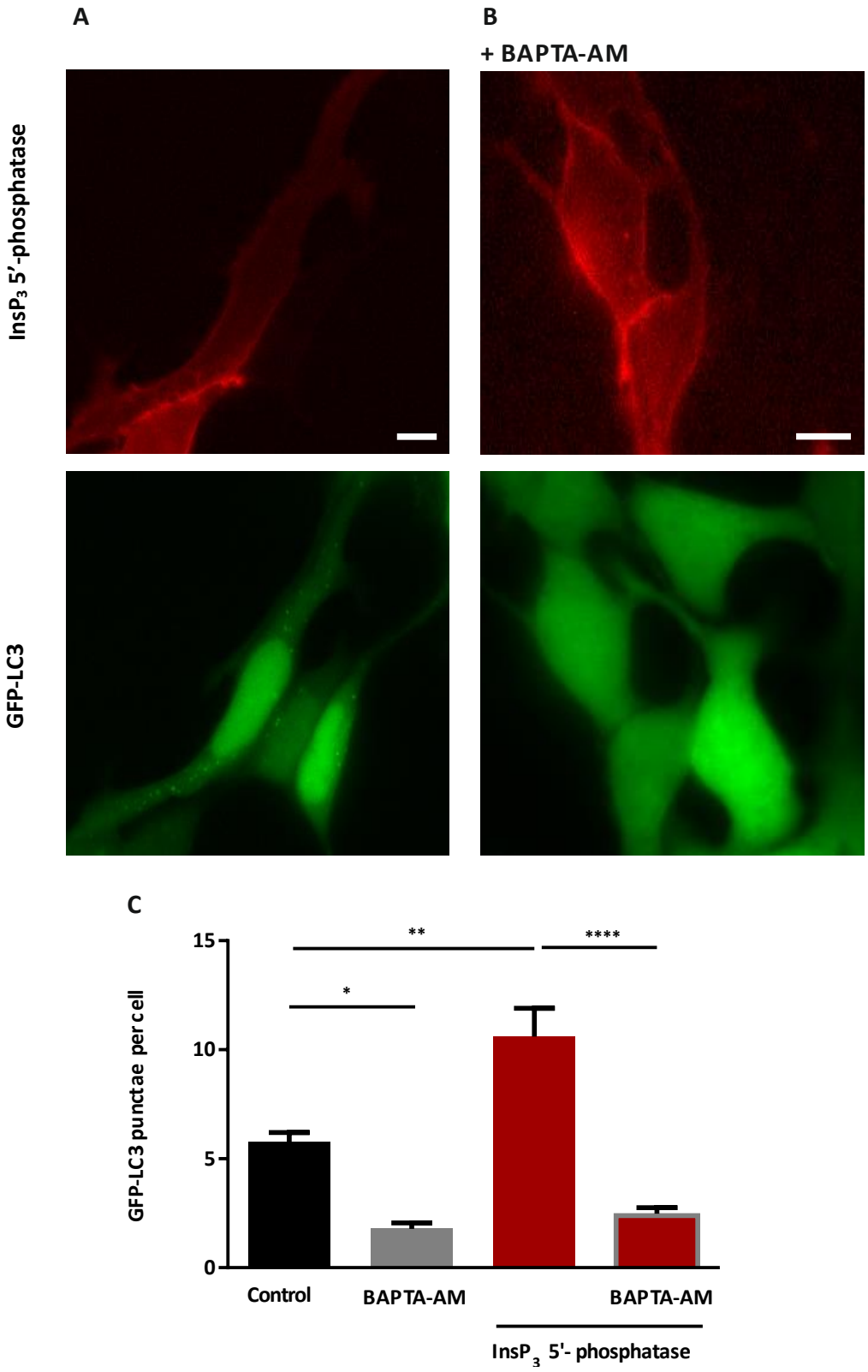
A
B
+ BAPTA-AM
InsP3 5'-phosphatase
GFP-LC3
C
GFP-LC3 punctae per cell
15
10
5
0
**
****
*
Control
BAPTA-AM
BAPTA-AM
InsP3 5'- phosphatase

Figure 4.14. Preincubation of HEK cells with BAPTA-AM inhibited the induction of autophagy by $InsP_3$ 5'-phosphatase. Panel A shows an image of GFP-LC3-expressing HEK cells that were transfected with mCherry-tagged $InsP_3$ 5'-phosphatase (12-hour transfection). An increased number of GFP-LC3 punctae is evident in the GFP-LC3 image (Panel A, bottom). Panel B represents GFP-LC3-expressing HEK cells treated with BAPTA-AM (10 μM) for one hour at the 11^{th} hour of the $InsP_3$ 5'-phosphatase transfection. Autophagy was significantly inhibited by the BAPTA-AM incubation, and GFP-LC3 punctae numbers were similar to the basal levels observed in control cells (untransfected cells). Panel C is a quantitative representation of the effects of $InsP_3$ 5'-phosphatase, and $InsP_3$ 5'-phosphatase + BAPTA-AM, on autophagy. The data are mean ± S.E.M of 3 - 4 experiments (40 - 50 cells per condition). The data were analysed with a one-way ANOVA. * indicates $p < 0.05$, ** indicates $p < 0.01$ and **** indicates $p < 0.0001$. The scale bars in Panels A and B indicate 10 μm.

4.3.8 Confirming autophagic flux in $InsP_3$ 5'-phosphatase-transfected cells

Accumulation of GFP-LC3 punctae can occur in situations where the processing of autophagic vesicles is blocked [225]. It was therefore important to examine whether the increase of GFP-LC3 punctae seen following $InsP_3$ 5'-phosphatase transfection was due to interference with autophagic flux. For this purpose, control experiments were performed using 3-MA and BafA1, as described in Chapter 3. HeLa and HEK cells were transfected with the mCherry-$InsP_3$ 5'-phosphatase for 12 hours, and BafA1 or 3-MA were added to the cells for the hour prior to imaging cells (i.e., at the 11^{th} hour post-transfection). As expected, BafA1 caused an accumulation of GFP-LC3 punctae when applied to untransfected cells, but also increased the number of GFP-LC3 punctae in $InsP_3$ 5'-phosphatase-transfected cells (Figures 4.15 and 4.16). Correspondingly, incubation with 3-MA reduced the numbers of GFP-LC3 punctae in both untransfected and $InsP_3$ 5'-phosphatase-transfected cells (Figures 4.17 and 4.18). These data are consistent with expression of the $InsP_3$ 5'-phosphatase triggering an increase in autophagic flux via the canonical PI3-kinase-dependent autophagy pathway.

An important point to make about the results obtained using BAPTA-AM (Figures 4.13 and 4.14) and 3-MA (Figures 4.17 and 4.18) is that the stimulation of autophagy by the $InsP_3$ 5'-phosphatase, and GFP-LC3 punctae accumulation, would have occurred before the compounds were applied to the cells (i.e., autophagy would have been activated during the 12-hour transfection with $InsP_3$ 5'-phosphatase). Therefore, the reduction of GFP-LC3 punctae caused by BAPTA-AM and 3-MA suggests that the existing autophagic vesicles completed their processing, and that no new vesicles were formed. This is significant because it indicates that vesicles can be processed in cells transfected with $InsP_3$ 5'-phosphatase, again consistent with functional autophagic flux.

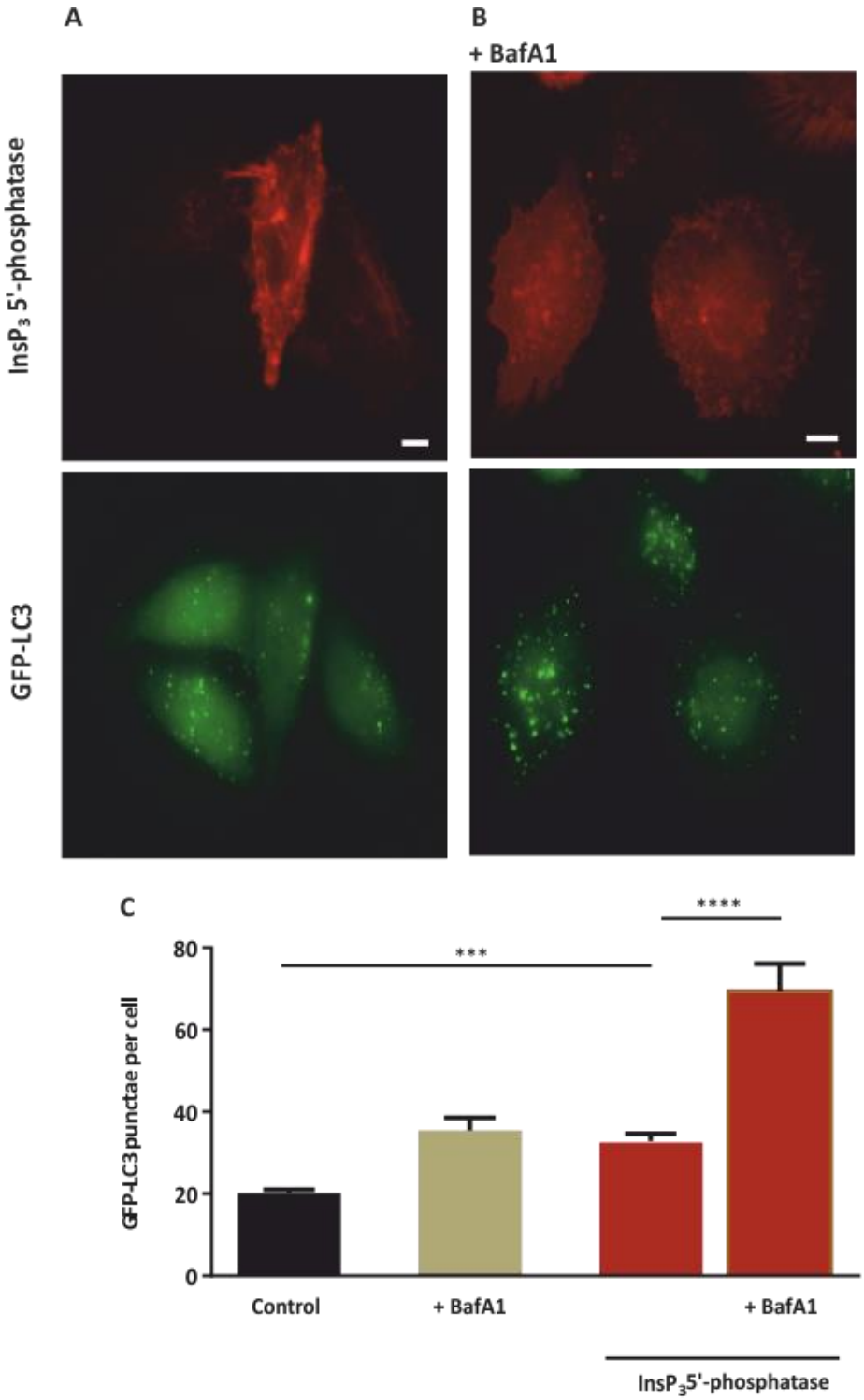

Figure 4.15. Expression of an $InsP_3$ 5'-phosphatase stimulated autophagic flux in HeLa cells. Panel A represents HeLa cells transfected with mCherry-tagged $InsP_3$ 5'-phosphatase (12-hour transfection), showing an increased number of GFP-LC3 punctae. Panel B represents cells treated with 0.1 µM BafA1 for one hour at the 11^{th} hour of $InsP_3$ 5'-phosphatase transfection; the number of GFP-LC3 punctae was further increased. Panel C is a quantitative representation of the effects of $InsP_3$ 5'-phosphatase and BafA1 on autophagy. The data are mean ± S.E.M of 3 experiments (25 - 40 cells per condition). The data were analysed with a one-way ANOVA. *** indicates $p < 0.001$ and **** indicates $p < 0.0001$. The scale bars in Panels A and B indicate 10 µm.

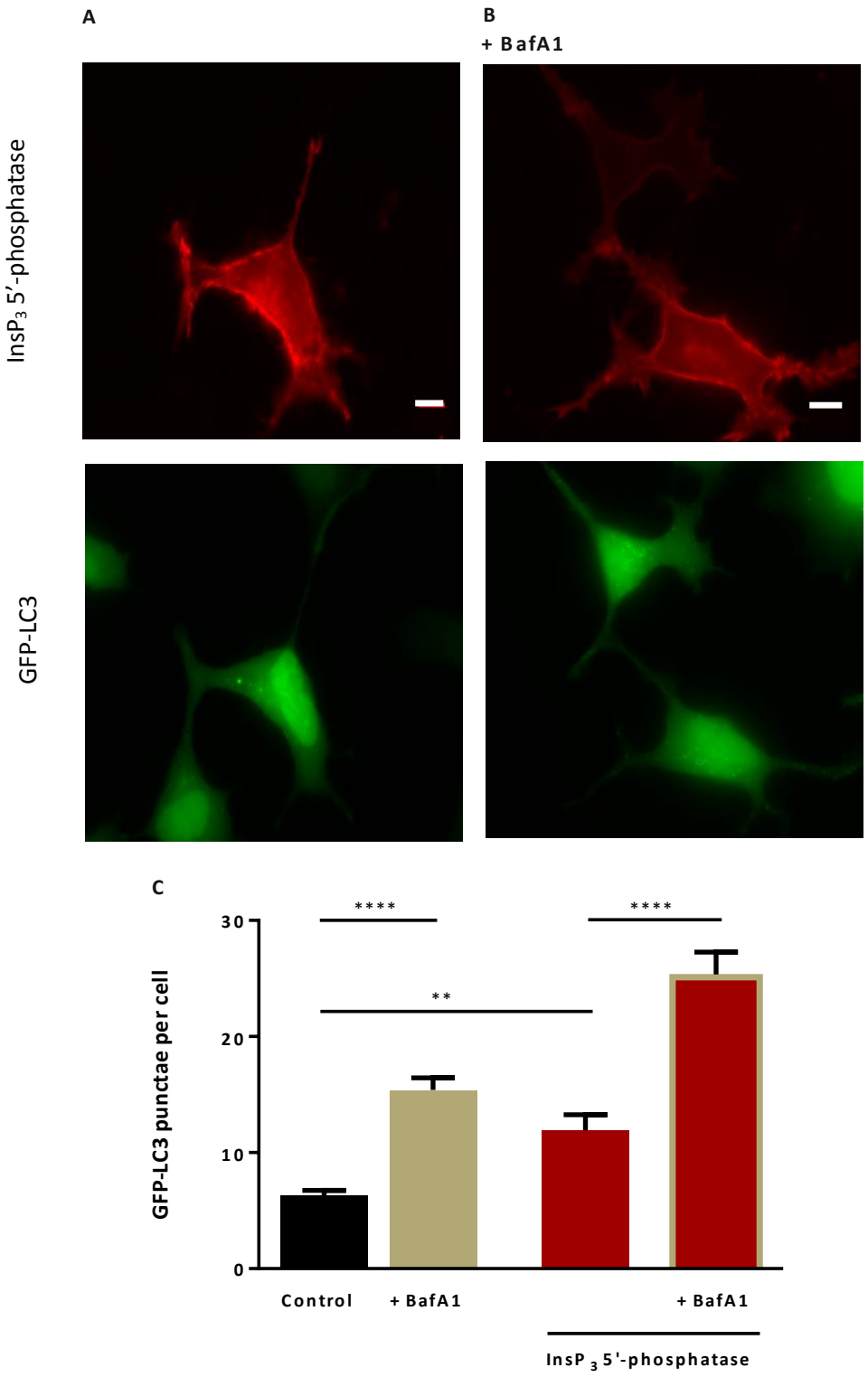

Figure 4.16. Expression of an $InsP_3$ 5'-phosphatase stimulated autophagic flux in HEK cells. Panel A represents HEK cells transfected with mCherry-tagged $InsP_3$ 5'-phosphatase (12-hour transfection), showing an increased number of GFP-LC3 punctae. Panel B represents cells treated with 0.1 µM BafA1 for one hour at the 11th hour of $InsP_3$ 5'-phosphatase transfection; the number of GFP-LC3 punctae was further increased. Panel C is a quantitative representation of the effects of $InsP_3$ 5'-phosphatase and BafA1 on autophagy. The data are mean ± S.E.M of 3 experiments (40 - 50 cells per condition). The data were analysed with a one-way ANOVA. ** indicates $p < 0.01$ and **** indicates $p < 0.0001$. The scale bars in Panels A and B indicate 10 µm.

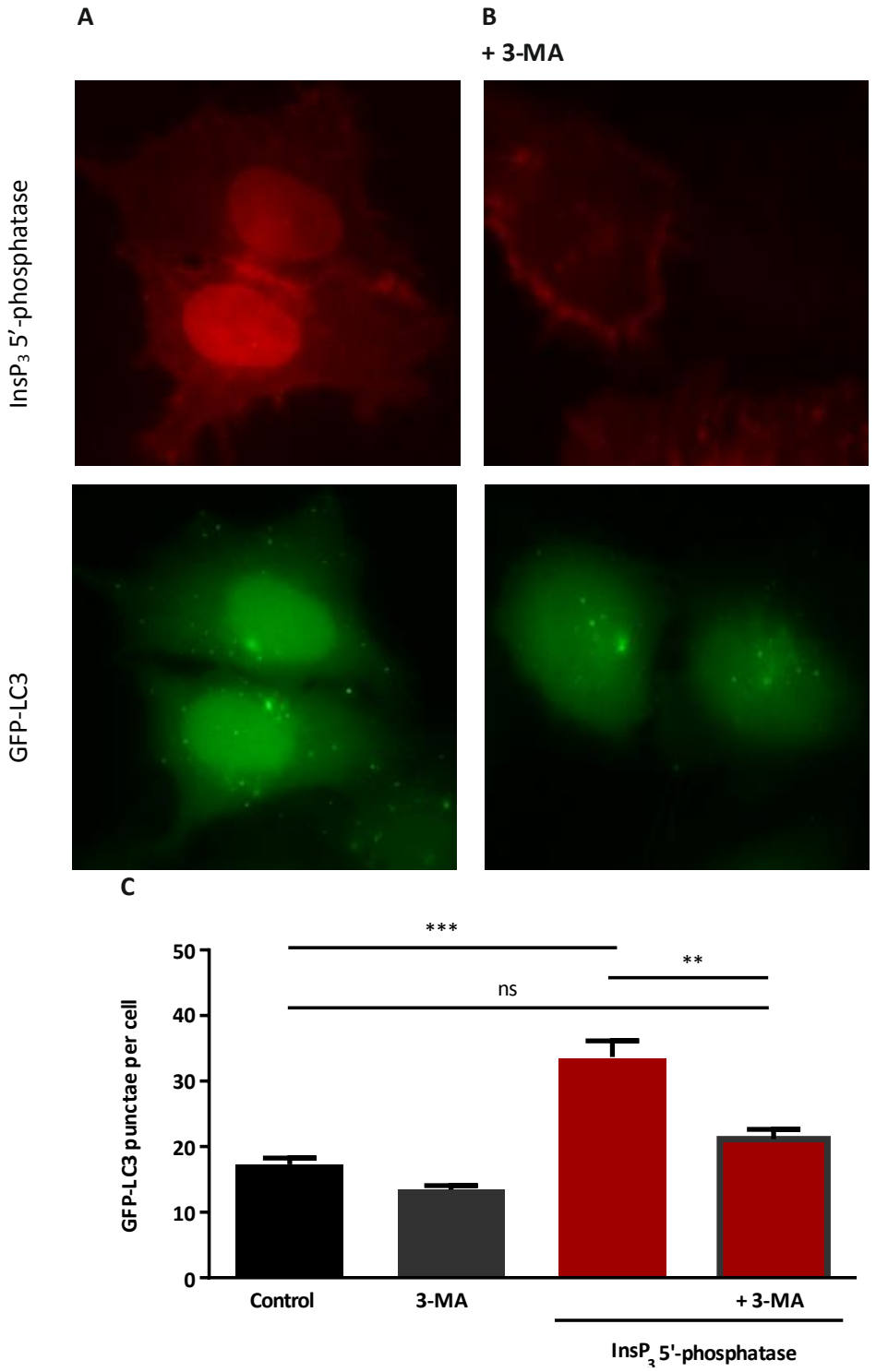

Figure 4.17. Autophagy induced by expression of an $InsP_3$ 5'-phosphatase was inhibited by 3-MA in HeLa cells. Panel A represents cells transfected with mCherry-tagged $InsP_3$ 5'-phosphatase (12-hour transfection), showing an increased number of GFP-LC3 punctae. Panel B represents cells treated with 5 mM 3-MA for one hour at the 11th hour of $InsP_3$ 5'-phosphatase transfection; autophagy was significantly inhibited and GFP-LC3 punctae numbers are similar to those at basal level. Panel C is a quantitative representation of the effects of $InsP_3$ 5'-phosphatase and 3-MA on autophagy. The data are mean ± S.E.M of 3 - 4 experiments (25 - 55 cells per condition). The data were analysed with a one-way ANOVA. ** indicates $p < 0.01$ and *** indicates $p < 0.001$. The scale bars in Panels A and B indicate 10 μm.

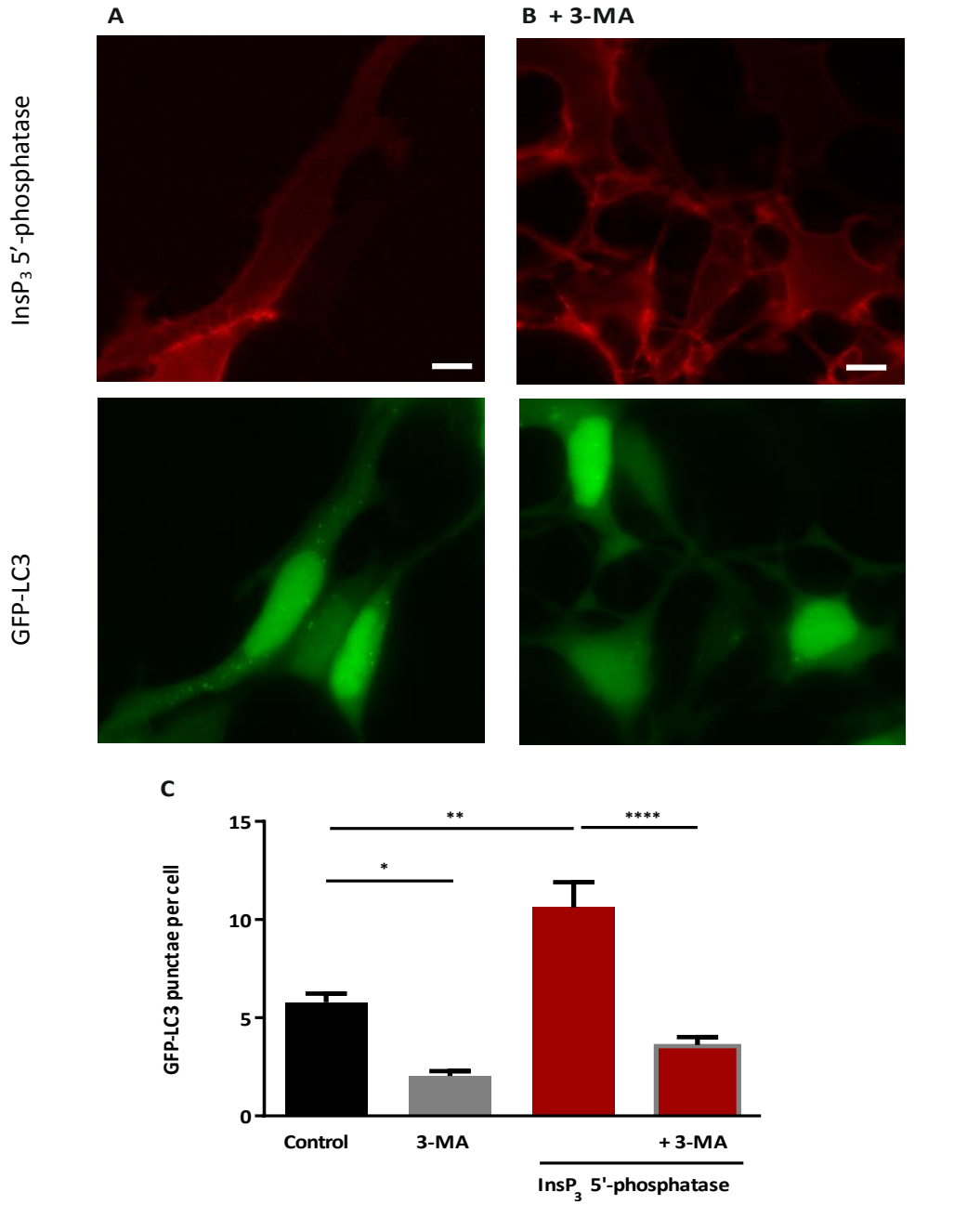

Figure 4.18. Autophagy induced by expression of an $InsP_3$ 5'-phosphatase was inhibited by 3-MA in HEK cells. Panel A shows an image of GFP-LC3-expressing HEK cells that were transfected with mCherry-tagged $InsP_3$ 5'-phosphatase (12-hour transfection). An increased number of GFP-LC3 punctae is evident in the GFP-LC3 image (Panel A, bottom). Panel B shows an image of GFP-LC3-expressing HEK cells that were transfected with mCherry-tagged $InsP_3$ 5'-phosphatase (12-hour transfection) and treated with 5 mM 3-MA for one hour at the 11^{th} hour of the $InsP_3$ 5'-phosphatase transfection. Autophagy was significantly inhibited by the 3-MA treatment, and GFP-LC3 punctae numbers are similar to the basal levels observed in control (untransfected) cells. Panel C is a quantitative representation of the effects of the $InsP_3$ 5'-phosphatase, and the $InsP_3$ 5'-phosphatase + 3-MA, on autophagy. The data are mean ± S.E.M of 3 - 4 experiments (50 - 60 cells per condition). The data were analysed with a one-way ANOVA. * indicates $p < 0.05$, ** indicates $p < 0.01$ and **** indicates $p < 0.0001$. The scale bars in Panels A and B indicate 10 µm.

4.3.9 Expression of the $InsP_3$ 5'-phosphatase caused a reduction in cellular ATP levels, but did not trigger ER stress

The accumulation of GFP-LC3 punctae caused by 2-APB (Figure 4.9), U73122 (Figure 4.10) and the $InsP_3$ 5'-phosphatase (Figures 4.1 and 4.2), suggest that inhibition of $InsP_3$Rs induced a cellular response that triggers autophagy. Since the expression of the $InsP_3$ 5'-phosphatase reduced the Ca^{2+} transfer from $InsP_3$Rs to mitochondria (Figures 4.3 and 4.4), it was considered plausible that there could have been a change in mitochondrial respiration. In addition, alteration of $InsP_3$R activity could potentially lead to ER stress by changing the environment within the lumen of the ER. Both a change in mitochondrial respiration and ER stress have been linked to the induction of autophagy [281, 293, 389] Therefore, both potential outcomes were assessed.

To examine changes in mitochondrial respiration that might result from a reduced flux of Ca^{2+} from $InsP_3$Rs to the mitochondrial matrix, cellular ATP levels were measured. Specifically, ATP levels were examined in untreated HeLa and HEK cells, and in those transfected with the $InsP_3$ 5'-phosphatase. In addition, oligomycin and antimycin A (inhibitors of mitochondrial respiration) and 2-deoxyglucose (2-DG) (a glucose molecule used to inhibit glycolysis), were applied to untransfected cells as positive controls to deplete cellular ATP levels. Expression of the $InsP_3$ 5'-phosphatase significantly reduced ATP levels in both HeLa and HEK cells, whereas expression of a catalytically inactive $InsP_3$ 5'-phosphatase did not (Figures 4.19 and 4.20). The reduction in ATP levels due to $InsP_3$ 5'-phosphatase expression was comparable to that obtained with addition of oligomycin + antimycin A (Figure 4.20B), but less than that seen when cells were treated with oligomycin + antimycin A + 2-DG (Figure 4.20).

ER stress can be induced when the Ca^{2+} stores are chronically empty, or when the physiological Ca^{2+} signalling is disturbed. Along with the unfolded protein response (UPR),

ER stress can cause ER-associated degradation (ERAD) and autophagy [390]. ER stress was measured with two methods; Thioflavin T labelling of living cells, and qRT-PCR measurement of GRP78/BiP expression. Thioflavin T is a cell-permeant fluorescence molecule that selectively binds protein aggregates, especially β-sheets, and consequently displays enhanced fluorescence upon binding [391]. HeLa cells were transfected with the $InsP_3$ 5'-phosphatase, and then acutely labelled with Thioflavin T at 12-, 24- and 48-hours post-transfection. Hydrogen peroxide (H_2O_2) was used as a positive control for ER stress induction. Treatment of cells with H_2O_2 caused a significant labelling of cells with Thioflavin T (Figure 4.21). However, cells expressing either the catalytically active or inactive $InsP_3$ 5'-phosphatase displayed the same intensity of Thioflavin T labelling as control cells at all time points measured (Figure 4.21). These data suggest that expression of the $InsP_3$ 5'-phosphatase did not cause accumulation of misfolded proteins, which could be indicative of ER stress. Moreover, qRT-PCR analysis of GRP78/BiP expression indicated that expression of the $InsP_3$ 5'-phosphatase did not alter the mRNA level of this ER protein chaperone (Figure 4.22). Whereas, application of H_2O_2 caused a significant increase in GRP78/BiP mRNA (Figure 4.22).

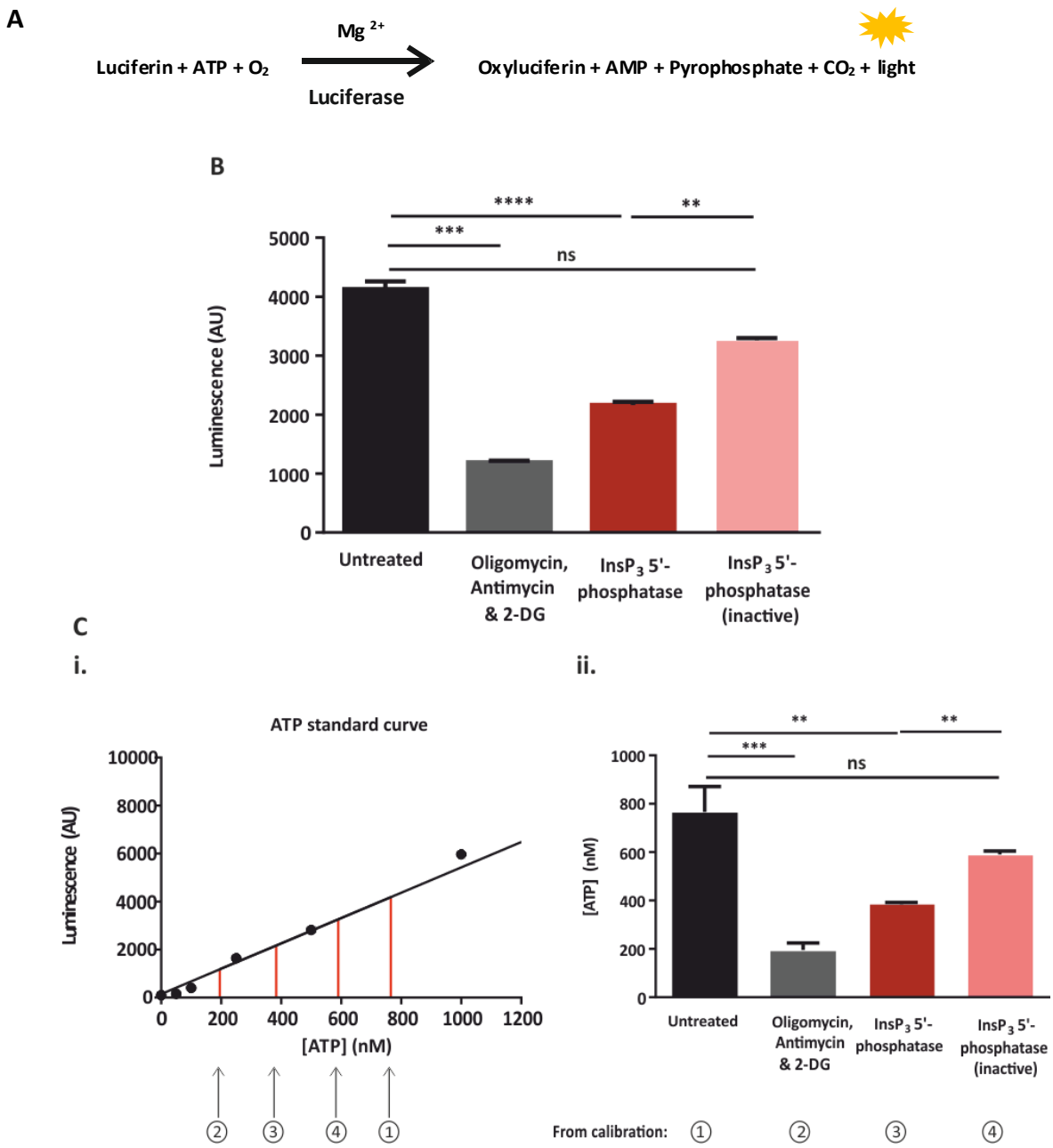

Figure 4.19. Cellular ATP levels were reduced in HeLa cells transfected with $InsP_3$ 5'-phosphatase. The cellular ATP concentration was determined via the production of bioluminescence from a luciferin-luciferase assay reaction (Panel A)**.** Panel B shows background-subtracted luminescence data values (mean ± S.E.M of 3 experiments) obtained from untreated cells, cells transfected with active and inactive forms of $InsP_3$ 5'-phosphatase, and cells treated with oligomycin, antimycin A (5 µM) and 2-DG (5.5 mM) (positive controls). Luminescence levels were reduced following a 1-hour treatment of HeLa cells with oligomycin, antimycin A and 2-DG. Luminescence counts in cells transfected with the active $InsP_3$ 5'-phosphatase were also significantly reduced. Panel Ci represents luminescence versus ATP concentration relationship that was generated by using a series of ATP concentrations ranging from 50 nM to 1000 nM. Panel Cii represents the calibrated concentrations of ATP in cells following the various treatments shown. The data were analysed with a one-way ANOVA test. ** indicates $p < 0.01$, *** indicates $p < 0.001$ and **** indicates $p < 0.0001$.

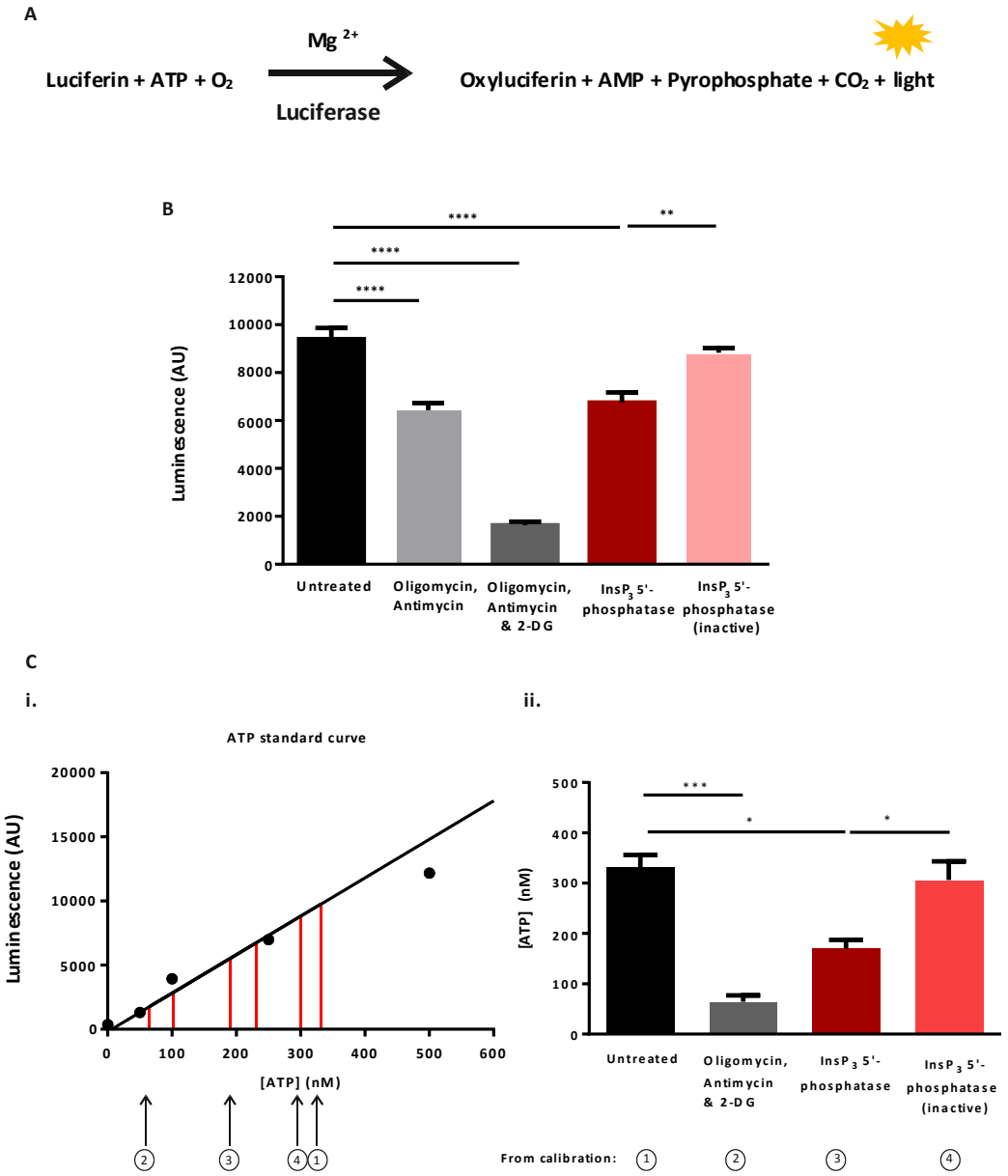

Figure 4.20. Cellular ATP levels were reduced in HEK cells transfected with $InsP_3$ 5'-phosphatase. The cellular ATP concentration was determined via the production of bioluminescence from a luciferin-luciferase assay reaction (Panel A)**.** Panel B shows background-subtracted luminescence data values (mean ± S.E.M of 3 experiments) obtained from untreated cells, cells transfected with the active and inactive forms of $InsP_3$ 5'-phosphatase, and cells treated with oligomycin, antimycin A (5 µM) and 2-DG (5.5 mM) (positive controls). Luminescence levels were reduced following a 1-hour treatment of HEK cells with oligomycin and antimycin A, and further reduced by a combination of oligomycin, antimycin A and 2-DG. Luminescence counts in cells transfected with the active $InsP_3$ 5'-phosphatase were also significantly reduced. Panel Ci represents luminescence versus ATP concentration relationship that was generated by using a series of ATP concentrations ranging from 50 nM to 500 nM. Panel Cii represents the calibrated concentrations of ATP in cells with the various treatments shown, obtained using the standard curve in Panel Ci. The data were analysed with a one-way ANOVA test. * indicates $p < 0.05$, ** indicates $p < 0.01$, *** indicates $p < 0.001$ and **** indicates $p < 0.0001$.

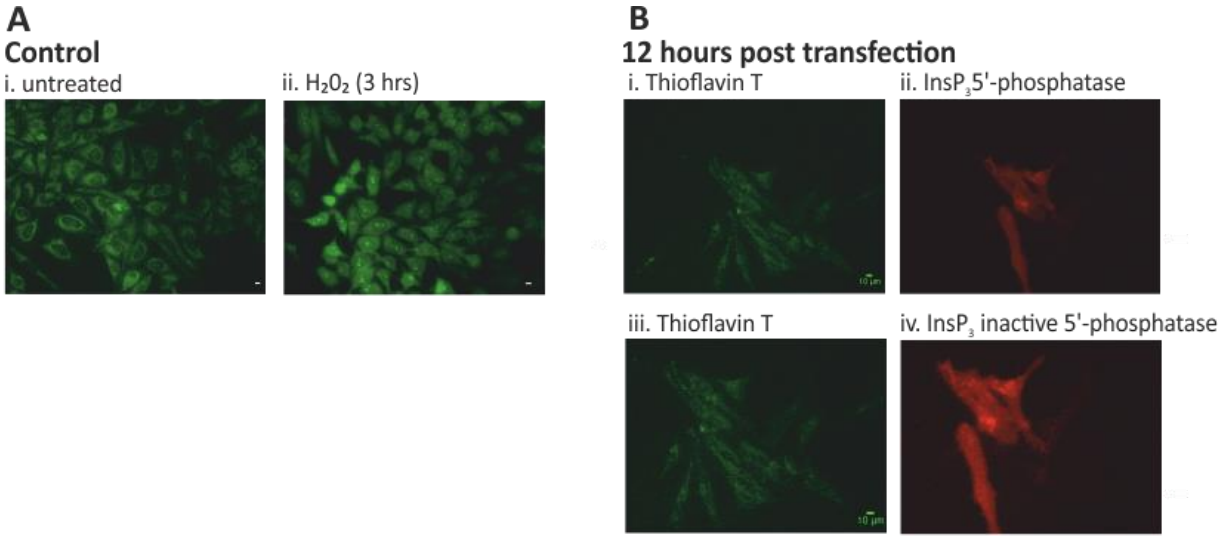
A
Control
i. untreated
ii. H_2O_2 (3 hrs)
B
12 hours post transfection
i. Thioflavin T
ii. $InsP_3$5'-phosphatase
iii. Thioflavin T
iv. $InsP_3$ inactive 5'-phosphatase
C
24 hours post transfection
i. Thioflavin T
ii. $InsP_3$5'-phosphatase
iii. Thioflavin T
iv. $InsP_3$ inactive 5'-phosphatase
D
48 hours post transfection
i. Thioflavin T
ii. $InsP_3$5'-phosphatase
iii. Thioflavin T
iv. $InsP_3$ inactive 5'-phosphatase

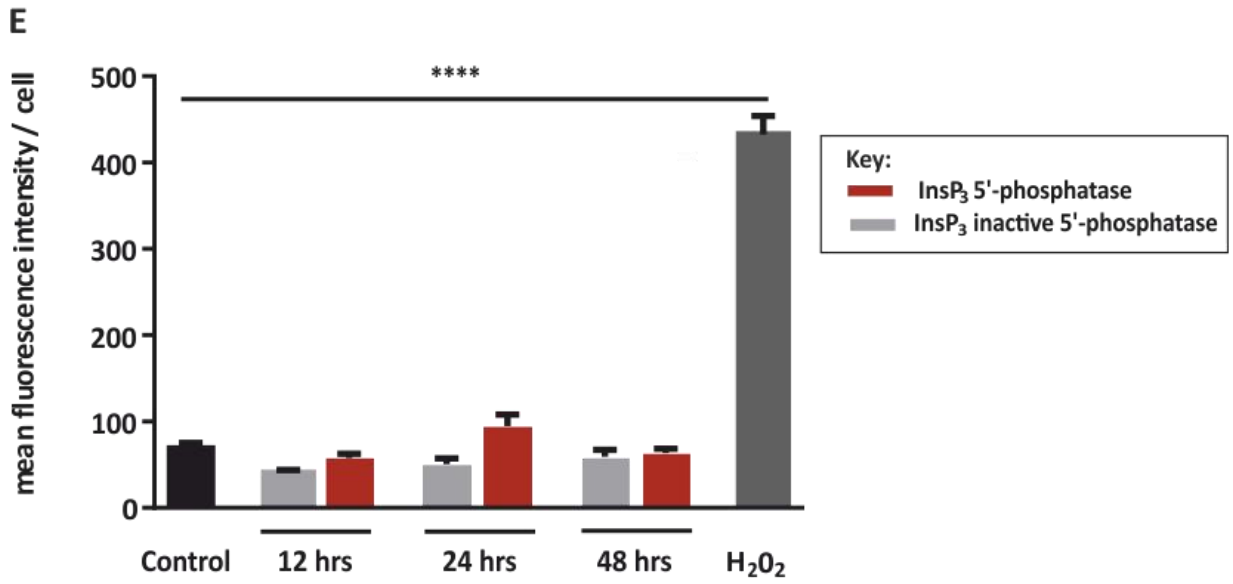
E
mean fluorescence intensity / cell
500
400
300
200
100
0
****
Control
12 hrs
24 hrs
48 hrs
H_2O_2
Key:
$InsP_3$ 5'-phosphatase
$InsP_3$ inactive 5'-phosphatase

Figure 4.21 Expression of the $InsP_3$ 5'-phosphatase did not cause accumulation of protein aggregates in HeLa cells. To assess the accumulation of misfolded protein aggregates, cells were incubated with 0.5 µM Thioflavin T for 10 minutes prior to acquiring fluorescence images. Panel Ai shows a representative image of Thioflavin T-labelled cells in complete imaging medium. Panel Aii shows a representative image of Thioflavin T-labelled cells in complete imaging medium, which were treated with hydrogen peroxide (H_2O_2; 100 µM) for 3 hours. Panels B, C and D show images of Thioflavin T fluorescence in cells transfected with either a functional or inactive $InsP_3$ 5'-phosphatase enzyme, for 12, 24 and 48 hours. These time points were chosen since they correlated with the times when transfection of a functional $InsP_3$ 5'-phosphatase enzyme would induce autophagy. Panel E is a quantitative representation of the effect of active and inactive $InsP_3$ 5'-phosphatase transfection on misfolded protein levels. The data are mean ± S.E.M of 3 - 4 experiments (35 - 150 cells per condition). The data were analysed with a one-way ANOVA test. **** indicates $p < 0.0001$. The scale bars in Panels A-C indicate 10 µm.

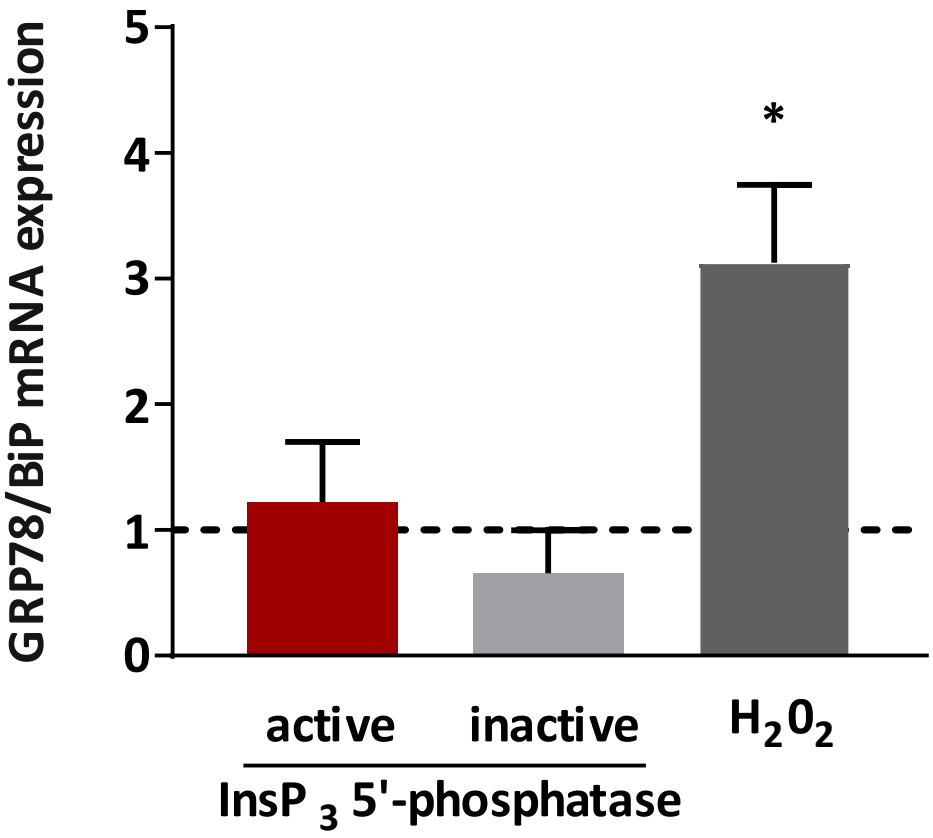

Figure 4.22. The concentration of GRP78/BiP mRNA in HEK cells was not affected by expression of an $InsP_3$ 5'-phosphatase. The column graph depicts the quantitation of GRP78/BiP mRNA expression in HEK cells calculated from qRT PCR results, as a measure of ER stress. HEK cells were either non-transfected, or transfected for 24 hours with expression vectors encoding active or inactive forms of the $InsP_3$ 5'-phosphatase, as indicated. The addition of hydrogen peroxide (H_2O_2; 100 µM) for 3 hours as a positive control resulted in a ~3-fold increase in GRP78/BiP expression relative to GAPDH and normalised to untreated conditions using the ΔΔCt method. Whereas, transfection of the cells with either active or inactive forms of $InsP_3$ 5'-phosphatase had no effect on GRP78/BiP expression. The data are mean ± S.E.M of 3-5 experiments. The data were analysed with a one-sample t-test. * indicates $p < 0.05$.

4.3.10 Expression of $InsP_3$ 5'-phosphatase did not protect HeLa or HEK cells from cell death induced by menadione, an apoptotic agent

A number of publications have shown a connection between apoptosis and autophagy [268, 273, 392]. For example, it has been shown that autophagy can inhibit the induction of apoptosis, but, in some circumstances, autophagy or autophagy-associated proteins may trigger apoptosis or necrosis. It was therefore of interest to examine whether the expression of $InsP_3$ 5'-phosphatase, which activates autophagy, affected the sensitivity of cells to apoptotic stimulation. For this purpose, HeLa and HEK cells were transfected with the catalytically active and inactive mCherry-$InsP_3$ 5'-phosphatase constructs, and treated with menadione to induce apoptotic cell death. Following menadione application (100 µM for 24 hours), cellular metabolic activity was measured using an MTT assay. Although MTT measurements are not a direct measure of cell death or cell viability, they monitor changes in cellular dehydrogenase activity, which is an indicator of metabolic homeostasis. The expression of neither the catalytically active or inactive mCherry-$InsP_3$ 5'-phosphatase forms reduced the effect of menadione on cellular metabolism (Figure 4.23). These data indicate that an increase in autophagy as a result of $InsP_3$ 5'-phosphatase expression did not protect cells from apoptotic cell death.

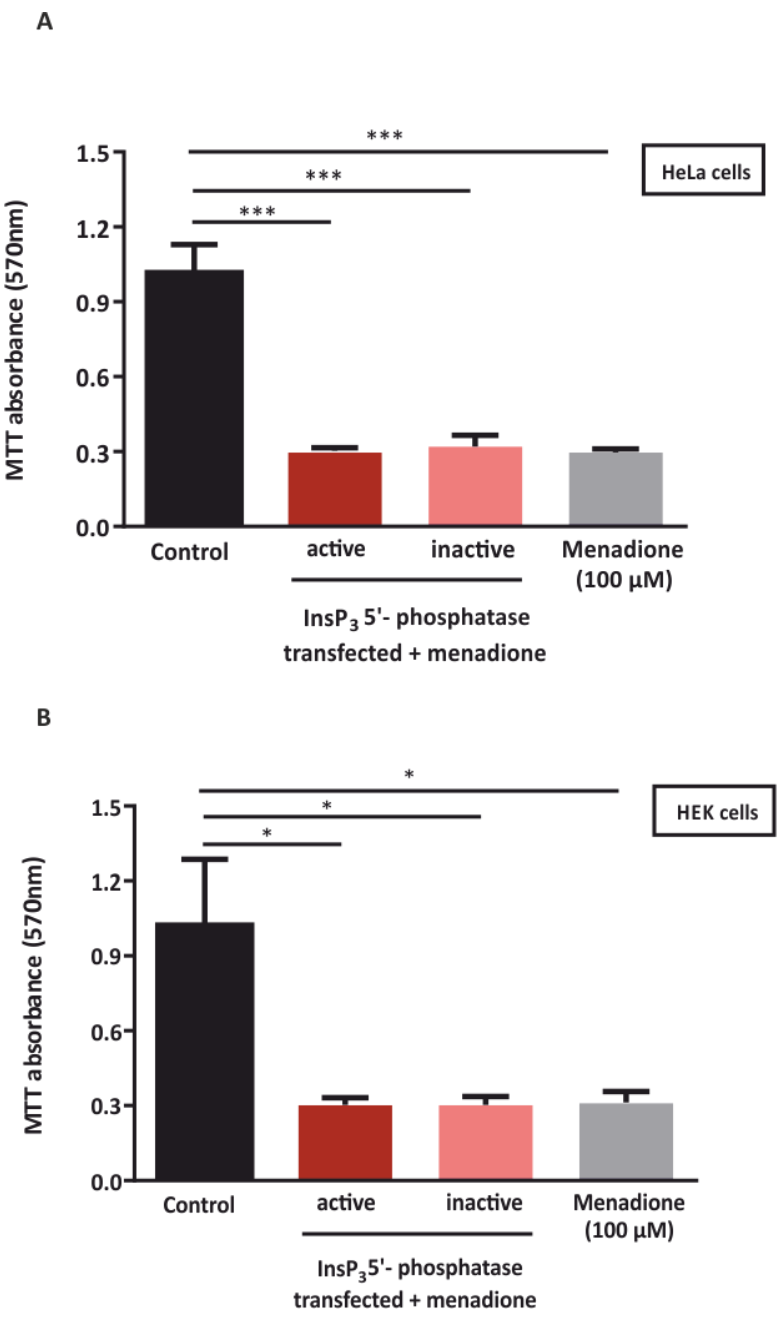

Figure 4.23 Expression of $InsP_3$ 5'-phosphatase did not protect HeLa or HEK cells from reduced metabolic activity induced by menadione, an apoptotic agent. HeLa and HEK cells were transfected with the catalytically active and inactive mCherry-$InsP_3$ 5'-phosphatase constructs, and exposed to 100 µM menadione for 24 hours prior to performing an MTT assay. The column graphs (A, HeLa cells; B, HEK cells) show that menadione had a similar effect on the cells whether or not they were transfected with $InsP_3$ 5'-phosphatase (or the inactive form of $InsP_3$ 5'-phosphatase). The data are mean ± S.E.M of 3 experiments and were analysed with a one-way ANOVA. * indicates $p < 0.05$ and *** indicates $p < 0.001$.

4.3.11 Inhibiting Ca^{2+} uptake into the mitochondria by blocking MCU increased cellular autophagy levels

Given the importance of MCU in mediating Ca^{2+} uptake into the mitochondria, we sought to determine whether this mitochondrial protein was critical in maintaining cellular autophagy at basal levels. The MCU gene encodes a Ca^{2+} transporter that localises to the inner membrane of the mitochondria [393, 394]. Experiments were carried out using siRNA to reduce expression of the MCU, and pharmacological inhibition of MCU-dependent Ca^{2+} uptake into the mitochondria. For this purpose, HEK Cells were transfected with 25 nM siRNA MCU or a negative control (non-silencing) siRNA as described in *Chapter 2: Materials & methods.* MCU Protein expression was consequently determined with Western blotting, confirming siRNA-mediated knockdown of the MCU (Figure 4.25A-B). Following the confirmation that the siRNA substantially reduced MCU expression, GFP-LC3 HEK cells were seeded on glass coverslips for imaging experiments, as described in *Chapter 2: Materials & methods*. The cells were transfected with the siRNAs described above, and their GFP-LC3 punctae numbers were counted. As shown in Figure 4.25C, cells with a reduced expression of MCU displayed elevated GFP-LC3 punctae numbers compared to cells in control conditions, or cells transfected with the non-silencing siRNA.

Ru360 is a ruthenium amine complex that binds to mitochondria, and has been shown to inhibit mitochondrial Ca^{2+} uptake [395, 396]. Incubation of cells in complete imaging medium with Ru360 (10 µM for 1 hour), and was used at to inhibit Ca^{2+} uptake into mitochondria in HEK cells. Similar to the effect of MCU siRNA (Figure 4.25C), Ru360 triggered an increase in GFP-LC3 punctae (Figure 4.25D).

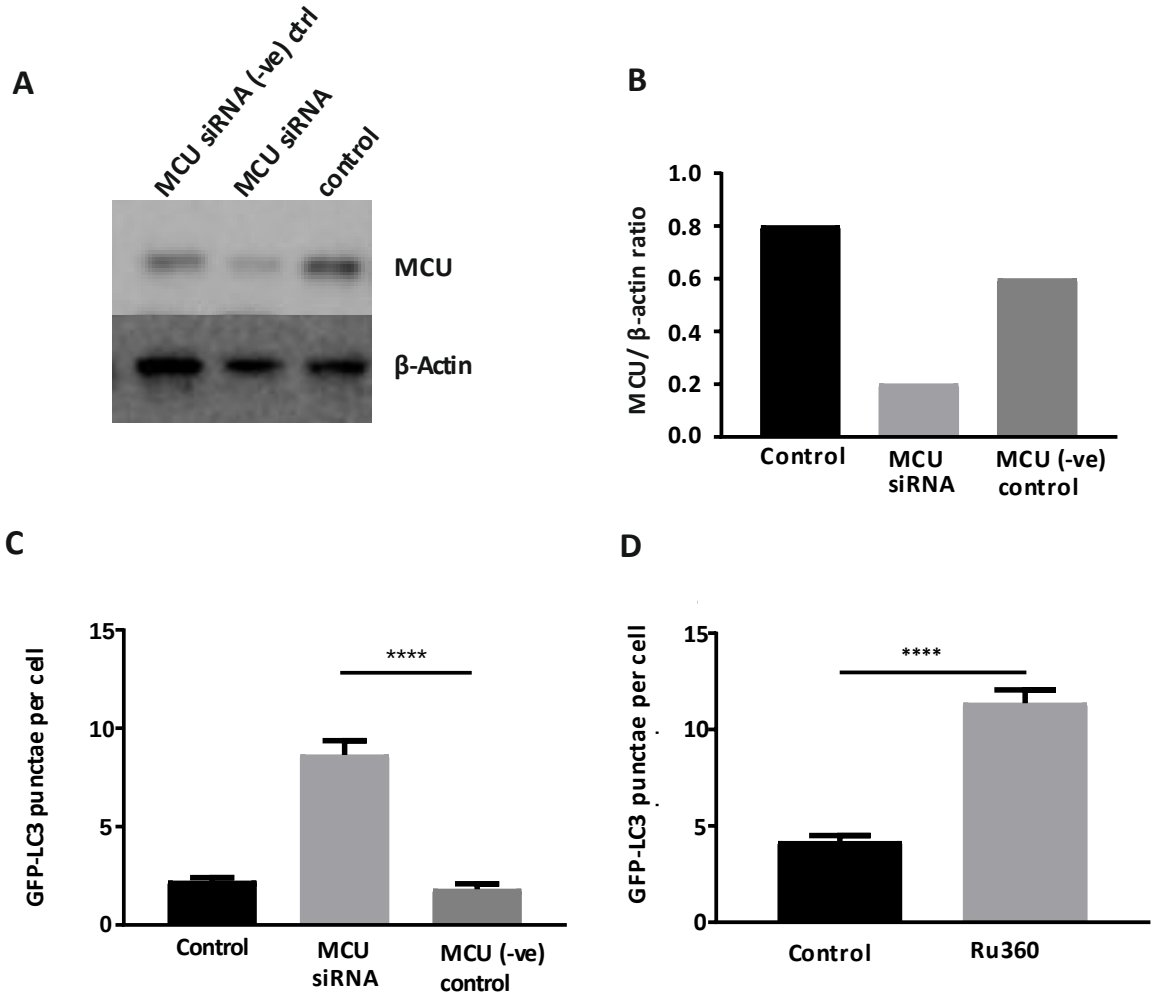

Figure 4.25. The inhibition of MCU by siRNA transfection, and the inhibition of mitochondrial Ca^{2+} uptake by Ru360, elevated autophagy in HEK cells. Panels A – B (n=1) show Western blot analysis of MCU expression using protein lysates obtained from HEK cells in complete imaging medium that were transfected with either human MCU siRNA or a negative control siRNA (non-targeting siRNA). β-actin was used as a loading control. Panel C is a quantification of GFP-LC3 punctae within the cells following the siRNA treatments. Panel D is a quantification of the effect of Ru360 (10 µM for 1 hour) application to HEK cells in a complete imaging medium on GFP-LC3 punctae accumulation. The data were analysed with a one-way ANOVA. **** indicates $p < 0.0001$. The data are mean ± S.E.M of 3 experiments (for Panels C and D).

4.3.12 Expression of the $InsP_3$ 5'-phosphatase did not affect the cell cycle

Foskett *et al.*, proposed that $InsP_3R$-mediated Ca^{2+} signalling was necessary for the viability of cancer cells [397]. In their model, the constitutive transfer of Ca^{2+} from the ER to mitochondria via $InsP_3Rs$ is important in maintaining mitochondrial bioenergetics and metabolism. They demonstrated that inhibition of $InsP_3Rs$ caused the selective killing of cancer cells due to the lack of mitochondrial metabolism, and an ensuing catastrophic necrotic death during cytokinesis [378]. Since the expression of the $InsP_3$ 5'-phosphatase used in this study also caused an apparent decline in both mitochondrial Ca^{2+} uptake (Figures 4.3 and 4.4) and mitochondrial ATP production (Figurex 4.19 and 4.20), similar to the effects shown by Foskett and colleagues, it was plausible that a similar defect in cytokinesis was occurring. This could potentially confound the interpretation of the results in this study, since the cells could be unhealthy and undergoing necrotic cell death. Therefore, cells were transfected with the catalytically active and inactive mCherry-$InsP_3$ 5'-phosphatase constructs, and the distribution of cells within the stages of the cell cycle was assessed using an image-based cytometer. Mitotic catastrophe occurs as a result of G2/M checkpoint blockade, and therefore nocodazole was used as a positive control in these experiments. The analysis of cell cycle distributions indicated that $InsP_3$ 5'-phosphatase-transfected cells had a similar cell cycle progression as control cells (Figure 4.26). In contrast, nocodazole-treated cells showed a significantly increased proportion of cells in the G2/M phase, and a reduced fraction of cells in G1. These results suggest that $InsP_3$ 5'-phosphatase expression did not induce alteration in the cell cycle, or cause mitotic catastrophe. Moreover, the lack of cells in the sub-G1 population, which are typically associated with apoptosis [398], indicates that mCherry-$InsP_3$ 5'-phosphatase constructs did not trigger apoptotic cell death.

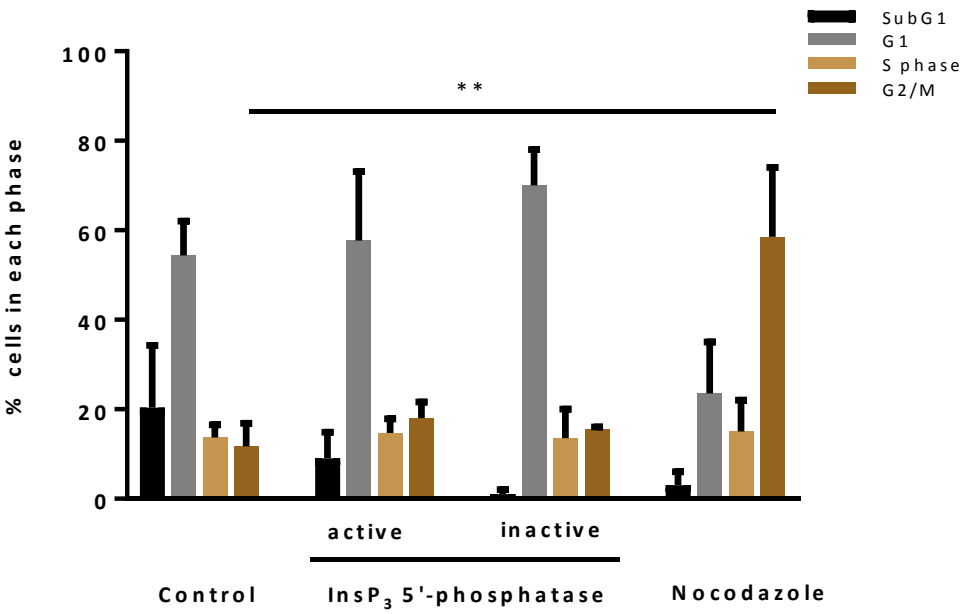

Figure 4.26 Expression of an $InsP_3$ 5'-phosphatase did not induce mitotic catastrophe or apoptosis in HEK cells. The column graph depicts the percentage of cells in each phase of the cell cycle under the conditions shown. The positive control for cell cycle arrest at G2/M was nocodazole (100 nM for 12 hours). HEK cells were either non-transfected or transfected with vectors encoding active or inactive forms of $InsP_3$ 5'-phosphatase. The untreated sample (control) and $InsP_3$ 5'-phosphatase transfected cells show a similar cell cycle progression with highest percentages of cells present in the G1 phase. The data are mean ± S.E.M of 3 experiments. The data were analysed with a Two-way ANOVA. ** indicates $p < 0.01$.

4.3.13 Expression of $InsP_3$ 5'-phosphatase did not induce autophagy during methyl pyruvate treatment

Following expression of the $InsP_3$ 5'-phosphatase, cellular ATP levels were reduced (Figures 4.19 and 4.20). To determine whether an increased mitochondrial substrate supply could rectify the induction of autophagy caused by $InsP_3R$ inhibition, cells were treated with methyl pyruvate (MP), a compound used for stimulating ATP production in cells. MP (5mM) was added to $InsP_3$ 5'-phosphatase expressing cells, and compared to $InsP_3$ 5'-phosphatase expressing cells only, GFP-LC3 punctae numbers were significantly reduced to basal numbers (Figure 4.27). By increasing mitochondrial metabolism with MP alone was sufficient to maintain autophagy at a basal state.

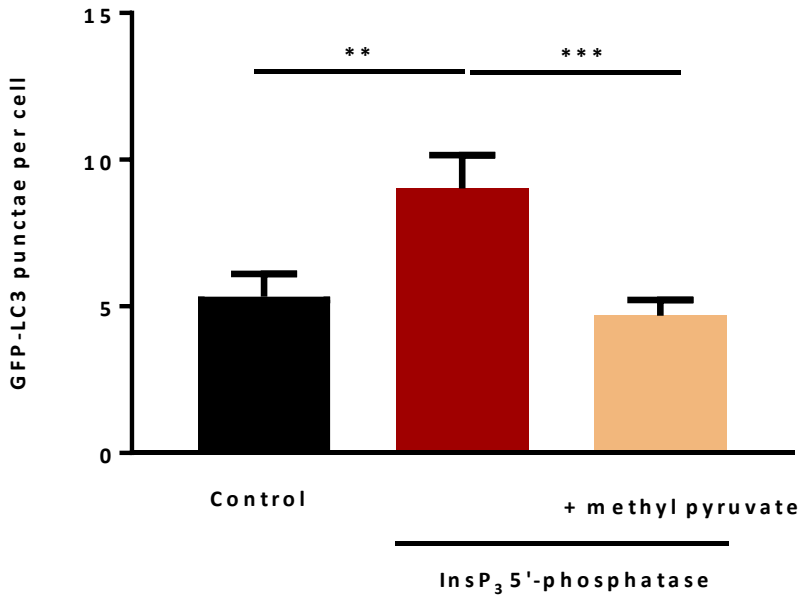

Figure 4.27. Expression of $InsP_3$ 5'-phosphatase did not induce autophagy in presence of methyl pyruvate HEK cells. The column graph is a quantitative representation of the effect of mCherry-tagged $InsP_3$ 5'-phosphatase on the accumulation of GFP-LC3 punctae in HEK cells in the presence or absence of methyl pyruvate (5 mM). Cells transfected with mCherry-tagged $InsP_3$ 5'-phosphatase (12-hour transfection) displayed an increased number of GFP-LC3 punctae, whereas the supplementation of methyl pyruvate concurrently with transfection reduced the number of punctae to basal levels. The data are mean ± S.E.M of 3 experiments (35 - 70 cells per condition). The data were analysed with a one-way ANOVA. ** indicates $p < 0.01$ and *** indicates $p < 0.001$.

4.3.14 Electron microscopic visualisation of autophagic vesicles in $InsP_3$ 5'-phosphatase-expressing cells

As discussed in Chapter 3, electron microscopy has been used in many studies to establish the presence and form of autophagic vesicles. In this study, electron microscopy was used to examine whether expression of the $InsP_3$ 5'-phosphatase altered the form or clustering of autophagy vesicles. Studies have shown that Tg, an inhibitor of SERCA, led to the persistent accumulation of mature autophagosomes by blocking autophagosomal fusion with lysosomes as well as clustering of punctae with more dense labelling of LC3 and changes in vesicle shape. It is rather difficult to detect any clustering in $InsP_3$ 5'-phosphatase treated cells using fluorescence microscopy, therefore it was important to examine any abnormalities by employing electron microscopy.

As depicted in Figures 4.28 and 4.29, autophagic vesicles could be clearly identified within cells under nutrient-replete conditions, and also following $InsP_3$ 5'-phosphatase transfection. No obvious differences in the structure or size of the autophagosomes/autolysosomes were evident between control cells and $InsP_3$ 5'-phosphatase-expressing cells. The contents of autophagosomes also appeared to be heterogeneous, with no evidence of a specific type of material having being engulfed.

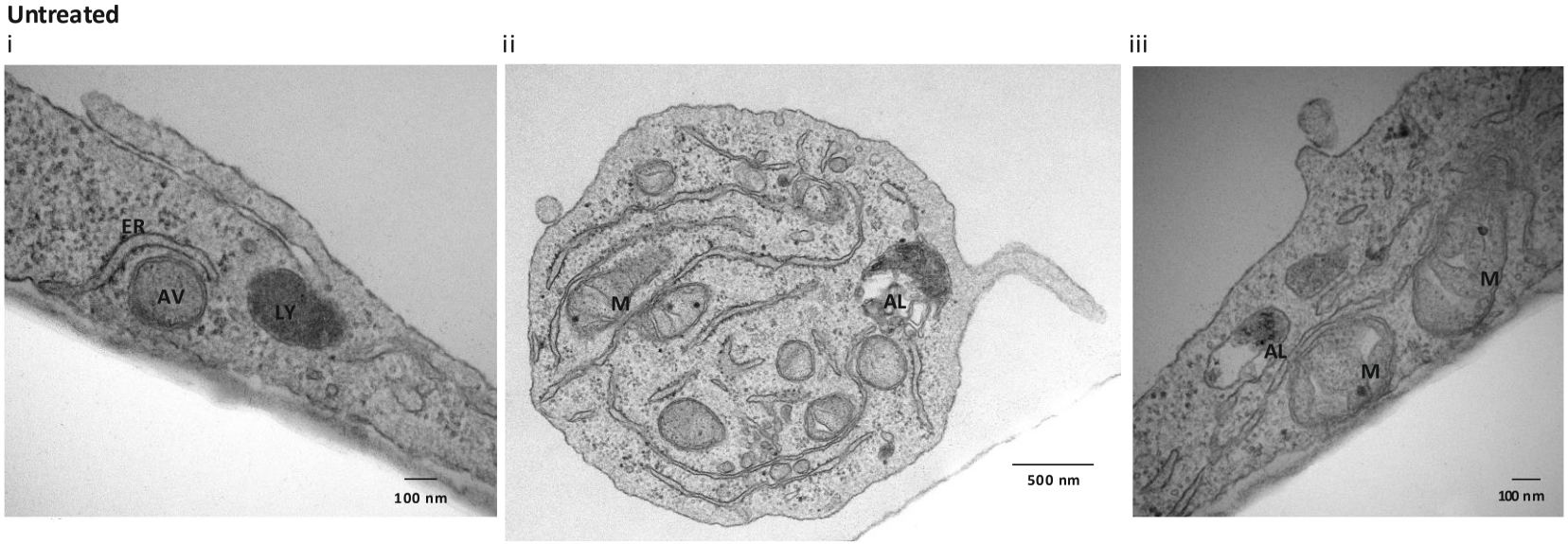

Figure 4.28 (same as Figure 3.18). Detection of autophagic vesicles in untreated HEK cells using electron microscopy. Electron micrographs showing sections of different cells incubated in complete imaging medium. The labels indicate autophagosomes and autolysosomes in various locations within the cells, along with mitochondria, ER and lysosomes. No gross differences in the structure or size of the autophagosomes/autolysosomes were obvious between the two treatments. Heterogeneity in the contents of autophagosomes is evident. AL: autolysosome, AV: autophagosome, ER: endoplasmic reticulum, M: mitochondrion, LY: lysosome.

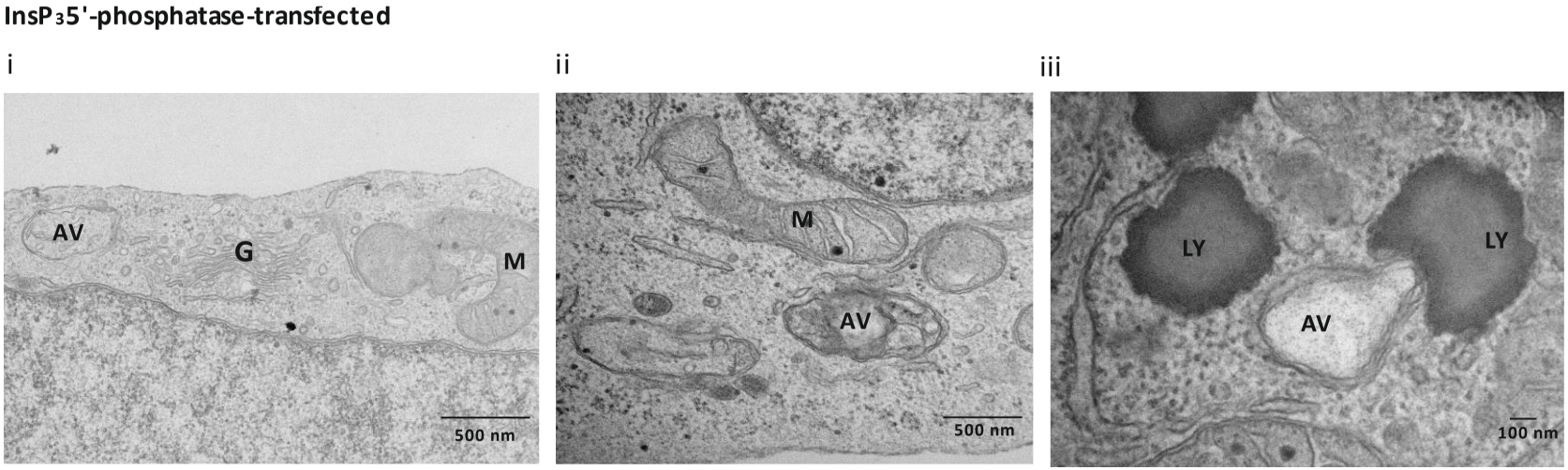

Figure 4.29. Detection of autophagic vesicles in $InsP_3$ 5'-phosphatase expressing HEK cells using electron microscopy. Electron micrographs showing sections of different cells that were transfected with $InsP_3$ 5'-phosphatase. The labels indicate autophagosomes and autolysosomes in various locations within the cells. Heterogeneity in the contents of autophagosomes is evident. AV: autophagosome, G: Golgi, M: mitochondrion, LY: lysosome.

4.3.15 Expression of $InsP_3$ 5'-phosphatase did not alter the expression of calreticulin or SERCA2

The results present earlier in this chapter indicated that expression of the mCherry-$InsP_3$ 5'-phosphatase altered both cytosolic and mitochondrial Ca^{2+} signalling (Figure 4.3 and Figure 4.4), but did not cause ER stress or accumulation of misfolded proteins (Figure 4.21 and Figure 4.22) or trigger cell death. To assess whether expression of the mCherry-$InsP_3$ 5'-phosphatase caused cells to alter the expression of components of their Ca^{2+} signalling toolkit, Western blotting was used to measure two proteins, calreticulin (CRT) [399] and SERCA2 [34], which are critical for ER Ca^{2+} storage and homeostasis.The results shown in Figure 4.30 indicate that CRT and SERCA2 expression levels were similar in $InsP_3$ 5'-phosphatase-transfected cells compared to untransfected cells, suggesting that inhibition of Ca^{2+} release from the ER does not provoke wholesale changes in the expression of the cells' Ca^{2+} signalling toolkit. Moreover, the addition of BAPTA-AM to $InsP_3$ 5'-phosphatase-transfected cells did not cause any change in CRT and SERCA2 expression (Figure 4.29).

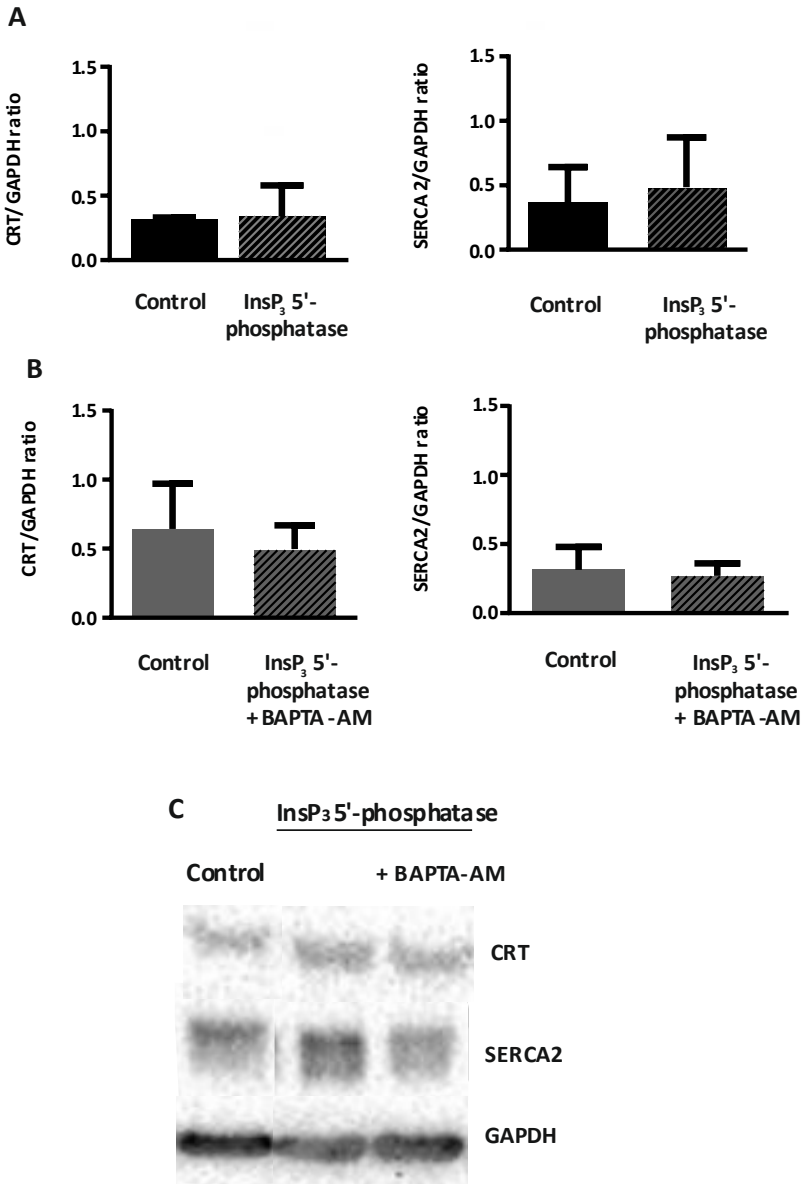

Figure 4.30. **$InsP_3$ 5'-phosphatase transfection did not alter the expression in CRT or SERCA2 levels.** Panels A and B show Western blot analysis of CRT and SERCA2 expression using protein lysates obtained from HeLa cells in complete imaging medium that were either transfected with $InsP_3$ 5'-phosphatase (12-hour transfection; Panel A), or transfected with $InsP_3$ 5'-phosphatase and loaded with BAPTA-AM (10 µM, added for one hour at the 11^{th} hour of $InsP_3$ 5'-phosphatase transfection; Panel B). Panel C shows a Western blot illustrating expression of CRT and SERCA2 proteins with GAPDH used as a loading control. The data are mean ± S.E.M of 3 experiments.

4.3.16 The nutrients present in complete imaging medium triggered Ca^{2+} oscillations

The data presented in this chapter support the hypothesis that expression of $InsP_3$ 5'-phosphatase blocks $InsP_3R$-mediated Ca^{2+} transfer from the ER to mitochondria (Figures 4.4 and 4.4), thereby causing a decrease in ATP production (Figures 4.19 and 4.20). For this hypothesis to be correct, $InsP_3$ 5'-phosphatase-sensitive Ca^{2+} signals should occur under nutrient-replete conditions (i.e., when cells are superfused with complete imaging medium). To examine this notion, HEK cells were loaded with Fura-2 whilst in starvation medium (i.e., imaging medium without amino acids, FBS, L-glutamine or sodium pyruvate, described in Chapter 3), and then placed on the stage of the microscope ready for imaging. Following 10 minutes of recording, the cells were superfused with complete imaging medium, followed by ATP (100 μM) as a positive control (Figure 4.31). Spontaneous Ca^{2+} signals were infrequently observed in cells maintained in starvation medium, whereas 60 - 90% of cells (*n* = 120, 3 independent experiments) responded to superfusion of complete imaging medium with one, or more, Ca^{2+} oscillations (Figure 4.31C and D). As shown in Figure 4.31B, the Ca^{2+} oscillations persisted, albeit infrequently, for tens of minutes. Application of a maximum ATP concentration evoked a Ca^{2+} increase in 100% of cells (*n* = 120, 3 independent experiments), with typically larger Ca^{2+} signal amplitudes than those evoked by complete imaging medium (Figure 4.31A and B).

To examine whether the $InsP_3$ 5'-phosphatase could affect the Ca^{2+} signals evoked by completed imaging medium, GFP-$InsP_3$ 5'-phophatase-transfected HEK cells were loaded with Fura-2 whilst in starvation medium, as described above. No spontaneous Ca^{2+} signals were observed in cells that expressed the $InsP_3$ 5'-phosphatase when they were maintained in starvation medium (*n* = 120, 3 independent experiments). Moreover, the expression of the $InsP_3$ 5'-phosphatase prevented Ca^{2+} responses to superfusion with complete imaging

medium, and substantially blunted the response of cells to application of ATP (Figure 4.32). These data suggest that the supplements added to complete imaging medium caused both acute and long-lasting Ca^{2+} signals, albeit more weakly than stimulation with a maximum dose of ATP, and that these Ca^{2+} signals were inhibited by expression of the $InsP_3$ 5'-phosphatase enzyme.

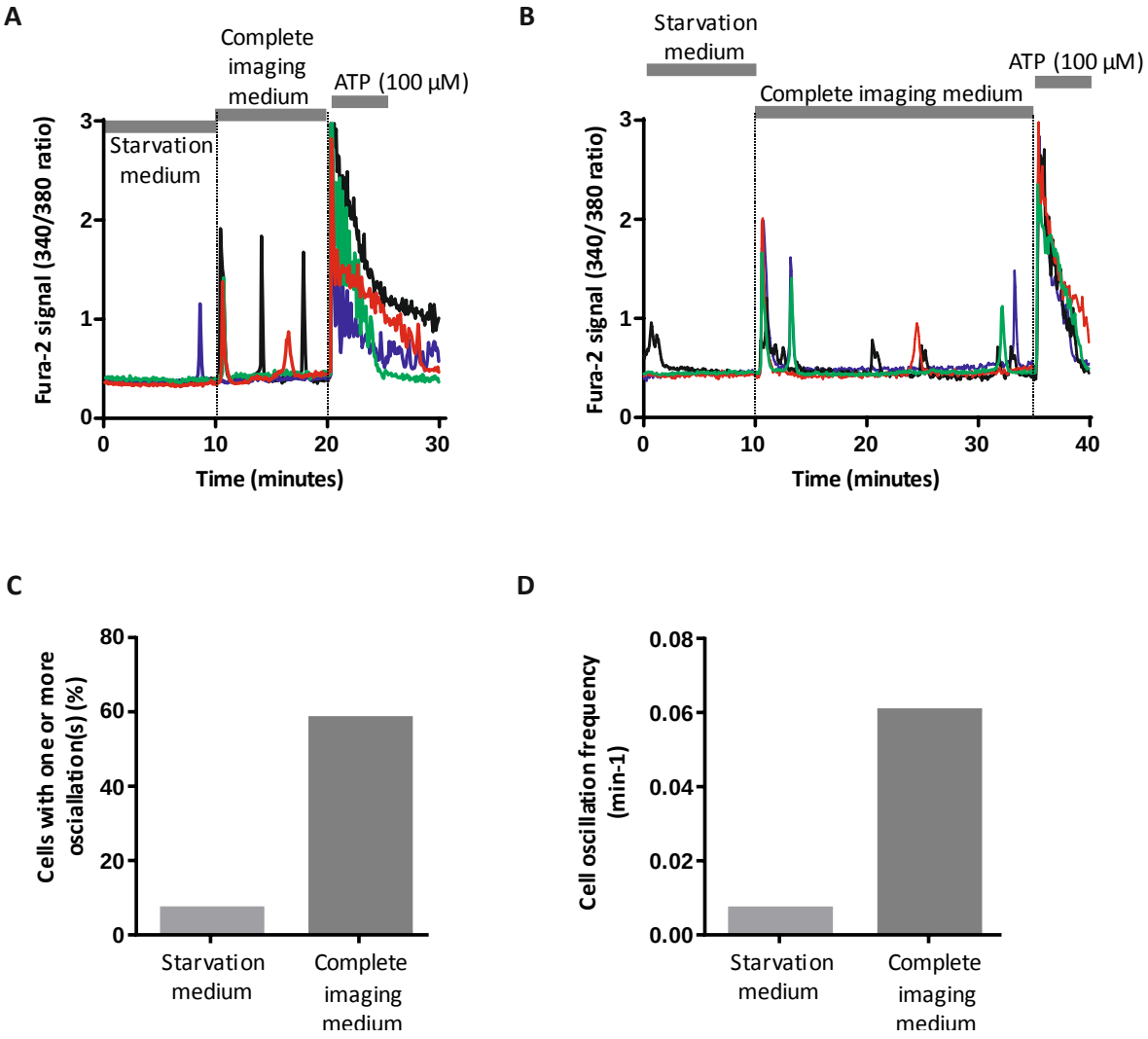

Figure 4.31. Complete imaging medium evoked Ca^{2+} oscillations in HEK cells. Panels A and B illustrate cytosolic Ca^{2+} signals recorded in individual representative Fura-2-loaded HEK cells during superfusion with starvation medium, complete imaging medium, and ATP. Panels C and D are a quantitative analysis of cell responses for the experiment shown in Panel A. For both Panels A and B, typical cellular responses are shown from individual experiments, but both experiments were repeated three times with similar outcomes.

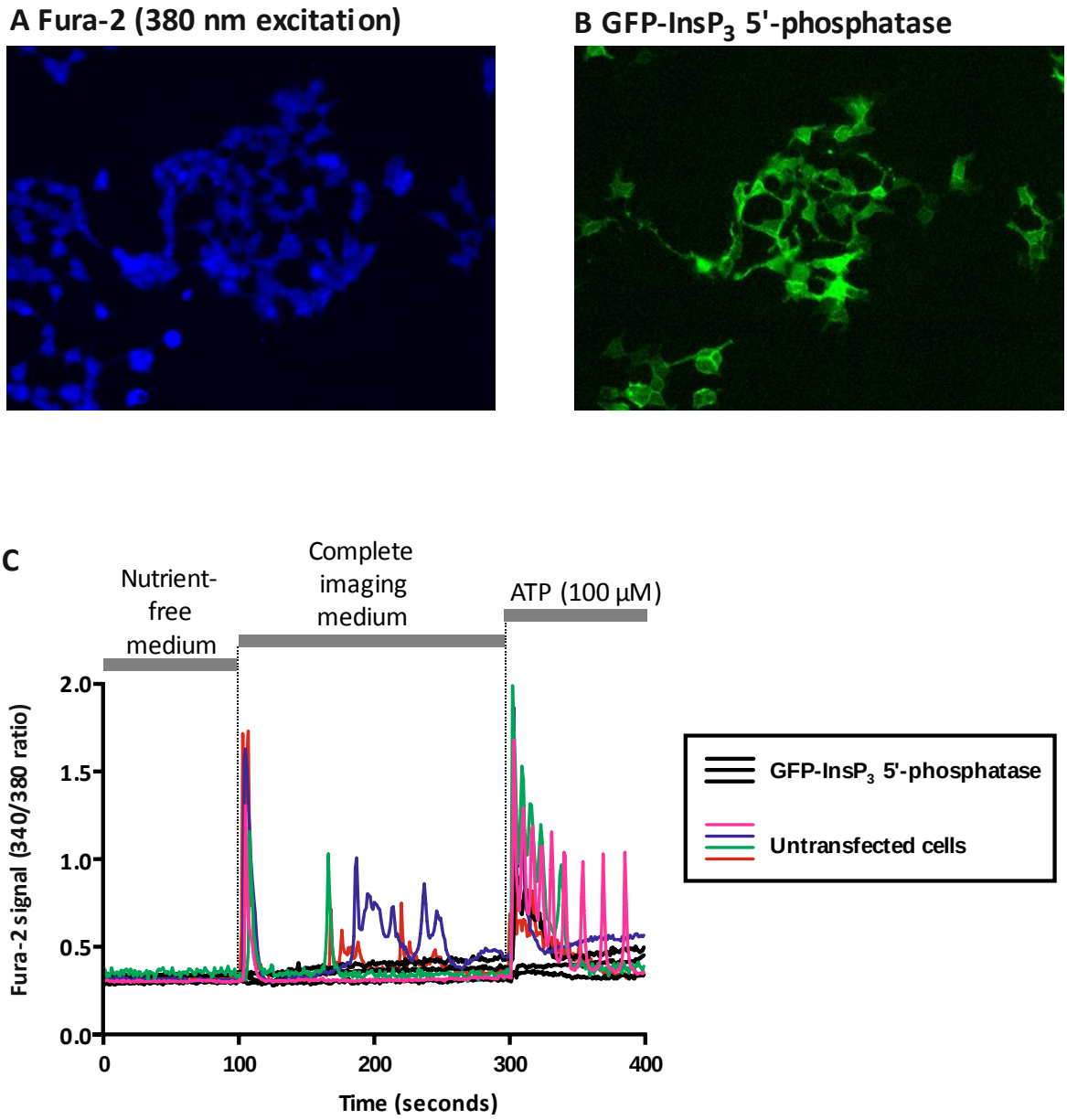

Figure 4.32 The expression of $InsP_3$ 5-phosphatase prevented Ca^{2+} signals in HEK cells in response to superfusion with complete imaging medium and ATP. Panel A is an image of a field of HEK cells loaded with Fura-2. Panel B is an image of the same field of cells indicating those cells that were transfected with GFP-$InsP_3$ 5'-phosphatase**.** Panel C illustrates cytosolic Ca^{2+} signals recorded in individual representative Fura-2-loaded HEK cells during superfusion with starvation medium, complete imaging medium, and ATP. For Panel C, typical cellular responses are shown from an individual experiment. The experiment was repeated three times with similar outcomes.

4.4 Summary of Chapter 4

The work described in this chapter investigated the role of $InsP_3R$ -mediated Ca^{2+} signals in autophagy. A range of tools were used to either inhibit $InsP_3Rs$ or Ca^{2+} release from $InsP_3Rs$, and their consequent effect on autophagy was measured using GFP-LC3 expressing HeLa and HEK cells. The cells were also tested for signs of ER stress that may occur as a consequence of interfering with Ca^{2+} signalling. Additionally, the role of autophagy in relation to cell death was briefly investigated where apoptosis was induced in cells to determine whether autophagy acts as a protective mechanism.

The key findings in this Chapter are:

- The expression of $InsP_3$ 5'-phosphatase in HeLa and HEK cells resulted in an increase of autophagic flux (Figures 4.1, 4.2, 4.15-4.18). BafA1 and 3-MA treatments given in the last 1 hour of $InsP_3$ 5'-phosphatase transfection caused an increase or a decrease in GFP-LC3 punctae numbers, respectively.

- The addition of rapamycin to $InsP_3$ 5'-phosphatase-expressing cells did not show any additive effects on autophagy induced by $InsP_3$ 5'-phosphatase autophagy (Figure 4.11).

- Cytosolic and mitochondrial Ca^{2+} signals were reduced in $InsP_3$ 5'-phosphatase–expressing HeLa and HEK cells (Figures 4.3 to 4.6).

- ATP levels were reduced in $InsP_3$ 5'-phosphatase transfected HeLa and HEK cells (Figures 4.19 and 4.20).

- Elevated autophagy levels induced by $InsP_3$ 5'-phosphatase expression, did not protect HeLa or HEK cells from apoptosis (Figure 4.23).

- The supplementation of cells with methyl pyruvate suppressed the increase in GFP-LC3 punctae accumulation caused by expression of the $InsP_3$ 5'-phosphatase (Figure 4.27).

- Electron microscopy showed that autophagic vesicles in $InsP_3$ 5'-phosphatase-expressing cells were similar in shape and size to those in control cells (Figures 4.28 and 4.29).

- Analysis of cell stress markers using qRT-PCR or Thioflavin T indicated that transfection of $InsP_3$ 5'-phosphatase did not induce cell stress or accumulation of misfolded protein aggregates (Figures 4.21 and 4.22).

- Acute incubation with Ru360 stimulated the accumulation of GFP-LC3 punctae in HEK cells (Figure 4.25).

- Cells expressing $InsP_3$ 5'-phosphatase showed a similar cell cycle distribution to control cells (Figure 4.26).

- BAPTA-AM inhibited $InsP_3$ 5'-phosphatase-induced autophagy (Figures 4.13 and 4.14).

4.5 Discussion

The studies presented in this chapter investigated the regulation of autophagy by Ca^{2+} release from $InsP_3$Rs. Previous studies from other laboratories have indicated that these Ca^{2+} release channels having both pro- or anti-autophagic effects in a range of cell lines [287-289] . The results in this chapter support the hypothesis that the transfer of Ca^{2+} from $InsP_3$Rs to mitochondria suppresses autophagy. This was demonstrated using HeLa and HEK cell lines expressing an $InsP_3$ 5'-phosphatase enzyme that significantly decreased both

cytosolic and mitochondrial Ca^{2+} signals (Figures 4.3 and Figure 4.4). Expression of the $InsP_3$ 5'-phosphatase reversibly increased autophagic flux in both cell types (Figures 4.15 - 4.18). These results agree with other evidence whereby a reduction in $InsP_3$ signalling is pro-autophagic. For example, studies using lithium to inhibit the production of $InsP_3$ [286, 291] and treatment of T cells with glucocorticoid to decrease $InsP_3R$-mediated Ca^{2+} signalling [400], also triggered autophagy. Xestospongin B (XeB), an $InsP_3R$ antagonist, was found to trigger autophagy in various cell lines, but not in DT40 cells that had a triple knockout of all $InsP_3R$ isoforms (DT40 TKO; [287]). In this study, the putative role of mitochondria Ca^{2+} uptake in suppressing autophagy was supported by finding that the mitochondrial uniporter (MCU) is important for maintaining basal level autophagy. Inhibition of the MCU (with either Ru360 or siRNA knockdown), significantly increased autophagosome numbers in HEK cells (Figure 4.25). These observations agree with results of Foskett *et al*., where MCU inhibition induced autophagy in DT40 cells [288].

The notion that of $InsP_3R$-mediated Ca^{2+} release suppresses autophagy was further validated by treatment of cells with the $InsP_3R$ inhibitor 2-APB (Figure 4.9), and the phospholipase C inhibitor U-73122 (Figure 4.10). It is, however, important to note that 2-APB is not fully specific for $InsP_3Rs$, and can affect a number of cellular targets including TRP channels, SERCA and Orai channels [8] [388, 401]. Other groups have also found that 2-APB can trigger autophagy. For example, breast cancer cells showed increased cell death when exposed to 2-APB, which was correlated with increased autophagy [402]. The addition of autophagy inhibitors such as BafA1 or 3-MA suppressed the breast cancer cell death. Contrary to the findings presented in this chapter, and those of others, some studies have suggested that inhibiting $InsP_3Rs$ with 2-APB suppresses autophagy. For example, cadmium- and evodiamine-induced autophagy were suppressed by 2-APB [377, 403]. These results suggest that $InsP_3Rs$ can be pro-autophagic, and are important for cadmium-

and evodiamine-induced autophagy, whereas the studies presented here show that $InsP_3R$-mediated Ca^{2+} signalling is vital for suppressing autophagy. Further work is clearly required to understand the different cellular contexts in which $InsP_3Rs$ can be either pro- or anti-autophagic. Plausibly, these different outcomes could depend on the cell type, their dependence on $InsP_3R$-mediated Ca^{2+} signals, or the nature of the autophagic stimulus.

ATP levels were found to be reduced in $InsP_3$ 5'-phosphatase-expressing cells (Figures 4.19 and 4.20). The observation of reduced ATP levels following $InsP_3R$ inhibition agrees with results obtained by Foskett and colleagues, whereby DT40 cells with reduced Ca^{2+} transfer from $InsP_3Rs$ to mitochondria had lesser ATP levels [288]. In addition, Foskett and colleagues demonstrated that reduced $InsP_3R$ opening lead to activation of AMPK, and subsequently elevated autophagy even in the presence of nutrients [288].Due to time constraints, the mechanism(s) leading from reduced cellular ATP levels to autophagy were not investigated. However, it is likely that AMPK will be implicated [136, 404].

Foskett *et al.*, have additionally shown that inhibiting $InsP_3R$-mediated Ca^{2+} release killed a higher percentage of tumour cells compared to non-tumorigenic cells and induced autophagy in both cell types [378]. In those studies, autophagy upregulated in the tumour cells was not enough for their survival. Cell death occurred as a consequence of the bioenergetic crisis following $InsP_3R$ inhibition, which lead to a failure in complete mitosis and a consequent triggering of necrosis. However, cell cycle studies carried out in this chapter revealed that $InsP_3$ 5'-phosphatase-expressing cells have a normal cell cycle profile (Figure 4.26). Therefore, the lack of $InsP_3R$ activity does not necessarily cause failure of mitosis.

The addition of rapamycin to $InsP_3$ 5'-phosphatase-expressing cells did not show any additive effects on autophagy (Figure 4.11). It is possible that both treatments might be

inducing autophagy through mTOR inhibition, and therefore cannot have an additive action. Studies have shown that nutrient starvation of DT40 cells devoid of $InsP_3R$ expression (which have increased autophagy), upregulated autophagy levels even further than in non-starved cells [288]. Although the additive effect of nutrient starvation with $InsP_3$ 5'-phosphatase-expressing cells was not tested in this chapter, since nutrient starvation and rapamycin induce autophagy via mTOR, our results show a different outcome than those in the literature.

Similar to our earlier findings with rapamycin presented in Chapter 3, Figure 3.24, BAPTA-AM prevented autophagy evoked by $InsP_3R$ inhibition (Figures 4.13 and 4.14). These observations indicate that the lack of $InsP_3R$-mediated Ca^{2+} signals triggers autophagy, and that a BAPTA-sensitive source of Ca^{2+} is required for autophagy to proceed. Although the source of Ca^{2+} signals chelated by BAPTA-AM is unknown, these data show that that cytosolic Ca^{2+} has both suppressive and activating roles in the regulation of autophagy.

Expression of the $InsP_3$ 5'-phosphatase was the principal approach used in this study to prevent $InsP_3R$ opening. Importantly, the expression of this enzyme did not cause ER stress (Figures 4.21 and 4.22), accumulation of misfolded proteins (Figure 4.21), changes in the expression of components of the Ca^{2+} signalling toolkit (Figure 4.30), alteration of the cell cycle (Figure 4.26) or trigger apoptosis (Figure 4.26). These observations concur with other studies from my lab that have used the $InsP_3$ 5'-phosphatase to efficiently block $InsP_3R$ opening without deleterious effects on cells [386]. Studies using HeLa cells have shown that $InsP_3R$ inhibition with XeB, which also induces autophagy, did not provoke ER stress or mitochondrial toxicity [286].

Interestingly, the autophagy induced by $InsP_3$ 5'-phosphatase expression did not protect HeLa or HEK cells from apoptotic cell death (Figure 4.23). Published studies have shown

autophagy can have a cytoprotective effect on cells undergoing apoptosis [270, 405]. For example, the induction of autophagy following treatment with rapamycin, or Beclin-1 overexpression, protected PC12, NRK, COS-7 and CSM-14 cells from pro-apoptotic agents [406]. The authors proposed that autophagy is able to reduce the mitochondrial load in cells, thereby lowering the amount of pro-apoptotic molecules, such as cytochrome *c* released from mitochondria, following apoptotic stimulants. The reason why a cytoprotective effect of autophagy was not seen in the studies presented here is unclear. It is plausible that autophagy would be protective against a weaker apoptotic stimulus than menadione.

Since the expression of the $InsP_3$ 5'-phosphatase was observed to reduce mitochondrial Ca^{2+} uptake (Figures 4.3 and 4.4) and lower cellular ATP levels (Figures 4.19 and4.20), it was considered that the lack of Ca^{2+} transfer from $InsP_3$Rs to mitochondria was decreasing mitochondrial bioenergetics and thereby triggering autophagy. To test whether increased mitochondrial substrate supply could rectify the induction of autophagy caused by $InsP_3$R inhibition cells were treated with methyl pyruvate (Figure 4.27). A number of studies have shown that methyl pyruvate is a membrane-permeant mitochondrial substrate that leads to increased energetics and ATP production [407-410]. Cells that were expressing the $InsP_3$ 5'-phosphatase and treated with methyl pyruvate showed similar levels of autophagy to control cells (Figure 4.27). These observations suggest that the key effect of the $InsP_3$ 5'-phosphatase was to decrease mitochondrial bioenergetics and ATP production.

If Ca^{2+} uptake by mitochondria is necessary to maintain mitochondrial bioenergetics and cellular ATP levels, and thereby suppress autophagy, there should be some evident form of Ca^{2+} signalling occurring within cells under nutrient rich conditions. Supporting this hypothesis it was observed that the supplements (amino acids, FBS, L-glutamine and

sodium pyruvate) contained in the complete imaging medium triggered Ca^{2+} oscillations (Figure 4.31). These Ca^{2+} responses were inhibited in $InsP_3$ 5'-phosphatase expressing cells incubated in complete imaging medium (Figure 4.32). Presumably these Ca^{2+} oscillations are nutrient-evoked Ca^{2+} signals that support mitochondrial bioenergetics, however further work is required to confirm this hypothesis.

It is evident that $InsP_3Rs$ play a dual role in autophagy, but it is presently difficult to reconcile the discrepant literature. It could be that the cellular context determines the autophagic role of $InsP_3Rs$. For example, during chronic starvation, when autophagy is upregulated, $InsP_3R$-mediated Ca^{2+} signalling may be pro-autophagic [317]. Whereas, under nutrient-replete conditions, such as those used in this study, $InsP_3R$-mediated Ca^{2+} signalling suppressed autophagy. Additional studies will be needed to resolve these seemingly contradictory findings.

Interest in the role of $InsP_3Rs$ in cancer has surged in the last few years, with the suggestions that cancer cells rely on $InsP_3R$-mediated Ca^{2+} signalling for survival and growth [319, 397]. Cancer cells undergo a remodelling of their metabolism, which is often denoted as the 'Warburg effect', where glycolysis is principally used for ATP production rather than oxidation of pyruvate within mitochondria [411]. However, evidence also shows that cancer cells also rely on mitochondrial respiration for energy and for the production of metabolites, lipids, DNA and proteins [307, 378]. Therefore it is possible that transfer of Ca^{2+} from $InsP_3Rs$ to mitochondria maintains the synthesis of essential building blocks for cancer cell survival and cytokinesis. Indeed, cancer cells were shown to be addicted to the ER-mitochondrial Ca^{2+} signals to fuel mitochondrial metabolism in order to maintain their fast and uncontrolled proliferation [402, 412]. Future opportunities might benefit from combination therapies for manipulating Ca^{2+} signals/sources to trigger a specific

autophagic outcome along with cancer therapies by exploiting some of the autophagy inducers and inhibitors that have been tested in clinical trials.

Chapter 5: Regulation of autophagy by store-operated Ca^{2+} entry (SOCE)

5.1 Introduction

As discussed earlier, a number of studies have shown that intracellular Ca^{2+} is involved in either activation or inhibition of autophagy [7, 8, 290, 371]. Several Ca^{2+} sources have been proposed, along with a number of downstream signalling steps. In many situations, it is experimentally difficult to dissociate cytosolic Ca^{2+} signals arising from different sources. Moreover, it can be tricky to precisely control the delivery of Ca^{2+} so that specific Ca^{2+} signals can be correlated with a particular cellular outcome. One experimental approach that has been used for this purpose is photolytic liberation of caged messengers such as $InsP_3$ and Ca^{2+}. Although for a process such as autophagy, which takes many minutes to develop, photolysis of caged precursors would require the continual delivery of energy for uncaging. The work presented in this Chapter describes a different approach to control cytosolic Ca^{2+} signals so that autophagy could be stimulated in a Ca^{2+}-dependent manner. The rationale for these experiments was to compare the kinetics of cytosolic Ca^{2+} signals and autophagy, and to develop a simple system to undertake a screen of signalling processes that mediate the effects of Ca^{2+} on autophagy.

Store-operated Ca^{2+} entry (SOCE) is a common mechanism for Ca^{2+} entry into cells [413] [414] and operates in almost all cell types, except perhaps some electrically-excitable cells [38]. SOCE is triggered following depletion of intracellular Ca^{2+} stores as a means of replenishing their Ca^{2+} content, but may also be constitutively active with minimal store depletion [415]. Ca^{2+} influx arising from SOCE supports global, whole-cell signals such as Ca^{2+} oscillations, which are known to affect various aspects of cell function and fate [416]. In addition, Ca^{2+} signals occurring in the vicinity of SOCE channels may have local signalling functions [417]. A similar approach, using depleted Ca^{2+} stores to activate SOCE and thereby allow the deliberate generation of Ca^{2+} signals upon superfusion with medium

containing extracellular Ca^{2+}, has been employed to investigate cellular responses in other studies [418].

Some previous studies have investigated the role of SOCE in the regulation of autophagy. However, as with other aspects of the relationship between Ca^{2+} and autophagy, the published literature is somewhat contradictory. It has been demonstrated that inhibiting SOCE via knock down of STIM1, or by pharmacological blockade, prevented cell cycle progression from G1 to S phase and also activated autophagy in cervical cancer cells, although the link between lack of Ca^{2+} influx and autophagy was not determined [419]. Plausibly, an absence of SOCE could cause the progressive decline of Ca^{2+} within cellular organelles such as the ER, which would activate the unfolded protein response (UPR) and lead to cellular stress [420]. Indeed, a link between ER stress, consequent UPR and autophagy has been demonstrated [421]. Pharmacological blockage of SOCE in colorectal cancer cells with SKF-96365 was shown to induce cell death via apoptosis, but cell death was slowed by the concomitant triggering of autophagy. Autophagy had a cytoprotective effect by preventing the release of cytochrome c from mitochondria [295]. Additionally, resveratrol was shown to downregulate STIM1 expression and thereby inhibit SOCE in prostate cancer cells, which consequently caused ER stress and autophagy-mediated cell death. These studies indicate that a lack of SOCE is pro-autophagic and can affect cell fate.

Conversely, it has been shown that activation of SOCE can trigger autophagy. It was observed that autophagy induction correlated with both increased STIM1 expression and intracellular Ca^{2+} concentration in bone marrow-derived endothelial progenitor cells (EPCs) [299]. The authors found that oxidized low-density lipoprotein (ox-LD), used to mimic hypercholesterolemia, inhibited cellular proliferation as well as activating autophagic flux in the EPCs. Inhibition of autophagy further reduced cellular proliferation, revealing that

autophagy acted as a protective response against ox-LDL-induced proliferative inhibition [299]. *In vivo* studies using murine pancreatic acini have shown that deletion of TRPC3 (*Trpc3*$^{-/-}$) reduced SOCE activity by about 50%, indicating that the native TRPC3 functions as a store-operated Ca^{2+} channel. Moreover, the reduced Ca^{2+} influx in the *Trpc3*$^{-/-}$ cells protected the cells by lowering ER stress and self-destruction by autophagy. Further research suggests that inhibition of autophagy prevents acute pancreatitis [422], and that a sustained increase of cytosolic Ca^{2+} concentration is a trigger for the cell damage that occurs during pancreatitis [423]. It is therefore plausible that inhibition of acinar cell TRPC3, and other Ca^{2+} influx channels, may reduce the severity of pancreatitis by preventing autophagic cell demise.

Although the studies described above have invoked a role for SOCE and Ca^{2+} influx in the triggering, or inhibition, of autophagy, they largely correlated the effect of long-term inhibition of cells with various compounds with autophagic markers. To induce autophagy in a Ca^{2+}-dependent manner, whilst avoiding the pleiotropic effects of membrane receptor stimulation, this study used the SERCA inhibitors thapsigargin (Tg) or cyclopiazonic acid (CPA) along with the controlled removal and re-addition of extracellular Ca^{2+}. In particular, experimental conditions were sought that allowed both Ca^{2+} and autophagy to be monitored over the same time course, without appreciable cell stress, and the least experimental time that allowed significant measurement of cytosolic Ca^{2+} and autophagy. Tg and CPA are well known inhibitors of SERCA pumps, and both are widely employed for depleting intracellular Ca^{2+} stores. To examine the role of SOCE on autophagy, GFP-LC3-expressing HeLa and HEK cells were treated with Tg or CPA in the presence or absence of extracellular Ca^{2+} for one hour. In the absence of extracellular Ca^{2+}, the Tg- or CPA-mediated release of Ca^{2+} from intracellular stores caused a transient (~3 minutes) cytosolic Ca^{2+}signal that eventually returned to basal levels. In the continual presence of Tg or CPA

the intracellular Ca^{2+} stores were not able to refill. Therefore, using Tg- or CPA-treated cells enabled the distinction between Ca^{2+} signals arising from intracellular stores and SOCE. The effect of SOCE on autophagy in HEK cells was compared with ionomycin, which also causes Ca^{2+} influx when cells are suspended in medium containing Ca^{2+}.

5.2 Results

Imaging medium contains Ca^{2+} (Complete imaging medium)	**Imaging medium does not contain Ca^{2+} (Ca^{2+}-free medium)**
Figure 5.1	Figure 5.5
Figure 5.2	Figure 5.6
Figure 5.3	Figure 5.7
Figure 5.4	Figure 5.8
Figure 5.8	Figure 5.9
Figure 5.9	Figure 5.11
Figure 5.10	Figure 5.12
Figure 5.14	Figure 5.13
Figure 5.15	Figure 5.14
Figure 5.16	Figure 5.15
Figure 5.17	
Figure 5.18	

Table 5.1 *Experiments of Chapter 5 which were carried out in either complete imaging medium or Ca^{2+}-free medium.*

5.2.1 Inhibiting SERCA pumps with Tg or CPA stimulated autophagic flux in HeLa cells.

Tg and CPA are both commonly used to inhibit SERCA pumps, thereby causing the gradual depletion of ER Ca^{2+} stores and activation of SOCE [424]. Tg and CPA are often considered to have a similar action. Although, Tg is lipophilic and has a nanomolar affinity for SERCA, whereas CPA is hydrophilic and inhibits SERCA pumps when applied in micromolar concentrations. In addition, Tg is irreversible and can permanently block SERCA function, whilst CPA is reversible and can be readily washed out of cells. An effect of Tg on autophagy has been reported in several studies. However, the effect of Tg on autophagy was variable, with some reports suggesting that autophagy was activated [199] [293] [425], whilst others

observed an inhibitory effect [6] [291]. Moreover, Ganley *et al*. [372] found that Tg did not affect the initial steps of autophagy, such as the formation of autophagosomes, but led to the persistent accumulation of mature autophagosomes by blocking autophagosomal fusion with lysosomes. The authors concluded that the reported accumulation of autophagosomes in Tg-treated cells was not due to induction of autophagy, but rather due to failure to clear existing autophagic vesicles. Since the principal method used in this study for detecting the dynamic activation of autophagy was accumulation of GFP-LC3-labelled punctae, it was important to examine whether SERCA inhibition blocked autophagic flux in the cell types used here. GFP-LC3-expressing HeLa cells were therefore treated with Tg (3 µM) for 1 or 5 hour(s) in Ca^{2+}-containing medium in the presence or absence of BafA1, and the numbers of GFP-LC3 punctae were subsequently monitored. As depicted in Figure 5.1, Tg elevated the number of GFP-LC3 punctae in HeLa cells. Importantly, BafA1 significantly increased the number of GFP-LC3 punctae in Tg-treated cells, consistent with an activation of autophagic flux by Tg (if Tg had blocked autophagic flux, BafA1 would have been ineffective). These data indicate that Tg increased autophagic flux when applied in Ca^{2+}-containing medium.

Similar to Tg, CPA induced an increase in GFP-LC3 punctae numbers that was also enhanced by concurrent incubation with BafA1 (described in detail below). For reasons that are presently unclear, CPA evoked a more rapid accumulation of autophagic vesicles than Tg (Figure 5.2). With CPA, a statistically significant increase in autophagic vesicles was observed after one hour, whereas Tg required longer. From an experimental perspective, CPA is much simpler to use than Tg. CPA is water soluble, easier to make up in solution, cheaper, reversible, and unlike Tg, CPA did not persistently stick to the imaging chambers used in this study. Following experiments with Tg, the imaging chambers needed treatment

with ethanol and copious washing to remove all of the compound. For these reasons, the bulk of the studies presented in this Chapter used CPA as a SERCA inhibitor.

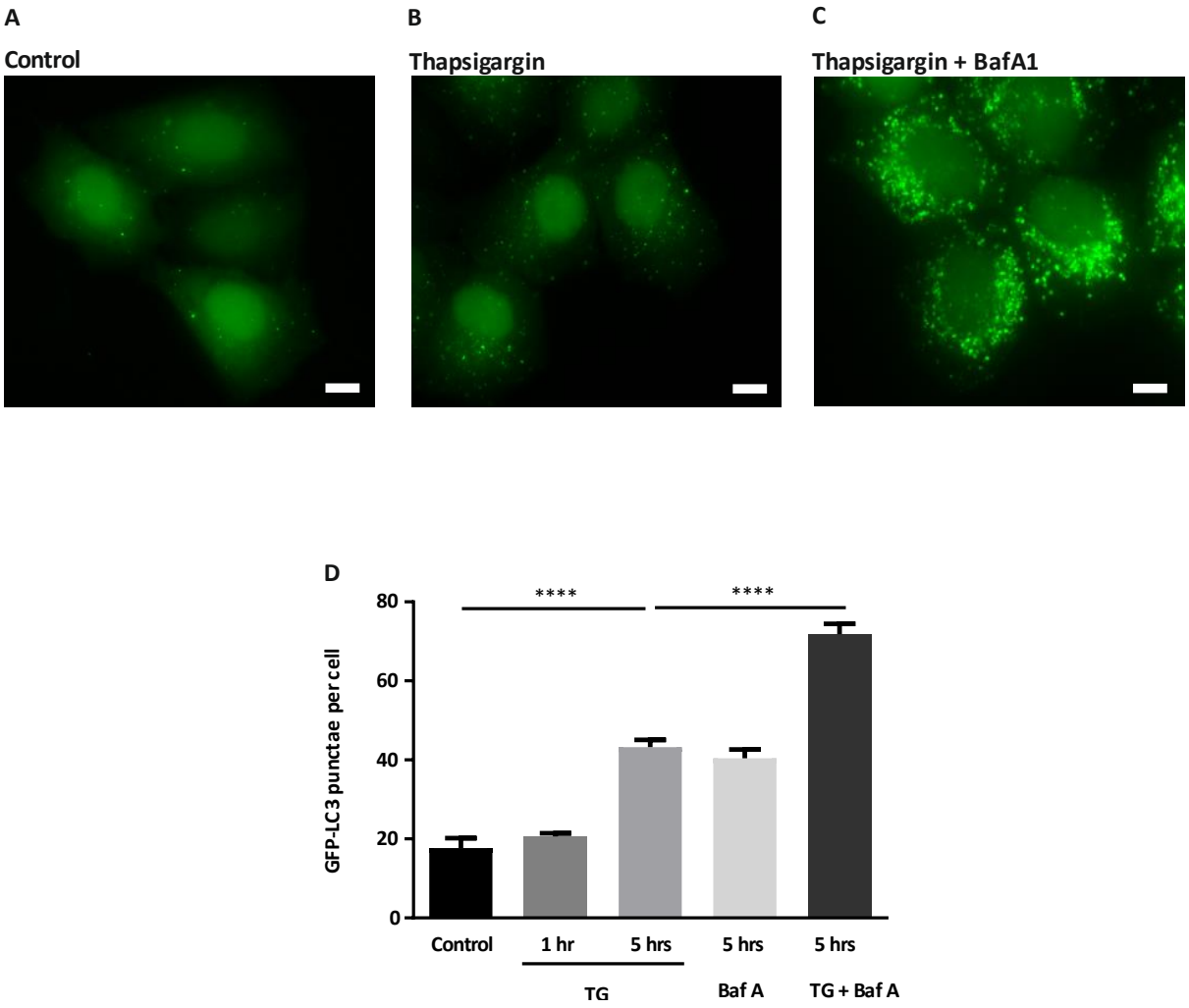

Figure 5.1. Thapsigargin, an inhibitor of SERCA pumps, increased the number of GFP-LC3 punctae in HeLa cells and did not block the autophagic flux. Panel A is a representative image of cells in complete imaging medium. Panel B is a representative image of cells incubated with 3 µM thapsigargin (TG) in complete imaging medium for five hours. Panel C represents cells treated similarly to those shown in Panel B, but with the addition of 0.1 µM BafA1 in the last one hour of incubation**.** Panel D is a quantitative representation of the effect of TG, BafA1 and TG + BafA1 on autophagy; the number of GFP-LC3 punctae per cell was increased by TG following a 5-hour incubation. Autophagy was further increased by the addition of BafA1. The data are mean ± S.E.M of 3 - 5 experiments (45 - 100 cells per condition). The data were analysed with an one-way ANOVA test. **** indicates $p < 0.0001$. The scale bars in Panels A-C indicate 10 µm.

5.2.2 Activating SOCE with CPA induces autophagy in Ca^{2+}-containing media

To monitor the influence of SOCE on cytosolic Ca^{2+} signals and autophagy, GFP-LC3-expressing HeLa and HEK cells were loaded with Fura-2 and placed on the stage of an epifluorescence microscope, as described in *Chapter 2: Materials and Methods*. Following a 1-minute recording of the basal 340/380 Fura-2 ratio, the HeLa and HEK cells were either incubated in complete imaging medium supplemented with 50 µM CPA for a further 59 minutes, or they were maintained in complete imaging medium without CPA. For both conditions, the 340/380 Fura-2 ratio was monitored for the duration of the experiment. To examine the status of the intracellular Ca^{2+} stores, $InsP_3$-generating agonists (histamine for HeLa and ATP for HEK cells) were added for the last 10 minutes of the experiment. At the end of the experiment, the numbers of autophagic vesicles were counted in both the CPA-treated cells and the untreated control cells. As depicted in Figures 5.2 and 5.3, it is evident that treatment of both cell types with CPA stimulated a significant increase in GFP-LC3 punctae accumulation. With both cell types, the Fura-2 measurements indicated that CPA caused a sustained elevation of cytosolic Ca^{2+}, consistent with perpetual activation of SOCE (Figures 5.2D and 5.3D), although, the amplitude of the SOCE response was greater and more sustained in HeLa cells than in HEK cells. The lack of responses to addition of $InsP_3$-generating agonists indicated that CPA had depleted the cells' intracellular Ca^{2+} stores. To show that processing of autophagic vesicles was not chronically affected by SERCA inhibition, an important control experiment was to wash out CPA following a 1-hour treatment in complete imaging medium. Results (Figure 5.4) show that incubation with CPA increased the number of GFP-LC3 punctae, and subsequently removing the CPA led to a reduction in the numbers of punctae. SOCE-induced autophagy was therefore found to be reversible.

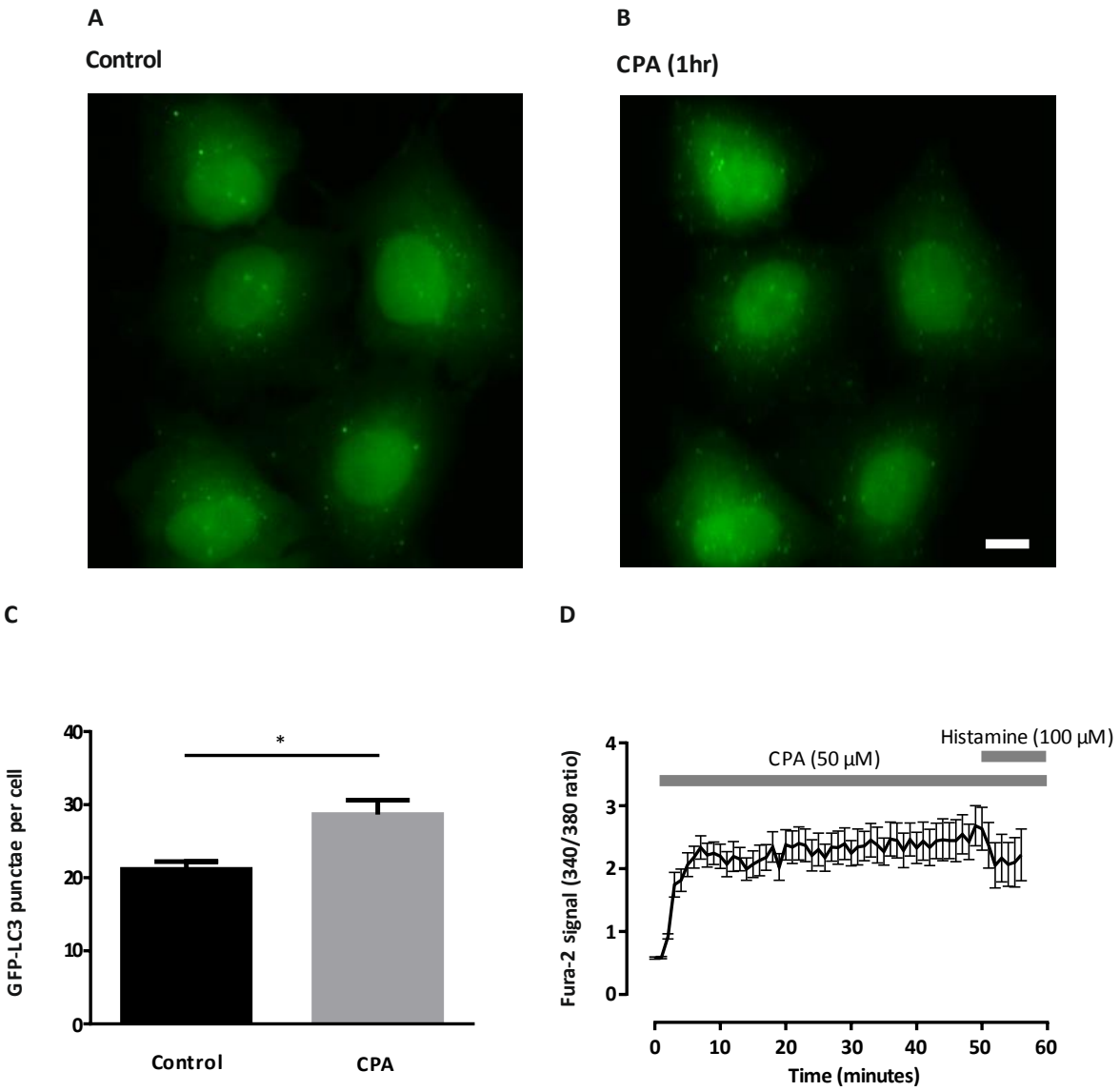

Figure 5.2. Activating SOCE with cyclopiazonic acid (CPA) increased the number of GFP-LC3 punctae in HeLa cells. Panel A is an image of cells in complete imaging medium. Panel B is an image of the same region of cells as shown in Panel A, but following treatment with 50 µM CPA for one hour. Panel C is a quantitative representation of the effect of CPA on autophagy; there was a significant increase in GFP-LC3 punctae. Panel D is the profile of cytosolic Ca^{2+} signals in cells incubated with CPA, following a one-minute baseline recording, with an addition of 100 µM histamine for the last 10 minutes. The data are mean ± S.E.M of 3 experiments (30 cells per condition). The data were analysed with an unpaired Student's t-test. * indicates $p < 0.05$. The scale bar in Panel B indicates 10 µm.

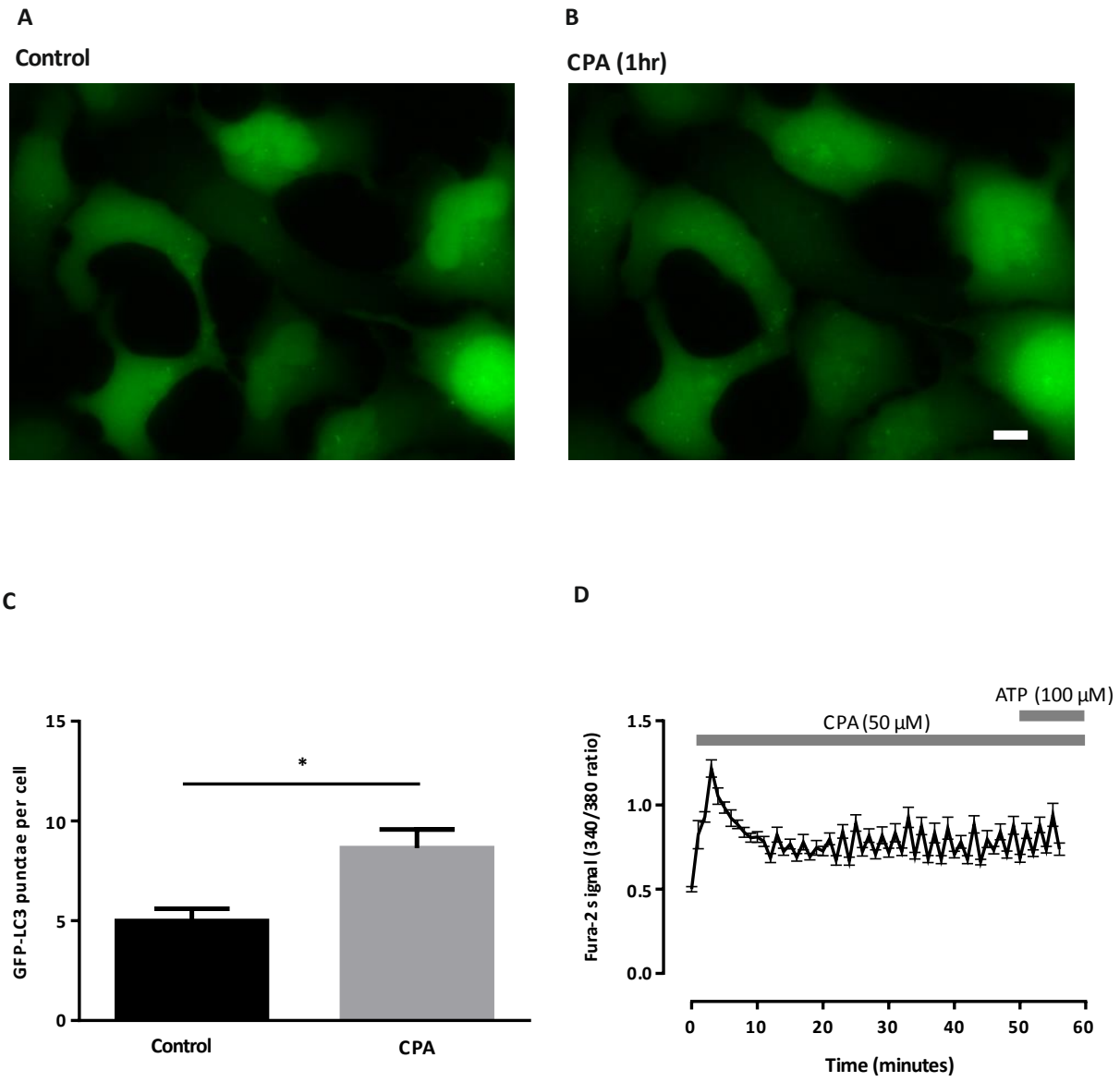

Figure 5.3. Activating SOCE with cyclopiazonic acid (CPA) increased the number of GFP-LC3 punctae in HEK cells. Panel A is an image of cells in complete imaging medium. Panel B is an image of the same region of cells as shown in Panel A, but following treatment with 50 µM CPA for one hour. Panel C is a quantitative representation of the effect of CPA on autophagy; GFP-LC3 punctae numbers increased nearly two-fold. Panel D is the profile of cytosolic Ca^{2+} signals in cells incubated with CPA, following a one-minute baseline recording, with addition of 100 µM ATP during the last 10 minutes. The data are mean ± S.E.M of 3 experiments (20 cells per condition). The data were analysed with a paired Student's t-test. * indicates $p < 0.05$. The scale bar in Panel B indicates 10 µm.

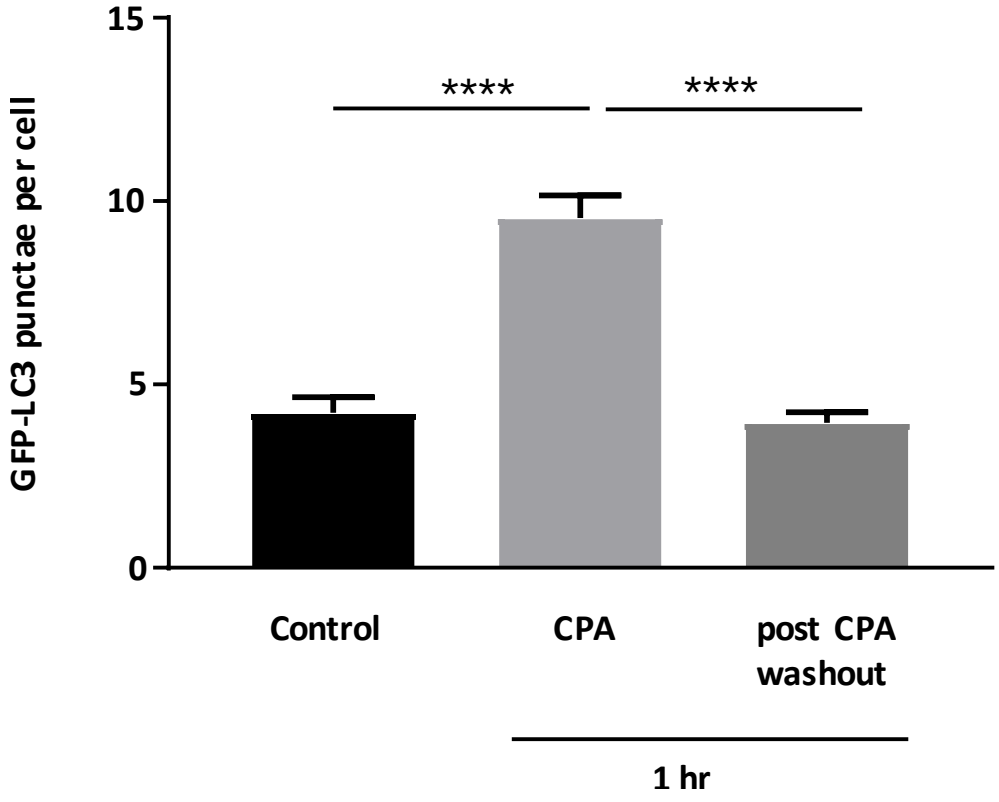

Figure 5.4. CPA reversibly increased the number of GFP-LC3 punctae in HEK cells. The column graph is a quantitative representation of numbers of GFP-LC3 punctae in HEK cells incubated in complete imaging medium (control), followed by treatment with CPA (50 μM) for 1 hour, followed by washout of CPA using superfusion with fresh complete imaging medium and recovery for 1 hour. The graph shows that incubation with CPA increased the number of GFP-LC3 punctae, and that subsequently removing the CPA led to a reduction in the numbers of GFP-LC3 punctae. The data are mean ± S.E.M of 3 experiments (60 - 100 cells per condition). The data were analysed with one-way ANOVA test. **** indicates $p < 0.0001$.

5.2.3 Inhibiting SERCA pumps with CPA does not induce autophagy in a Ca^{2+}-free media

To examine whether Ca^{2+} influx was necessary for the CPA-evoked increase of autophagy depicted in Figures 5.2 and 5.3, GFP-LC3-expressing HeLa and HEK cells were treated with 50 μM CPA using a similar experimental protocol, but for these experiments Ca^{2+} was omitted during the preparation of the extracellular medium. Moreover, 0.5 mM EGTA was included in order to chelate Ca^{2+} ions that might be present in distilled water or other chemicals that were used to prepare the medium. This Ca^{2+}-free, EGTA-containing medium (hereafter denoted 'Ca^{2+}-free medium') had the same supplements as complete imaging medium (i.e., it was supplemented with glutamine, amino acids and growth factors to prevent the induction of autophagy due to starvation). HeLa and HEK cells were either incubated in Ca^{2+}-free medium supplemented with 50 μM CPA for 59 minutes, or they were maintained in Ca^{2+}-free medium without CPA (control). For both conditions, the 340/380 Fura-2 ratio was monitored for the duration of the experiment. To examine the status of the intracellular Ca^{2+} stores, $InsP_3$-generating agonists (histamine or ATP for HeLa and HEK cells, respectively) were added for the last 10 minutes of the experiment. At the end of the experiment, the numbers of GFP-LC3 punctae were counted in both CPA-treated and control cells. As depicted in Figures 5.5 and 5.6, it is evident that the numbers of GFP-LC3 punctae were not affected by treatment with CPA in Ca^{2+}-free medium for either cell type. With both cell types, the Fura-2 measurements indicated that CPA caused a transient elevation of cytosolic Ca^{2+} that lasted for a few minutes (black traces of Figures 5.5D and 5.6D). The lack of responses to addition of $InsP_3$-generating agonists indicated that CPA had depleted the cells' intracellular Ca^{2+} stores. These data suggest that a sustained Ca^{2+} influx induces autophagy, but depletion of intracellular Ca^{2+} stores with CPA for 1 hour does not.

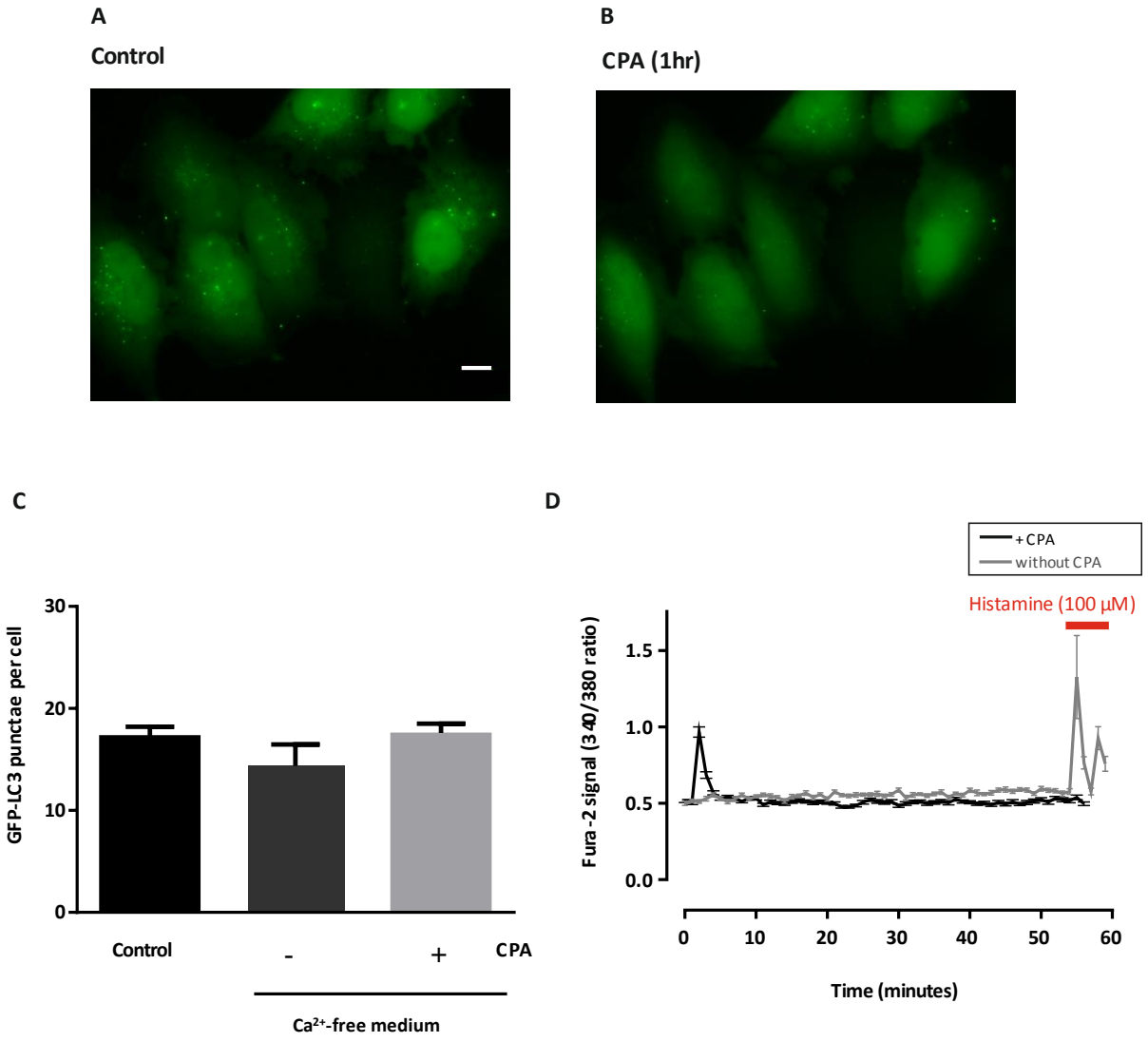

Figure 5.5. Treatment of HeLa cells with cyclopiazonic acid (CPA) in the absence of extracellular Ca^{2+} did not alter the number of GFP-LC3 punctae. Panel A is a representative image of HeLa cells in complete imaging medium. Panel B shows the same field of cells as in Panel A, but after treatment with CPA (50 µM) for one hour in a Ca^{2+}-free medium. Panel C is a quantitative representation of the effect of CPA on autophagy in Ca^{2+} free medium; there was no difference in the number of GFP-LC3 punctae. Panel D shows the profile of cytosolic Ca^{2+} in HeLa cells incubated in Ca^{2+}-free medium. The black trace was recorded from cells treated with CPA (50 µM). The CPA was added following a one-minute baseline recording. The grey trace was recorded from cells that were solely incubated in Ca^{2+}-free medium (i.e., no addition of CPA). Histamine (100 µM) was applied to the cells for the last 10 minutes of the recordings to examine the Ca^{2+} content of the ER. The data are mean ± S.E.M of 3 - 4 experiments (25 – 50 cells per condition). The data were analysed with a one-way ANOVA. The scale bar in Panel A indicates 10 µm.

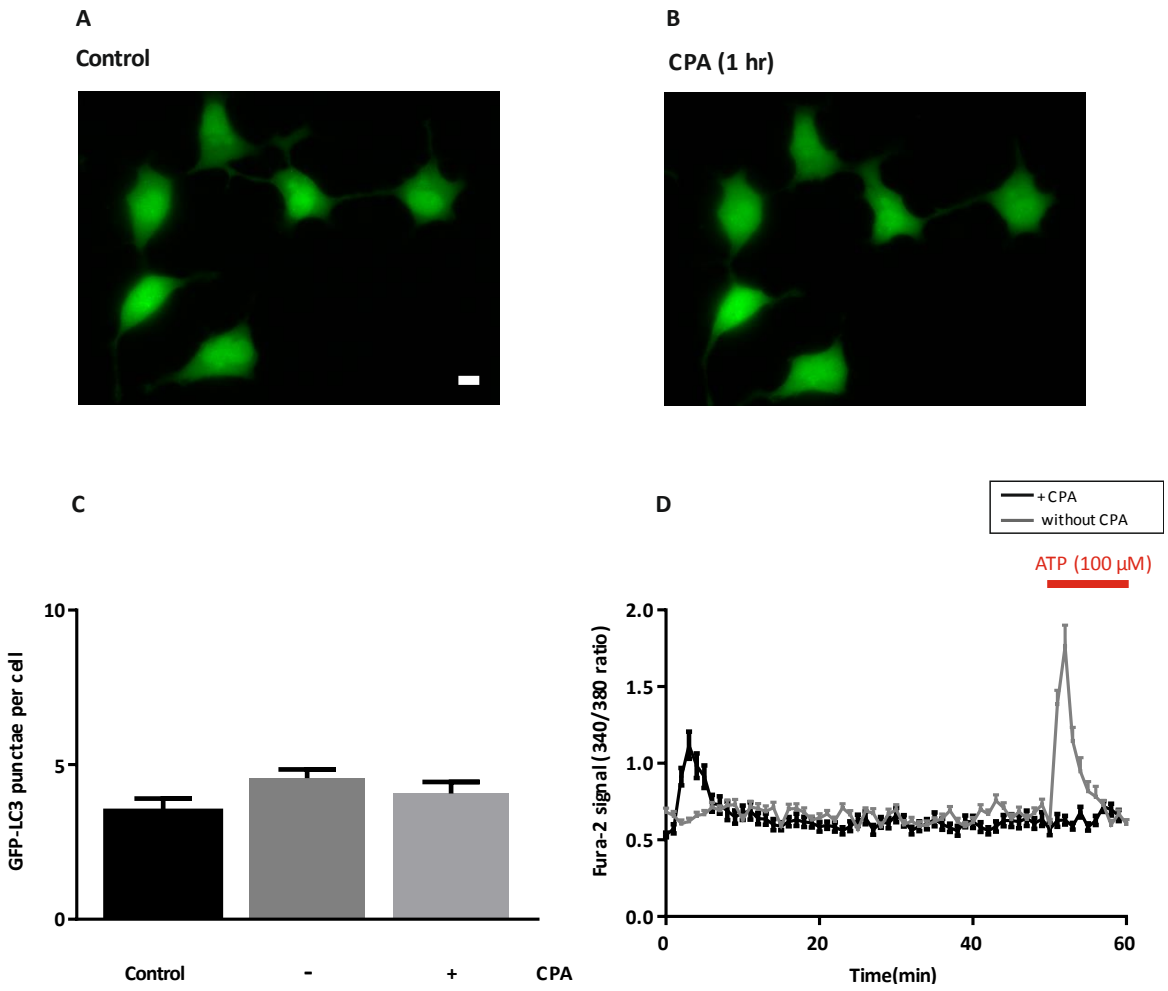

Figure 5.6. Treatment of HEK cells with cyclopiazonic acid (CPA) in the absence of extracellular Ca^{2+} did not alter the number of GFP-LC3 punctae. Panel A is a representative image of HEK cells in complete imaging medium. Panel B is the same field of cells as in Panel A, but following treatment with CPA (50 µM) for one hour in Ca^{2+}-free medium. Panel C is a quantitative representation of the effect of CPA on autophagy in Ca^{2+}-free medium; there was no difference in the number of GFP-LC3 punctae. Panel D shows the profile of cytosolic Ca^{2+} in HEK cells incubated in Ca^{2+}-free medium. The black trace was recorded from cells treated with CPA (50 µM); CPA was added following a one-minute baseline recording. The grey trace was recorded from cells that were solely incubated in Ca^{2+}-free medium (i.e., no addition of CPA). For both traces, ATP (100 µM) was applied to cells for the last 10 minutes of the recordings to examine the Ca^{2+} content of the ER. The data are mean ± S.E.M of 3 - 4 experiments (40 - 50 cells per condition). The data were analysed with a one-way ANOVA. The scale bar in Panel A indicates 10 µm.

5.2.4 The transient release of intracellular Ca^{2+} stores evoked by inhibiting SERCA pumps with CPA did not induce autophagy

To explore whether the transient release of Ca^{2+} from intracellular stores evoked by inhibition of SERCA pumps with CPA affected autophagy, the numbers of GFP-LC3 punctae in HeLa cells were monitored at 10 minute intervals after the addition of CPA in Ca^{2+}-free medium. As depicted in Figure 5.7A, addition of 50 µM CPA in Ca^{2+}-free medium caused a transient cytosolic Ca^{2+} signal that returned to basal levels within 2 minutes. Monitoring GFP-LC3 punctae numbers in the same CPA-treated cells indicated that the transient release of Ca^{2+} evoked by CPA did not affect autophagy (Figure 5.7B). Taken together, these data indicate that a sustained Ca^{2+} influx signal triggers autophagic flux in HeLa cells, whereas neither a transient release of Ca^{2+} from intracellular stores, nor Ca^{2+} store depletion, induces autophagy.

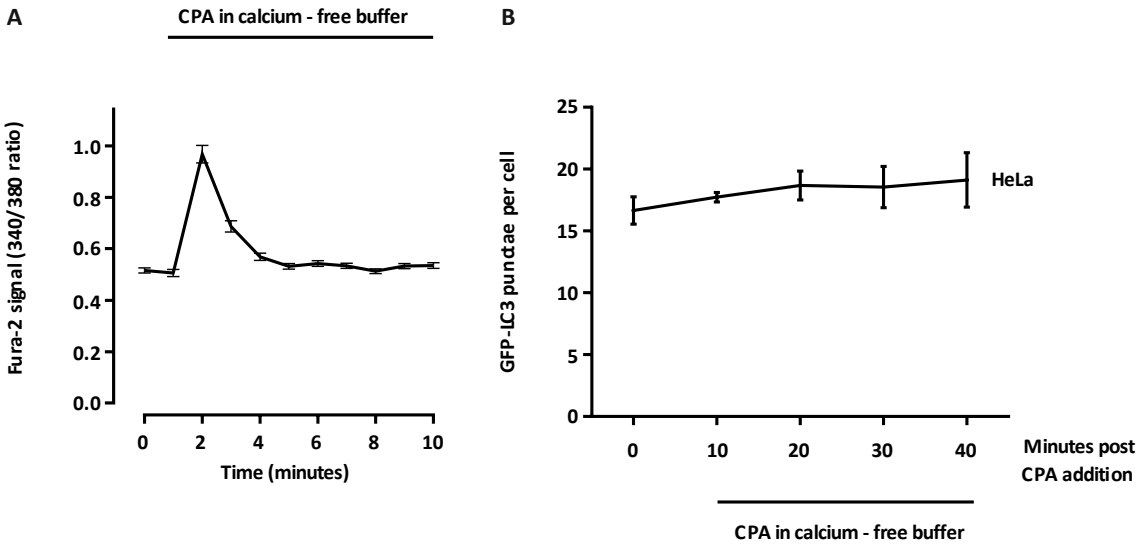

Figure 5.7. Exposing HeLa cells to cyclopiazonic acid (CPA) in the absence of extracellular Ca^{2+} did not alter the number of GFP-LC3 punctae. To examine whether a transient Ca^{2+} release from intracellular stores was able to affect autophagy, GFP-LC3-expressing HeLa cells were stimulated with CPA (50 µM) in Ca^{2+}-free medium. Panel A shows an averaged response of HeLa cells to addition of CPA in Ca^{2+}-free medium; a transient cytosolic Ca^{2+} signal was evident. Panel B shows the number of GFP-LC3 punctae within HeLa cells during the CPA treatment. The data are mean ± S.E.M of 3 experiments.

5.2.5 CPA stimulated *autophagic flux* in the presence of extracellular Ca^{2+}, but not in its absence.

To explore whether in the absence of extracellular Ca^{2+} CPA had interfered with the autophagic flux, control tests were carried out with BafA1. As shown in Figures 5.8 and 5.9, CPA did not prevent the enhanced accumulation of GFP-LC3 punctae in cells incubated with BafA1, suggesting that autophagic flux was occurring in the presence of CPA in Ca^{2+}-free medium. Moreover, the co-addition of 3-MA with CPA in complete imaging medium prevented GFP-LC3 punctae accumulation, revealing that CPA-induced autophagy was sensitive to a blocker of the canonical autophagy pathway (Figure 5.10).

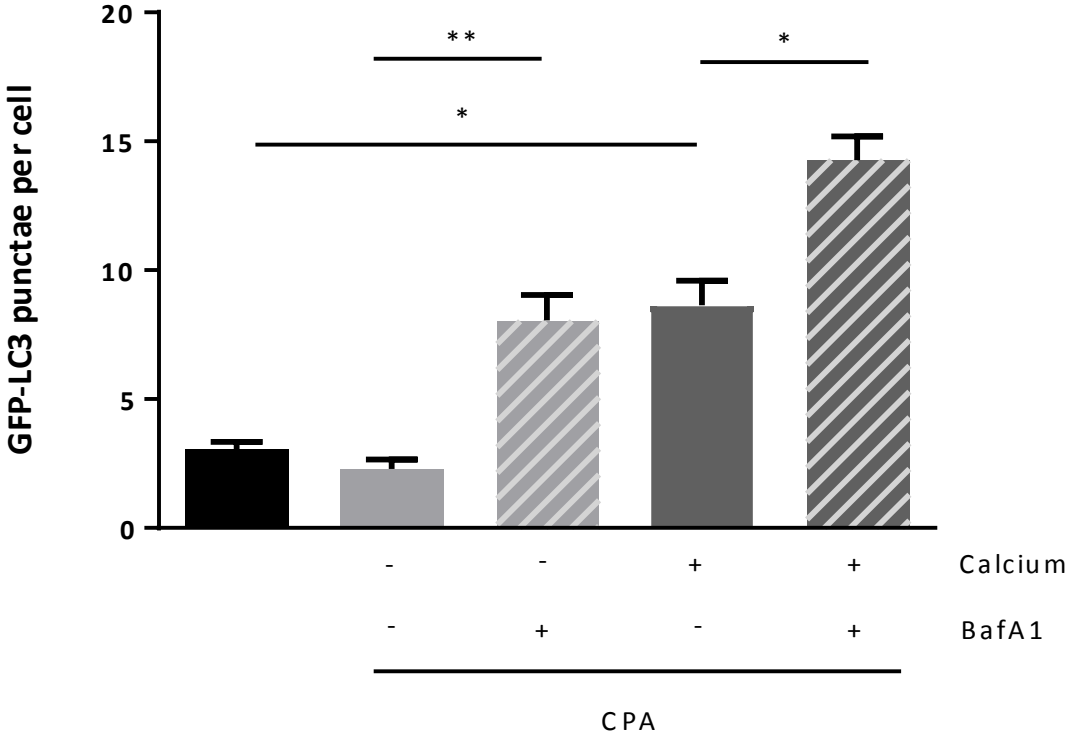

Figure 5.8. CPA stimulated *autophagic flux* within HEK cells in presence of extracellular Ca^{2+}, but not in its absence. The column graph is a quantitative representation of the effect of CPA (50 µM for 1 hour) on GFP-LC3 punctae accumulation in HEK cells in a Ca^{2+}-free or Ca^{2+}-containing, complete medium. Co-addition of BafA1 (0.1 µM) with CPA caused an increase in GFP-LC3 punctae compared to CPA treatment only. The data are mean ± S.E.M of 3 experiments (25 - 75 cells per condition). The data were analysed with a one-way ANOVA. * indicates $p < 0.05$ and ** indicates $p < 0.01$.

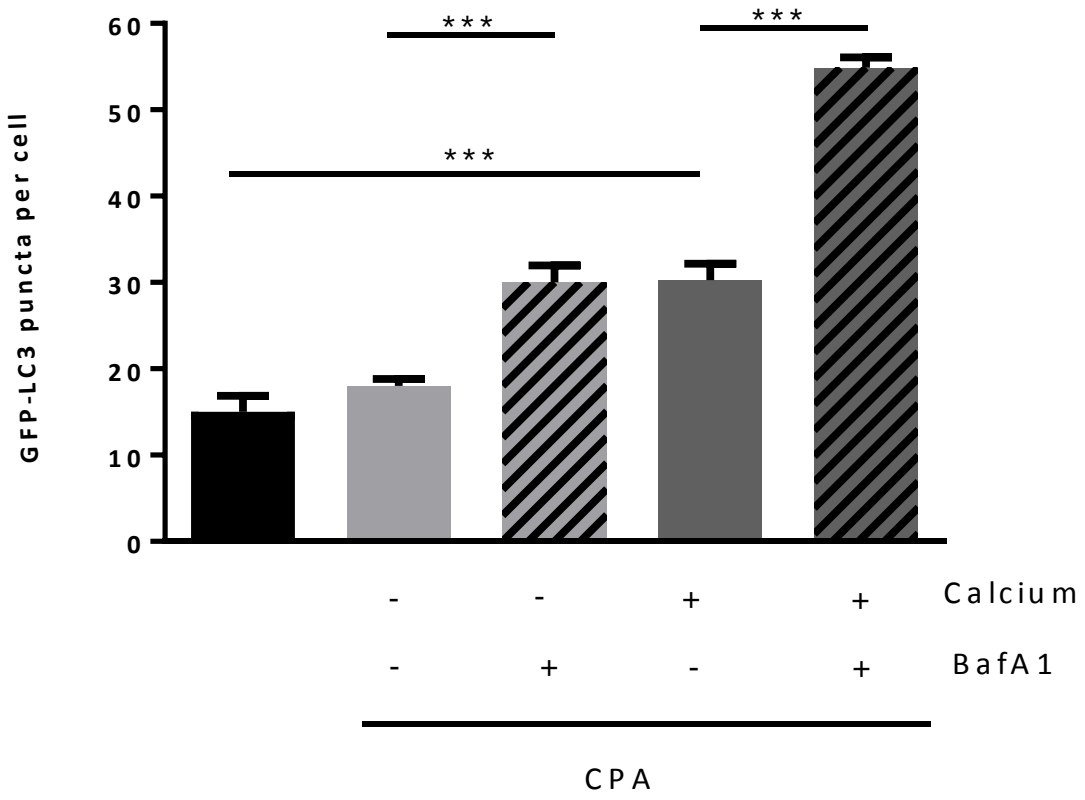

Figure 5.9. CPA stimulated *autophagic flux* in HeLa cells in presence of extracellular Ca^{2+}, but not in its absence. The column graph is a quantitative representation of the effect of CPA (50 µM for 1 hour) on GFP-LC3 punctae accumulation in HeLa cells in a Ca^{2+}-free or Ca^{2+}-containing, complete medium. Co-addition of BafA1 (0.1 µM) with CPA caused an increase in GFP-LC3 punctae compared to CPA treatment only. The data are mean ± S.E.M of 3 experiments (20 - 30 cells per condition). The data were analysed with a one-way ANOVA. *** indicates $p < 0.001$.

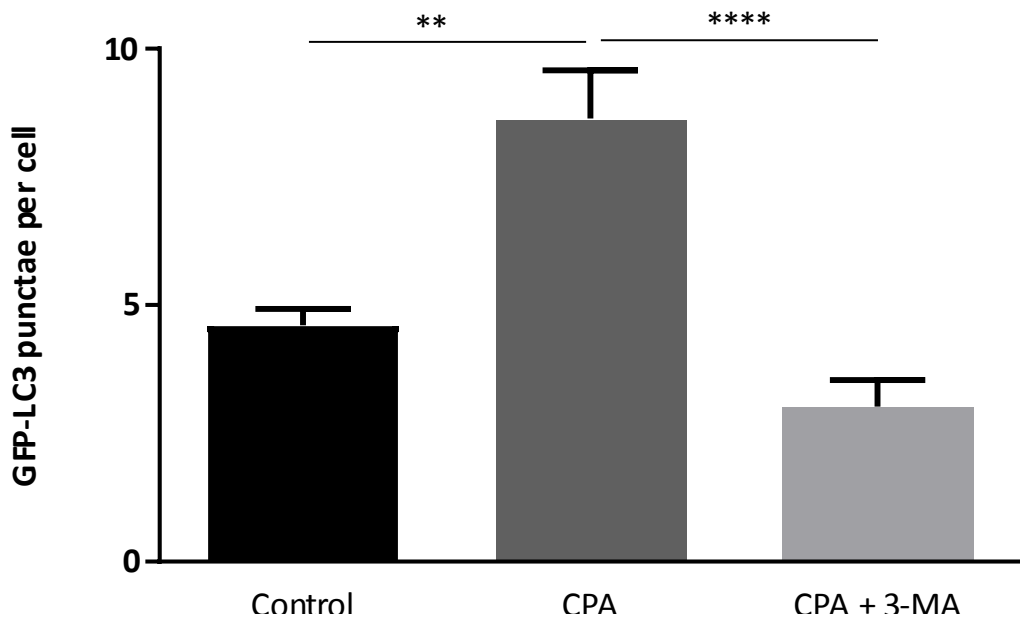

Figure 5.10. 3-MA, an inhibitor of class III PI 3-kinases, prevented the increase of GFP-LC3 punctae induced by CPA in HEK cells. The panel is a quantitative representation on the effect of CPA (50 μM) in complete imaging medium on numbers of GFP-LC3 punctae in GFP-LC3 HEK cells, following a 1-hour incubation. CPA significantly increased the number of GFP-LC3 punctae, but the concurrent addition of 3-MA (5 mM) with CPA suppressed the increase in GFP-LC3 punctae numbers to near basal levels. The data are mean ± S.E.M of 3 experiments (40 cells per condition). The data were analysed with a one-way ANOVA. ** indicates $p < 0.01$ and **** indicates $p < 0.0001$.

5.2.6 Chronic CPA treatment in a Ca^{2+}-free media induces autophagy

The observation that treatment of cells with CPA for 1 hour in the absence of extracellular Ca^{2+} did not induce an increase in GFP-LC3 punctae suggests that the Ca^{2+} entry occurring during activation of SOCE was critical to the triggering of autophagy. However, the depletion of ER Ca^{2+} stores with agents such as CPA is known to trigger cell stress responses that can subsequently activate autophagy [426] [427]. To examine whether the cells used in this study behaved in a similar manner to other those used in other reports, the effects of a prolonged incubation with CPA in Ca^{2+}-free medium were investigated. To this end, HeLa and HEK cells were treated for 12 hours with CPA in the Ca^{2+}-free medium described above. The prolonged incubation of cells with CPA in Ca^{2+}-free medium evoked an increase in GFP-LC3 punctae numbers (Figure 5.11 and Figure 5.12). Incubating the cells in Ca^{2+}-free medium for 12 hours without CPA had no effect on GFP-LC3 punctae accumulation. Importantly, the addition of BafA1 during the CPA treatment increased the number of GFP-LC3 punctae, consistent with CPA triggering autophagic flux.

A plausible explanation for the autophagic flux triggered by prolonged incubation of cells with CPA in Ca^{2+}-free medium would be the triggering of ER stress due to chronic Ca^{2+} store depletion. However, qRT-PCR analysis of GRP78/BiP mRNA indicated that treatment of cells with CPA for either 1 hour or 12 hours did not induce an increase in ER stress (Figure 5.13). Whereas, treatment of cells with H_2O_2, used as a positive control, evoked a significant increase in GRP78/BiP mRNA.

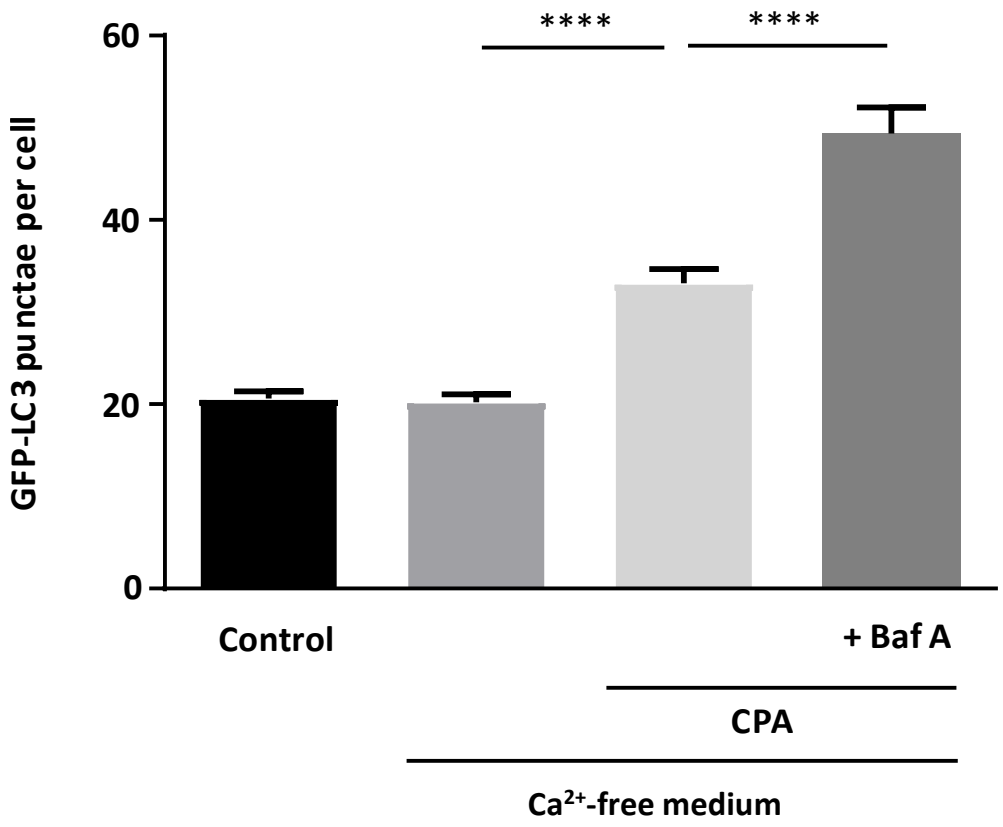

Figure 5.11. Prolonged treatment of HeLa cells with cyclopiazonic acid (CPA) in the absence of extracellular Ca^{2+} stimulated an increase in GFP-LC3 punctae. The column graph is a quantitative representation of the effect of treating HeLa cells with CPA (50 µM) for 12 hours in Ca^{2+}-free medium. The addition of CPA to cells in a Ca^{2+}-free medium increased GFP-LC3 punctae numbers significantly, with greater punctae accumulation in the presence of BafA1. The data are mean ± S.E.M of 3 experiments (40 - 60 cells per condition). The data were analysed with a one-way ANOVA. **** indicates $p < 0.0001$.

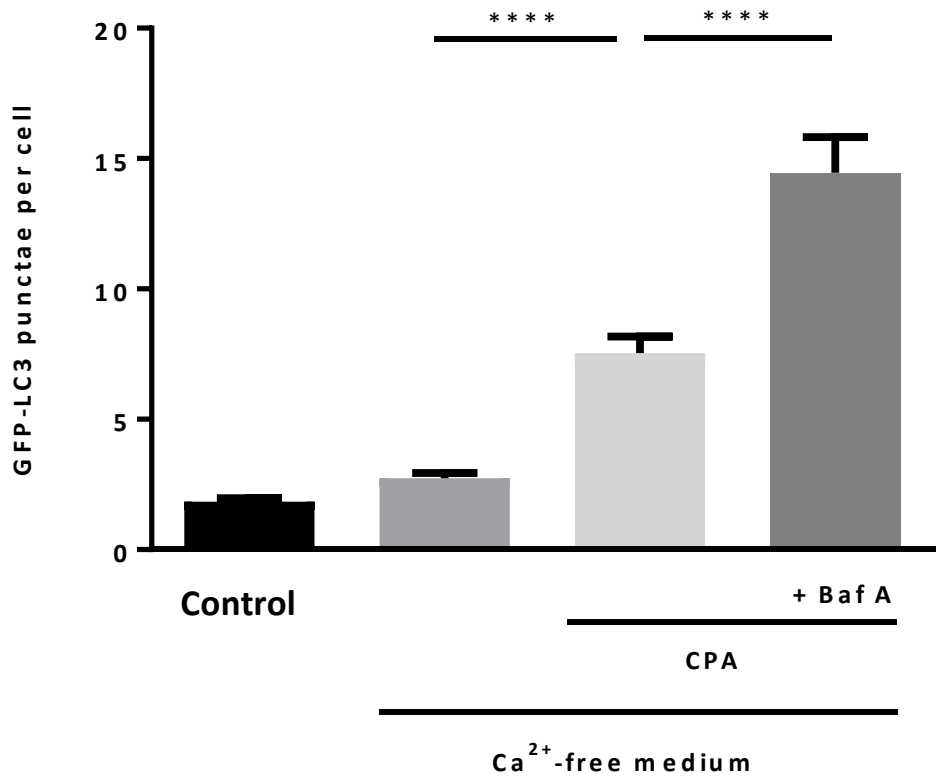

Figure 5.12. Prolonged treatment of HEK cells with cyclopiazonic acid (CPA) in the absence of extracellular Ca^{2+} stimulated an increase in GFP-LC3 punctae. The column graph is a quantitative representation of the effect of treating HEK cells with CPA (50 µM) for 12 hours in Ca^{2+}-free medium. The addition of CPA to cells in a Ca^{2+}-free medium increased GFP-LC3 punctae numbers significantly, with greater punctae accumulation in the presence of BafA1. The data are mean ± S.E.M of 3 experiments (40 - 60 cells per condition). The data were analysed with a one-way ANOVA. **** indicates $p < 0.0001$.

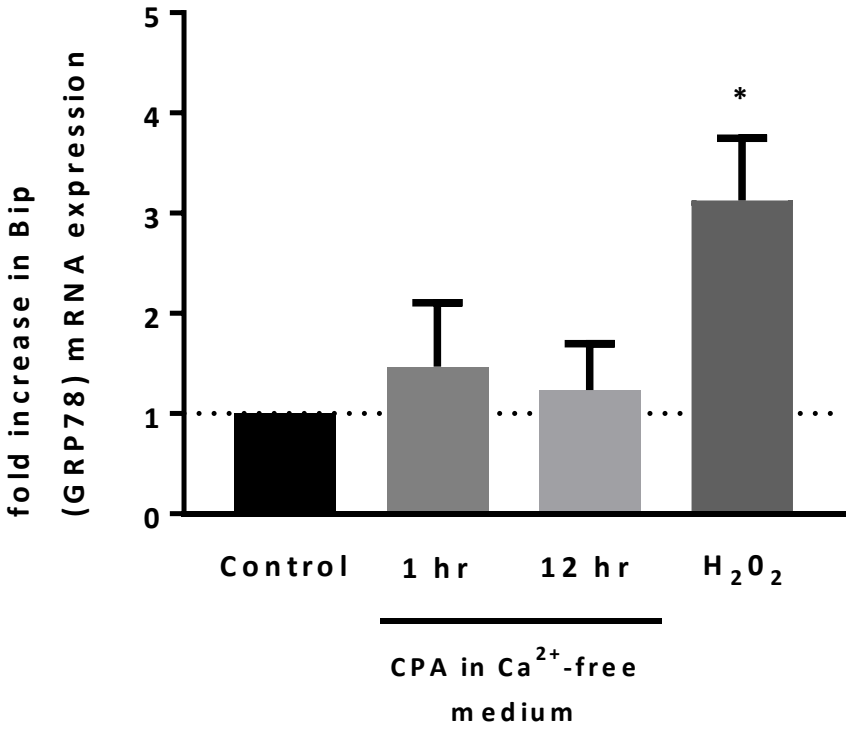

Figure 5.13. Prolonged treatment of HEK cells with CPA for 12 hours in the absence of extracellular Ca^{2+} did not alter the transcription of GRP78/BiP mRNA. The column graph depicts the quantitation of GRP78/BiP mRNA in HEK cells assayed using qRT-PCR, as a measure of ER stress. HEK cells were treated for 1 or 12 hours with CPA (50 µM) in Ca^{2+}-free medium. The addition of hydrogen peroxide (H_2O_2; 100 µM) for 3 hours as a positive control resulted in a ~2-fold increase in GRP78/BiP expression relative to GAPDH and normalised to untreated conditions using the ΔΔCt method. Neither acute nor prolonged CPA treatment affected GRP78/BiP transcription. The data are mean ± S.E.M of 3 experiments. The data were analysed with a one-way ANOVA. * indicates $p < 0.05$.

5.2.7 The absence of extracellular Ca^{2+} prevented the induction of autophagy by rapamycin

The data presented in Chapter 3, Figures 3.12 to 3.15, showed that incubation of cells in complete imaging medium with rapamycin increased GFP-LC3 punctae accumulation that was enhanced by BafA1 and prevented by 3-MA. To investigate whether canonical mTOR-dependent autophagy requires Ca^{2+} storage within the ER or extracellular Ca^{2+} influx, cells were treated with rapamycin in complete imaging medium or in Ca^{2+} -free medium, with or without (CPA 50 μM) for 1 hour. As depicted in Figures 5.14 and 5.15, and shown in Figures 3.12 and 3.13, application of rapamycin in complete imaging medium stimulated an increase in the number of GFP-LC3 punctae. However, application of rapamycin to cells in the absence of extracellular Ca^{2+} did not alter the number of GFP-LC3 punctae, whether the cells were treated with CPA or not. Since HeLa cells retain their ER Ca^{2+} stores when incubated in Ca^{2+}-free medium without CPA (Figure 5.5), these data indicate that rapamycin-evoked autophagy does not depend on Ca^{2+} release from the ER, but does require Ca^{2+} influx.

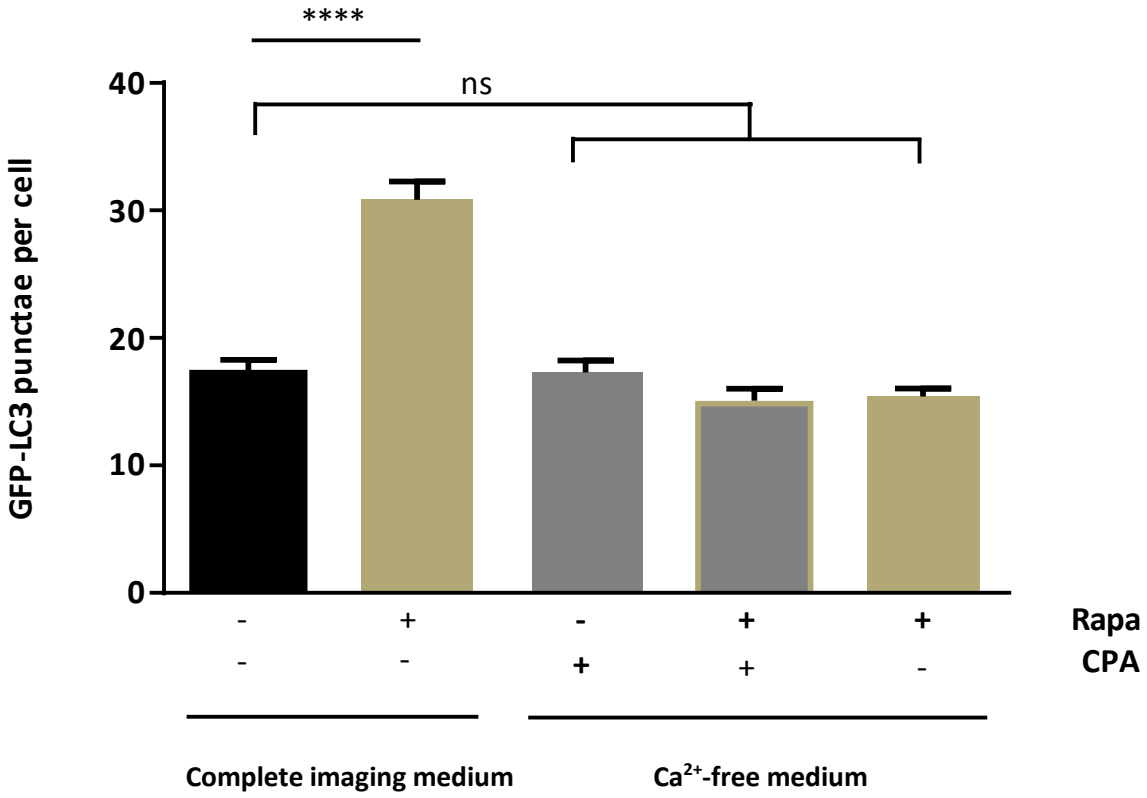

Figure 5.14. Rapamycin-stimulated induction of autophagy in HeLa cells was dependent on the presence of extracellular Ca^{2+}, but not Ca^{2+} storage in the ER. The column graph is a quantitative representation of the effects of rapamycin (1 µM) on GFP-LC3 punctae formation in the presence or absence of extracellular Ca^{2+}, with or without application of CPA (50 µM). All incubations were for 1 hour. The addition of rapamycin caused a significant increase in GFP-LC3 punctae only if extracellular Ca^{2+} was present. The data are mean ± S.E.M of 3 - 5 experiments (25 - 60 cells per condition). The data were analysed with a one-way ANOVA. **** indicates $p < 0.0001$.

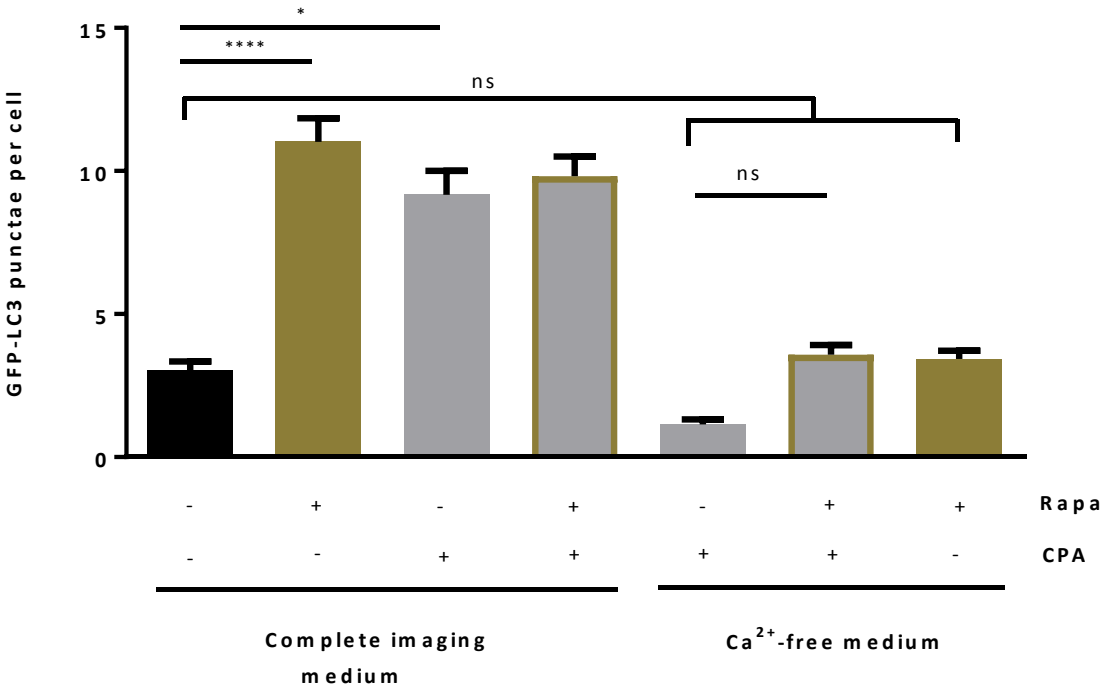

Figure 5.15. Rapamycin-stimulated induction of autophagy in HEK cells was dependent on the presence of extracellular Ca^{2+}, but not Ca^{2+} storage in the ER. The column graph is a quantitative representation of the effects of CPA (used to deplete ER calcium) for 1 hour and Ca^{2+}-free medium (used to prevent calcium entry) on rapamycin-induced autophagy. The addition of rapamycin for 1 hour to HEK cells caused a significant increase in GFP-LC3 punctae only if extracellular Ca^{2+} was present. Also, the addition of rapamycin and CPA together in a Ca^{2+}-containing medium showed similar punctae numbers to CPA or rapamycin treatments alone, which reveals that the two compounds did not have additive effects. The data are mean ± S.E.M of 3 experiments (20 - 60 cells per condition). The data were analysed with a one-way ANOVA. * indicates $p < 0.05$ and **** indicates $p < 0.0001$.

5.2.8 Ionomycin-mediated Ca^{2+} influx does not trigger autophagy in HEK cells

The data presented in this Chapter indicate that prolonged activation of SOCE leads to the induction of autophagy in HEK cells (Figure 5.3). Ca^{2+} influx via SOCE can lead to a global cytosolic Ca^{2+} rise, which may affect cellular functions. In addition, SOCE has been shown to have specific local signalling actions [417]. To examine whether the pro-autophagic effect of SOCE was due to global or local Ca^{2+} signalling, ionomycin was used to generate a prolonged Ca^{2+} influx signal that was not dependent on plasma membrane channel activation.

The effect of ionomycin on autophagy was investigated using Fura-2-loaded GFP-LC3-expressing HEK cells with an experimental protocol similar to that used for the experiments shown in Figure 5.3. Following a 1-minute recording of the basal 340/380 Fura-2 ratio, HEK cells were incubated in complete imaging medium supplemented with 1 µM ionomycin for a further 59 minutes. The 340/380 Fura-2 ratio was monitored for the duration of the experiment. To examine the status of the intracellular Ca^{2+} stores, 100 µM ATP was added for the last 10 minutes of the experiment. At the end of the experiment, the numbers of GFP-LC3 punctae were counted. As shown in Figure 5.16, treatment with ionomycin did not affect GFP-LC3 punctae accumulation in HEK cells (Figures 5.16 A-C). The Fura-2 measurements indicated that ionomycin caused a sustained elevation of cytosolic Ca^{2+}, consistent with perpetual Ca^{2+} influx (Figure 5.16D). The lack of responses to addition of ATP indicated that ionomycin had depleted intracellular Ca^{2+} stores. Increasing the extracellular Ca^{2+} concentration to 5 mM during ionomycin application did not enhance the number of GFP-LC3 punctae (Figure 5.16C).

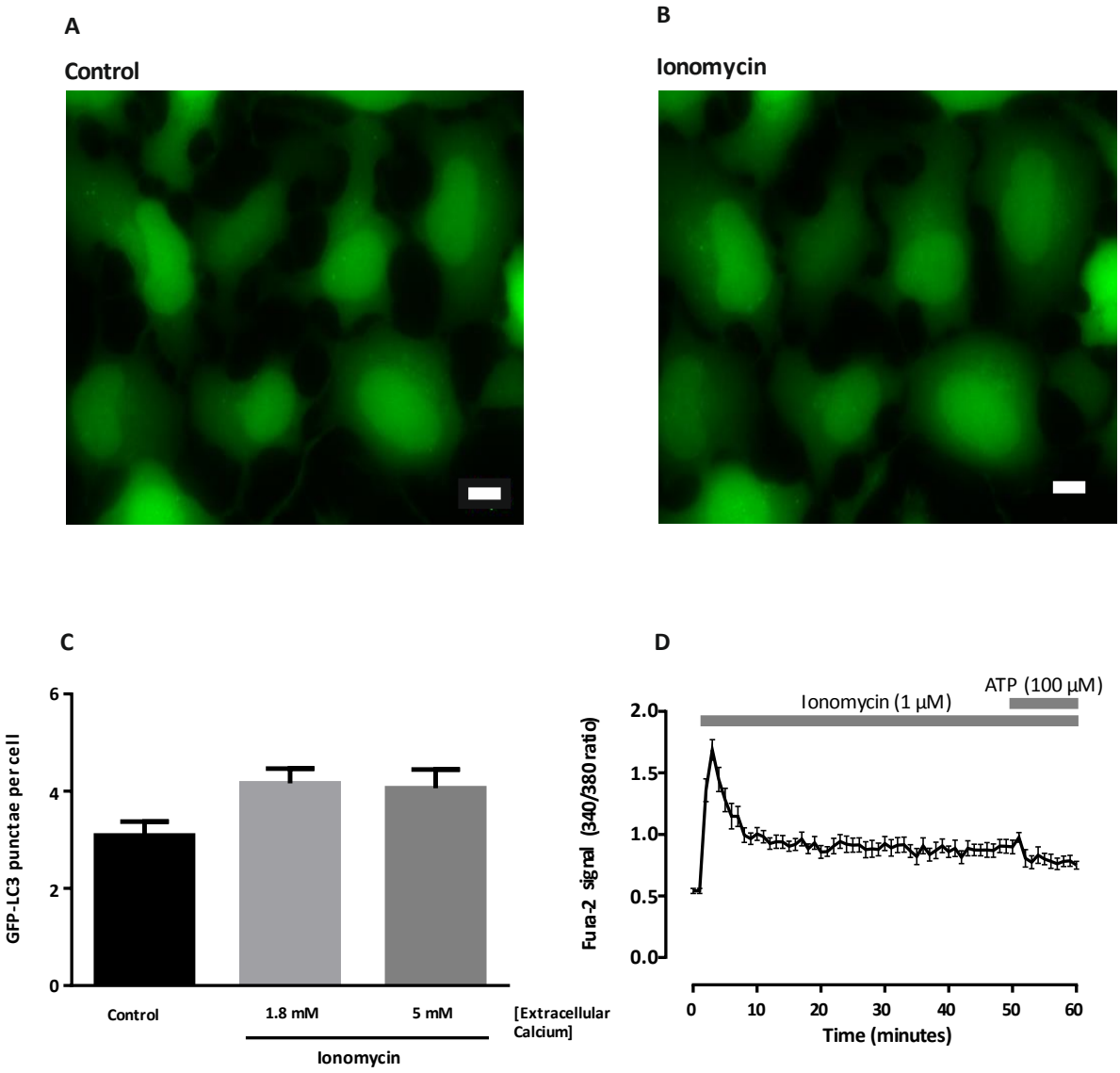

Figure 5.16. Increasing cytosolic Ca^{2+} concentration with ionomycin did not affect GFP-LC3 punctae accumulation in HEK cells. Panel A is a representative image of cells in complete imaging medium. Panel B is an image of the same cells as in Panel A, but following incubation with 1 µM Ionomycin for one hour. Panel C is a quantitative representation of GFP-LC3 punctae numbers in control cells and cells treated with ionomycin in complete imaging media containing either 1.8 mM or 5 mM Ca^{2+}. Panel D is the profile of cytosolic Ca^{2+} signals recorded from cells in complete imaging medium containing 1.8 mM Ca^{2+}. A one-minute baseline recording was followed by addition of 1 µM Ionomycin. 100 µM ATP was added to cells for the last 10 minutes of the recording. The data are mean ± S.E.M of 3 experiments (15 - 45 cells per condition). The data were analysed with a one-way ANOVA test. The scale bars in Panels A and B indicate 10 µm.

5.2.9 Ionomycin does not prevent autophagic flux

Unlike CPA, ionomycin did not stimulate a significant accumulation of GFP-LC3 punctae in HEK cells, despite both treatments giving similar cytosolic Ca^{2+} signals that were dependent on Ca^{2+} influx (Figures 5.3 and 5.16). To test whether ionomycin prevented the accumulation of GFP-LC3 punctae by inhibiting the formation of autophagosomes, HEK cells were incubated with BafA1 to assess autophagic flux. As shown in Figure 5.17, ionomycin did not trigger a significant increase in GFP-LC3 punctae accumulation. Moreover, ionomycin did not prevent the significant accumulation of GFP-LC3 punctae in cells incubated with BafA1, suggesting that there was on-going autophagic flux in the presence of ionomycin.

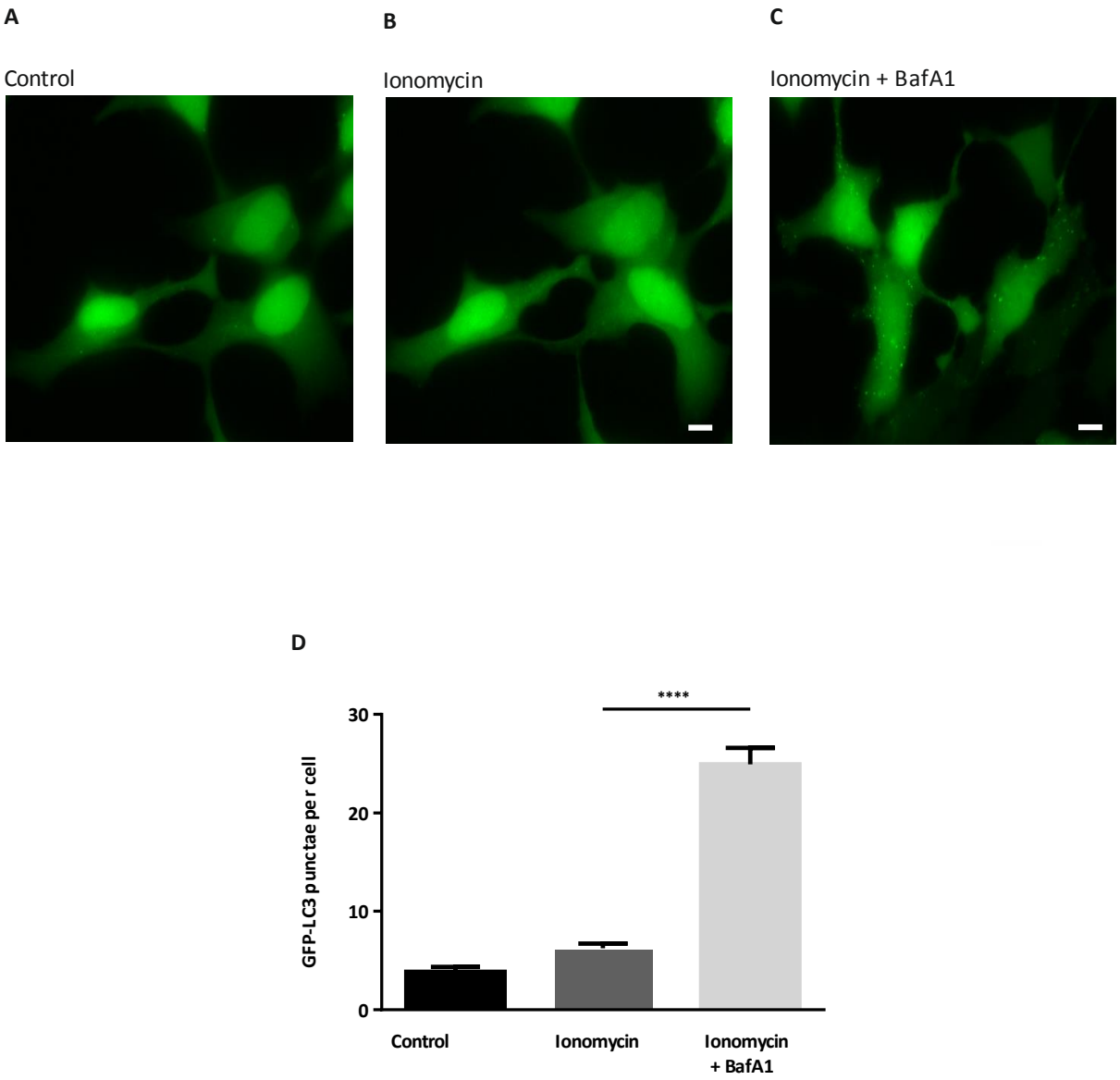

Figure 5.17. Ionomycin did not prevent autophagic flux in HEK cells. Panel A is a representative image of cells in complete imaging medium. Panels B and C are representative images of cells in complete imaging medium treated with 1 µM ionomycin for one hour, in the absence or presence of BafA1, respectively. Panel D is a quantitative representation of the effect of ionomycin and ionomycin + BafA1 on autophagy; no significant change in GFP-LC3 punctae number was obtained with ionomycin alone. The data are mean ± S.E.M of 3 experiments (35 - 80 cells per condition). The data were analysed with a one-way ANOVA. **** indicates $p < 0.0001$. The scale bars in Panels A - C indicate 10 µm.

5.2.10 Inhibition of Ca^{2+}/calmodulin-dependent kinase kinase (CaMKK) with STO-609 prevented CPA-induced autophagy

To investigate the molecular pathways involved in CPA-induced autophagy, HeLa cells were treated with compounds that inhibit three signalling mediators commonly reported in the literature to be involved in autophagy induction [428-430]. Go6983, Sto-609 and KN-93 (and its inactive form KN-92) were used to inhibit PKC, CaMKK-α/β and CaMKII respectively. Control conditions involved cells either incubated in complete imaging medium, or cells treated with the compounds mentioned above in the absence of CPA to determine if they have any effect on basal autophagy. As shown earlier (Figure 5.2 and Figure 5.3), incubation of cells with CPA for 1 hour in complete imaging medium caused an increase in GFP-LC3 punctae accumulation (Figure 5.18). Of the compounds applied to the cells with CPA, only STO-609 caused a significant decrease of GFP-LC3 punctae numbers. None of the compounds had any effect on the basal level of GFP-LC3 punctae formation in the absence of CPA.

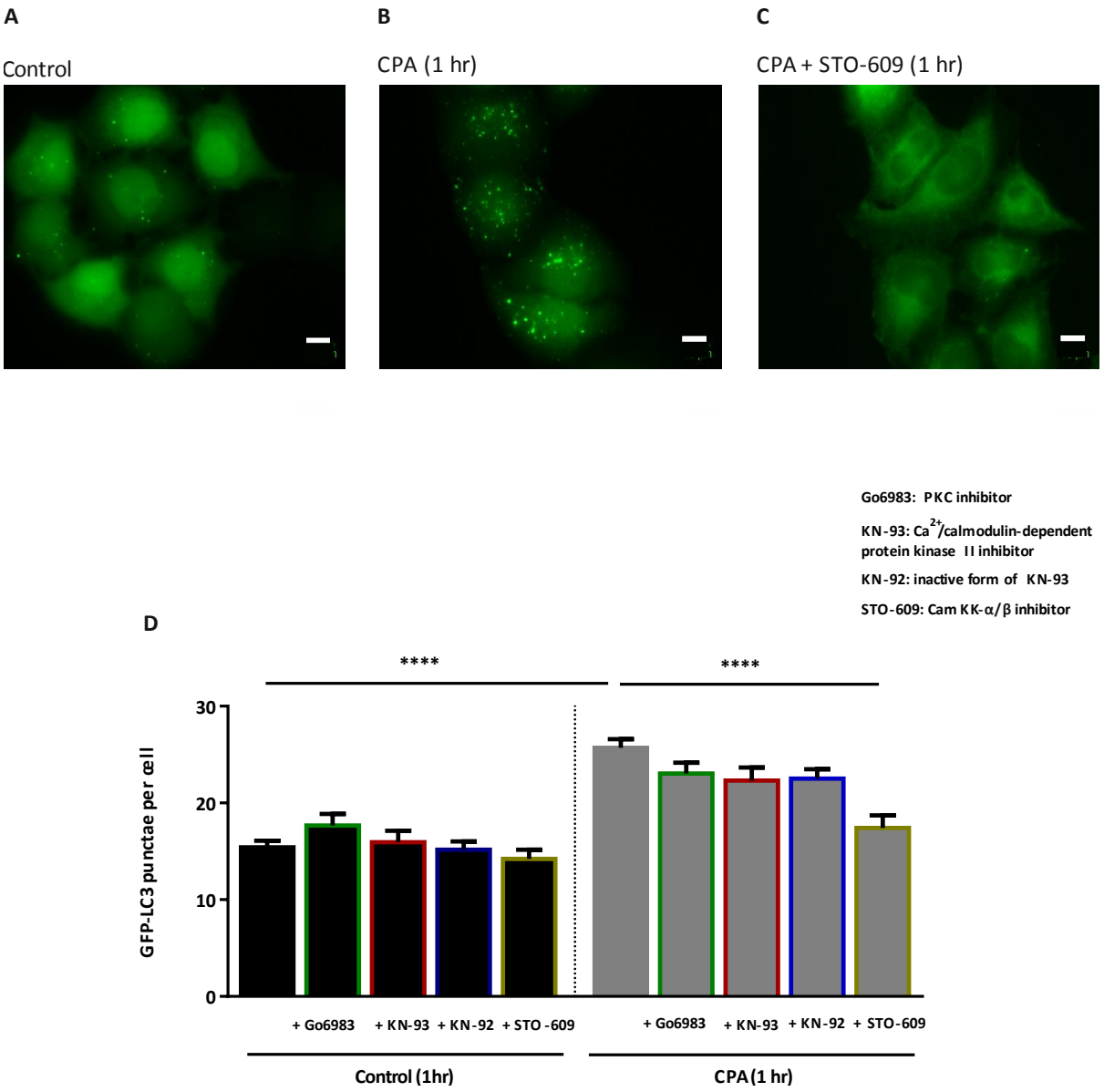

Figure 5.18. The CaMKK-α/β antagonist STO-609 inhibited GFP-LC3 punctae accumulation induced by CPA in HeLa cells. Panel A is a representative image of cells in complete imaging medium. Panel B shows cells that were incubated in complete imaging medium supplemented with CPA (50 µM) for 1 hour. Panel C shows cells that were incubated in complete imaging medium supplemented with both CPA and STO-609 (25 µM). Panel D is a quantitative representation of the effect of CPA and the compounds on autophagy; only STO-609, an inhibitor of CaMKK-α/β**,** reduced CPA-evoked autophagy, whereas neither PKC nor CaM Kinase II inhibitors had a significant effect. The data are mean ± S.E.M of 3 experiments (25-70 cells per condition). The data were analysed with a one-way ANOVA. **** indicates $p < 0.0001$. The scale bars in Panels A - C indicate 10 µm.

5.3 Summary

The work presented in this Chapter examined the ability of Ca^{2+} influx via SOCE, or Ca^{2+} release from intracellular stores, to regulate autophagy. All experiments were performed using supplements that maintain cells in a basal autophagic state with consistent numbers of GFP-LC3 punctae for several hours (Chapter 3, Figures 3.3 and 3.4). Any change in GFP-LC3 punctae numbers would therefore result from stimulation or inhibition of autophagy, or an effect on autophagic flux. The key findings in this Chapter are:

- Prolonged Ca^{2+} influx via CPA-evoked SOCE triggered an increase in autophagic flux in HeLa and HEK cells (Figures 5.2 and 5.3).
- ER Ca^{2+} store depletion for 1 hour, in the absence of Ca^{2+} influx, did not induce or inhibit autophagy; GFP-LC3 punctae numbers remained similar to basal levels in HeLa and HEK cells (Figures 5.5 and 5.6).
- ER Ca^{2+} store depletion for 12 hours, in the absence of Ca^{2+} influx, induced autophagy (Figures 5.11 and 5.12). However, autophagy was not upregulated due to ER stress.
- Rapamycin-induced autophagy required the presence of extracellular Ca^{2+}, but not ER Ca^{2+} stores (Figures 5.14 and 5.15).
- Thapsigargin, another activator of SOCE, triggered autophagy in HeLa cells (Fig. 5.1)
- CPA and Thapsigargin do not inhibit autophagic flux.
- Ionomycin evoked a similar cytosolic Ca^{2+} signal to CPA, but did not significantly stimulate autophagy in HEK cells (Figures 5.16).
- The lack of effect of ionomycin on autophagy was not due to inhibition of autophagic flux.

- Cytosolic Ca^{2+} elevation with CPA treatment induced autophagy via CaMKK-mediated phosphorylation in HeLa cells (Figure 5.18).

5.4 Discussion

This Chapter investigated the role of Ca^{2+} influx via SOCE on autophagy in two distinct cell lines. The results reveal that a prolonged cytosolic Ca^{2+} signal, caused by application of Tg or CPA in Ca^{2+}-containing medium, induced autophagy. The experiments carried out in the presence or absence of extracellular Ca^{2+} suggest that a sustained Ca^{2+} influx via SOCE induces autophagy (Figures 5.2 & 5.3), but depletion of ER Ca^{2+} stores does not change autophagy levels (Figures 5.5 & 5.6). The lack of autophagy induction by ER Ca^{2+} store release during CPA application does not necessarily indicate that Ca^{2+} release cannot trigger autophagy. Rather, it is possible that prolonged Ca^{2+} signals (i.e., longer than the 15 minutes for ER Ca^{2+} store depletion; Figure 5.7) are required for the induction of autophagy, and that ER Ca^{2+} release, when triggered by SERCA inhibition, is too brief. The induction of autophagy by rapamycin similarly relied on extracellular Ca^{2+}, suggesting that mTOR-induced autophagy requires constitutive Ca^{2+} signals (Figure 5.14 and 5.15), and that Ca^{2+} release from ER stores is not sufficient. Further work is required to understand why rapamycin-induced autophagy is reliant on Ca^{2+} influx. SOCE-induced autophagy was found to be reversible (Figure 5.4). This was an important control to show that processing of autophagic vesicles was not chronically affected by SERCA inhibition. Published evidence has shown that CPA-induced Ca^{2+} signals are reversible [431] [432].

Neither CPA nor Tg halted autophagic flux (Figures 5.1, 5.8 and 5.9). This result differs from that reported by Ganley *et al.* [372], who suggested that SERCA inhibition led to the accumulation of GFP-LC3 punctae due to a blockade or autophagosome/lysosome fusion. The reasons why Ganley *et al.* observed an inhibition of autophagic flux when using Tg,

whereas the data presented in this study show that using either Tg or CPA did not block autophagic flux, are unclear. The conditions used by Ganley *et al.* (5 μM Tg for 7 hours with MEF cells) are not that different from those used in this study (e.g., Figure 5.1). Consistent with the data shown in this study, Ganley *et al.* found that punctae formed in the presence of Tg were susceptible to inhibition of PI3-kinase (in their case using wortmanin, rather than 3-MA), but they could not find any enhancement of punctae numbers by addition of BafA1 with Tg. Moreover, Ganley *et al*. reported that the GFP-LC3 punctae observed during TG application were larger in diameter, and proposed that they represented clusters of unprocessed autophagosomes. In the present study, the size of the GFP-LC3 punctae observed during Tg or CPA application did not obviously change (e.g., Figure 5.1, Figure 5.2 and Figure 5.3). Also, whereas Ganley *et al*, found that Tg evoked only a modest change in GFP-LC3 punctae numbers over basal conditions, the present study found a marked fold increase in GFP-LC3 puncate numbers (Figure 5.1). The study by Ganley *et al*. did not show the effect of Tg on cytosolic Ca^{2+} concentration, and it is therefore impossible to compare the effects of SERCA inhibition in the MEF cells those authors used versus the HEK and HeLa cells employed in this study with regards to Ca^{2+} signalling. Although, it is presently unclear why SERCA inhibition led to a blockade of autophagic flux in the work by Ganley *et al.*, whereas the present study found that autophagic flux was evident in Tg- and CPA-treated cells, both studies agree that SERCA inhibition does not affect the initial stages of autophagosome formation. This validates the approach employed in this study to use SOCE as a means for activating a Ca^{2+}-dependent form of autophagy. The use of CPA to cause SOCE-dependent autophagic flux therefore provides a useful system in which autophagy is Ca^{2+}-dependent, and screening for factors that mediate the effects of Ca^{2+} can be performed.

Ionomycin, however, did not have a significant effect on autophagy in HEK cells, despite evoking a similar prolonged cytosolic Ca^{2+} elevation to that seen with CPA (Figures 5.16). This outcome could be due to the fact that SOCE allows local Ca^{2+} signalling around the mouth of a channel, whereas ionomycin gives a more global Ca^{2+}signal and therefore does not trigger effectors that are local to SOCE channels [433]. Contrary to these findings, ionomycin elevated autophagy levels in MCF-7 cells [199]. However, the upregulation of autophagy in that study might not have been due to a direct effect of cytosolic Ca^{2+}, but as a consequence of long-term effects of ionomycin such as mitochondrial depolarisation and fragmentation of organelles [434], since the ionophore was applied for 24 hours.

A number of experimental studies, using a variety of means to elevate cytosolic Ca^{2+} concentration, have suggested that Ca^{2+} can cause an increase in autophagy through a Ca^{2+}/CaMKK-β-stimulated pathway [199]. Similarly, the findings in this chapter showed that CPA-induced SOCE increased autophagy following a 1 hour incubation in HeLa cells through a CaMKK-α/β-dependent pathway. Although a number of different cellular signalling pathways have been suggested to mediate the effects of Ca^{2+} on autophagy, a majority of studies have pinpointed CaMKK-α/β, which can phosphorylate and activate AMPK thereby leading to autophagy. In support of our data, Racioppi *et al*., have highlighted a critical link between Ca^{2+} and AMPK, where an increase in intracellular Ca^{2+} activates AMPK via CaMKK2 and CaMKK2 forms a complex with AMPK [435].

The findings in this chapter also suggest that the Ca^{2+} sensor must have a high affinity for Ca^{2+}, given that the sustained SOCE-dependent cytosolic Ca^{2+} increase is most cell types is ~100 nM. The published literature has shown SOCE to have both pro- and anti- autophagic roles [13] [14]. The findings in this study support the notion that SOCE is pro-autophagic, since acute depletion of ER Ca^{2+} stores triggered GFP-LC3 punctae accumulation when

extracellular Ca^{2+} was present (Figure 5.2 and Figure 5.3). With colorectal cells, inhibition of Ca^{2+} influx following application of SKF-96365 triggered autophagy, suggesting that constitutive Ca^{2+} entry is required to suppress basal autophagy. However, in this study, the removal of extracellular Ca^{2+} did not alter the basal number of GFP-LC3 punctae (Figure 5.5, Figure 5.11 and Figure 5.12), suggesting that for the cells used here SOCE was not required to suppress autophagy. This study did not therefore furnish any results suggesting that SOCE is anti-autophagic. Long term treatment of cells with CPA in absence of extracellular Ca^{2+} did induce accumulation of GFP-LC3 punctae, however, this induction of autophagy was evidently not dependent on SOCE since no extracellular Ca^{2+} was present. Further work is required to understand why long-term depletion of ER Ca^{2+} stores in the absence of extracellular Ca^{2+} lead to autophagy.

Although a number of studies have directly, or indirectly, used SOCE to examine the role of Ca^{2+} signalling in the regulation of autophagy, the results are not entirely consistent. However, it is clear from the present study that Ca^{2+} influx can trigger autophagy, and is vital for the induction of autophagy via mTOR inhibition. Which channels underlie the effects of SOCE on autophagy were not examined in this study. Whilst STIM1-activated Orai channels are believed to account for substantial proportion of SOCE, they are not the only channels that may respond to ER Ca^{2+} depletion [436]. For example, transient receptor potential canonical channel-1 (TRPC1), is also believed to mediate Ca^{2+} entry in response to depletion of ER Ca^{2+} stores, and increased in intracellular Ca^{2+} arising through TRPC1 activation has been demonstrated to trigger autophagy [437]. Interestingly, a common finding with studies that have investigated the role of SOCE in autophagy is that the resulting autophagy is cytoprotective and acts to delay cell death [295] [437]. These studies suggest that extracellular Ca^{2+} is necessary to trigger autophagy that promotes cell survival.

Plausibly, inhibiting SOCE-dependent autophagy, and its cytoprotective effect, may help in situations where increased cell death is required, such as during chemotherapy for cancer.

Chapter 6: General Discussion and Future Perspectives

6.1 General Discussion

The work described in this thesis sought to develop an understanding of the spatial and temporal characteristics of Ca^{2+} signals that control autophagy in mammalian cells, and to characterise sources of Ca^{2+} that lead to the generation of these Ca^{2+} signals. In particular, this project aimed to understand the regulation of autophagy by cytosolic and mitochondrial Ca^{2+} signals.

The experiments described in *Chapter 3* characterised the utility of fluorescence for studying Ca^{2+} signalling and autophagy within the same cells over an acute time period, as opposed to the many hours of cell stimulation that had been used in previously published studies. Different stimuli were employed to induce autophagy in HeLa and HEK cell lines, two commonly used cell lines in the Ca^{2+} and autophagy fields respectively. A microscopy-based method measuring GFP-LC3 punctae was validated for use in real-time monitoring of autophagic flux with the use of autophagy modulators such as 3-MA and BafA1 to determine any defects in the early and late stages of the process respectively. Additionally, results revealed that chelating cytosolic Ca^{2+} with BAPTA-AM prevented the induction of basal or stimulated autophagy. However the source and nature of the Ca^{2+} signals necessary for these putative Ca^{2+}-sensitive steps is unclear.

The work presented in *Chapter 4* investigated the regulation of autophagy by Ca^{2+} release from $InsP_3Rs$. Recent studies investigating the regulation of autophagy have indicated that $InsP_3Rs$ are involved in both anchoring proteins involved in autophagy (e.g., Beclin-1 and Bcl-2) and providing Ca^{2+} signals that impact on the induction of autophagy. However, as with much of the literature on Ca^{2+} and autophagy, the actual role of $InsP_3Rs$ (whether pro- or anti-autophagic) is controversial. Moreover, $InsP_3Rs$ have received great attention in

relation to cancer in the last few years, with proposals that cancer cells are addicted to $InsP_3R$-mediated Ca^{2+} signalling for survival and growth in order to keep up with their fast and uncontrolled proliferation [402, 412]. The results presented in this study support the hypothesis that the transfer of Ca^{2+} from $InsP_3Rs$ to mitochondria suppresses autophagy, and agree with other evidence whereby a reduction in $InsP_3$ signalling is pro-autophagic. Reduced Ca^{2+} transfer from $InsP_3Rs$ to mitochondria in $InsP_3$ 5'-phosphatase-expressing cells caused reduced ATP levels. Additionally, the mitochondrial uniporter (MCU) was found to be vital for maintaining suppression of autophagy. $InsP_3$ 5'-phosphatase-expressing cells were shown to have a normal cell cycle profile without failure of mitosis, which is contrary to literature findings [320]. BAPTA-AM prevented autophagy induction by $InsP_3R$ inhibition, revealing that a BAPTA-sensitive source of Ca^{2+} is required for autophagy to proceed. These data show that that cytosolic Ca^{2+} has both suppressive and activating roles in the regulation of autophagy. The effectiveness of BAPTA-AM loading as a blocker of autophagy is the seemingly one universal finding in the Ca^{2+} and autophagy literature, and has been interpreted to mean that there is an essential, permissive Ca^{2+} signal at the core of the canonical autophagic pathway. Although, the source of Ca^{2+} signals chelated by BAPTA-AM has not been identified, its identification could provide a key mechanism for regulating autophagy in most cell types. Additional results in *Chapter 4* supported the concept that Ca^{2+} uptake by mitochondria is vital for maintaining mitochondrial bioenergetics and consequently maintaining basal autophagy. Ca^{2+} oscillations were shown to occur in cells under nutrient replete conditions. These oscillations were inhibited in $InsP_3$ 5'-phosphatase expressing cells, supporting the notion that the pro-autophagic effect of the InsP3 5'-phosphatase was to inhibit Ca^{2+} signals stimulated by the nutrients in the complete imaging medium, and that the nutrients themselves were not sufficient to suppress autophagy..

The findings in *Chapter 5* revealed that a prolonged cytosolic Ca^{2+} signal via SOCE upregulated autophagy in HeLa and HEK cell lines. Given that the sustained SOCE-dependent cytosolic Ca^{2+} increase is most cell types is ~100 nM, the Ca^{2+} sensor must have a high affinity for Ca^{2+}. Depletion of ER Ca^{2+} stores did not acutely affect autophagy levels. However, the lack of autophagy induction by ER Ca^{2+} store release does not imply that Ca^{2+} release cannot trigger autophagy, rather that a prolonged Ca^{2+} signal (>15 minutes) is required. Ca^{2+} release from ER stores was not sufficient for rapamycin-induced autophagy, suggesting that autophagy caused by direct inhibition of mTOR also required constitutive Ca^{2+} signals. Ionomycin, however, did not have a significant effect on autophagy in HEK cells, despite evoking a similar prolonged cytosolic Ca^{2+} elevation to that seen with CPA. SOCE allows local Ca^{2+} signalling around the vicinity of a channel, whereas ionomycin gives a more global Ca^{2+} signal and therefore does not trigger effectors that are local to SOCE channels. Studies reporting the role of SOCE in autophagy are not entirely consistent. The findings in this study support the notion that SOCE is pro-autophagic; CPA-induced SOCE upregulated autophagy in HeLa cells through a CaMKK-α/β-dependent pathway. An anti-autophagic role, which is also reported in literature, was not evident in our studies. However, one common finding with SOCE studies in autophagy is that the resulting autophagy acts to delay cell death, suggesting that extracellular Ca^{2+} is necessary to trigger cytoprotective autophagy.

Whereas the published literature has shown Ca^{2+} to be either pro- or anti-autophagic in different cell types and experimental systems, the results presented here reveal the novel finding that Ca^{2+} exerted both suppressive and stimulatory effects in the same cell models. This is the first reported case where Ca^{2+} is having a dual role in the same study. Indeed a triple effect of Ca^{2+} was evident in this study with Ca^{2+} providing three different forms of control of autophagy; $InsP_3R$-mediated Ca^{2+} signals were anti-autophagic via mitochondrial

effects (*Chapter 4*), SOCE-evoked Ca^{2+} signals were pro-autophagy in part via CaMKK2 (*Chapter 5*) and BAPTA-AM was anti-autophagic for all stimuli (*Chapters 3, 4 and 5*). These findings provide additional evidence that Ca^{2+} is essential for both acute and chronic autophagy induction, and that it can have multiple roles in the same cells. Discrepancies between pro- and anti-autophagic Ca^{2+} roles reported in the literature are sometimes attributed to the use of differing cell lines/incubation times with Ca^{2+} modulators. The evidence gathered in this study implies that intracellular Ca^{2+} can indeed switch roles in the same cells depending on cellular conditions. Opposing observations in literature could be due to the behaviour of different cell lines used such as primary cell lines compared to immortal cell lines used in this study.

6.2 Future perspectives

Collectively, the data in this thesis demonstrate that Ca^{2+} signals arising from different sources have contrasting effects on autophagy. Ca^{2+} release from $InsP_3Rs$ suppresses autophagy, plausibly by stimulating mitochondrial ATP production (Figures 4.1-4.4). Whereas, Ca^{2+} entry via SOCE stimulates autophagy, at least in part via activation of CaMKK-β (Figure 5.18). Despite these findings, there is clearly more to understand about the regulation of autophagy by Ca^{2+}. For example, the profound inhibitory role of BAPTA-AM loading on autophagy is presently unexplained (Figure 3.24). BAPTA-AM loading does not solely block autophagy in response to stimuli that elevate cytosolic Ca^{2+} concentration [290].Rather, BAPTA-AM blocks autophagy evoked by seemingly all stimuli, such as rapamycin which is a direct inhibitor of mTOR (Figure 3.24). The block of autophagy by BAPTA-AM must be proximal to phagophore formation, since BAPTA-AM loading prevents accumulation of autophagic vesicles rather than blocking their processing. These observations suggest that there is a critical Ca^{2+}-dependent step required for the initiation of autophagy that is plausibly part of the core autophagy signalling pathway. Understanding the source and characteristics of the BAPTA-AM-sensitive Ca^{2+} signals are obviously critical to understanding how autophagy could be regulated in pathological conditions in which altered autophagic flux would be desired.

The induction of autophagy following activation of SOCE, but not by ionomycin (Figures 5.2 and 5.3), is consistent with a scheme in which local Ca^{2+} signals arising near to the mouth of Orai or TRP cation channels activate signalling pathways leading to autophagy. It is becoming apparent that TRP, Orai and STIM proteins can associate with multiple accessory protein partners [438], and it is plausible that local Ca^{2+} signals activate an as yet unknown signalling pathway (containing CaMKK-β) that leads to the activation of autophagy. Further

work is required to establish how the SOCE-CaMKK-β-autophagy pathway functions within cells, and whether there are other signalling components in the pathway.

Additional studies are required to establish the role of other Ca^{2+} sources and channels in the regulation of autophagy. For example, endosomes/lysosomes have been proposed as a Ca^{2+} store that modulates autophagy, potentially with Ca^{2+} being release by two-pore channels (TPCs) [325, 439]. Preliminary experiments were conducted in this study to investigate the role of TPCs, which indicated that they may have a significant role in the regulation of autophagy, but a lack of time precluded a full investigation. Rapamycin- and nutrient starvation-induced autophagy was inhibited in TPC 1/2 knockout murine embryonic fibroblast cells (MEF cells) (Figure 6.1). Additionally, it was observed that $TPC^{-/-}$ cells showed signs of cell death following starvation.

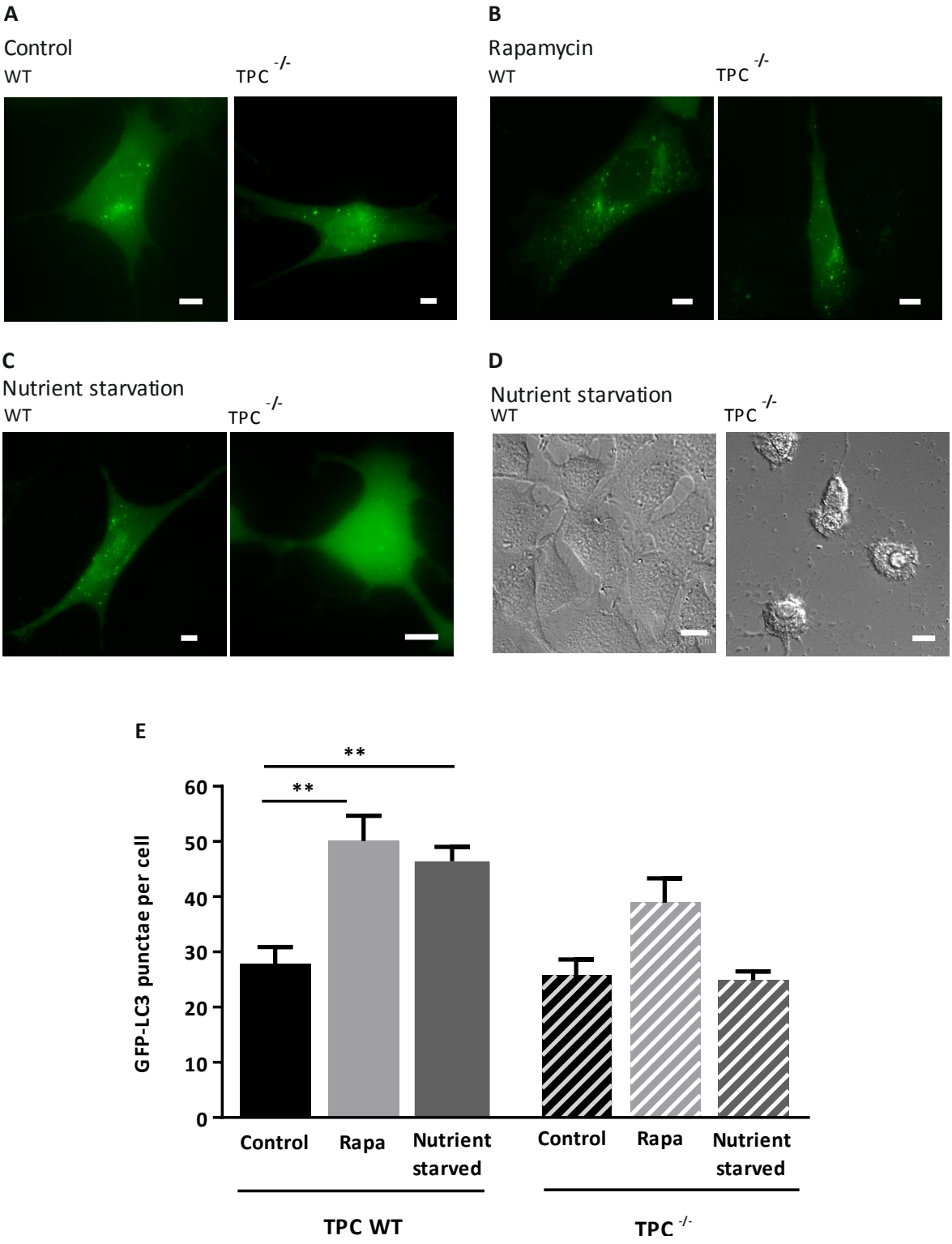

Figure 6.1. Rapamycin and nutrient starvation did not stimulate autophagy in two-pore channel null (TPC$^{-/-}$) MEF cells. Autophagy was monitored by transiently transfecting the MEF cells with GFP-LC3. Panel A shows representative images of wild-type (WT) and TPC$^{-/-}$ cells in complete imaging medium. Panel B shows images of WT and TPC$^{-/-}$ cells incubated with rapamycin (1 µM for 1 hour). Panel C shows images of WT and TPC$^{-/-}$ cells in starvation medium (2 hours). Panel D shows images of WT and TPC$^{-/-}$ cells, where TPC$^{-/-}$ cells showed signs of cell death when nutrient starved in two out of three independent experiments. Panel E is a quantitative representation of the effect of rapamycin and nutrient starvation on autophagy in WT and TPC$^{-/-}$ cells; rapamycin and nutrient starvation increased autophagy in WT but not in TPC$^{-/-}$ cells. The data are mean ± S.E.M of 3 experiments (25 - 50 cells per condition). The data were analysed with one-way ANOVA. ** indicates $p < 0.01$. The scale bar in Panels A, B and C indicate 10 µm.

Whilst GFP-LC3 provided a reliable and convenient method for assessing autophagy in this study, it would be beneficial to develop other quantitative measures of autophagic flux. A considerable amount of effort was given to using Western blotting, but the results were rather mixed. In particular, with Beclin-1 and p62, which have been used with Western blotting in other studies. Beclin-1 is vital for the initiation of autophagy, and has been widely used as a marker for autophagy in studies using Western blotting, alongside LC3 [440]. Beclin-1 is involved in sensitisation of $InsP_3Rs$ [441] which is essential in increasing autophagic flux. Expression of Beclin-1 is expected to increase upon induction of autophagy [171, 172]. Western blots were carried out to determine Beclin-1 expression in HeLa cells following $InsP_3$ 5'-phosphatase transfection, however, results showed an unexpectedly decreased expression (Figure 6.2), and should be repeated in future studies.

p62, another commonly used marker of autophagy, was also evaluated. Since p62 is constantly degraded, p62 levels are expected to decrease with autophagy induction making it a popular choice for determining the autophagic flux. However, in this study, Western blotting for p62 was found to give inconsistent results; p62 expression levels were increased when they were expected to decrease, and *vice versa* (Figure 6.2). This work was performed in the laboratory of Dr Geert Bultynck (KU Leuven, Belgium), and other members of the lab had found that p62 could be an unreliable marker for autophagy. Due to time constraints, this marker was not further used in this study, but it would be ideal to resolve the use of p62 as an autophagy marker in future work.

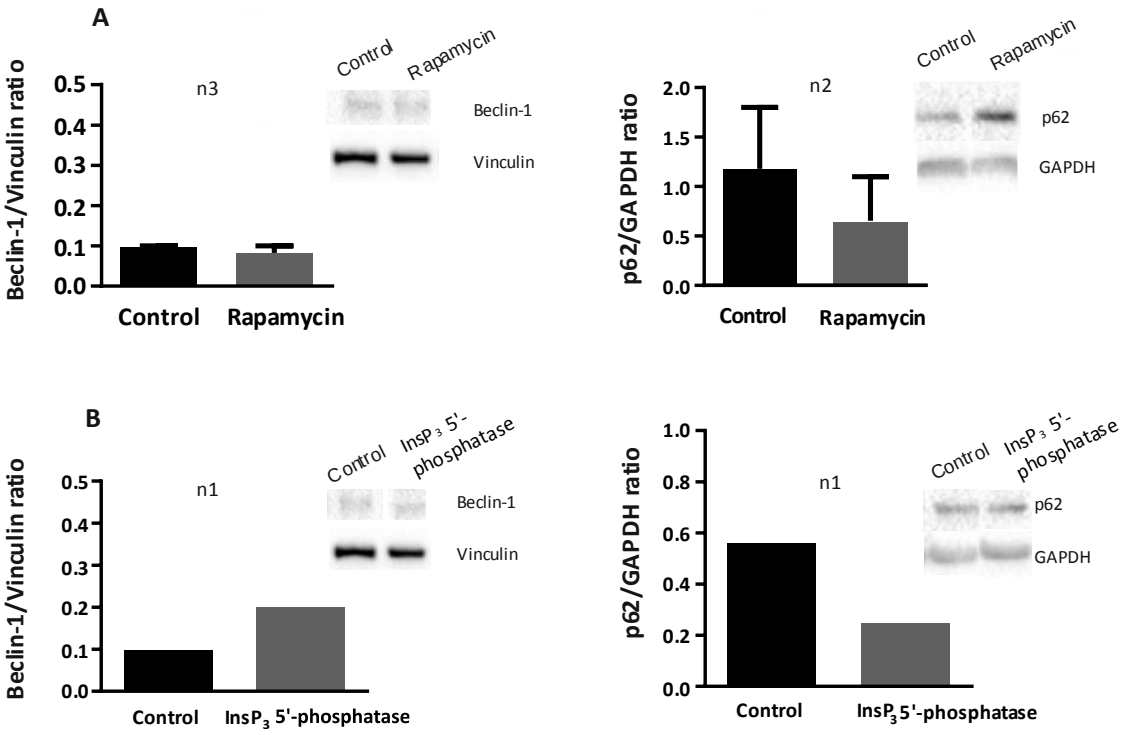

Figure 6.2. Western blotting for Beclin-1 and p62 expression in HeLa cells. Panels A and B show Western blot analysis for Beclin-1 and p62, with GAPDH and vinculin used as loading controls. The Western blots were performed using protein lysates obtained from HeLa cells superfused with complete imaging medium (control), and treated with 1 μM rapamycin (1 hour) or transfected with 1 μg $InsP_3$ 5'-phosphatase for 12 -24 hours.

The induction of autophagy by Ca^{2+} has been shown to occur via a few signalling pathways, including AMPK. The results in *Chapter 4* reveal that methyl pyruvate suppressed the autophagy increase in $InsP_3$ 5'-phosphatase-expressing cells. Whilst these observations suggest that the main effect of the $InsP_3$ 5'-phosphatase was to reduce mitochondrial bioenergetics and ATP production, further studies are required to ensure that cellular ATP levels were indeed restored by methyl pyruvate treatment, and to test whether AMPK, which is sensitive to the AMP: ATP ratio inside cells, was mediating the effect of $InsP_3R$ inhibition on autophagy. Additionally, studying mitochondrial bioenergetics in more detail (with the use of a Seahorse analyser) could give us insights into the metabolic and enzymatic processes in cells with treatments which modify ER-mitochondrial Ca^{2+} signalling.

Exploring additional cellular systems, such as primary cell lines, might prove beneficial for the further understanding of how Ca^{2+} signals exert its dual role in autophagy. Differences in the kinetics, amplitude or spatial extent of cytosolic Ca^{2+} signals presumably determine a pro- or anti-autophagic fate.

If the opportunity arises, investigating the relationship between autophagy and Ca^{2+} in disease states *in vivo* would be one vision. This research would allow the translation some of the findings in this thesis into therapeutic use, by looking at autophagy and Ca^{2+} in combination as potential approach for manipulating Ca^{2+} permeable channels and autophagy levels. Possibly the use of compounds such as HCQ, which is already approved by the FDA together with well-known inhibitors or activators of Ca^{2+} permeable channels might give insights into the best compound combinations for specific desired autophagy outcomes needed in relation to a particular state of a disease.

Chapter 7: References

1. Berridge, M.J., *Calcium signalling in health and disease.* Biochem Biophys Res Commun, 2017. **485**(1): p. 5.
2. Clapham, D.E., *Calcium signaling.* Cell, 2007. **131**(6): p. 1047-58.
3. White, P.J. and M.R. Broadley, *Calcium in plants.* Ann Bot, 2003. **92**(4): p. 487-511.
4. Berridge, M.J., *Inositol trisphosphate and calcium signalling mechanisms.* Biochim Biophys Acta, 2009. **1793**(6): p. 933-40.
5. Smajilovic, S. and J. Tfelt-Hansen, *Calcium acts as a first messenger through the calcium-sensing receptor in the cardiovascular system.* Cardiovasc Res, 2007. **75**(3): p. 457-67.
6. Gordon, P.B., et al., *Dependence of hepatocytic autophagy on intracellularly sequestered calcium.* J Biol Chem, 1993. **268**(35): p. 26107-12.
7. Decuypere, J.P., G. Bultynck, and J.B. Parys, *A dual role for Ca(2+) in autophagy regulation.* Cell Calcium, 2011. **50**(3): p. 242-50.
8. Kondratskyi, A., et al., *Calcium-permeable ion channels in control of autophagy and cancer.* Front Physiol, 2013. **4**: p. 272.
9. Zare-Shahabadi, A., et al., *Autophagy in Alzheimer's disease.* Rev Neurosci, 2015. **26**(4): p. 385-95.
10. Funderburk, S.F., B.K. Marcellino, and Z. Yue, *Cell "self-eating" (autophagy) mechanism in Alzheimer's disease.* Mt Sinai J Med, 2010. **77**(1): p. 59-68.
11. Yang, Z.J., et al., *The role of autophagy in cancer: therapeutic implications.* Mol Cancer Ther, 2011. **10**(9): p. 1533-41.
12. Kimura, T., et al., *Chloroquine in cancer therapy: a double-edged sword of autophagy*. Cancer Res, 2013. **73**(1): p. 3-7.
13. Chude, C.I. and R.K. Amaravadi, *Targeting Autophagy in Cancer: Update on Clinical Trials and Novel Inhibitors.* Int J Mol Sci, 2017. **18**(6).
14. Berridge, M.J., P. Lipp, and M.D. Bootman, *The versatility and universality of calcium signalling.* Nat Rev Mol Cell Biol, 2000. **1**(1): p. 11-21.
15. Islam, M.S., *Calcium Signaling*. 2012: Springer Netherlands.
16. Morgan, A.J., et al., *Bidirectional Ca(2)(+) signaling occurs between the endoplasmic reticulum and acidic organelles.* J Cell Biol, 2013. **200**(6): p. 789-805.
17. Rizzuto, R. and T. Pozzan, *Microdomains of intracellular Ca2+: molecular determinants and functional consequences.* Physiol Rev, 2006. **86**(1): p. 369-408.
18. Raffaello, A., et al., *Calcium at the Center of Cell Signaling: Interplay between Endoplasmic Reticulum, Mitochondria, and Lysosomes.* Trends Biochem Sci, 2016. **41**(12): p. 1035-1049.
19. Berridge, M.J., M.D. Bootman, and H.L. Roderick, *Calcium signalling: dynamics, homeostasis and remodelling.* Nat Rev Mol Cell Biol, 2003. **4**(7): p. 517-29.
20. Bootman, M.D., *Calcium signaling.* Cold Spring Harb Perspect Biol, 2012. **4**(7): p. a011171.
21. Munaron, L., *Shuffling the cards in signal transduction: Calcium, arachidonic acid and mechanosensitivity.* World J Biol Chem, 2011. **2**(4): p. 59-66.
22. Groschner, K., W.F. Graier, and C. Romanin, *Store-Operated Ca2+ Entry (SOCE) Pathways: Emerging Signaling Concepts in Human (Patho)physiology*. 2017: Springer International Publishing.
23. Hermosura, M.C., et al., *InsP4 facilitates store-operated calcium influx by inhibition of InsP3 5-phosphatase.* Nature, 2000. **408**(6813): p. 735-40.
24. Berridge, M.J., *The Inositol Trisphosphate/Calcium Signaling Pathway in Health and Disease.* Physiol Rev, 2016. **96**(4): p. 1261-96.
25. Guse, A.H., *Second messenger function and the structure-activity relationship of cyclic adenosine diphosphoribose (cADPR).* FEBS J, 2005. **272**(18): p. 4590-7.
26. Fliegert, R., A. Gasser, and A.H. Guse, *Regulation of calcium signalling by adenine-based second messengers.* Biochem Soc Trans, 2007. **35**(Pt 1): p. 109-14.
27. Santella, L., D. Lim, and F. Moccia, *Calcium and fertilization: the beginning of life.* Trends Biochem Sci, 2004. **29**(8): p. 400-8.

28. Whitaker, M., *Calcium at fertilization and in early development.* Physiol Rev, 2006. **86**(1): p. 25-88.
29. Dufour, J.F., I.M. Arias, and T.J. Turner, *Inositol 1,4,5-trisphosphate and calcium regulate the calcium channel function of the hepatic inositol 1,4,5-trisphosphate receptor.* J Biol Chem, 1997. **272**(5): p. 2675-81.
30. Lim, W., B. Mayer, and T. Pawson, *Cell Signaling: principles and mechanisms*. 2014: Taylor & Francis Group.
31. Kuo, I.Y. and B.E. Ehrlich, *Signaling in muscle contraction.* Cold Spring Harb Perspect Biol, 2015. **7**(2): p. a006023.
32. Brini, M. and E. Carafoli, *The plasma membrane Ca(2)+ ATPase and the plasma membrane sodium calcium exchanger cooperate in the regulation of cell calcium.* Cold Spring Harb Perspect Biol, 2011. **3**(2).
33. Blaustein, M.P. and W.J. Lederer, *Sodium/calcium exchange: its physiological implications.* Physiol Rev, 1999. **79**(3): p. 763-854.
34. Periasamy, M. and A. Kalyanasundaram, *SERCA pump isoforms: their role in calcium transport and disease.* Muscle Nerve, 2007. **35**(4): p. 430-42.
35. Brini, M. and E. Carafoli, *Calcium pumps in health and disease.* Physiol Rev, 2009. **89**(4): p. 1341-78.
36. Caride, A.J., et al., *The plasma membrane calcium pump displays memory of past calcium spikes. Differences between isoforms 2b and 4b.* J Biol Chem, 2001. **276**(43): p. 39797-804.
37. Putney, J.W., Jr., *Capacitative calcium entry revisited.* Cell Calcium, 1990. **11**(10): p. 611-24.
38. Levitan, I. and A.M. Dopico, *Vascular Ion Channels in Physiology and Disease*. 2016: Springer International Publishing.
39. Parekh, A.B. and J.W. Putney, Jr., *Store-operated calcium channels.* Physiol Rev, 2005. **85**(2): p. 757-810.
40. Bootman, M.D., et al., *Extracellular calcium concentration controls the frequency of intracellular calcium spiking independently of inositol 1,4,5-trisphosphate production in HeLa cells.* Biochem J, 1996. **314 (Pt 1)**: p. 347-54.
41. Putney, J.W. and G.S. Bird, *Cytoplasmic calcium oscillations and store-operated calcium influx.* J Physiol, 2008. **586**(13): p. 3055-9.
42. Fahrner, M., et al., *The STIM1/Orai signaling machinery.* Channels (Austin), 2013. **7**(5): p. 330-43.
43. Roos, J., et al., *STIM1, an essential and conserved component of store-operated Ca^{2+} channel function.* J Cell Biol, 2005. **169**(3): p. 435-45.
44. Liou, J., et al., *STIM is a Ca^{2+} sensor essential for Ca^{2+}-store-depletion-triggered Ca^{2+} influx.* Curr Biol, 2005. **15**(13): p. 1235-41.
45. Feske, S., et al., *A mutation in Orai1 causes immune deficiency by abrogating CRAC channel function.* Nature, 2006. **441**(7090): p. 179-85.
46. Vig, M., et al., *CRACM1 is a plasma membrane protein essential for store-operated Ca2+ entry.* Science, 2006. **312**(5777): p. 1220-3.
47. Zhang, S.L., et al., *Genome-wide RNAi screen of Ca^{2+} influx identifies genes that regulate Ca^{2+} release-activated Ca^{2+} channel activity.* Proc Natl Acad Sci U S A, 2006. **103**(24): p. 9357-62.
48. Oh-Hora, M., et al., *Dual functions for the endoplasmic reticulum calcium sensors STIM1 and STIM2 in T cell activation and tolerance.* Nat Immunol, 2008. **9**(4): p. 432-43.
49. Watson, R. and A.B. Parekh, *Mitochondrial regulation of CRAC channel-driven cellular responses.* Cell Calcium, 2012. **52**(1): p. 52-6.
50. Touchberry, C.D., et al., *Store-operated calcium entry is present in HL-1 cardiomyocytes and contributes to resting calcium.* Biochem Biophys Res Commun, 2011. **416**(1-2): p. 45-50.
51. Peppiatt, C.M., et al., *2-Aminoethoxydiphenyl borate (2-APB) antagonises inositol 1,4,5-trisphosphate-induced calcium release, inhibits calcium pumps and has a use-dependent and slowly reversible action on store-operated calcium entry channels.* Cell Calcium, 2003. **34**(1): p. 97-108.

52. Chen, K.H., et al., *SKF-96365 strongly inhibits voltage-gated sodium current in rat ventricular myocytes.* Pflugers Arch, 2015. **467**(6): p. 1227-36.
53. Sabourin, J., E. Robin, and E. Raddatz, *A key role of TRPC channels in the regulation of electromechanical activity of the developing heart.* Cardiovasc Res, 2011. **92**(2): p. 226-36.
54. Dominguez-Rodriguez, A., et al., *Proarrhythmic effect of sustained EPAC activation on TRPC3/4 in rat ventricular cardiomyocytes.* J Mol Cell Cardiol, 2015. **87**: p. 74-8.
55. Nilius, B. and A. Szallasi, *Transient receptor potential channels as drug targets: from the science of basic research to the art of medicine.* Pharmacol Rev, 2014. **66**(3): p. 676-814.
56. Ong, H.L., L.B. de Souza, and I.S. Ambudkar, *Role of TRPC Channels in Store-Operated Calcium Entry.* Adv Exp Med Biol, 2016. **898**: p. 87-109.
57. Cheng, K.T., et al., *Local Ca(2)+ entry via Orai1 regulates plasma membrane recruitment of TRPC1 and controls cytosolic Ca(2)+ signals required for specific cell functions.* PLoS Biol, 2011. **9**(3): p. e1001025.
58. Desai, P.N., et al., *Multiple types of calcium channels arising from alternative translation initiation of the Orai1 message.* Sci Signal, 2015. **8**(387): p. ra74.
59. Zitt, C., C.R. Halaszovich, and A. Luckhoff, *The TRP family of cation channels: probing and advancing the concepts on receptor-activated calcium entry.* Prog Neurobiol, 2002. **66**(4): p. 243-64.
60. Rizzuto, R., et al., *Ca(2+) transfer from the ER to mitochondria: when, how and why.* Biochim Biophys Acta, 2009. **1787**(11): p. 1342-51.
61. Dellis, O., et al., *Ca2+ entry through plasma membrane IP3 receptors.* Science, 2006. **313**(5784): p. 229-33.
62. Prakriya, M., *The molecular physiology of CRAC channels.* Immunol Rev, 2009. **231**(1): p. 88-98.
63. McFadzean, I. and A. Gibson, *The developing relationship between receptor-operated and store-operated calcium channels in smooth muscle.* Br J Pharmacol, 2002. **135**(1): p. 1-13.
64. Coderre, T.J. and R. Melzack, *The role of NMDA receptor-operated calcium channels in persistent nociception after formalin-induced tissue injury.* J Neurosci, 1992. **12**(9): p. 3671-5.
65. Antkiewicz-Michaluk, L., *Voltage-operated calcium channels: characteristics and their role in the mechanism of action of psychotropic drugs.* Pol J Pharmacol, 1999. **51**(2): p. 179-86.
66. Sher, E., et al., *Physiopathology of neuronal voltage-operated calcium channels.* FASEB J, 1991. **5**(12): p. 2677-83.
67. Talarico, E.F., Jr., et al., *Expression and immunolocalization of plasma membrane calcium ATPase isoforms in human corneal epithelium.* Mol Vis, 2005. **11**: p. 169-78.
68. Guerini, D., et al., *The calcium pump of the plasma membrane: membrane targeting, calcium binding sites, tissue-specific isoform expression.* Acta Physiol Scand Suppl, 1998. **643**: p. 265-73.
69. Brini, M., et al., *The plasma membrane calcium pump in health and disease.* FEBS J, 2013. **280**(21): p. 5385-97.
70. Smith, I.C., et al., *ATP consumption by sarcoplasmic reticulum Ca(2)(+) pumps accounts for 40-50% of resting metabolic rate in mouse fast and slow twitch skeletal muscle.* PLoS One, 2013. **8**(7): p. e68924.
71. Corvazier, E., et al., *Expression of sarco/endoplasmic reticulum Ca(2+) ATPase (SERCA) 3 proteins in two major conformational states in native human cell membranes.* Biochim Biophys Acta, 2009. **1788**(3): p. 587-99.
72. MacLennan, D.H., W.J. Rice, and N.M. Green, *The mechanism of Ca2+ transport by sarco(endo)plasmic reticulum Ca2+-ATPases.* J Biol Chem, 1997. **272**(46): p. 28815-8.
73. Espinoza-Fonseca, L.M., J.M. Autry, and D.D. Thomas, *Sarcolipin and phospholamban inhibit the calcium pump by populating a similar metal ion-free intermediate state.* Biochem Biophys Res Commun, 2015. **463**(1-2): p. 37-41.
74. Mahmmoud, Y.A., *Capsaicin stimulates uncoupled ATP hydrolysis by the sarcoplasmic reticulum calcium pump.* J Biol Chem, 2008. **283**(31): p. 21418-26.

75. Vandecaetsbeek, I., et al., *The Ca2+ pumps of the endoplasmic reticulum and Golgi apparatus.* Cold Spring Harb Perspect Biol, 2011. **3**(5).
76. Dode, L., et al., *Functional comparison between secretory pathway Ca2+/Mn2+-ATPase (SPCA) 1 and sarcoplasmic reticulum Ca2+-ATPase (SERCA) 1 isoforms by steady-state and transient kinetic analyses.* J Biol Chem, 2005. **280**(47): p. 39124-34.
77. Yu, S.P. and D.W. Choi, *Na(+)-Ca2+ exchange currents in cortical neurons: concomitant forward and reverse operation and effect of glutamate.* Eur J Neurosci, 1997. **9**(6): p. 1273-81.
78. DiPolo, R. and L. Beauge, *Sodium/calcium exchanger: influence of metabolic regulation on ion carrier interactions.* Physiol Rev, 2006. **86**(1): p. 155-203.
79. Boyman, L., et al., *NCLX: the mitochondrial sodium calcium exchanger.* J Mol Cell Cardiol, 2013. **59**: p. 205-13.
80. Van Baelen, K., et al., *The Ca2+/Mn2+ pumps in the Golgi apparatus.* Biochim Biophys Acta, 2004. **1742**(1-3): p. 103-12.
81. He, W. and Z. Hu, *The role of the Golgi-resident SPCA Ca(2)(+)/Mn(2)(+) pump in ionic homeostasis and neural function.* Neurochem Res, 2012. **37**(3): p. 455-68.
82. Kirichok, Y., G. Krapivinsky, and D.E. Clapham, *The mitochondrial calcium uniporter is a highly selective ion channel.* Nature, 2004. **427**(6972): p. 360-4.
83. Patergnani, S., et al., *Calcium signaling around Mitochondria Associated Membranes (MAMs).* Cell Commun Signal, 2011. **9**: p. 19.
84. De Stefani, D., R. Rizzuto, and T. Pozzan, *Enjoy the Trip: Calcium in Mitochondria Back and Forth.* Annu Rev Biochem, 2016. **85**: p. 161-92.
85. Kamer, K.J. and V.K. Mootha, *The molecular era of the mitochondrial calcium uniporter.* Nat Rev Mol Cell Biol, 2015. **16**(9): p. 545-53.
86. Deluca, H.F. and G.W. Engstrom, *Calcium uptake by rat kidney mitochondria.* Proc Natl Acad Sci U S A, 1961. **47**: p. 1744-50.
87. Vasington, F.D. and J.V. Murphy, *Ca ion uptake by rat kidney mitochondria and its dependence on respiration and phosphorylation.* J Biol Chem, 1962. **237**: p. 2670-7.
88. Rizzuto, R., et al., *Close Contacts with the Endoplasmic Reticulum as Determinants of Mitochondrial Ca^{2+} Responses.* Science, 1998. **280**(5370): p. 1763-1766.
89. Csordas, G., et al., *Structural and functional features and significance of the physical linkage between ER and mitochondria.* J Cell Biol, 2006. **174**(7): p. 915-21.
90. Bravo, R., et al., *Increased ER-mitochondrial coupling promotes mitochondrial respiration and bioenergetics during early phases of ER stress.* J Cell Sci, 2011. **124**(Pt 13): p. 2143-52.
91. Raturi, A. and T. Simmen, *Where the endoplasmic reticulum and the mitochondrion tie the knot: the mitochondria-associated membrane (MAM).* Biochim Biophys Acta, 2013. **1833**(1): p. 213-24.
92. Rodriguez-Arribas, M., et al., *Mitochondria-Associated Membranes (MAMs): Overview and Its Role in Parkinson's Disease.* Mol Neurobiol, 2016.
93. Marchi, S., S. Patergnani, and P. Pinton, *The endoplasmic reticulum-mitochondria connection: one touch, multiple functions.* Biochim Biophys Acta, 2014. **1837**(4): p. 461-9.
94. Missiroli, S., et al., *Endoplasmic reticulum-mitochondria Ca^{2+} crosstalk in the control of the tumor cell fate.* Biochim Biophys Acta, 2017. **1864**(6): p. 858-864.
95. Marchi, S., et al., *Oncogenic and oncosuppressive signal transduction at mitochondria-associated endoplasmic reticulum membranes.* Mol Cell Oncol, 2014. **1**(2): p. e956469.
96. Vance, J.E., *MAM (mitochondria-associated membranes) in mammalian cells: lipids and beyond.* Biochim Biophys Acta, 2014. **1841**(4): p. 595-609.
97. Paillusson, S., et al., *There's Something Wrong with my MAM; the ER-Mitochondria Axis and Neurodegenerative Diseases.* Trends Neurosci, 2016. **39**(3): p. 146-57.
98. Filadi, R., P. Theurey, and P. Pizzo, *The endoplasmic reticulum-mitochondria coupling in health and disease: Molecules, functions and significance.* Cell Calcium, 2017. **62**: p. 1-15.
99. Stoica, R., et al., *ER-mitochondria associations are regulated by the VAPB-PTPIP51 interaction and are disrupted by ALS/FTD-associated TDP-43.* Nat Commun, 2014. **5**: p. 3996.

100. Collins, T.J., et al., *Mitochondria are morphologically and functionally heterogeneous within cells.* EMBO J, 2002. **21**(7): p. 1616-27.
101. Yang, J.S., et al., *Spatial and functional organization of mitochondrial protein network.* Sci Rep, 2013. **3**: p. 1403.
102. Cogliati, S., J.A. Enriquez, and L. Scorrano, *Mitochondrial Cristae: Where Beauty Meets Functionality.* Trends Biochem Sci, 2016. **41**(3): p. 261-73.
103. Xu, T., et al., *Kinetic studies of Ca2+ binding and Ca2+ clearance in the cytosol of adrenal chromaffin cells.* Biophys J, 1997. **73**(1): p. 532-45.
104. Hansford, R.G. and D. Zorov, *Role of mitochondrial calcium transport in the control of substrate oxidation.* Mol Cell Biochem, 1998. **184**(1-2): p. 359-69.
105. Harris, M.H. and C.B. Thompson, *The role of the Bcl-2 family in the regulation of outer mitochondrial membrane permeability.* Cell Death Differ, 2000. **7**(12): p. 1182-91.
106. De Pinto, V., et al., *Voltage-dependent anion-selective channel (VDAC) in the plasma membrane.* FEBS Lett, 2010. **584**(9): p. 1793-9.
107. Csordás, G., A.P. Thomas, and G. Hajnóczky, *Quasi-synaptic calcium signal transmission between endoplasmic reticulum and mitochondria.* EMBO J, 1999. **18**(1): p. 96-108.
108. Palty, R., et al., *NCLX is an essential component of mitochondrial Na^+/Ca^{2+} exchange.* Proc Natl Acad Sci U S A, 2010. **107**(1): p. 436-41.
109. Herrera-Cruz, M.S. and T. Simmen, *Of yeast, mice and men: MAMs come in two flavors.* Biol Direct, 2017. **12**(1): p. 3.
110. Jouaville, L.S., et al., *Synchronization of calcium waves by mitochondrial substrates in Xenopus laevis oocytes.* Nature 1995. **377**(6548): p. 438-41.
111. Collins, T., et al., *Inositol 1,4,5-trisphosphate-induced Ca^{2+} release is inhibited by mitochondrial depolarization.* Biochem J, 2000. **347**(Pt 2): p. 593-600.
112. Haak, L.L., et al., *Mitochondria regulate Ca^{2+} wave initiation and inositol trisphosphate signal transduction in oligodendrocyte progenitors.* J Neurochem, 2002. **80**(3): p. 405-15.
113. McCarron, J.G. and T.C. Muir, *Mitochondrial regulation of the cytosolic Ca^{2+} concentration and the $InsP_3$-sensitive Ca^{2+} store in guinea-pig colonic smooth muscle.* J Physiol 1999. **516**(Pt 1): p. 149-61.
114. Ashrafi, G. and T.L. Schwarz, *The pathways of mitophagy for quality control and clearance of mitochondria.* Cell Death Differ, 2013. **20**(1): p. 31-42.
115. Narendra, D., et al., *Parkin is recruited selectively to impaired mitochondria and promotes their autophagy.* J Cell Biol, 2008. **183**(5): p. 795-803.
116. Jung, M., et al., *Cathepsin inhibition-induced lysosomal dysfunction enhances pancreatic beta-cell apoptosis in high glucose.* PLoS One, 2015. **10**(1): p. e0116972.
117. Korolchuk, V.I., et al., *Lysosomal positioning coordinates cellular nutrient responses.* Nat Cell Biol, 2011. **13**(4): p. 453-60.
118. Appelqvist, H., et al., *The lysosome: from waste bag to potential therapeutic target.* J Mol Cell Biol, 2013. **5**(4): p. 214-26.
119. Lloyd-Evans, E., *Acidic Ca2+ stores in neurodegeneration.* Messenger (Los Angel), 2016. **5**(1-2): p. 37-55.
120. Morgan, A.J., et al., *Molecular mechanisms of endolysosomal Ca2+ signalling in health and disease.* Biochem J, 2011. **439**(3): p. 349-74.
121. Lloyd-Evans, E., et al., *Niemann-Pick disease type C1 is a sphingosine storage disease that causes deregulation of lysosomal calcium.* Nat Med, 2008. **14**(11): p. 1247-55.
122. Churchill, G.C., et al., *Sperm deliver a new second messenger: NAADP.* Curr Biol, 2003. **13**(2): p. 125-8.
123. Galione, A., et al., *The acid test: the discovery of two-pore channels (TPCs) as NAADP-gated endolysosomal Ca(2+) release channels.* Pflugers Arch, 2009. **458**(5): p. 869-76.
124. Galione, A., *NAADP receptors.* Cold Spring Harb Perspect Biol, 2011. **3**(1): p. a004036.
125. Allison, R., et al., *Defects in ER-endosome contacts impact lysosome function in hereditary spastic paraplegia.* J Cell Biol, 2017. **216**(5): p. 1337-1355.
126. Lin-Moshier, Y., et al., *Photoaffinity labeling of nicotinic acid adenine dinucleotide phosphate (NAADP) targets in mammalian cells.* J Biol Chem, 2012. **287**(4): p. 2296-307.

127. Brailoiu, E., et al., *Essential requirement for two-pore channel 1 in NAADP-mediated calcium signaling.* J Cell Biol, 2009. **186**(2): p. 201-9.
128. Calcraft, P.J., et al., *NAADP mobilizes calcium from acidic organelles through two-pore channels.* Nature, 2009. **459**(7246): p. 596-600.
129. Beck, A., et al., *Nicotinic acid adenine dinucleotide phosphate and cyclic ADP-ribose regulate TRPM2 channels in T lymphocytes.* FASEB J, 2006. **20**(7): p. 962-4.
130. Zhang, F., et al., *TRP-ML1 functions as a lysosomal NAADP-sensitive Ca2+ release channel in coronary arterial myocytes.* J Cell Mol Med, 2009. **13**(9B): p. 3174-85.
131. Lange, I., et al., *TRPM2 functions as a lysosomal Ca2+-release channel in beta cells.* Sci Signal, 2009. **2**(71): p. ra23.
132. Zhu, M.X., et al., *TPCs: Endolysosomal channels for Ca2+ mobilization from acidic organelles triggered by NAADP.* FEBS Lett, 2010. **584**(10): p. 1966-74.
133. Kintzer, A.F. and R.M. Stroud, *On the structure and mechanism of two-pore channels.* FEBS J, 2017.
134. Ruas, M., et al., *TPC1 has two variant isoforms, and their removal has different effects on endo-lysosomal functions compared to loss of TPC2.* Mol Cell Biol, 2014. **34**(21): p. 3981-92.
135. Sancak, Y., et al., *Ragulator-Rag complex targets mTORC1 to the lysosomal surface and is necessary for its activation by amino acids.* Cell, 2010. **141**(2): p. 290-303.
136. Gomez-Suaga, P., et al., *Leucine-rich repeat kinase 2 regulates autophagy through a calcium-dependent pathway involving NAADP.* Hum Mol Genet, 2012. **21**(3): p. 511-25.
137. Nazio, F., et al., *Fine-tuning of ULK1 mRNA and protein levels is required for autophagy oscillation.* J Cell Biol, 2016. **215**(6): p. 841-856.
138. Zhao, Y.G. and H. Zhang, *ULK1 cycling: The ups and downs of the autophagy response.* J Cell Biol, 2016. **215**(6): p. 757-759.
139. Sammels, E., et al., *Intracellular Ca2+ storage in health and disease: a dynamic equilibrium.* Cell Calcium, 2010. **47**(4): p. 297-314.
140. Rodriguez, A., et al., *Lysosomes behave as Ca2+-regulated exocytic vesicles in fibroblasts and epithelial cells.* J Cell Biol, 1997. **137**(1): p. 93-104.
141. Andrews, N.W., *Regulated secretion of conventional lysosomes.* Trends Cell Biol, 2000. **10**(8): p. 316-21.
142. Jaiswal, J.K., N.W. Andrews, and S.M. Simon, *Membrane proximal lysosomes are the major vesicles responsible for calcium-dependent exocytosis in nonsecretory cells.* J Cell Biol, 2002. **159**(4): p. 625-35.
143. Zhang, Z., et al., *Regulated ATP release from astrocytes through lysosome exocytosis.* Nat Cell Biol, 2007. **9**(8): p. 945-53.
144. Ralevic, V. and G. Burnstock, *Receptors for purines and pyrimidines.* Pharmacol Rev, 1998. **50**(3): p. 413-92.
145. Roczniak-Ferguson, A., et al., *The transcription factor TFEB links mTORC1 signaling to transcriptional control of lysosome homeostasis.* Sci Signal, 2012. **5**(228): p. ra42.
146. Deter, R.L. and C. De Duve, *Influence of glucagon, an inducer of cellular autophagy, on some physical properties of rat liver lysosomes.* J Cell Biol, 1967. **33**(2): p. 437-49.
147. Wang, C. and X. Wang, *The interplay between autophagy and the ubiquitin-proteasome system in cardiac proteotoxicity.* Biochim Biophys Acta, 2015. **1852**(2): p. 188-94.
148. Lilienbaum, A., *Relationship between the proteasomal system and autophagy.* Int J Biochem Mol Biol, 2013. **4**(1): p. 1-26.
149. Melendez, A. and T.P. Neufeld, *The cell biology of autophagy in metazoans: a developing story.* Development, 2008. **135**(14): p. 2347-60.
150. Russell, R.C., H.X. Yuan, and K.L. Guan, *Autophagy regulation by nutrient signaling.* Cell Res, 2014. **24**(1): p. 42-57.
151. Fulda, S., et al., *Cellular stress responses: cell survival and cell death.* Int J Cell Biol, 2010. **2010**: p. 214074.
152. Mizushima, N., T. Yoshimori, and B. Levine, *Methods in mammalian autophagy research.* Cell, 2010. **140**(3): p. 313-26.

153. Mari, M., S.A. Tooze, and F. Reggiori, *The puzzling origin of the autophagosomal membrane.* F1000 Biol Rep, 2011. **3**: p. 25.
154. Klionsky, D.J., A.M. Cuervo, and P.O. Seglen, *Methods for monitoring autophagy from yeast to human.* Autophagy, 2007. **3**(3): p. 181-206.
155. Tooze, S.A. and T. Yoshimori, *The origin of the autophagosomal membrane.* Nat Cell Biol, 2010. **12**(9): p. 831-5.
156. Wesselborg, S. and B. Stork, *Autophagy signal transduction by ATG proteins: from hierarchies to networks.* Cell Mol Life Sci, 2015. **72**(24): p. 4721-57.
157. Klionsky, D.J., *Look people, "Atg" is an abbreviation for "autophagy-related." That's it.* Autophagy, 2012. **8**(9): p. 1281-2.
158. Roberts, R. and N.T. Ktistakis, *Omegasomes: PI3P platforms that manufacture autophagosomes.* Essays Biochem, 2013. **55**: p. 17-27.
159. Esclatine, A., M. Chaumorcel, and P. Codogno, *Macroautophagy signaling and regulation.* Curr Top Microbiol Immunol, 2009. **335**: p. 33-70.
160. Eskelinen, E.L. and P. Saftig, *Autophagy: a lysosomal degradation pathway with a central role in health and disease.* Biochim Biophys Acta, 2009. **1793**(4): p. 664-73.
161. Mauvezin, C., et al., *Autophagosome-lysosome fusion is independent of V-ATPase-mediated acidification.* Nat Commun, 2015. **6**: p. 7007.
162. Mizushima, N., *Autophagy: process and function.* Genes Dev, 2007. **21**(22): p. 2861-73.
163. Zhou, J., et al., *Activation of lysosomal function in the course of autophagy via mTORC1 suppression and autophagosome-lysosome fusion.* Cell Res, 2013. **23**(4): p. 508-23.
164. Monastyrska, I., et al., *Multiple roles of the cytoskeleton in autophagy.* Biol Rev Camb Philos Soc, 2009. **84**(3): p. 431-48.
165. Mizushima, N. and B. Levine, *Autophagy in mammalian development and differentiation.* Nat Cell Biol, 2010. **12**(9): p. 823-30.
166. De Duve, C. and R. Wattiaux, *Functions of lysosomes.* Annu Rev Physiol, 1966. **28**: p. 435-92.
167. Reggiori, F. and D.J. Klionsky, *Autophagy in the eukaryotic cell.* Eukaryot Cell, 2002. **1**(1): p. 11-21.
168. Wang, C.W. and D.J. Klionsky, *The molecular mechanism of autophagy.* Mol Med, 2003. **9**(3-4): p. 65-76.
169. Levine, B. and D.J. Klionsky, *Development by self-digestion: molecular mechanisms and biological functions of autophagy.* Dev Cell, 2004. **6**(4): p. 463-77.
170. Mizushima, N., T. Yoshimori, and Y. Ohsumi, *The role of Atg proteins in autophagosome formation.* Annu Rev Cell Dev Biol, 2011. **27**: p. 107-32.
171. Meyer, G., et al., *The cellular autophagy markers Beclin-1 and LC3B-II are increased during reperfusion in fibrillated mouse hearts.* Curr Pharm Des, 2013. **19**(39): p. 6912-8.
172. Li, X., et al., *Beclin1 inhibition promotes autophagy and decreases gemcitabine-induced apoptosis in Miapaca2 pancreatic cancer cells.* Cancer Cell Int, 2013. **13**(1): p. 26.
173. Nascimbeni, A.C., P. Codogno, and E. Morel, *Phosphatidylinositol-3-phosphate in the regulation of autophagy membrane dynamics.* FEBS J, 2017. **284**(9): p. 1267-1278.
174. Geng, J. and D.J. Klionsky, *The Atg8 and Atg12 ubiquitin-like conjugation systems in macroautophagy. 'Protein modifications: beyond the usual suspects' review series.* EMBO Rep, 2008. **9**(9): p. 859-64.
175. Yamamoto, H., et al., *Atg9 vesicles are an important membrane source during early steps of autophagosome formation.* J Cell Biol, 2012. **198**(2): p. 219-33.
176. Jung, C.H., et al., *mTOR regulation of autophagy.* FEBS Lett, 2010. **584**(7): p. 1287-95.
177. Laplante, M. and D.M. Sabatini, *mTOR signaling in growth control and disease.* Cell, 2012. **149**(2): p. 274-93.
178. Populo, H., J.M. Lopes, and P. Soares, *The mTOR signalling pathway in human cancer.* Int J Mol Sci, 2012. **13**(2): p. 1886-918.
179. Wong, M., *Mammalian target of rapamycin (mTOR) pathways in neurological diseases.* Biomed J, 2013. **36**(2): p. 40-50.

180. Saini, K.S., et al., *Targeting the PI3K/AKT/mTOR and Raf/MEK/ERK pathways in the treatment of breast cancer.* Cancer Treat Rev, 2013. **39**(8): p. 935-46.
181. Caron, E., et al., *A comprehensive map of the mTOR signaling network.* Mol Syst Biol, 2010. **6**: p. 453.
182. Zhang, X., et al., *The dual mTORC1 and mTORC2 inhibitor PP242 shows strong antitumor activity in a pheochromocytoma PC12 cell tumor model.* Urology, 2015. **85**(1): p. 273 e1-7.
183. Evangelisti, C., et al., *Targeted inhibition of mTORC1 and mTORC2 by active-site mTOR inhibitors has cytotoxic effects in T-cell acute lymphoblastic leukemia.* Leukemia, 2011. **25**(5): p. 781-91.
184. Ono, A., et al., *Comparative effects of PP242 and rapamycin on mTOR signalling and NOTCH signalling in leukemia cells.* Anticancer Res, 2013. **33**(3): p. 809-13.
185. Gulati, P., et al., *Amino acids activate mTOR complex 1 via Ca2+/CaM signaling to hVps34.* Cell Metab, 2008. **7**(5): p. 456-65.
186. Juhasz, G., et al., *The class III PI(3)K Vps34 promotes autophagy and endocytosis but not TOR signaling in Drosophila.* J Cell Biol, 2008. **181**(4): p. 655-66.
187. Backer, J.M., *The regulation and function of Class III PI3Ks: novel roles for Vps34.* Biochem J, 2008. **410**(1): p. 1-17.
188. He, C. and D.J. Klionsky, *Regulation mechanisms and signaling pathways of autophagy.* Annu Rev Genet, 2009. **43**: p. 67-93.
189. Levine, B., N. Mizushima, and H.W. Virgin, *Autophagy in immunity and inflammation.* Nature, 2011. **469**(7330): p. 323-35.
190. Mordier, S., et al., *Leucine limitation induces autophagy and activation of lysosome-dependent proteolysis in C2C12 myotubes through a mammalian target of rapamycin-independent signaling pathway.* J Biol Chem, 2000. **275**(38): p. 29900-6.
191. Kanazawa, T., et al., *Amino acids and insulin control autophagic proteolysis through different signaling pathways in relation to mTOR in isolated rat hepatocytes.* J Biol Chem, 2004. **279**(9): p. 8452-9.
192. Sarkar, S., et al., *Small molecules enhance autophagy and reduce toxicity in Huntington's disease models.* Nat Chem Biol, 2007. **3**(6): p. 331-8.
193. Meijer, A.J., et al., *Regulation of autophagy by amino acids and MTOR-dependent signal transduction.* Amino Acids, 2015. **47**(10): p. 2037-63.
194. Lardeux, B.R. and G.E. Mortimore, *Amino acid and hormonal control of macromolecular turnover in perfused rat liver. Evidence for selective autophagy.* J Biol Chem, 1987. **262**(30): p. 14514-9.
195. Codogno, P. and A.J. Meijer, *Autophagy and signaling: their role in cell survival and cell death.* Cell Death Differ, 2005. **12 Suppl 2**: p. 1509-18.
196. Djavaheri-Mergny, M., et al., *NF-kappaB activation represses tumor necrosis factor-alpha-induced autophagy.* J Biol Chem, 2006. **281**(41): p. 30373-82.
197. Scherz-Shouval, R., et al., *Reactive oxygen species are essential for autophagy and specifically regulate the activity of Atg4.* EMBO J, 2007. **26**(7): p. 1749-60.
198. Xiong, Y., et al., *Degradation of oxidized proteins by autophagy during oxidative stress in Arabidopsis.* Plant Physiol, 2007. **143**(1): p. 291-9.
199. Hoyer-Hansen, M., et al., *Control of macroautophagy by calcium, calmodulin-dependent kinase kinase-beta, and Bcl-2.* Mol Cell, 2007. **25**(2): p. 193-205.
200. Meley, D., et al., *AMP-activated protein kinase and the regulation of autophagic proteolysis.* J Biol Chem, 2006. **281**(46): p. 34870-9.
201. Reggiori, F., et al., *Autophagy: more than a nonselective pathway.* Int J Cell Biol, 2012. **2012**: p. 219625.
202. Suzuki, K., *Selective autophagy in budding yeast.* Cell Death Differ, 2013. **20**(1): p. 43-8.
203. Behrends, C. and S. Fulda, *Receptor proteins in selective autophagy.* Int J Cell Biol, 2012. **2012**: p. 673290.
204. Katsuragi, Y., Y. Ichimura, and M. Komatsu, *p62/SQSTM1 functions as a signaling hub and an autophagy adaptor.* FEBS J, 2015. **282**(24): p. 4672-8.

205. Shaid, S., et al., *Ubiquitination and selective autophagy.* Cell Death Differ, 2013. **20**(1): p. 21-30.
206. Mancias, J.D. and A.C. Kimmelman, *Mechanisms of Selective Autophagy in Normal Physiology and Cancer.* J Mol Biol, 2016. **428**(9 Pt A): p. 1659-80.
207. Zhang, J., M. Kundu, and P.A. Ney, *Mitophagy in mammalian cells: the reticulocyte model.* Methods Enzymol, 2009. **452**: p. 227-45.
208. Jin, S.M. and R.J. Youle, *PINK1- and Parkin-mediated mitophagy at a glance.* J Cell Sci, 2012. **125**(Pt 4): p. 795-9.
209. Lemasters, J.J., *Selective mitochondrial autophagy, or mitophagy, as a targeted defense against oxidative stress, mitochondrial dysfunction, and aging.* Rejuvenation Res, 2005. **8**(1): p. 3-5.
210. Deas, E., N.W. Wood, and H. Plun-Favreau, *Mitophagy and Parkinson's disease: the PINK1-parkin link.* Biochim Biophys Acta, 2011. **1813**(4): p. 623-33.
211. Durcan, T.M. and E.A. Fon, *The three 'P's of mitophagy: PARKIN, PINK1, and post-translational modifications.* Genes Dev, 2015. **29**(10): p. 989-99.
212. Vives-Bauza, C., et al., *PINK1-dependent recruitment of Parkin to mitochondria in mitophagy.* Proc Natl Acad Sci U S A, 2010. **107**(1): p. 378-83.
213. Pickrell, A.M. and R.J. Youle, *The roles of PINK1, parkin, and mitochondrial fidelity in Parkinson's disease.* Neuron, 2015. **85**(2): p. 257-73.
214. Chan, N.C., et al., *Broad activation of the ubiquitin-proteasome system by Parkin is critical for mitophagy.* Hum Mol Genet, 2011. **20**(9): p. 1726-37.
215. Barth, S., D. Glick, and K.F. Macleod, *Autophagy: assays and artifacts.* J Pathol, 2010. **221**(2): p. 117-24.
216. Warner, J.R., *The economics of ribosome biosynthesis in yeast.* Trends Biochem Sci, 1999. **24**(11): p. 437-40.
217. Kraft, C., F. Reggiori, and M. Peter, *Selective types of autophagy in yeast.* Biochim Biophys Acta, 2009. **1793**(9): p. 1404-12.
218. Cebollero, E., F. Reggiori, and C. Kraft, *Reticulophagy and ribophagy: regulated degradation of protein production factories.* Int J Cell Biol, 2012. **2012**: p. 182834.
219. Karim, M.R., et al., *Cytosolic LC3 ratio as a sensitive index of macroautophagy in isolated rat hepatocytes and H4-II-E cells.* Autophagy, 2007. **3**(6): p. 553-60.
220. Kimura, S., T. Noda, and T. Yoshimori, *Dissection of the autophagosome maturation process by a novel reporter protein, tandem fluorescent-tagged LC3.* Autophagy, 2007. **3**(5): p. 452-60.
221. Proikas-Cezanne, T., et al., *WIPI proteins: essential PtdIns3P effectors at the nascent autophagosome.* J Cell Sci, 2015. **128**(2): p. 207-17.
222. Szalai, P., et al., *Autophagic bulk sequestration of cytosolic cargo is independent of LC3, but requires GABARAPs.* Exp Cell Res, 2015. **333**(1): p. 21-38.
223. Engedal, N. and P.O. Seglen, *Autophagy of cytoplasmic bulk cargo does not require LC3.* Autophagy, 2016. **12**(2): p. 439-41.
224. Kimmelman, A.C., *The dynamic nature of autophagy in cancer.* Genes Dev, 2011. **25**(19): p. 1999-2010.
225. Klionsky, D.J., et al., *Guidelines for the use and interpretation of assays for monitoring autophagy (3rd edition).* Autophagy, 2016. **12**(1): p. 1-222.
226. Zhao, J., et al., *mTOR inhibition activates overall protein degradation by the ubiquitin proteasome system as well as by autophagy.* Proc Natl Acad Sci U S A, 2015. **112**(52): p. 15790-7.
227. Maycotte, P. and A. Thorburn, *Autophagy and cancer therapy.* Cancer Biol Ther, 2011. **11**(2): p. 127-37.
228. Wu, Y.T., et al., *Dual role of 3-methyladenine in modulation of autophagy via different temporal patterns of inhibition on class I and III phosphoinositide 3-kinase.* J Biol Chem, 2010. **285**(14): p. 10850-61.
229. Levine, B. and G. Kroemer, *Autophagy in the pathogenesis of disease.* Cell, 2008. **132**(1): p. 27-42.

230. Jiang, P. and N. Mizushima, *Autophagy and human diseases.* Cell Res, 2014. **24**(1): p. 69-79.
231. Son, J.H., et al., *Neuronal autophagy and neurodegenerative diseases.* Exp Mol Med, 2012. **44**(2): p. 89-98.
232. Barnett, A. and G.J. Brewer, *Autophagy in aging and Alzheimer's disease: pathologic or protective?* J Alzheimers Dis, 2011. **25**(3): p. 385-94.
233. Pickford, F., et al., *The autophagy-related protein beclin 1 shows reduced expression in early Alzheimer disease and regulates amyloid beta accumulation in mice.* J Clin Invest, 2008. **118**(6): p. 2190-9.
234. Orr, M.E. and S. Oddo, *Autophagic/lysosomal dysfunction in Alzheimer's disease.* Alzheimers Res Ther, 2013. **5**(5): p. 53.
235. Cai, Z. and L.J. Yan, *Rapamycin, Autophagy, and Alzheimer's Disease.* J Biochem Pharmacol Res, 2013. **1**(2): p. 84-90.
236. Yang, D.S., et al., *Reversal of autophagy dysfunction in the TgCRND8 mouse model of Alzheimer's disease ameliorates amyloid pathologies and memory deficits.* Brain, 2011. **134**(Pt 1): p. 258-77.
237. Webb, J.L., et al., *Alpha-Synuclein is degraded by both autophagy and the proteasome.* J Biol Chem, 2003. **278**(27): p. 25009-13.
238. Spencer, B., et al., *Beclin 1 gene transfer activates autophagy and ameliorates the neurodegenerative pathology in alpha-synuclein models of Parkinson's and Lewy body diseases.* J Neurosci, 2009. **29**(43): p. 13578-88.
239. Finkbeiner, S., *Huntington's Disease.* Cold Spring Harb Perspect Biol, 2011. **3**(6).
240. Jia, K., A.C. Hart, and B. Levine, *Autophagy genes protect against disease caused by polyglutamine expansion proteins in Caenorhabditis elegans.* Autophagy, 2007. **3**(1): p. 21-5.
241. Terman, A. and U.T. Brunk, *Autophagy in cardiac myocyte homeostasis, aging, and pathology.* Cardiovasc Res, 2005. **68**(3): p. 355-65.
242. Pattison, J.S., H. Osinska, and J. Robbins, *Atg7 induces basal autophagy and rescues autophagic deficiency in CryABR120G cardiomyocytes.* Circ Res, 2011. **109**(2): p. 151-60.
243. Salabei, J.K. and D.J. Conklin, *Cardiovascular autophagy: crossroads of pathology, pharmacology and toxicology.* Cardiovasc Toxicol, 2013. **13**(3): p. 220-9.
244. Tanaka, Y., et al., *Accumulation of autophagic vacuoles and cardiomyopathy in LAMP-2-deficient mice.* Nature, 2000. **406**(6798): p. 902-6.
245. Degenhardt, K., et al., *Autophagy promotes tumor cell survival and restricts necrosis, inflammation, and tumorigenesis.* Cancer Cell, 2006. **10**(1): p. 51-64.
246. Schoenlein, P.V., et al., *Autophagy facilitates the progression of ERalpha-positive breast cancer cells to antiestrogen resistance.* Autophagy, 2009. **5**(3): p. 400-3.
247. Amaravadi, R.K., et al., *Autophagy inhibition enhances therapy-induced apoptosis in a Myc-induced model of lymphoma.* J Clin Invest, 2007. **117**(2): p. 326-36.
248. Takamura, A., et al., *Autophagy-deficient mice develop multiple liver tumors.* Genes Dev, 2011. **25**(8): p. 795-800.
249. Liberti, M.V. and J.W. Locasale, *The Warburg Effect: How Does it Benefit Cancer Cells?* Trends Biochem Sci, 2016. **41**(3): p. 211-8.
250. Ivanova, H., et al., *Endoplasmic Reticulum-Mitochondrial Ca2+ Fluxes Underlying Cancer Cell Survival.* Front Oncol, 2017. **7**: p. 70.
251. Bultynck, G., *Onco-IP3Rs Feed Cancerous Cravings for Mitochondrial Ca(2.).* Trends Biochem Sci, 2016. **41**(5): p. 390-3.
252. Singh, A., et al., *Inhibition of Inositol 1, 4, 5-Trisphosphate Receptor Induce Breast Cancer Cell Death Through Deregulated Autophagy and Cellular Bioenergetics.* J Cell Biochem, 2017. **118**(8): p. 2333-2346.
253. White, E., *The role for autophagy in cancer.* J Clin Invest, 2015. **125**(1): p. 42-6.
254. Yang, S., et al., *Pancreatic cancers require autophagy for tumor growth.* Genes Dev, 2011. **25**(7): p. 717-29.
255. Lock, R., et al., *Autophagy-dependent production of secreted factors facilitates oncogenic RAS-driven invasion.* Cancer Discov, 2014. **4**(4): p. 466-79.

256. Avalos, Y., et al., *Tumor suppression and promotion by autophagy.* Biomed Res Int, 2014. **2014**: p. 603980.
257. Quail, D.F. and J.A. Joyce, *Microenvironmental regulation of tumor progression and metastasis.* Nat Med, 2013. **19**(11): p. 1423-37.
258. Poillet-Perez, L., et al., *Interplay between ROS and autophagy in cancer cells, from tumor initiation to cancer therapy.* Redox Biol, 2015. **4**: p. 184-92.
259. Elgendy, M., et al., *Oncogenic Ras-induced expression of Noxa and Beclin-1 promotes autophagic cell death and limits clonogenic survival.* Mol Cell, 2011. **42**(1): p. 23-35.
260. Young, A.R., et al., *Autophagy mediates the mitotic senescence transition.* Genes Dev, 2009. **23**(7): p. 798-803.
261. Thorburn, A., D.H. Thamm, and D.L. Gustafson, *Autophagy and cancer therapy.* Mol Pharmacol, 2014. **85**(6): p. 830-8.
262. Cook, K.L., et al., *Hydroxychloroquine inhibits autophagy to potentiate antiestrogen responsiveness in ER+ breast cancer.* Clin Cancer Res, 2014. **20**(12): p. 3222-32.
263. Lloyd-Evans, E. and L.J. Haslett, *The lysosomal storage disease continuum with ageing-related neurodegenerative disease.* Ageing Res Rev, 2016. **32**: p. 104-121.
264. Levine, B. and J. Yuan, *Autophagy in cell death: an innocent convict?* J Clin Invest, 2005. **115**(10): p. 2679-88.
265. Schweichel, J.U. and H.J. Merker, *The morphology of various types of cell death in prenatal tissues.* Teratology, 1973. **7**(3): p. 253-66.
266. Liu, Y., et al., *Autosis is a Na+,K+-ATPase-regulated form of cell death triggered by autophagy-inducing peptides, starvation, and hypoxia-ischemia.* Proc Natl Acad Sci U S A, 2013. **110**(51): p. 20364-71.
267. Tsujimoto, Y. and S. Shimizu, *Another way to die: autophagic programmed cell death.* Cell Death Differ, 2005. **12 Suppl 2**: p. 1528-34.
268. Gump, J.M. and A. Thorburn, *Autophagy and apoptosis: what is the connection?* Trends Cell Biol, 2011. **21**(7): p. 387-92.
269. Fulda, S., *Regulation of cell death in cancer-possible implications for immunotherapy.* Front Oncol, 2013. **3**: p. 29.
270. Maiuri, M.C., et al., *Self-eating and self-killing: crosstalk between autophagy and apoptosis.* Nat Rev Mol Cell Biol, 2007. **8**(9): p. 741-52.
271. Moscat, J. and M.T. Diaz-Meco, *p62 at the crossroads of autophagy, apoptosis, and cancer.* Cell, 2009. **137**(6): p. 1001-4.
272. Kang, R., et al., *The Beclin 1 network regulates autophagy and apoptosis.* Cell Death Differ, 2011. **18**(4): p. 571-80.
273. Fan, Y.J. and W.X. Zong, *The cellular decision between apoptosis and autophagy.* Chin J Cancer, 2013. **32**(3): p. 121-9.
274. Quinsay, M.N., et al., *Bnip3-mediated mitochondrial autophagy is independent of the mitochondrial permeability transition pore.* Autophagy, 2010. **6**(7): p. 855-62.
275. Gozuacik, D., et al., *DAP-kinase is a mediator of endoplasmic reticulum stress-induced caspase activation and autophagic cell death.* Cell Death Differ, 2008. **15**(12): p. 1875-86.
276. Bano, D., et al., *Cleavage of the plasma membrane Na+/Ca2+ exchanger in excitotoxicity.* Cell, 2005. **120**(2): p. 275-85.
277. Ogata, M., et al., *Autophagy is activated for cell survival after endoplasmic reticulum stress.* Mol Cell Biol, 2006. **26**(24): p. 9220-31.
278. Rashid, H.O., et al., *ER stress: Autophagy induction, inhibition and selection.* Autophagy, 2015. **11**(11): p. 1956-1977.
279. Gardner, B.M., et al., *Endoplasmic reticulum stress sensing in the unfolded protein response.* Cold Spring Harb Perspect Biol, 2013. **5**(3): p. a013169.
280. Pallepati, P. and D.A. Averill-Bates, *Activation of ER stress and apoptosis by hydrogen peroxide in HeLa cells: protective role of mild heat preconditioning at 40 degrees C.* Biochim Biophys Acta, 2011. **1813**(12): p. 1987-99.
281. Senft, D. and Z.A. Ronai, *UPR, autophagy, and mitochondria crosstalk underlies the ER stress response.* Trends Biochem Sci, 2015. **40**(3): p. 141-8.

282. Zheng, Q., J. Li, and X. Wang, *Interplay between the ubiquitin-proteasome system and autophagy in proteinopathies.* Int J Physiol Pathophysiol Pharmacol, 2009. **1**(2): p. 127-42.
283. Liu, Y. and B. Levine, *Autosis and autophagic cell death: the dark side of autophagy.* Cell Death Differ, 2015. **22**(3): p. 367-76.
284. Luan, Q., et al., *RIPK1 regulates survival of human melanoma cells upon endoplasmic reticulum stress through autophagy.* Autophagy, 2015. **11**(7): p. 975-94.
285. Decuypere, J.P., et al., *The IP(3) receptor-mitochondria connection in apoptosis and autophagy.* Biochim Biophys Acta, 2011. **1813**(5): p. 1003-13.
286. Criollo, A., et al., *Regulation of autophagy by the inositol trisphosphate receptor.* Cell Death Differ, 2007. **14**(5): p. 1029-39.
287. Vicencio, J.M., et al., *The inositol 1,4,5-trisphosphate receptor regulates autophagy through its interaction with Beclin 1.* Cell Death Differ, 2009. **16**(7): p. 1006-17.
288. Cardenas, C., et al., *Essential regulation of cell bioenergetics by constitutive $InsP_3$ receptor Ca^{2+} transfer to mitochondria.* Cell, 2010. **142**(2): p. 270-83.
289. Khan, M.T. and S.K. Joseph, *Role of inositol trisphosphate receptors in autophagy in DT40 cells.* J Biol Chem, 2010. **285**(22): p. 16912-20.
290. Bootman, M.D., et al., *The regulation of autophagy by calcium signals: Do we have a consensus?* Cell Calcium, 2017.
291. Williams, A., et al., *Novel targets for Huntington's disease in an mTOR-independent autophagy pathway.* Nat Chem Biol, 2008. **4**(5): p. 295-305.
292. Itakura, E. and N. Mizushima, *Characterization of autophagosome formation site by a hierarchical analysis of mammalian Atg proteins.* Autophagy, 2010. **6**(6): p. 764-76.
293. Sakaki, K., J. Wu, and R.J. Kaufman, *Protein kinase Ctheta is required for autophagy in response to stress in the endoplasmic reticulum.* J Biol Chem, 2008. **283**(22): p. 15370-80.
294. Brady, N.R., et al., *The autophagic response to nutrient deprivation in the hl-1 cardiac myocyte is modulated by Bcl-2 and sarco/endoplasmic reticulum calcium stores.* FEBS J, 2007. **274**(12): p. 3184-97.
295. Jing, Z., et al., *SKF-96365 activates cytoprotective autophagy to delay apoptosis in colorectal cancer cells through inhibition of the calcium/CaMKIIgamma/AKT-mediated pathway.* Cancer Lett, 2016. **372**(2): p. 226-38.
296. Vingtdeux, V., et al., *AMP-activated protein kinase signaling activation by resveratrol modulates amyloid-beta peptide metabolism.* J Biol Chem, 2010. **285**(12): p. 9100-13.
297. Ghislat, G., et al., *Withdrawal of essential amino acids increases autophagy by a pathway involving Ca^{2+}/calmodulin-dependent kinase kinase-beta (CaMKK-beta).* J Biol Chem, 2012. **287**(46): p. 38625-36.
298. Egan, D.F., et al., *Phosphorylation of ULK1 (hATG1) by AMP-activated protein kinase connects energy sensing to mitophagy.* Science, 2011. **331**(6016): p. 456-61.
299. Yang, J., et al., *Store-operated calcium entry-activated autophagy protects EPC proliferation via the CAMKK2-MTOR pathway in ox-LDL exposure.* Autophagy, 2017. **13**(1): p. 82-98.
300. Gao, W., et al., *Induction of macroautophagy by exogenously introduced calcium.* Autophagy, 2008. **4**(6): p. 754-61.
301. Kim, H.J., et al., *The Ca(2+) channel TRPML3 regulates membrane trafficking and autophagy.* Traffic, 2009. **10**(8): p. 1157-67.
302. Decrock, E., et al., *Connexin and pannexin signaling pathways, an architectural blueprint for CNS physiology and pathology?* Cell Mol Life Sci, 2015. **72**(15): p. 2823-51.
303. Lu, N., et al., *Autophagy occurs within an hour of adenosine triphosphate treatment after nerve cell damage: the neuroprotective effects of adenosine triphosphate against apoptosis.* Neural Regen Res, 2014. **9**(17): p. 1599-605.
304. Das, S., et al., *Purinergic receptor X7 is a key modulator of metabolic oxidative stress-mediated autophagy and inflammation in experimental nonalcoholic steatohepatitis.* Am J Physiol Gastrointest Liver Physiol, 2013. **305**(12): p. G950-63.
305. Biswas, D., et al., *ATP-induced autophagy is associated with rapid killing of intracellular mycobacteria within human monocytes/macrophages.* BMC Immunol, 2008. **9**: p. 35.

306. Wei, Q., et al., *High dose of extracellular ATP switched autophagy to apoptosis in anchorage-dependent and anchorage-independent hepatoma cells.* Purinergic Signal, 2013. **9**(4): p. 585-98.
307. Boroughs, L.K. and R.J. DeBerardinis, *Metabolic pathways promoting cancer cell survival and growth.* Nat Cell Biol, 2015. **17**(4): p. 351-9.
308. Decuypere, J.P., J.B. Parys, and G. Bultynck, *ITPRs/inositol 1,4,5-trisphosphate receptors in autophagy: From enemy to ally.* Autophagy, 2015. **11**(10): p. 1944-8.
309. Vervliet, T., et al., *Basal ryanodine receptor activity suppresses autophagic flux.* Biochem Pharmacol, 2017. **132**: p. 133-142.
310. Cardenas, C. and J.K. Foskett, *Mitochondrial Ca(2+) signals in autophagy.* Cell Calcium, 2012. **52**(1): p. 44-51.
311. Rizzuto, R., et al., *Mitochondria as sensors and regulators of calcium signalling.* Nat Rev Mol Cell Biol, 2012. **13**(9): p. 566-78.
312. Mallilankaraman, K., et al., *MICU1 is an essential gatekeeper for MCU-mediated mitochondrial Ca(2+) uptake that regulates cell survival.* Cell, 2012. **151**(3): p. 630-44.
313. Rojas-Rivera, D. and C. Hetz, *TMBIM protein family: ancestral regulators of cell death.* Oncogene, 2015. **34**(3): p. 269-80.
314. Sano, R., et al., *Endoplasmic reticulum protein BI-1 regulates Ca(2)(+)-mediated bioenergetics to promote autophagy.* Genes Dev, 2012. **26**(10): p. 1041-54.
315. Bultynck, G., et al., *The C terminus of Bax inhibitor-1 forms a Ca2+-permeable channel pore.* J Biol Chem, 2012. **287**(4): p. 2544-57.
316. Kiviluoto, S., et al., *Bax inhibitor-1 is a novel IP(3) receptor-interacting and -sensitizing protein.* Cell Death Dis, 2012. **3**: p. e367.
317. Decuypere, J.P., et al., *Ins(1,4,5)P3 receptor-mediated Ca2+ signaling and autophagy induction are interrelated.* Autophagy, 2011. **7**(12): p. 1472-89.
318. Luyten, T., et al., *Resveratrol-induced autophagy is dependent on IP3Rs and on cytosolic Ca2.* Biochim Biophys Acta, 2017. **1864**(6): p. 947-956.
319. Messai, Y., et al., *ITPR1 protects renal cancer cells against natural killer cells by inducing autophagy.* Cancer Res, 2014. **74**(23): p. 6820-32.
320. Cardenas, C., et al., *Selective Vulnerability of Cancer Cells by Inhibition of Ca(2+) Transfer from Endoplasmic Reticulum to Mitochondria.* Cell Rep, 2016. **14**(10): p. 2313-24.
321. Bennett, D.L., et al., *Expression and function of ryanodine receptors in nonexcitable cells.* J Biol Chem, 1996. **271**(11): p. 6356-62.
322. Hazama, A., T. Yada, and Y. Okada, *HeLa cells have histamine H1-receptors which mediate activation of the K+ conductance.* Biochim Biophys Acta, 1985. **845**(2): p. 249-53.
323. Graham, F.L., et al., *Characteristics of a human cell line transformed by DNA from human adenovirus type 5.* J Gen Virol, 1977. **36**(1): p. 59-74.
324. Wojcikiewicz, R.J., *Type I, II, and III inositol 1,4,5-trisphosphate receptors are unequally susceptible to down-regulation and are expressed in markedly different proportions in different cell types.* J Biol Chem, 1995. **270**(19): p. 11678-83.
325. Ruas, M., et al., *Expression of Ca(2)(+)-permeable two-pore channels rescues NAADP signalling in TPC-deficient cells.* EMBO J, 2015. **34**(13): p. 1743-58.
326. Verjans, B., et al., *Cloning and expression in Escherichia coli of a dog thyroid cDNA encoding a novel inositol 1,4,5-trisphosphate 5-phosphatase.* Biochem J, 1994. **300 (Pt 1)**: p. 85-90.
327. Whisstock, J.C., et al., *The inositol polyphosphate 5-phosphatases and the apurinic/apyrimidinic base excision repair endonucleases share a common mechanism for catalysis.* J Biol Chem, 2000. **275**(47): p. 37055-61.
328. Livak, K.J. and T.D. Schmittgen, *Analysis of relative gene expression data using real-time quantitative PCR and the 2(-Delta Delta C(T)) Method.* Methods, 2001. **25**(4): p. 402-8.
329. Bootman, M.D., et al., *Ca2+-sensitive fluorescent dyes and intracellular Ca2+ imaging.* Cold Spring Harb Protoc, 2013. **2013**(2): p. 83-99.
330. Grynkiewicz, G., M. Poenie, and R.Y. Tsien, *A new generation of Ca2+ indicators with greatly improved fluorescence properties.* J Biol Chem, 1985. **260**(6): p. 3440-50.
331. Paredes, R.M., et al., *Chemical calcium indicators.* Methods, 2008. **46**(3): p. 143-51.

332. Tasdemir, E., et al., *Methods for assessing autophagy and autophagic cell death.* Methods Mol Biol, 2008. **445**: p. 29-76.
333. Kabeya, Y., et al., *LC3, a mammalian homologue of yeast Apg8p, is localized in autophagosome membranes after processing.* EMBO J, 2000. **19**(21): p. 5720-8.
334. Chandrachud, U., et al., *Unbiased Cell-based Screening in a Neuronal Cell Model of Batten Disease Highlights an Interaction between Ca2+ Homeostasis, Autophagy, and CLN3 Protein Function.* J Biol Chem, 2015. **290**(23): p. 14361-80.
335. Bootman, M.D. and M.J. Berridge, *Subcellular Ca2+ signals underlying waves and graded responses in HeLa cells.* Curr Biol, 1996. **6**(7): p. 855-65.
336. Hornstein, B.D., et al., *Effects of Circular DNA Length on Transfection Efficiency by Electroporation into HeLa Cells.* PLoS One, 2016. **11**(12): p. e0167537.
337. Thomas, P. and T.G. Smart, *HEK293 cell line: a vehicle for the expression of recombinant proteins.* J Pharmacol Toxicol Methods, 2005. **51**(3): p. 187-200.
338. Ermak, G. and K.J. Davies, *Calcium and oxidative stress: from cell signaling to cell death.* Mol Immunol, 2002. **38**(10): p. 713-21.
339. Bauvy, C., A.J. Meijer, and P. Codogno, *Assaying of autophagic protein degradation.* Methods Enzymol, 2009. **452**: p. 47-61.
340. Hirota, Y., et al., *Mitophagy is primarily due to alternative autophagy and requires the MAPK1 and MAPK14 signaling pathways.* Autophagy, 2015. **11**(2): p. 332-43.
341. Chen, R., et al., *The general amino acid control pathway regulates mTOR and autophagy during serum/glutamine starvation.* J Cell Biol, 2014. **206**(2): p. 173-82.
342. Zhu, Y., et al., *L-Glutamine deprivation induces autophagy and alters the mTOR and MAPK signaling pathways in porcine intestinal epithelial cells.* Amino Acids, 2015. **47**(10): p. 2185-97.
343. Mauvezin, C. and T.P. Neufeld, *Bafilomycin A1 disrupts autophagic flux by inhibiting both V-ATPase-dependent acidification and Ca-P60A/SERCA-dependent autophagosome-lysosome fusion.* Autophagy, 2015. **11**(8): p. 1437-8.
344. Juhasz, G., *Interpretation of bafilomycin, pH neutralizing or protease inhibitor treatments in autophagic flux experiments: novel considerations.* Autophagy, 2012. **8**(12): p. 1875-6.
345. Devereaux, K., et al., *Regulation of mammalian autophagy by class II and III PI 3-kinases through PI3P synthesis.* PLoS One, 2013. **8**(10): p. e76405.
346. Heckmann, B.L., et al., *The autophagic inhibitor 3-methyladenine potently stimulates PKA-dependent lipolysis in adipocytes.* Br J Pharmacol, 2013. **168**(1): p. 163-71.
347. Decuypere, J.P., et al., *mTOR-Controlled Autophagy Requires Intracellular Ca(2+) Signaling.* PLoS One, 2013. **8**(4): p. e61020.
348. Kim, Y.C. and K.L. Guan, *mTOR: a pharmacologic target for autophagy regulation.* J Clin Invest, 2015. **125**(1): p. 25-32.
349. Mukherjee, A., S. Koli, and K.V. Reddy, *Rapamycin (Sirolimus) alters mechanistic target of rapamycin pathway regulation and microRNA expression in mouse meiotic spermatocytes.* Andrology, 2015. **3**(5): p. 979-90.
350. Weichhart, T., *Mammalian target of rapamycin: a signaling kinase for every aspect of cellular life.* Methods Mol Biol, 2012. **821**: p. 1-14.
351. Di Virgilio, F., T.H. Steinberg, and S.C. Silverstein, *Inhibition of Fura-2 sequestration and secretion with organic anion transport blockers.* Cell Calcium, 1990. **11**(2-3): p. 57-62.
352. Palmer, A.E. and R.Y. Tsien, *Measuring calcium signaling using genetically targetable fluorescent indicators.* Nat Protoc, 2006. **1**(3): p. 1057-65.
353. Chan, L.L., et al., *A novel image-based cytometry method for autophagy detection in living cells.* Autophagy, 2012. **8**(9): p. 1371-82.
354. Yla-Anttila, P., et al., *Monitoring autophagy by electron microscopy in Mammalian cells.* Methods Enzymol, 2009. **452**: p. 143-64.
355. Engedal, N., et al., *Modulation of intracellular calcium homeostasis blocks autophagosome formation.* Autophagy, 2013. **9**(10): p. 1475-90.
356. Bultynck, G., et al., *Calcineurin and intracellular Ca2+-release channels: regulation or association?* Biochem Biophys Res Commun, 2003. **311**(4): p. 1181-93.

357. Wu, L., et al., *Rapamycin upregulates autophagy by inhibiting the mTOR-ULK1 pathway, resulting in reduced podocyte injury.* PLoS One, 2013. **8**(5): p. e63799.
358. Liu, C., et al., *Impaired autophagy in mouse embryonic fibroblasts null for Kruppel-like Factor 4 promotes DNA damage and increases apoptosis upon serum starvation.* Mol Cancer, 2015. **14**: p. 101.
359. Shang, L., et al., *Nutrient starvation elicits an acute autophagic response mediated by Ulk1 dephosphorylation and its subsequent dissociation from AMPK.* Proc Natl Acad Sci U S A, 2011. **108**(12): p. 4788-93.
360. Yan, X., et al., *Reconstitution of leucine-mediated autophagy via the mTORC1-Barkor pathway in vitro.* Autophagy, 2012. **8**(2): p. 213-21.
361. Tanemura, M., et al., *Role of rapamycin-induced autophagy in pancreatic islets.* Am J Transplant, 2012. **12**(4): p. 1067.
362. Steiger-Barraissoul, S. and A. Rami, *Serum deprivation induced autophagy and predominantly an AIF-dependent apoptosis in hippocampal HT22 neurons.* Apoptosis, 2009. **14**(11): p. 1274-88.
363. Demetriades, C., N. Doumpas, and A.A. Teleman, *Regulation of TORC1 in response to amino acid starvation via lysosomal recruitment of TSC2.* Cell, 2014. **156**(4): p. 786-99.
364. Fung, C., et al., *Induction of autophagy during extracellular matrix detachment promotes cell survival.* Mol Biol Cell, 2008. **19**(3): p. 797-806.
365. Chen, X., et al., *Autophagy induced by calcium phosphate precipitates involves endoplasmic reticulum membranes in autophagosome biogenesis.* PLoS One, 2012. **7**(12): p. e52347.
366. N'Diaye, E.N., et al., *PLIC proteins or ubiquilins regulate autophagy-dependent cell survival during nutrient starvation.* EMBO Rep, 2009. **10**(2): p. 173-9.
367. Tanida, I., T. Ueno, and E. Kominami, *LC3 and Autophagy.* Methods Mol Biol, 2008. **445**: p. 77-88.
368. Asano, K., et al., *Suppression of starvation-induced autophagy by recombinant toxic shock syndrome toxin-1 in epithelial cells.* PLoS One, 2014. **9**(11): p. e113018.
369. Melendez, A., et al., *Autophagy genes are essential for dauer development and life-span extension in C. elegans.* Science, 2003. **301**(5638): p. 1387-91.
370. Wang, Q.J., et al., *Induction of autophagy in axonal dystrophy and degeneration.* J Neurosci, 2006. **26**(31): p. 8057-68.
371. Sun, F., et al., *Regulation of autophagy by Ca2.* Tumour Biol, 2016.
372. Ganley, I.G., et al., *Distinct autophagosomal-lysosomal fusion mechanism revealed by thapsigargin-induced autophagy arrest.* Mol Cell, 2011. **42**(6): p. 731-43.
373. Pryor, P.R., et al., *The role of intraorganellar Ca(2+) in late endosome-lysosome heterotypic fusion and in the reformation of lysosomes from hybrid organelles.* J Cell Biol, 2000. **149**(5): p. 1053-62.
374. Pankiv, S., et al., *p62/SQSTM1 binds directly to Atg8/LC3 to facilitate degradation of ubiquitinated protein aggregates by autophagy.* J Biol Chem, 2007. **282**(33): p. 24131-45.
375. Shpilka, T., et al., *Atg8: an autophagy-related ubiquitin-like protein family.* Genome Biol, 2011. **12**(7): p. 226.
376. Eickholt, B.J., et al., *Effects of valproic acid derivatives on inositol trisphosphate depletion, teratogenicity, glycogen synthase kinase-3beta inhibition, and viral replication: a screening approach for new bipolar disorder drugs derived from the valproic acid core structure.* Mol Pharmacol, 2005. **67**(5): p. 1426-33.
377. Wang, S.H., et al., *Cadmium-induced autophagy and apoptosis are mediated by a calcium signaling pathway.* Cell Mol Life Sci, 2008. **65**(22): p. 3640-52.
378. Cardenas, C., et al., *Selective Vulnerability of Cancer Cells by Inhibition of Ca^{2+} Transfer from Endoplasmic Reticulum to Mitochondria.* Cell Rep, 2016. **14**(10): p. 2313-24.
379. Jouaville, L.S., et al., *Regulation of mitochondrial ATP synthesis by calcium: evidence for a long-term metabolic priming.* Proc Natl Acad Sci U S A, 1999. **96**(24): p. 13807-12.
380. Territo, P.R., et al., *Ca(2+) activation of heart mitochondrial oxidative phosphorylation: role of the F(0)/F(1)-ATPase.* Am J Physiol Cell Physiol, 2000. **278**(2): p. C423-35.

381. Glancy, B. and R.S. Balaban, *Role of mitochondrial Ca2+ in the regulation of cellular energetics.* Biochemistry, 2012. **51**(14): p. 2959-73.
382. Decuypere, J.P., J.B. Parys, and G. Bultynck, *Regulation of the autophagic bcl-2/beclin 1 interaction.* Cells, 2012. **1**(3): p. 284-312.
383. Regimbald-Dumas, Y., M.O. Fregeau, and G. Guillemette, *Mammalian target of rapamycin (mTOR) phosphorylates inositol 1,4,5-trisphosphate receptor type 2 and increases its Ca(2+) release activity.* Cell Signal, 2011. **23**(1): p. 71-9.
384. Qazi, S. and B.A. Trimmer, *The role of inositol 1,4,5-trisphosphate 5-phosphatase in inositol signaling in the CNS of larval Manduca sexta.* Insect Biochem Mol Biol, 1999. **29**(2): p. 161-75.
385. Hidaka, H. and M. Watanabe, *[Calcium protein signaling].* Nihon Rinsho, 1993. **51**(5): p. 1151-5.
386. Higazi, D.R., et al., *Endothelin-1-stimulated InsP3-induced Ca2+ release is a nexus for hypertrophic signaling in cardiac myocytes.* Mol Cell, 2009. **33**(4): p. 472-82.
387. Collins, T.J., et al., *Mitochondrial Ca(2+) uptake depends on the spatial and temporal profile of cytosolic Ca(2+) signals.* J Biol Chem, 2001. **276**(28): p. 26411-20.
388. Bootman, M.D., et al., *2-aminoethoxydiphenyl borate (2-APB) is a reliable blocker of store-operated Ca2+ entry but an inconsistent inhibitor of InsP3-induced Ca2+ release.* FASEB J, 2002. **16**(10): p. 1145-50.
389. Selvaraj, S., et al., *Resveratrol activates autophagic cell death in prostate cancer cells via downregulation of STIM1 and the mTOR pathway.* Mol Carcinog, 2016. **55**(5): p. 818-31.
390. Oslowski, C.M. and F. Urano, *Measuring ER stress and the unfolded protein response using mammalian tissue culture system.* Methods Enzymol, 2011. **490**: p. 71-92.
391. Beriault, D.R. and G.H. Werstuck, *Detection and quantification of endoplasmic reticulum stress in living cells using the fluorescent compound, Thioflavin T.* Biochim Biophys Acta, 2013. **1833**(10): p. 2293-301.
392. Delou, J.M., D. Biasoli, and H.L. Borges, *The Complex Link between Apoptosis and Autophagy: a Promising New Role for RB.* An Acad Bras Cienc, 2016. **88**(4): p. 2257-2275.
393. De Stefani, D., et al., *A forty-kilodalton protein of the inner membrane is the mitochondrial calcium uniporter.* Nature, 2011. **476**(7360): p. 336-40.
394. Baughman, J.M., et al., *Integrative genomics identifies MCU as an essential component of the mitochondrial calcium uniporter.* Nature, 2011. **476**(7360): p. 341-5.
395. Matlib, M.A., et al., *Oxygen-bridged dinuclear ruthenium amine complex specifically inhibits Ca2+ uptake into mitochondria in vitro and in situ in single cardiac myocytes.* J Biol Chem, 1998. **273**(17): p. 10223-31.
396. Garcia-Rivas Gde, J., et al., *Ru360, a specific mitochondrial calcium uptake inhibitor, improves cardiac post-ischaemic functional recovery in rats in vivo.* Br J Pharmacol, 2006. **149**(7): p. 829-37.
397. Cardenas, C., et al., *Selective Vulnerability of Cancer Cells by Inhibition of Ca(2+) Transfer from Endoplasmic Reticulum to Mitochondria.* Cell Rep, 2016. **15**(1): p. 219-20.
398. Hanson, C.J., M.D. Bootman, and H.L. Roderick, *Cell signalling: IP3 receptors channel calcium into cell death.* Curr Biol, 2004. **14**(21): p. R933-5.
399. Michalak, M., et al., *Calreticulin, a multi-process calcium-buffering chaperone of the endoplasmic reticulum.* Biochem J, 2009. **417**(3): p. 651-66.
400. Harr, M.W., et al., *Glucocorticoids downregulate Fyn and inhibit IP_3-mediated calcium signaling to promote autophagy in T lymphocytes.* Autophagy, 2010. **6**(7): p. 912-21.
401. Missiaen, L., et al., *2-Aminoethoxydiphenyl borate affects the inositol 1,4,5-trisphosphate receptor, the intracellular Ca2+ pump and the non-specific Ca2+ leak from the non-mitochondrial Ca2+ stores in permeabilized A7r5 cells.* Cell Calcium, 2001. **29**(2): p. 111-6.
402. Ivanova, H., et al., *Endoplasmic Reticulum–Mitochondrial Ca^{2+} Fluxes Underlying Cancer Cell Survival.* Frontiers in Oncology, 2017. **7**.
403. Liu, A.J., et al., *Evodiamine, a plant alkaloid, induces calcium/JNK-mediated autophagy and calcium/mitochondria-mediated apoptosis in human glioblastoma cells.* Chem Biol Interact, 2013. **205**(1): p. 20-8.

404. Kim, J., et al., *AMPK and mTOR regulate autophagy through direct phosphorylation of Ulk1.* Nat Cell Biol, 2011. **13**(2): p. 132-41.
405. Thorburn, A., *Apoptosis and autophagy: regulatory connections between two supposedly different processes.* Apoptosis, 2008. **13**(1): p. 1-9.
406. Ravikumar, B., et al., *Rapamycin pre-treatment protects against apoptosis.* Hum Mol Genet, 2006. **15**(7): p. 1209-16.
407. Tagashira, H., et al., *Methyl pyruvate rescues mitochondrial damage caused by SIGMAR1 mutation related to amyotrophic lateral sclerosis.* Biochim Biophys Acta, 2014. **1840**(12): p. 3320-34.
408. Santulli, G., et al., *Calcium release channel RyR2 regulates insulin release and glucose homeostasis.* J Clin Invest, 2015. **125**(5): p. 1968-78.
409. Santulli, G., et al., *Calcium release channel RyR2 regulates insulin release and glucose homeostasis.* J Clin Invest, 2015. **125**(11): p. 4316.
410. Dufer, M., et al., *Methyl pyruvate stimulates pancreatic beta-cells by a direct effect on KATP channels, and not as a mitochondrial substrate.* Biochem J, 2002. **368**(Pt 3): p. 817-25.
411. He, X., et al., *Down-regulation of adenosine monophosphate-activated protein kinase activity: A driver of cancer.* Tumour Biol, 2017. **39**(4): p. 1010428317697576.
412. Bultynck, G., *Onco-IP_3Rs Feed Cancerous Cravings for Mitochondrial Ca^{2+}.* Trends Biochem Sci, 2016. **41**(5): p. 390-3.
413. Nurbaeva, M.K., et al., *Store-operated Ca2+ Entry Modulates the Expression of Enamel Genes.* J Dent Res, 2015. **94**(10): p. 1471-7.
414. Pan, Z., M. Brotto, and J. Ma, *Store-operated Ca2+ entry in muscle physiology and diseases.* BMB Rep, 2014. **47**(2): p. 69-79.
415. Rosado, J.A., *Calcium Entry Pathways in Non-excitable Cells. Preface.* Adv Exp Med Biol, 2016. **898**: p. vii-viii.
416. Toth, A.B., A.K. Shum, and M. Prakriya, *Regulation of neurogenesis by calcium signaling.* Cell Calcium, 2016. **59**(2-3): p. 124-34.
417. Luik, R.M., et al., *The elementary unit of store-operated Ca2+ entry: local activation of CRAC channels by STIM1 at ER-plasma membrane junctions.* J Cell Biol, 2006. **174**(6): p. 815-25.
418. Dolmetsch, R.E., K. Xu, and R.S. Lewis, *Calcium oscillations increase the efficiency and specificity of gene expression.* Nature, 1998. **392**(6679): p. 933-6.
419. Chen, Y.W., et al., *The STIM1-Orai1 pathway of store-operated Ca2+ entry controls the checkpoint in cell cycle G1/S transition.* Sci Rep, 2016. **6**: p. 22142.
420. Bravo, R., et al., *Endoplasmic reticulum and the unfolded protein response: dynamics and metabolic integration.* Int Rev Cell Mol Biol, 2013. **301**: p. 215-90.
421. Zhang, X.Y., et al., *Endoplasmic reticulum chaperone GRP78 is involved in autophagy activation induced by ischemic preconditioning in neural cells.* Mol Brain, 2015. **8**: p. 20.
422. Hashimoto, D., et al., *Involvement of autophagy in trypsinogen activation within the pancreatic acinar cells.* J Cell Biol, 2008. **181**(7): p. 1065-72.
423. Sutton, R., O.H. Petersen, and S.J. Pandol, *Pancreatitis and calcium signalling: report of an international workshop.* Pancreas, 2008. **36**(4): p. e1-14.
424. Parekh, A.B., *Store-operated Ca2+ entry: dynamic interplay between endoplasmic reticulum, mitochondria and plasma membrane.* J Physiol, 2003. **547**(Pt 2): p. 333-48.
425. Grotemeier, A., et al., *AMPK-independent induction of autophagy by cytosolic Ca^{2+} increase.* Cell Signal, 2010. **22**(6): p. 914-25.
426. Nakanishi, K., et al., *Transient Ca2+ depletion from the endoplasmic reticulum is critical for skeletal myoblast differentiation.* FASEB J, 2015. **29**(5): p. 2137-49.
427. Petremand, J., et al., *HDLs protect pancreatic beta-cells against ER stress by restoring protein folding and trafficking.* Diabetes, 2012. **61**(5): p. 1100-11.
428. Saberi, B., et al., *Protein kinase C (PKC) participates in acetaminophen hepatotoxicity through c-jun-N-terminal kinase (JNK)-dependent and -independent signaling pathways.* Hepatology, 2014. **59**(4): p. 1543-1554.
429. Tokumitsu, H., et al., *STO-609, a specific inhibitor of the Ca(2+)/calmodulin-dependent protein kinase kinase.* J Biol Chem, 2002. **277**(18): p. 15813-8.

430. Pfisterer, S.G., et al., *Ca2+/calmodulin-dependent kinase (CaMK) signaling via CaMKI and AMP-activated protein kinase contributes to the regulation of WIPI-1 at the onset of autophagy.* Mol Pharmacol, 2011. **80**(6): p. 1066-75.
431. Burdyga, T.V. and S. Wray, *The effect of cyclopiazonic acid on excitation-contraction coupling in guinea-pig ureteric smooth muscle: role of the sarcoplasmic reticulum.* J Physiol, 1999. **517 (Pt 3)**: p. 855-65.
432. Moncoq, K., C.A. Trieber, and H.S. Young, *The molecular basis for cyclopiazonic acid inhibition of the sarcoplasmic reticulum calcium pump.* J Biol Chem, 2007. **282**(13): p. 9748-57.
433. Curry, M.C., et al., *Distinct regulation of cytoplasmic calcium signals and cell death pathways by different plasma membrane calcium ATPase isoforms in MDA-MB-231 breast cancer cells.* J Biol Chem, 2012. **287**(34): p. 28598-608.
434. Bonora, M., et al., *Comprehensive analysis of mitochondrial permeability transition pore activity in living cells using fluorescence-imaging-based techniques.* Nat Protoc, 2016. **11**(6): p. 1067-80.
435. Racioppi, L. and A.R. Means, *Calcium/calmodulin-dependent protein kinase kinase 2: roles in signaling and pathophysiology.* J Biol Chem, 2012. **287**(38): p. 31658-65.
436. Prakriya, M. and R.S. Lewis, *Store-Operated Calcium Channels.* Physiol Rev, 2015. **95**(4): p. 1383-436.
437. Sukumaran, P., et al., *TRPC1-mediated Ca(2)(+) entry is essential for the regulation of hypoxia and nutrient depletion-dependent autophagy.* Cell Death Dis, 2015. **6**: p. e1674.
438. Bootman, M.D. and K. Rietdorf, *Tissue Specificity: Store-Operated Ca2+ Entry in Cardiac Myocytes.* Adv Exp Med Biol, 2017. **993**: p. 363-387.
439. Lin, P.H., et al., *Lysosomal two-pore channel subtype 2 (TPC2) regulates skeletal muscle autophagic signaling.* J Biol Chem, 2015. **290**(6): p. 3377-89.
440. Liu, Y., et al., *Knockdown of RAB25 promotes autophagy and inhibits cell growth in ovarian cancer cells.* Mol Med Rep, 2012. **6**(5): p. 1006-12.
441. Kania, E., et al., *IP3 Receptor-Mediated Calcium Signaling and Its Role in Autophagy in Cancer.* Front Oncol, 2017. **7**: p. 140.

Copyright

NATURE PUBLISHING GROUP LICENSE
TERMS AND CONDITIONS

Sep 29, 2017

This Agreement between Ms. Tala Chehab ("You") and Nature Publishing Group ("Nature Publishing Group") consists of your license details and the terms and conditions provided by Nature Publishing Group and Copyright Clearance Center.

License Number	4198121025293
License date	Sep 29, 2017
Licensed Content Publisher	Nature Publishing Group
Licensed Content Publication	Nature Reviews Molecular Cell Biology
Licensed Content Title	Calcium signalling: dynamics, homeostasis and remodelling
Licensed Content Author	Michael J. Berridge, Martin D. Bootman and H. Llewelyn Roderick
Licensed Content Date	Jul 1, 2003
Licensed Content Volume	4
Licensed Content Issue	7
Type of Use	reuse in a dissertation / thesis
Requestor type	academic/educational
Format	print
Portion	figures/tables/illustrations
Number of figures/tables/illustrations	1
High-res required	no
Figures	figure 1
Author of this NPG article	no
Your reference number	
Title of your thesis / dissertation	The role of calcium signalling in autophagy
Expected completion date	Dec 2017
Estimated size (number of pages)	300
Requestor Location	Ms. Tala Chehab Walton Hall Milton Keynes, mk7 6aa United Kingdom Attn: Ms. Tala Chehab

ELSEVIER LICENSE
TERMS AND CONDITIONS

Sep 29, 2017

This Agreement between Ms. Tala Chehab ("You") and Elsevier ("Elsevier") consists of your license details and the terms and conditions provided by Elsevier and Copyright Clearance Center.

License Number	4198080691389
License date	Sep 29, 2017
Licensed Content Publisher	Elsevier
Licensed Content Publication	Trends in Biochemical Sciences
Licensed Content Title	Calcium at the Center of Cell Signaling: Interplay between Endoplasmic Reticulum, Mitochondria, and Lysosomes
Licensed Content Author	Anna Raffaello,Cristina Mammucari,Gaia Gherardi,Rosario Rizzuto
Licensed Content Date	Dec 1, 2016
Licensed Content Volume	41
Licensed Content Issue	12
Licensed Content Pages	15
Start Page	1035
End Page	1049
Type of Use	reuse in a thesis/dissertation
Portion	figures/tables/illustrations
Number of figures/tables/illustrations	1
Format	both print and electronic
Are you the author of this Elsevier article?	No
Will you be translating?	No
Original figure numbers	figure 1
Title of your thesis/dissertation	The role of calcium signalling in autophagy
Expected completion date	Dec 2017
Estimated size (number of pages)	300
Requestor Location	Ms. Tala Chehab Walton Hall Milton Keynes, mk7 6aa United Kingdom Attn: Ms. Tala Chehab
Publisher Tax ID	GB 494 6272 12